Siderophile Element Partitioning at high Pressures and Temperatures

-

Implications for Core Formation Processes

Dissertation

Zur Erlangung des akademischen Grades eines Doktors der Naturwissenschaften (Dr. rer. nat.) an der Bayreuther Graduiertenschule für Mathematik und Naturwissenschaften (BayNAT) der Universität Bayreuth

vorgelegt von

Dipl.-Min. Antje Kathrin Vogel
aus Mayen

Bayreuth, 2014

Die vorliegende Arbeit wurde in der Zeit von März 2011 bis September 2014 in Bayreuth am Bayerischen Geoinstitut Bayreuth, Universität Bayreuth unter der Betreuung von Herrn Professor Dr. David C. Rubie angefertigt.

Vollständiger Abdruck der von der Bayreuther Graduiertenschule für Mathematik und Naturwisseschaften (BayNAT) der Universität Bayreuth genehmigten Dissertation zur Erlangung des akademischen Grades eines Doktors der Naturwissenschaften (Dr. rer. nat.).

Dissertation eingereicht am: 16.09.2014
Zulassung durch das Leitungsgremium: 25.09.2014
Wissenschaftliches Kolloquium: 20.02.2015

Amtierender Direktor: Prof. Dr. Franz Xaver Schmid

Prüfungsausschuss:

Prof. Dr. David C. Rubie	(Erstgutachter)
Prof. Dr. Herbert Palme	(Zweitgutachter)
Prof. Dr. Daniel J. Frost	(Vorsitz)
Prof. Dr. Leonid Dubrovinsky	
Prof. Dr. Birgit Weber	

Table of Contents

Abstract

Siderophile (Fe-loving) elements are depleted in the Earth´s mantle because they have been extracted into the Earth´s core by core formation processes. Metal – silicate partitioning of siderophile elements can provide major constraints on the conditions that prevailed during core formation of the Earth because partitioning is dependent on pressure, temperature, oxygen fugacity and the silicate and metal compositions. The liquid metal – liquid silicate partitioning behaviour of the non-volatile elements Ni, Co, Mo and W and the volatile elements Cu, Sn, Sb, Ge, Pb, Ag, Au, P and As has been studied at pressures between 11 and 23 GPa and temperatures of 2342 K to 2911 K by performing partitioning experiments in a multi-anvil apparatus. This work has been primarily focused on volatile elements, because previous studies and therefore core formation models lack data for this group of elements. The silicate starting material of the experiments had a peridotitic composition and the starting Fe-rich metal has been varied by adding S in the case of non-volatile elements and Si or S when investigating volatile element partitioning. This enables the influence of these light elements, that potentially contribute to the Earth´s core density deficit, on the partitioning of siderophile elements to be quantified. The metal, ferropericlase and silicate phases of 104 samples have subsequently been analysed with the electron probe micro-analyser for the first two phases and the laser ablation inductively coupled plasma mass spectrometer in the case of silicate. Subsequently partition and exchange coefficients have been calculated on a molar basis. The partitioning was analysed by employing the ε-approach as formulated by Ma et al. (2001). It was found that over the experimentally investigated pressure and temperature range the partitioning of all elements studied does not change significantly. The addition of Si to the starting metal powder resulted in decreased siderophility for all volatile elements. Since the addition of Si is accompanied by a decrease in oxygen fugacity this implies that for each volatile element studied the interaction of Si with these elements in the metal counteracts the effect of low fO_2 which normally results in increased siderophile behaviour. This shows that reducing conditions in the early stages of core formation do not necessarily result in complete or even strong depletion of siderophile elements when Si is present as a light element in the metal phase. The quantification of the effect of Si on the metal – silicate partitioning of volatile elements furthermore facilitates the identification of the valence states of these elements in the silicate phase. It was found that Cu and Ag are present as 1+ cations, Au and Pb are divalent, Sn and Ge have a valence of 3+ and Sb and As are tetravalent and pentavalent

respectively. The addition of S to the metal phase of the experiments resulted in increased siderophility for the elements Ag, Cu, Pb and Ni and vise versa for all other elements studied. Finally, the parameterization of the metal – silicate partitioning behaviour of all elements – in the case of non-volatile elements including literature - was incorporated into a single stage core formation model, in which oxygen fugacity was set by the present day FeO content of the Earth´s mantle and the temperature was fixed by the peridotitic liquidus at a given pressure after Liebske et al. (2012). For the non-volatile elements it was attempted to match their absolute abundances in the Earth´s mantle or if not possible the ratio between the partition coefficients of two elements. In the case of volatile elements the ratio of the respective mantle abundances of two elements with similar 50% condensation temperature was tried to explain in order to be able to neglect any assumptions about the degree of volatility these elements might have experienced. It was found that increasing pressure facilitates the achievement of the correct relative abundances of Mo/W (29 GPa), Cu/Au (12 GPa), Cu/As (5 GPa) and Sn/Pb (21 GPa). It was furthermore possible to explain the absolute abundances of Ni and Co in the Earth by enormeously high pressures of 126 and 116 GPa respectively. Incorporating the influence of S on the partitioning behaviour of the elements of interest extended the pressure range that can explain the relative abundances of Ni/Co, Cu/Au, Cu/As, and Ag/Sb. In particular it has been found that the solutions for the element pairs Cu/Au and Cu/As intersect at 7 GPa and 4.5 wt% S, Cu/Au and Ag/Sb have the same solution at 2 GPa and 9 wt% S and the trends for Cu/As and Ag/Sb intersect at 9 GPa and 12 wt% S. These results clearly exceed the assumed abundance of around 2 wt % S in the Earth´s core (Dreibus and Palme, 1996), but are not in conflict with the theory of a late S-rich accretionary component as proposed by O´Neill (1991). For each pair of volatile elements (Cu/Au, Cu/As, Ag/Sb and Sn/Pb) a combination of S and Si in the metal prevents their fractionation from one another at various pressures. In particular it was found that S and Si contents of each less than 1 wt % at pressures between 6 and 9 GPa can explain the relative abundances of Cu, Au and As simultaneously. However a unique solution that is capable of explaining even the relative abundances of all elements studied has not been found. In summary a single stage core formation event can be excluded by the results of this study. It seems that increasing pressure and with it increasing temperature, as well as increasing S-contents of the metal facilitate the achievement of the relative mantle abundances of various elements. Best results have been obtained when the effects of Si- and S- metal contents on siderophile element partitioning have been taken into account simultaneously.

Zusammenfassung

Siderophile (Fe-liebende) Elemente sind im Erdmantel verarmt, da sie bei der Differentiation der Erde in den metallischen Kern extrahiert wurden. Das Verteilungsverhalten siderophiler Elemente zwischen Metall und Silikat ist abhängig vom herrschenden Druck, der Temperatur, der Sauerstofffugazität (fO_2) und der Zusammensetzung der Metall- und Silikatphasen und kann deshalb herangezogen werden um die herrschenden Bedingungen bei der Erdkernbildung einzugrenzen. Im Zuge dieser Arbeit wurde das Metall – Silikat Verteilungsverhalten der nicht-volatilen Elemente Ni, Co, Mo und W, sowie der volatilen Elemente Cu, Sn, Sb, Ge, Pb, Ag, Au, P und As experimentell untersucht. Der Schwerpunkt der vorliegenden Arbeit wurde auf die volatilen Elemente gelegt, da es zum jetzigen Zeitpunkt an ausreichenden Literaturdaten mangelt um das Verteilungsverhalten dieser in Kernbildungsmodelle einzubeziehen. Alle Experimente wurden mit mithilfe von Vielstempelpressen in einem Druckbereich zwischen 11 GPa und 23 GPa und Temperaturen zwischen 2342 K und 2911 K durchgeführt. Dabei wurden eine Silikatphase mit peridotitischer Zusammensetzung und ein Fe-reiches Metall equilibriert. Die Zusammensetzung der Metallphase wurde durch unterschiedliche S-Konzentrationen variiert. Im Falle von volatilen Elemente wurden zusätzliche Experimente mit variierender Si-Konzentration in der Metallphase durchgeführt. Beide Elemente (S und Si) könnten, falls im Erdkern vorhanden, dessen geringere Dichte im Vergleich zu einer reinen FeNi-Verbindung erklären. Die Zusammensetzung der experimentell entstandenen Metall- und Ferroperiklasphasen von insgesamt 104 Proben wurden im Anschluss an die Experimente mithilfe einer Elektronenstrahl-Mikrosonde analysiert, wohingegen die Silikatzusammensetzung durch Laserablation-ICP-Massenspektrometrie ermittelt wurde. Basierend auf den molaren Zusammensetzungen der Metall- und Silikatphasen wurden anschließend Verteilungs- und Austauschkoeffizienten berechnet und das Verteilungsverhalten der untersuchten Elemente mithilfe des ε-Models parameterisiert (Ma et al., 2011). Innerhalb des untersuchten Druck- und Temperaturbereichs änderte sich das Verteilungsverhalten der untersuchten Elemente nur geringfügig. Mit steigenden Si-Konzentrationen im Metall ist eine Verringerung der Sauerstofffugazität verbunden, was üblicherweise zu steigender Affinität der siderophilen Elemente für die Metallphase führt. Die Ergebnisse dieser Arbeit zeigen jedoch, dass die Anwesenheit von Si im Metall eine Verringerung der Verteilungskoeffizienten aller untersuchten volatilen Elemente zur Folge

hat. Dies bedeutet, dass bei Anwesenheit von Si im Erdkern reduzierende Bedingungen in den frühen Stadien der Erdkernbildung nicht notwendigerweise zu einer völligen Extrahierung siderophiler Elemente in den Erdkern geführt haben müssen. Durch die Parameterisierung des Einflusses von Si auf das Verteilungsverhalten von siderophilen Elementen konnten zudem deren Oxidationszustände in der Silikatphase ermittelt werden. Die Elemente Cu und Ag bilden einwertige Kationen, Pb und Au zweiwertige, Ge und Sn haben einen Oxidationszustand von 3+, Sb ist vierwertig und As fünfwertig. Die Zugabe von S zur Metallphase führte zu einer Steigerung der Verteilungs- und Austauschkoeffizienten von Ag, Cu, Pb und Ni und einer Verringerung derer aller anderen untersuchten Elemente. Alle Ergebnisse – im Falle von nicht-volatilen Elementen unter Einbeziehung von Literaturdaten - wurden im Zuge eines einstufigen Modells zur Erdkernbildung ausgewertet. In diesem Modell wurde die Sauerstofffugazität durch den heutigen FeO-Gehalt des Erdmantels fixiert und die Temperatur entlang des Peridotit-Liquidus bei gegebenem Druck berechnet (Liebske et al., 2012). Ziel war es die Absolutwerte der Konzentrationen der nicht-volatilen Elemente im Erdmantel oder das Verhältnis zweier Verteilungskoeffizienten zueinander zu modelieren. Im Falle von volatilen Elementen wurde versucht die Verhältnisse der Mantelkonzentrationen zweier Elemente mit annähernd gleicher 50% Kondensationstemperatur zu erzielen, um auf Annahmen über den Grad der Volatilität verzichten zu können. Die Ergebnisse zeigen, dass durch erhöhte Drücke die relativen Verhältnisse jeweils zweier Elemente zueinander erklärt werden können: Mo/W (29 GPa), Cu/Au (12 GPa), Cu/As (5 GPa) und Sn/Pb (21 GPa). Die Absolutwerte von Ni und Co im Erdmantel können durch enorm hohe Drücke von 126 GPa und 116 GPa erreicht werden. Durch den Einfluss von S wird der Druckbereich vergrößert indem die relativen Verhältnisse der Mantelkonzentrationen von Ni/Co, Cu/Au, Cu/As und Ag/Sb erklärt werden können. Das Verhältnis der Mantelkonzentrationen der Elemente Cu/Au, sowie Cu/As kann übereinstimmend bei 7 GPa und einer S-Konzentration im Metall von 4.5 Gew.% erreicht werden, die Elementpaare Cu/Au und Ag/Sb lassen sich bei 2 GPa und 9 Gew.% S erklären und im Falle von Cu/As und Ag/Sb werden 9 GPa und 12 Gew.% S benötigt. Die berechneten S-Konzentrationen übersteigen die geschätze Konzentration von 2 Gew.% S im Erdkern (Dreibus und Palme, 1996), die Ergebnisse stehen jedoch nicht im Widerspruch zur Theorie einer späten Akkretion einer sulphidreichen Phase. (O´Neill, 1991). Für alle volatilen Elementpaare (Cu/Au, Cu/As, Ag/Sb und Sn/Pb) wurde schließlich eine Kombination von Si und S bei unterschiedlichen Drücken ermittelt um die Verhältnisse der Mantelkonzentrationen beider Elemente zu erklären. Im Zuge dessen konnte gezeigt werden, dass S- und Si-Konzentrationen von je weniger als 1 Gew.% in einem Druckbereich von 6 – 9

GPa die relativen Mantelkonzentrationen von Cu, Au und As gleichzeitig erklären können. Eine gemeinsame Lösung zur Erklärung der relativen Verhältnisse aller Elemente konnte jedoch nicht ermittelt werden. Die Ergebnisse dieser Arbeit verdeutlichen, dass ein einstufiger Kernbildungsprozess ausgeschlossen werden kann. Steigende Drücke, sowie erhöhte S-Konzentrationen im Metall erklären die Verhältnisse einiger Elemente zueinander. Die besten Ergebnisse wurden jedoch durch den kombinierten Einfluss von Si und S auf das Metall – Silikat Verteilungsverhalten der siderophilen Elemente erzielt.

1. Introduction

1.1 Solar System evolution

The evolution of the Solar System began 4.567 billion years ago with the collapse of the Solar Nebula, the latter being one of many denser parts of a giant molecular cloud (Amelin et al., 2002; Weissman, 2007; Halliday and Chambers, 2007). According to Faure and Mensing (2007) the Solar Nebula consisted of gas and dust, mainly H and He atoms, but also contained all other chemical elements – the remnants of exploded Red Giant Stars. The dust particles amount to 2 % (by mass) of the collapsing matter and are composed of different interstellar grains like silicates, organics and condensed ices (Weissman, 2007). Initially triggered by an external source, the Solar Nebula contracted due to gravitational forces. The deaths of neighbouring red giant stars and the corresponding shockwaves or the pressure of photons radiated by other stars, as well as fortuitous movements of atoms and particles are considered to initiate the collapse (Faure and Mensing, 2007). Material of the collapsing nebula forms a rotating disk around a protostar continuously transporting mass into its center. This episode proceeds until hydrogen burning becomes possible and solar winds start to remove the remaining gas. Around 10^5 – 10^6 years are estimated to have elapsed until this stage of Solar System formation (Taylor, 2001).

The removal of gas by solar winds towards the outer and cooler regions of the disk was followed by the condensation of ices beyond the Snow Line at a distance around 5 AU (astronomical units) from the sun (Taylor, 2001; Taylor and McLennan, 2009). Due to the increasing density in this region the outer giant planets grew rapidly, forming from masses of ices and dust. Their early development facilitated the capture of gases (H and He) prior to the dispersion of the Solar Nebula gas. Following the growth of the outer giant planets, the inner terrestrial planets began to develop from dry rocky refractory material. In contrast to the rapid formation of the giant planets (timescale of 10^5 years), the accretion of the two largest inner planets, Earth and Venus, took around 10 to 100 Million years (Taylor and McLennan; 2009).

The growth of the terrestrial planets is dominated by gravitational attraction as soon as building blocks of 1 to 10 km in diameter have formed (Wetherill, 1989). Prior to this stage agglomeration of dust grains was induced by electrostatic forces. Furthermore it can be shown that collisions at low velocities (tens of m/s) are sufficient to result in adherence. With

increasing aggregation size however the possibility of fragmentation during collisions rises. At this point an incorporation mechanism of smaller objects into larger ones at velocities of more than 10 m/s becomes important (Halliday and Chambers, 2007). Further growth of kilometer-sized objects – now known as planetesimals – is then mainly driven by mutual gravitational interactions. The term "runaway growth" describes the fact that larger planetesimals will grow faster at the expense of smaller surrounding objects due to their greater gravitational influence (Chambers, 2004). As a result tens to hundreds of lunar- to Mars-sized embryos formed (Weidenschilling, 2000). According to Chambers (2004) it took approximately 0.1 – 1 million years to create only a few tens of these embryos. A late stage of planetary evolution then involves growth of the largest embryos, now called protoplanets, and is termed "oligarchic growth" (Thommes et al., 2003). At this point giant impacts occur when mutual gravitational influences of similarly sized bodies result in crossing orbits (Rubie et al., 2007). The late stages of planetary accretion are often modeled by N-body simulations in the course of which Raymond et al. (2004) showed that the development of the inner planets by oligarchic growth needs ~ 10^8 year.

It is now generally accepted by most scientists that the Earth´s Moon originated from a giant impact of a Mars-sized body with the Earth. This collision resulted in a protolunar disk from which the Moon quickly accumulated (Canup, 2012; Ćuk and Stewart, 2012; Geiss and Rossi, 2013). The latter authors report that the conversion of gravitational energy into heat during lunar accretion was sufficient to cause global melting. Subsequent cooling consequently led to the formation of an anorthositic crust and a mafic mantle on the Moon when gravitational segregation occurred (Geiss and Rossi, 2013).

Figure 1 shows a schematic picture of the Solar System that eventually emerged from the mechanisms described above. Here the relative sizes of all bodies are displayed, whereas distances are not correctly shown (modified after Brown and Mussett, 1981).

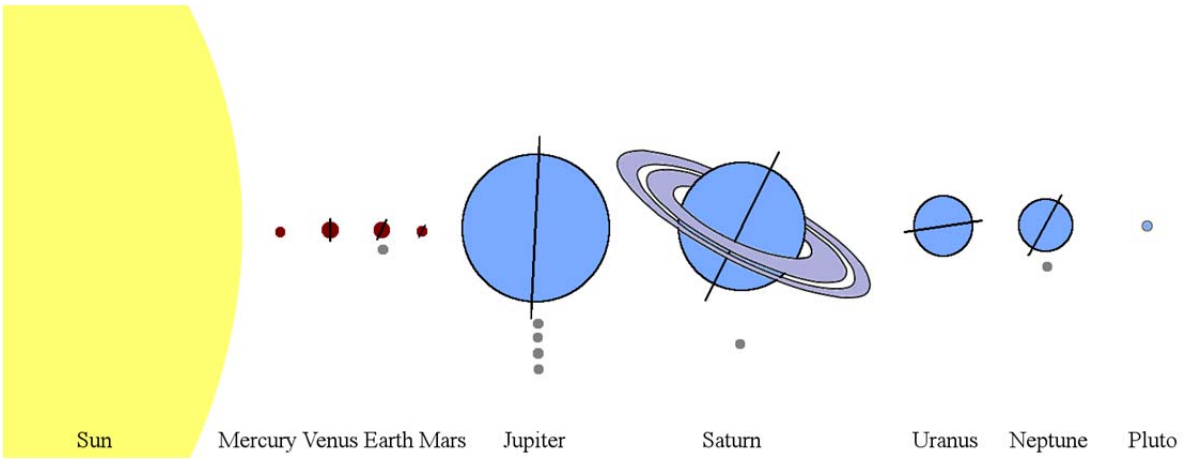

Figure 1: *Schematic picture of the Solar System. Mechanisms that lead to its formation are described in the text. The relative sizes are displayed correctly, whereas this is not the case for the distances between the objects. One should note that that according to the Resolutions B5 and B6 adopted by the International Astronomical Union (IAU) in 2006 "Pluto" is no longer recognized as a planet, but called a "dwarf planet". (modified after Brown and Mussett, 1981)*

At the time of accretion the terrestrial planets underwent differentiation, this means core formation occurred separating the silicate mantle from a Fe-rich core (Stevenson, 1981; Rushmer et al., 2000; Rubie et al., 2007). The mechanisms of differentiation are discussed in Section 1.3 Segregation Mechanisms.

1.2 Thermal evolution

It is crucial to understand the thermal evolution of the Earth, because core formation, in particular the segregation of metal from silicate, requires high temperatures, which may facilitate the development of a global magma ocean, or at least lead to partial melting. Furthermore heating in small bodies (e.g. planetesimals) needs to be considered, because it constrains whether the accreting material was already differentiated. The main heat sources are thought to be radioactive decay of short lived radioactive nuclides, energy that was delivered by giant impacts and finally the conversion of gravitational energy into heat induced by the segregation of metal from a silicate mantle (Rubie et al. 2007).

It has been shown, that collisions between asteroids with sizes of less than a few hundred kilometers in diameter are insufficient to cause global melting (Keil, 1997). Instead the decay of ^{26}Al and ^{60}Fe with half lives of 0.73 x 10^6 and 1.5 x 10^6 years respectively (Rubie et al., 2007) can increase the temperatures in smaller bodies up to 1000 °C or more that means above the Fe-FeS eutectic melting point. Thus the Earth might have accreted from already differentiated objects (Yoshino et al., 2003). The melting of small bodies induced by radioactive decay must have taken place in the very early stages of Solar System formation, probably within 1 million years (Baker et al., 2005). However the evidence of undifferentiated asteroids such as Ceres (Thomas et al., 2005) questions whether a mixture of differentiated and undifferentiated objects might have contributed to the Earth´s accretion (Rubie et al., 2007).

The late stages of accretion involved giant impacts that resulted in the formation of one or several global magma oceans (Rubie et al., 2007; Tonks and Melosh, 1993; Melosh, 1990; Benz and Cameron, 1990). It has been shown that the impact that probably led to the formation of the Earth´s Moon was able to cause melting of the entire Earth (Cameron, 2000; Canup and Asphaug, 2001). One should note that even the latter scenario is characterized by temperature gradients with the region close to the impact exhibiting the highest temperatures. Yet average temperatures reach values of several thousand K (Rubie et al., 2007).

The mechanisms of metal – silicate segregation on Earth will be discussed in detail in Section 1.3. However independent of the kind of segregation (e.g percolation or dyking) descending iron is always associated with the conversion of gravitational potential energy into heat. This causes an increase in core temperatures of hundreds up to a few thousand K (Rubie et al., 2007).

1.3 Segregation mechanisms

The formation of the Earth´s iron-rich metallic core results from the segregation of metal from the silicate mantle. Metal tends to separate from silicate due to the density contrast. Possible segregation mechanisms involve percolation, the separation of molten metal from molten silicate in a magma ocean and the processes of diapirism and dyking. The mechanisms

of metal – silicate segregation depend on the physical state of the early Earth, are visualized in Figure 2 (Rubie et al, 2007) and are discussed in detail further below.

However although metal – silicate segregation in a magma ocean is believed to be very efficient (Righter, 2005) it has been proposed that core formation might have been partially inefficient with some metal remaining in the silicate mantle (Rubie et al., 2007; Jones and Drake, 1986). It has furthermore been proposed that metal might have been added back from the core to the mantle, what could significantly influence the highly siderophile element abundances in the Earth´s mantle as discussed by Walker (2000), Brandon and Walker (2005) and Rubie et al. (2007).

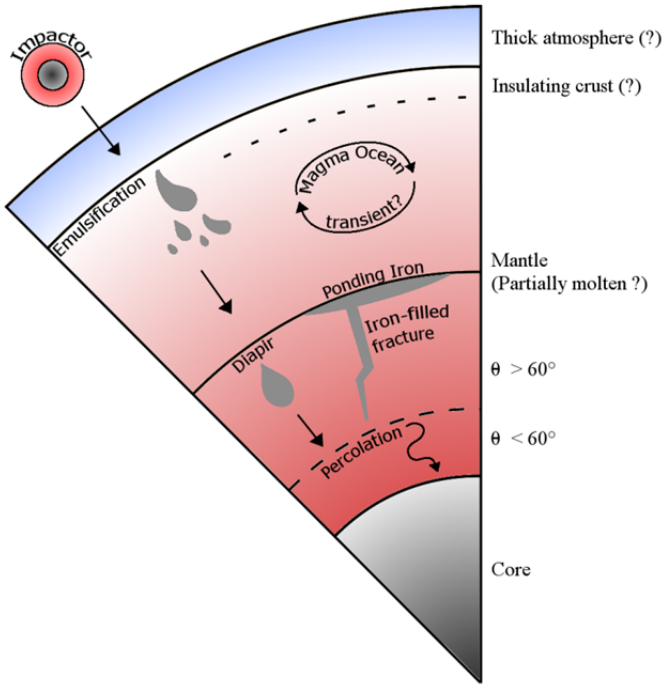

Figure 2: *Schematic image showing possible mechanisms of metal - silicate segregation during core formation. The base of the magma ocean is defined at a melt fraction of 60 % (Solomatov, 2000). Θ represents the dihedral (or wetting angle) in polycrystalline aggregates, which needs to be < 60° for efficient percolation to occur (von Bargen and Waff, 1986). For further details see text. (modified after Rubie et al., 2007)*

1.3.1 Percolation

Liquid metal can percolate through a mantle made of polycrystalline silicates by porous flow as long as the liquid is interconnected. The constraint on interconnection depends on the dihedral angle θ, which is defined as the angle of a liquid in contact with two solid grains (Rushmer et al., 2000). If the dihedral or wetting angle is less than 60° the liquid forms a network along the grain edges, whereas dihedral angles above 60° will lead to isolated melt pockets until a critical melt fraction is achieved (von Bargen and Waff, 1986). The critical melt fraction or "connection boundary" lies at 2 – 6 % when dihedral angles vary between 60 – 85°. Higher melt fractions enable sufficient percolation, but if the melt fraction drops to a certain value below the critical melt fraction, the rest of the liquid ends up stranded in the silicate mantle. Since the dihedral angle was found to exceed 60° in a typical core formation regime (Shannon and Agee, 1996 and 1998), percolation can be excluded as an efficient process for metal-silicate segregation, because the amount of stranded metal in the silicate mantle is inconsistent with the concentration of siderophile elements in the mantle (Rubie et al. 2011).

1.3.2 Metal – Silicate separation in a magma ocean

It has been shown that isostatic adjustment can lead to the development of a global magma ocean with a uniform depth after a giant impact (Tonks and Melosh, 1993). The base of the magma ocean can be defined at a melt fraction of 60 % and the time span until solidification is estimated to be only 10^3 years when neither a thick atmosphere nor an insulating crust delays cooling (Solomatov, 2000; Pritchard and Stevenson, 2000). The development of a thick atmosphere and/or an insulating lid can prolong magma ocean lifetimes to 10^7 to 10^8 years respectively (Spohn and Schubert, 1991 and Abe, 1997, respectively).

It has been proposed that equilibration between the core forming metal and the silicate mantle involves a metal layer that ponded at the base of a magma ocean (Righter et al., 1997; Solomotov, 2000). In contrast it has been argued that metal droplets equilibrate with the mantle while sinking through the magma ocean (Stevenson, 1990; Rushmer et al., 2000; Rubie et al., 2003). In particular the results of Rubie et al. (2003) showed that the first mechanism, equilibration between a ponded metal layer with the overlying silicate mantle, is

not capable of achieving chemical equilibrium between metal and silicate because equilibration timescales exceed the time span estimated for magma ocean cooling by some orders of magnitude. The latter authors found that accreting metal can emulsify to a stable droplet size of about 1 cm. Their settling velocities have been estimated to be 0.5 m s^{-1}. It should be noted that the convection velocity of a magma ocean is on the order of a few meters per second, thus leading to longer settling times for the metal droplets. The break up into stable metal droplets takes place at very short settling distances, most likely only a few times of the original size of the body. Therefore even the largest impacting bodies must exhibit a high degree of emulsification. This process is capable of allowing chemical equilibration between the metal and the silicate. However according to Rubie et al. (2003) the equilibration of metal droplets with the surrounding mantle depends significantly on the dynamics of the magma ocean properties such as convection and mixing.

Based on fluid dynamical models of turbulent mixing, Dahl and Stevenson (2010) showed that Rayleigh-Taylor instabilities can cause emulsification of Fe metal enabling siderophile elements to chemically equilibrate. However these authors found that impacting cores with sizes > 10 km do not disaggregate completely, because of which the last giant impact, that formed the Earth´s Moon, did not result in in complete re-equilibration. Dahl and Stevenson (2010) conclude that Hf-W chronometry (see Section 1.4) probably does not constrain the timing of the last giant impact, since the abundances of both elements in the Earth´s mantle are established by earlier core formation processes.

Partial disequilibrium is also considered by Nimmo et al. (2010) who combined N-body simulations with a Hf-W evolution model. They proposed that the Earth´s Hf-W characteristics can be explained if each impactor partly re-equilibrates with the Earth´s mantle to an extent between 30 and 80 %.

Similar to the results of Rubie et al. (2003), Samuel (2012) showed on the basis of numerical investigations and theoretical calculations that metal, that sinks through a magma ocean, breaks up until it reaches a stable droplet size of 0.2 m. In contrast to the results of Dahl and Stevenson (2010), Samuel (2012) predicts that only in the case of Fe bodies with sizes exceeding the thickness of the magma ocean are emulsification and re-equilibration hindered.

Recently also Deguen et al. (2014) found that Fe metal undergoes fragmentation when falling through a magma ocean, but the authors showed that this process is not essential for metal – silicate equilibration. Instead equilibration could be achieved prior to the metal break

up by turbulent mixing in a magma ocean at least for impactors with core diameters less than the magma ocean thickness.

1.3.3 Diapirism and dyking

Metal that accumulates at the base of a magma ocean can further sink towards the center of the Earth by forming large diapirs with this process being triggered by gravitational instabilities (Karato and Murthy, 1997).

The transport of molten metal through fractures in the surrounding host-material, termed dyking, is also capable of efficiently separating Fe from a silicate mantle (Rubin, 1995; Rubie et al., 2007).

However in contrast to the processes of emulsification and percolation, the descent of metal bodies via diapirs (> 1 - 10 km) or by dykes does not facilitate chemical equilibrium of the metal with the bulk of the surrounding silicate, i.e. with the lower mantle (Karato and Murthy, 1997; Rubie et al., 2007).

1.4 Constraints on the timing of core formation

Constraints on the timescales of core formation can be obtained by employing the Hf-W radioactive series. The mode of operation of the Hf-W chronometer has been summarized by Rubie et al. (2007). The major characteristics are the siderophile behaviour of W compared to the lithophile element Hf. The radioactive isotope ^{182}Hf decays to the stable isotope ^{182}W with a half-life of only 9 million years. Early core formation, prior to the entire decay of ^{182}Hf, will thus enrich the Earth´s mantle in the stable isotope ^{182}W due to ongoing decay processes, whereas late core formation will extract the siderophile decay product ^{182}W into the Earth´s core, leaving a W-depleted mantle.

Employing the Hf-W chronometer together with comparisons between the terrestrial radiogenic W-isotope composition and chondrites leads to the conclusion that core formation, here treated as a single stage event, was terminated after 30 million years (Jacobsen, 2005).

A major advantage of the Hf-W chronometer is that both elements are refractory. In contrast to other dating systems like U-Pb and Pd-Ag a volatility related loss of elements during accretion does not have to be considered (Rubie et al. 2007).

However, latest investigations have shown that the Hf-W chronometer depends on the degree of equilibration between the Earth´s mantle and core, as well as on the timing of core formation. On this account Rudge et al. (2010) estimated that at least 36 % of the terrestrial core was developed in equilibrium with the Earth´s mantle.

The siderophile behaviour of W is dependent on the conditions that prevailed during core formation, namely pressure, temperature, oxygen fugacity and composition. Moreover these conditions might have varied over the period of accretion (Halliday, 2004). For this reason it is necessary to precisely determine the partitioning behaviour of W as has been attempted, for example, by Cottrell (2009 and 2010) and Wade et al. (2012).

1.5 The late veneer hypothesis

Many scientists favor the idea of a late accretionary event, called the “late veneer” in the course of which ~ 1 % of the Earth´s mass was delivered by small leftover planetesimals after the giant impact stage (Kimura, 1974; Chou, 1978; Albarède, 2009; Palme and O´Neill, 2003; Mann et al., 2012; Rubie et al., 2007).

A major justification of the late veneer hypothesis is that it explains the abundances of highly siderophile elements in the Earth´s mantle and moreover their presence in chondritic relative proportions provided the accreting matter was either Fe-free or became oxidized after the impact, so that metal segregation and with it the extraction of highly siderophile elements into the Earth´s core was prohibited (Palme and O´Neill, 2003 and 2014). In this way Holzheid et al. (2000) were able to explain the upper mantle abundances of Pd and Pt by the addition of chondritic material after core formation was ceased. In addition also the results of

Mann et al. (2012) are in accordance with the constraint of a late chondritic veneer that led to an overprint of the HSE abundance pattern.

However the amount and type of the late accreting material as well as the diameters of the impactors are still under discussion: While some studies still doubt the necessity of a late accretionary component (Snow and Schmidt, 1998), other studies attempt to precisely characterize and quantify the impacting material. Where Javoy (1997) suggests the addition of CI compositional material, it has been proposed by O´Neill (1991) that both, the Earth and the Moon, were hit by reduced chondritic material – most likely H-group ordinary chondrites. Moreover it has been shown by Drake and Righter (2002) that water-bearing carbonaceous chondrites are inconsistent with the observed $^{187}Os/^{188}Os$ ratio of the primitive upper mantle. Instead they also consider anhydrous ordinary chondrites.

Schlichting et al. (2012) suggest that the late veneer mainly consisted of small residual, undifferentiated planetesimals of chondritic composition with radii less than 10 m beside a minority of larger planetesimals and that the late accretion delivered 1 % of the Earth´s total mass. On the other hand latest publications suggest a late accretionary stage which involved impactors with diameters of up to 4000 km (Bottke et al., 2010; Raymond et al., 2013).

1.6 Geochemistry

1.6.1 Geochemical classification of the elements after Goldschmidt

According to their geochemical affinities elements can be grouped into lithophile, chalcophile, siderophile and atmophile elements (Goldschmidt, 1937).

Siderophile elements are iron-loving elements. With respect to core formation processes this means that these elements partition preferentially into the metal phase and as a result are extracted from the Earth´s silicate mantle into the core. Lithophile elements in contrast are incorporated into the silicates of the Earth´s mantle and have thus not been depleted by core formation processes. Chalcophile elements will preferentially be enriched in sulphides, whereas atmophile elements are concentrated in the Earth´s atmosphere (Goldschmidt, 1937; Palme and O´Neill, 2003 and 2014).

However several elements do not exclusively belong to one of the above mentioned groups. Instead they show secondary affinities. The classification of elements into siderophile, lithophile, chalcophile and atmophile can be read from Figure 3 (modified after Faure, 1998), secondary affinities are additionally displayed (underlined elements).

H																	He
Li	Be											B	C	N	O	F	Ne
Na	Mg											Al	Si	P	S	Cl	Ar
K	Ca	Sc	Ti	V	Cr	Mn	Fe	Co	Ni	Cu	Zn	Ga	Ge	As	Se	Br	Kr
Rb	Sr	Y	Zr	Nb	Mo	Tc	Ru	Rh	Pd	Ag	Cd	In	Sn	Sb	Te	I	Xe
Cs	Ba	La-Lu	Hf	Ta	W	Re	Os	Ir	Pt	Au	Hg	Tl	Pb	Bi	Po	At	Rn
Fr	Ra	Ac-Lr	Rf	Db	Sg	Bh	Hs	Mt	Uun	Uuu	Uub		Uuq				

La	Ce	Pr	Nd	Pm	Sm	Eu	Gd	Tb	Dy	Ho	Er	Tm	Yb	Lu
Ac	Th	Pa	U	Np	Pu	Am	Cm	Bk	Cf	Es	Fm	Md	No	Lr

Geochemical Character
siderophile
chalcophile
lithophile
atmophile

*Secondary affinity
W, As, Pb
Ge, Sn, Cr, Fe, Mo
C, Ga, Ge, Tl, Fe, H
C, O

Figure 3: *The periodic system of the elements showing their geochemical characters. Underlined elements exhibit secondary affinites. The element P tends to be siderophile as well as lithophile. (modified after Faure, 1998)*

Siderophile elements that are the subject of this study can furthermore be divided into moderately siderophile and highly siderophile elements having partition coefficients $D^{met-sil}$ of less and more than 10^4 at 1 bar respectively. The boundary between lithophile and siderophile behavior is defined as $D^{met\text{-}sil} = 1$ (Rubie et al., 2007).

1.6.2 Volatile and refractory elements

Elements can furthermore be divided into volatile and refractory elements that exhibit lower and higher condensation temperatures than the three most abundant elements in terrestrial rocks, Mg, Si and Fe, respectively (Lodders, 2003).

The depletions of siderophile elements in the Earth´s mantle can be recognized in a diagram of their silicate Earth values, normalized to CI chondrite composition and the refractory element Ti (Palme and O´Neill, 2003) (Figure 4), plotted against their 50 % condensation temperatures (Lodders, 2003 or Wasson, 1985). At these temperatures the individual elements are one half each in the gas and in the condensate phase (Lodders, 2003). The volatility trend, defined by lithophile elements, is one reason for low element abundances in the Earth´s mantle, but additionally depletions due to siderophile behaviour, coming along with extraction into the metallic core, have to be considered. For example it has been shown by Rubie et al. (2010) that Cu does not simply follow the observed volatility trend but must be additionally affected by core formation processes.

A broad estimation of 50 % condensation temperatures has been published by Lodders (2003). The values have been computed simultaneously, taking into account that major elements might control minor element condensations. Total, partial and vapor pressures as well as elemental distributions between gases and condensates were employed as constraining parameters (Lodders, 2003). A total pressure of 10^{-4} bars was adopted for all calculations since it represents the likely pressure in the Solar Nebula at a distance of 1 AU (Lodders, 2003 and Fegley, 2000).

The classification of volatile elements into moderately volatile, volatile and highly volatile elements used in this study is from Lodders (2003). Moderately volatile elements exhibit 50 % condensation temperatures from 1290 to 704 K prior to the condensation of FeS. Volatile elements have 50 % condensation temperatures of 704 to 371 K that marks the boundary with the highly volatile elements. Lodders (2003) defines a group of “common elements”, namely Mg, Si, Fe, Co, Cr, Ni, Pd and Eu with 50 % condensation temperatures between 1360 and 1290 K that separates volatile elements from refractory elements. The refractory element group, exhibiting 50 % condensation temperatures above 1360 K is furthermore sub-divided, but this has been neglected in this study for simplification.

An older estimate of 50 % condensation temperatures was published by Wasson (1985). The determined values are generally in good agreement with the data given by Lodders

(2003). However, a major difference is found for the volatile element Pb. Lodders (2003) determined a 50 % condensation temperature of 727 K for Pb, whereas Wasson (1985) reports a temperature of only 496 K at a total pressure of 10^{-5} bar, thus leading to a discrepancy of 231 K (Figure 5). It is necessary to note that all conclusions that are based on the partitioning behaviour of Pb in this study are based on the values given by Lodders (2003). This in particular corresponds to the assumption of Sn and Pb being depleted to the same extent in the Earth´s mantle independent of the volatility trend.

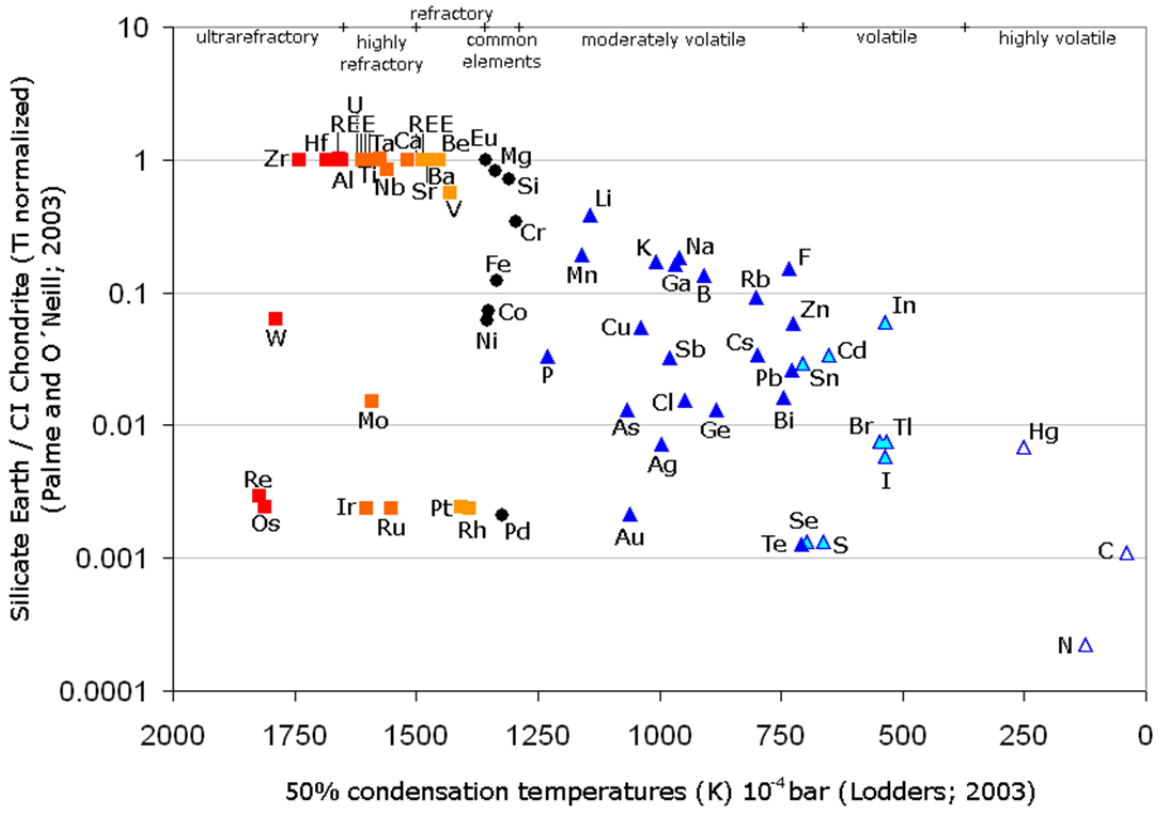

Figure 4: *Depletion diagram: Element abundances of the Earth´s mantle normalized to CI chondrites and the refractory element Ti (data after Palme and O´Neill, 2003) plotted against their 50 % condensation temperatures given by Lodders (2003). The distinction between volatile and refractory elements was adopted from Lodders (2003). Elements are depleted in the Earth´s mantle due to their volatility. However additional depletions due to siderophile behaviour and thus extraction of elements into the Earth´s core can be observed (Rubie et al., 2010).*

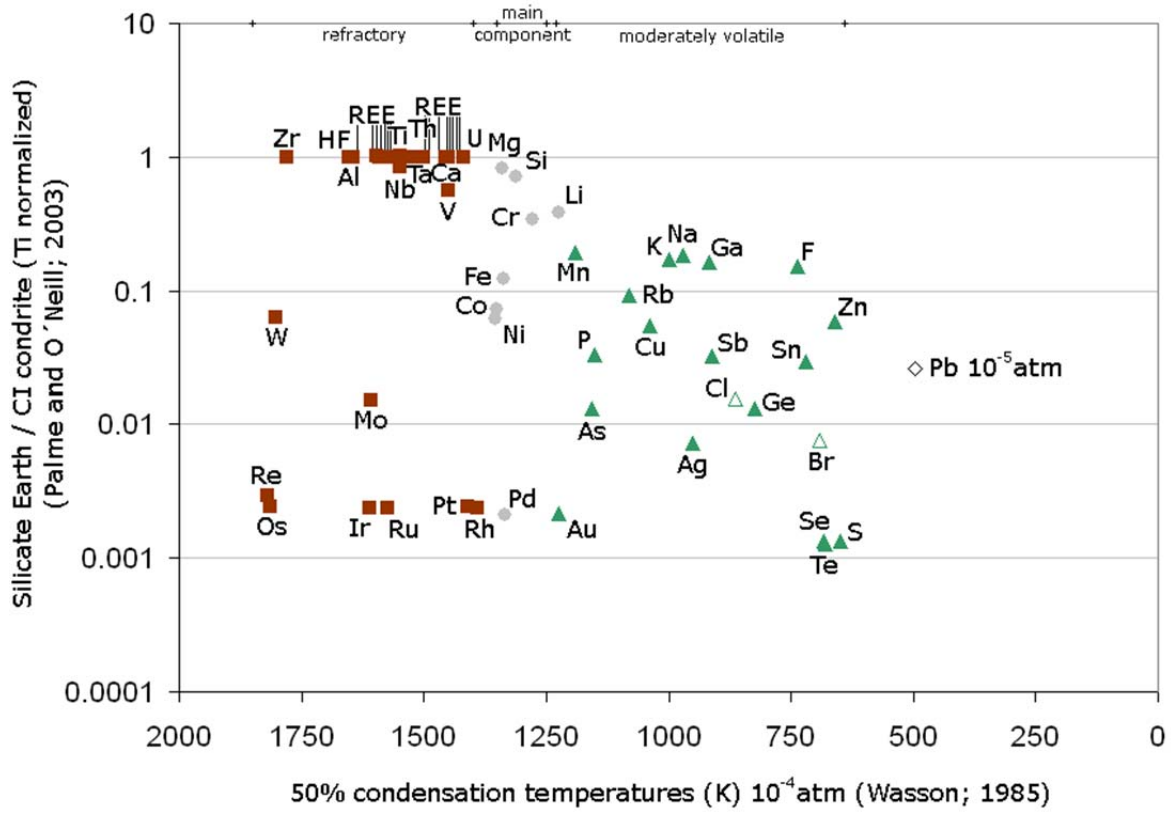

Figure 5: *Depletion diagram: Element abundances of the Earth´s mantle normalized to CI chondrites and the refractory element Ti (data after Palme and O´Neill, 2003) plotted against their 50 % condensation temperatures given by Wasson (1985). The 50 % condensation temperatures are very similar to those obtained by Lodders (2003) except for Pb. Its 50 % condensation temperature differs by 231 K compared to the value given by Lodders (2003). All conclusions in this study concerning Pb are based on the value given by Lodders (2003).*

Volatile elements are depleted in the Earth´s mantle most probably because they failed to condense at high temperatures in the inner part of the Solar Nebula, independent of their geochemical character and of geochemical processes (Palme and O´Neill, 2003 and 2014). Evidence against evaporation of formerly undepleted volatile elements in the Earth has been provided by Palme et al. (1988) who showed that recondensation would elsewhere lead to enrichments which have never been observed. Moreover Humayun and Cassen (2000) and Nebel et al. (2011) pointed out that isotopic fractionations, which are related to local volatilization processes, have not been discovered in samples from the Earth and meteorites.

1.7 Light elements in the core

The Earth´s core is generally considered to consist of Fe-Ni alloys, but it has been found that the outer core especially requires the admixture of one or more light elements, since its density is 5 to 10 % too low to consist only of Fe and Ni (e.g. Birch, 1952; Anderson and Issak, 2002). Additionally it has been suggested by Jephcoat and Olson (1987), that some light elements also must be present in the inner core, accounting for a density deficit that has been quantified as 2 – 3 % by Alfe et al. (2002).

Light elements, dissolved in liquid Fe, are known to influence the metal – silicate partitioning behaviour of siderophile elements (e.g. Li and Agee, 2001; Mann et al., 2009; Tuff et al., 2011; Wade et al., 2012; Buono et al., 2013). The knowledge of the composition of the Earth´s core is important, because it constrains not only the conditions that prevailed during core formation by influencing the metal-silicate partitioning behavior of siderophile elements, but also the Earth´s bulk composition (Rubie et al., 2007) and structure and dynamics of the Earth´s core (e.g. Helffrich and Kaneshima, 2004; Buffett and Seagle, 2010). Still questions remain about the number of and which elements come into question, as has been investigated by several authors.

Poirier (1994) argued that not one but several light elements contribute to the density deficit of the Earth´s outer core and he justified the presence of Si, S, O, H and C. Graphite and P are likely present, but only in minor concentrations. McDonough and Sun (1995) proposed 0.5 wt% P, while according to McDonough (2003) the amount of C and P each do not exceed 0.2 wt%. Zhang and Yin (2012) determined a similar value for C of 0.1 to 0.7 wt%. Several studies have concluded that the Earth´s core S-content does not exceed 1.7 - 1.9 wt% (Dreibus and Palme, 1996; McDonough, 2003).

It has been suggested by several authors that the outer core might contain large proportions of FeO (Ringwood, 1997; Ohtani and Ringwood, 1984; Ohtani et al., 1984). Later on both Rubie et al. (2004) and Asahara et al. (2007) yielded estimates of 7 - 8 wt% O indicating that O might be the main light element present in the core. Slightly lower values of 6 wt% have been obtained by Frost et al. (2010).

A study of isotopic fractionations of Si leads to a contribution of 6 wt% Si in the core (Ziegler et al. 2010). This is in good agreement with a determination of Si partitioning into the core that leads to a value of 7 wt% (Gessmann et al. 2001). The latter investigation was based on Si solubilities in liquid Fe-rich metal at pressures up to 23 GPa. Similar results, although

based on the idea that core equilibration took place in a low pressure regime, have earlier been obtained by Allegre et al. (1995), who predicted a contribution of 7.3 wt% Si and additionally a contribution of O by around 4 wt% to account for the density deficit.

By performing ab initio calculations of densities and chemical potentials of Si, O and S and taking into account seismic observations Alfe et al. (2002) have predicted that the Earth´s liquid outer core must contain 8.0 mole% O together with a combined amount of the light elements Si and S of 10 mole%. The high abundance of O in the liquid outer core is explained by its strong partitioning from solid to liquid Fe metal. The comparatively small size of O atoms causes its presence in solid metal to be less stable than in the liquid metal phase. According to Alfe et al. (2002) the Earth´s solid inner core accommodates only 0.2 mole% O but 8.5 mole% of Si + S.

On the basis of sound velocity measurements in alloys of Fe and either Si, O or S Badro et al. (2007) found that the Earth´s inner core contains 2.3 wt% Si and only 0.1 wt% O, whereas the presence of 5.3 wt% O and 2.8 wt% Si could account for the outer core´s density deficit.

However, the simultaneous contributions of O and Si to the light element budget of the Earth´s metallic core was for a long time thought to be mutually exclusive, because Si was found to be incorporated into metal at low oxygen fugacity (Rubie et al., 2007; Li and Fei, 2003, Kilburn and Wood, 1997; O´Neill, 1998; Hillgren, 2000). This point of view changed as soon as pressure and in particular temperature effects on the partitioning behaviour of these elements were taken into account.

Takafuji et al. (2005) recommended a combined contribution of 3 wt% O and 6 wt% Si at 135 GPa and 3500 K that can account for a density deficit of 7 %. Sakai et al. (2006) determined a possible incorporation into metallic iron of 6.3 wt% O and 4.0 wt% Si at 139 GPa and 3000 K. According to these studies high pressures and temperatures enable the incorporation of both elements into liquid iron, which has been verified recently by Tsuno et al. (2013).

To date the main element that causes the reduced density of the Earth´s core seems to be Si. Latest investigations quantified the light element budget of the Earth´s core to 8 wt% Si, 2 wt% S and 0.5 wt% O (Rubie et al., 2011), or 6 wt% Si and 1.3 wt% O (Siebert et al., 2013) .

1.8 Metal – silicate partitioning of elements

As will be shown in detail in Chapters 4 – 6 the liquid metal – liquid silicate partitioning behaviour of an element *M* potentially depends on temperature, pressure, oxygen fugacity and composition of both metal and silicate phases (e.g. Li and Agee, 1996; Kegler et al., 2008; Wood et al., 2008; Mann et al., 2009 and 2012; Cottrell et al., 2009 and 2010; Righter, 2010; Wood and Halliday, 2010; Wade at al., 2012; Siebert et al., 2013; Ballhaus et al., 2013).

Partitioning can be expressed by a metal – silicate partition coefficient $D^{met\text{-}sil}$ that is defined as the ratio of the abundance of an element of interest *M* in the metal phase over its amount in the silicate phase (equation 1).

$$D^{met-sil} = \frac{X_M^{met}}{X_{MO\frac{n}{2}}^{sil}} \quad [1]$$

For its determination, molar values have been employed in this study, whereas other investigations have been based on the mass ratio of the elements of interest. The concentrations of the elements of interest *M* in the metal phase have been calculated as pure elemental molar abundances, whereas the concentrations in the silicate phase have been computed as molar oxide values.

Another way of describing the partitioning behaviour of any element *M* is the formulation of an exchange coefficient K_D^{M-Fe} that can be understood as the normalization of the partition coefficient $D^{met\text{-}sil}$ to the partition coefficient of Fe with respect to the valence state *n* of the element of interest *M* (equation 2). Its advantage is that it is independent of oxygen fugacity.

$$K_D^{M-Fe} = \frac{D_M^{met-sil}}{\left(D_{Fe}^{met-sil}\right)^{\frac{n}{2}}} \quad [2]$$

The quantification of pressure, temperature, compositional and oxygen fugacity dependences together with present day abundances of elements in the Earth´s mantle and core provides information on the conditions that must have prevailed during core formation. In

particular it has been found that low pressure – moderate temperature conditions, based on partitioning experiments at 1 bar and 1200 °C – 1500 °C, cannot explain the abundances of a wide range of elements in the Earth´s mantle. The significant overabundance of these elements has been termed the "excess siderophile element problem". Figure 6 demonstrates the depletion of siderophile elements in the Earth´s mantle due to core formation, where red squares indicate refractory elements and blue triangles correspond to volatile elements. Green circles reflect the results that have been obtained from low pressure and temperature partitioning experiments of siderophile elements (Walter et al., 2000).

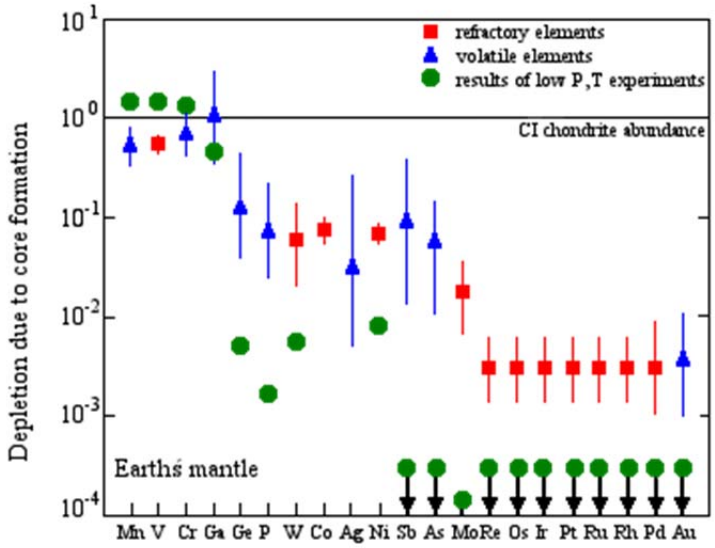

Figure 6: *Depiction of the "excess siderophile element problem". The depletion of siderophile elements in the Earth´s mantle due to core formation is shown. Red squares indicate refractory elements, whereas blue triangles denote volatile elements. Green circles indicate the results of low pressure – moderately temperature partitioning experiments. (modified after Walter et al., 2000)*

A major step in understanding the "excess siderophile element problem" was made by Li and Agee (1996), who showed that the partition coefficients of Ni and Co, two elements that are depleted by about the same amount in the Earth´s mantle, differ by around one order of magnitude at low pressures but converge with increasing pressures, and furthermore become consistent with Earth´s mantle abundances. The partitioning experiments of Li and Agee (1996) indicated a single stage core formation event at a pressure of 28 GPa, corresponding to a magma ocean of 750 to 1100 km depth. Afterwards the partitioning behaviour of Ni and Co

has been refined (e.g. Kegler et al., 2008) and together with investigations of the partitioning behaviour or solubilities of other siderophile elements a wide range of possible pressure and temperature conditions has been published, as summarized in Table 1 (modified after Rubie et al., 2007 and 2015).

Table 1: *Summary of conditions that could have prevailed during core formation. The results are based on partitioning or solubility studies of siderophile elements and refer to single stage core formation scenarios or to averaged conditions during core formation. (modified after Rubie et al., 2007 and 2015)*

P (Gpa)	T (K)	Elements employed for investigations	References
28	2400 – 2700	Ni, Co	Li and Agee (1996)
27	2200	Ni, Co, P, Mo, W	Righter et al. (1997)
37	2260	Ni, Co, Fe	O´Neill et al. (1998)
37	3360	Cr	O´Neill et al. (1998)
> 35	> 3600	V, Cr, Mn	Gessmann and Rubie (2000)
43 – 59	2400 – 4200	Ni, Co	Li and Agee (2001)
25	3350	Si	Gessmann et al. (2001)
27	2250	P, W, Co, Ni, Mo, Re, Ga, Sn, Cu	Righter and Drake (2003)
40	2800	Ni, Co	Walter and Tronnes (2004)
40	3750	V, Ni, Co, Mn, Si	Wade and Wood (2005)
30 – 60	> 2000	Ni, Co	Chabot et al. (2005)
10 – 40	-	Nb, V	Mann et al. (2009)
30 - 60	-	Ga, Mn, In, Zn	Mann et al. (2009)
22.5	2673	Mo, P	Righter et al. (2010)
27 - 33	3300 - 3600	Mn, V, Cr, Ni, Co, Mo, W, P, Cu, Ga, Pd	Righter (2011)

One should note that these proposed conditions refer mainly to single stage core formation scenarios, i.e. assuming equilibration of core and mantle at a single pressure, temperature and oxygen fugacity. However it has been argued that the siderophile element abundances in the Earth´s mantle cannot be explained within the framework of single stage core formation (Rubie et al., 2011). Instead multi-stage or continuous core formation scenarios with changing pressure, temperature and oxygen fugacity conditions should be considered.

1.9 Core formation models

The idea of a single stage core formation scenario including a magma ocean with a defined depth is unlikely to be realistic. Instead the Earth most probably experienced several giant

impacts with each of them causing a global magma ocean with different depths (Rubie et al., 2007).

A simplified heterogeneous two-stage accretion model has been proposed very early by Wänke (1981). This model suggests an early accretion of differentiated material under reducing conditions without any re-equilibration with the Earth´s mantle. In a second step oxidized chondritic material accretes and enhances the siderophile element abundances of the Earth´s mantle. A disadvantage of this model is that it assumes a low pressure scenario, which can be excluded according to the results of e.g. Mann et al. (2009) who showed that the chondritic ratios of the volatile element pairs Ga/Mn and In/Zn cannot be explained by core formation processes at low pressures, but rather equilibration occurred at pressures between 10 – 40 GPa and 30 – 60 GPa respectively.

To date, models can be distinguished into continuous and multistage core formation models. Continuous core formation was proposed by Wade and Wood (2005). According to this study the magma ocean on the early Earth increases in depth as the Earth grows by further accretion. With the constraint of a fixed peridotitic liquidus temperature at the base of the magma ocean, Wade and Wood (2005) were able to match the siderophile element abundances of the Earth´s mantle for V, Ni, Co and W only if the oxygen fugacity was increased over two logarithmic units, eventually being in accordance with the present day´s mantle FeO abundance.

Similar results have been obtained by Tuff et al. (2011), who established a continuous core formation model with respect to metal – silicate partitioning data of Si and its influence on the partitioning behaviour of siderophile elements.

Rubie et al. (2011) investigated a multistage core formation model, assuming episodically occurring metal – silicate segregations caused by collisions of the growing Earth with bodies that were 10 % of the actual Earth´s mass. This approach neglects any assumptions on oxygen fugacity, but constrains the bulk composition of the accreting bodies, which in turn defines oxygen fugacity by the partitioning of Fe between metal and silicate. The composition of the accreting matter is defined as CI chondritic with enhanced concentrations of Al, Ca, Ta, Nb, W and V. The cores of the impacting bodies are considered to react with the silicate mantle, before being segregated to the Earth´s core. The composition of metal and silicate has been calculated after each impact by employing mass balance equations for the elements Fe, Ni, Si and O together with partition coefficients of Ni, Si and O. The concentrations of Co, Cr, V, Nb, W and Ta have been determined exclusively from partition coefficients.

In summary Rubie et al. (2011) showed, that accretion of the initial 60 – 70 % of the Earth (by mass) involved highly reduced material, followed by 30 – 40 % of oxidized impactors. This model is consistent with high pressure metal – silicate equilibration but it requires some extent of disequilibrium between the cores of some large impactors and the silicate Earth. Similar to continuous core formation models the oxygen fugacity is found to increase during accretion due to the variations of the accreting material.

1.10 Aims of the study

The aim of this study was the systematic investigation of the liquid metal – liquid silicate partitioning behaviour for a wide range of elements in order to better constrain the conditions that prevailed during core formation.

Multi-anvil experiments have been performed to determine the pressure and temperature dependences of the partitioning and exchange coefficients for the refractory elements Ni, Co, W and Mo, the moderately volatile elements Cu, Sb, Ge, As, P, Au, Ag and the volatile elements Sn and Pb. The 50 % condensation temperatures cover a range from 704 K (Sn) to 1789 K (W) and the depletions of elements in the Earth´s mantle vary by around two orders of magnitude. Clearly the attention has been turned on volatile elements, because the literature and with it core formation models lack data for this group of elements.

It is well known that the Earth´s core contains one or several light elements (see Section 1.7) and that S is most probably one of these (Dreibus and Palme, 1996; McDonough, 2003). S furthermore has a major influence on the liquid metal – liquid silicate partitioning behaviour of siderophile elements (e.g. Wade et al., 2012; Mann et al., 2009) and was thus incorporated into the study to find additional constraints on the type and amount of light elements in the Earth´s core and their influence on metal - silicate equilibration. For this reason the same 13 elements as mentioned above have been chosen in order to quantify the effect of S on the corresponding partition and exchange coefficients, by performing isobaric multi anvil experiments at 11 GPa. S was added as FeS to the starting metal material and a range from S-free experiments, over 10 and 20 wt% S up to pure FeS has been covered.

Additionally the effect of Si, possibly the major contributor to the budget of light elements in the Earth´s core (Rubie et al., 2011; Siebert et al., 2013), and with it the influence of

different oxygen fugacities has been studied by determining partitioning behaviours with $Fe_{91}Si_9$ or $Fe_{83}Si_{17}$ plus element(s) of interest being employed as starting metal materials. The importance of this determination arises from the fact that latest core formation models have shown that the oxidation state of the Earth varied over time from an initially reduced to a more oxidized system (e.g. Wade and Wood, 2005), see Section 1.9. Moreover it was the aim of this study to identify the oxidation states of the volatile elements in the silicate phase

All partitioning data were quantified in form of regression coefficients and interaction parameters ε_i^k have been provided, that describe the influence on the activity of a given element i as a function of the concentration of another element k dissolved in Fe metal. Whenever possible, the derived expressions for the partitioning and exchange coefficients have been compared with other literature data sets in order to expand the experimental pressure and temperature ranges.

Finally the intention has been to derive accurate partitioning data for 13 elements that can be incorporated into future core formation models, themselves in turn being used to better define constraints on pressure, temperature and oxygen fugacity conditions during core formation scenarios, the amount and nature of light elements in the Earth´s core and the type of material that most probably accreted to the Earth in form of the late veneer.

2. Experimental and analytical methods

2.1 Experimental methods

2.1.1 Preparation of the starting materials

13 elements, namely the non-volatile elements Ni, Co, W and Mo, the moderately volatile elements Cu, Sb, Ge, P, Au, As and Ag and the volatile elements Sn and Pb have been chosen for the investigation of their partitioning behaviour. All experiments were performed with combinations of different metal and silicate powders, the preparation of which is described below.

2.1.1.1 Metal powders

The main component of the metal phase was Fe, $Fe_{91}Si_9$, $Fe_{83}Si_{17}$ or Fe plus S with the latter being added as FeS. The S contents ranged from 10 wt % up to pure FeS. One to five elements of interest have been added to the starting metal powders of the experiments either in form of pure elements or as oxides. The quantities ranged from 0.5 wt% to 3.5 wt%. Initially the elements of interest were grouped into three different batches:

a) Ni, Co, W, Mo
b) Cu, Sn, Sb, Ge and Pb
c) As, P, Au and Ag

However experiments performed with the latter two combinations of elements exhibited exsolutions within the metal spheres during quenching, which was found to be strongly facilitated by the presence of Ag and Pb. In subsequent experiments Ag and Pb have therefore been extracted from the mixes *b* and *c* and treated separately. Moreover their concentrations in the metal phase were halved to 0.5 wt% in order to prevent the formation of exsolutions in the metal phase. Table 2 summarizes the initial compositions of all starting metal powders

that were employed in this study. All components were mixed, ground under ethanol for at least 35 minutes and subsequently dried in an extractor hood at room temperatures or under an infrared lamp.

Table 2: *Composition of the starting metal powders in wt%.*

	met#1a	met#1b(S10)	met#1c(S20)	met#1d(FeS)
Fe	93.95	66.76	41.09	-
FeS	-	26.90	54.76	95.89
Ni	1.66	1.66	1.04	1.01
Co	1.27	1.56	1.04	1.03
W	1.66	1.56	1.02	1.03
Mo	1.46	1.56	1.05	1.03

	met#2	met#2a	met#2b(S10)	met#2c(S20)	met#2d(FeS)	met#2e(FeO5)	met#2f(FeO10)	met#2g($Fe_{83}Si_{17}$)	met#2h($Fe_{91}Si_9$)
Fe	92.18	95.33	65.40	41.11	-	91.00	86.00	-	-
FeS	-	-	26.72	54.78	95.90	-	-	-	-
FeO	-	-	-	-	-	5.00	10.00	-	-
$Fe_{83}Si_{17}$	-	-	-	-	-	-	-	96.00	-
$Fe_{91}Si_9$	-	-	-	-	-	-	-	-	96.00
Cu	1.74	1.19	1.46	1.03	1.02	1.00	1.00	1.00	1.00
SnO	1.16	0.99	1.85	1.02	1.04	1.00	1.00	1.00	1.00
Sb_2O_3	1.45	1.29	1.55	1.03	1.03	1.00	1.00	1.00	1.00
GeO_2	1.74	1.19	1.46	1.02	1.01	1.00	1.00	1.00	1.00
Pb_3O_4	1.74	-	1.55	-	-	-	-	-	-

	met#3	met#3a	met#3b(S10)	met#3c(S20)	met#3d(FeS)	met#3e(FeO5)	met#3f(FeO10)	met#3g($Fe_{83}Si_{17}$)	met#3h($Fe_{91}Si_9$)
Fe	92.53	94.66	65.48	39.91	-	89.84	84.83	-	-
FeS	-	-	27.40	54.59	94.93	-	-	-	-
FeO	-	-	-	-	-	5.00	9.98	-	-
$Fe_{83}Si_{17}$	-	-	-	-	-	-	-	94.72	-
$Fe_{91}Si_9$	-	-	-	-	-	-	-	-	94.77
As	1.28	1.02	1.09	1.00	1.03	1.04	1.04	1.03	1.00
Au	1.67	1.01	1.29	1.01	1.02	1.01	1.00	1.00	1.04
P_2O_5	3.44	3.32	3.66	3.48	3.03	3.11	3.15	3.26	3.19
Ag_2O	1.08	-	1.09	-	-	-	-	-	-

Table 2 continued

	met#4a	met#4c(S20)	met#4d(FeS)	met#4e(FeO5)	met#4f(FeO10)	met#4g($Fe_{83}Si_{17}$)	met#4h($Fe_{91}Si_9$)
Fe	99.35	44.66	-	94.50	89.50	-	-
FeS	-	54.84	99.49	-	-	-	-
FeO	-	-	-	5.00	10.00	-	-
$Fe_{83}Si_{17}$	-	-	-	-	-	99.50	-
$Fe_{91}Si_9$	-	-	-	-	-	-	99.50
Pb_3O_4	0.65	0.50	0.51	0.50	0.50	0.50	0.50

	met#5a	met#5c(S20)	met#5d(FeS)	met#5e(FeO5)	met#5f(FeO10)	met#5g($Fe_{83}Si_{17}$)	met#5h($Fe_{91}Si_9$)
Fe	99.50	44.65	-	94.50	89.50	-	-
FeS	-	54.84	99.50	-	-	-	-
FeO	-	-	-	5.00	10.00	-	-
$Fe_{83}Si_{17}$	-	-	-	-	-	99.50	-
$Fe_{91}Si_9$	-	-	-	-	-	-	99.50
Ag_2O	0.50	0.51	0.50	0.50	0.50	0.50	0.50

2.1.1.2 Silicate powders

For the silicate phases a peridotitic composition has been employed based on the primitive mantle composition of Palme and O´Neill (2003). However the initial amount of FeO was reduced by 4.1 wt% since reactions during the experiments lead to an increase in FeO abundances. In contrast to this primitive mantle (PM) composition several minor oxides, namely TiO_2, Cr_2O_3, Na_2O and K_2O were omitted for simplification. In order to prevent impurities due to reactions of CaO and FeO with O_2 and CO_2 respectively these compounds were added in form of Fe_2O_3 and $CaCO_3$. Subsequent reduction and decarbonation ensured that the initially sought composition was achieved (see below). Two batches of silicate powder were prepared, their initial compositions are given in Table 3.

Table 3: *Initial composition of the silicate powders in wt%.*

	sil#1	**sil#2**
SiO_2	46.56	46.68
MgO	37.56	37.79
Al_2O_3	4.61	4.62
$CaCO_3$	6.93	6.80
Fe_2O_3	4.34	4.11

Prior to the preparation of the peridotitic powders, all oxides were heated in order to remove water. The oxides $CaCO_3$ and Al_2O_3 were heated to 120°C for 3 hours. MgO and SiO_2 were placed into platinum crucibles and Fe_2O_3 was contained in an aluminum crucible in order to prevent reaction with the sample holder. The three powders were then heated to 1000°C for one hour employing a box furnace.

After cooling the powders were weighed, mixed and ground under ethanol for at least 40 minutes and subsequently dried in an extractor hood at room temperature or under the infrared lamp. Subsequently the powder was heated in a platinum crucible to 1000°C for five hours to decarbonate. Each silicate powder was reduced at an oxygen fugacity of 2 logarithmic units below the FMQ buffer in a CO-CO_2 atmosphere at 1273 K or 1373 K in a gas-mixing furnace.

2.1.1.3 Reversed experiment

In order to verify that choosing the metal to be the initial host phase for the elements of interest does not influence the outcome of the experiments a reversal experiment has been performed in which the starting material consisted of pure Fe metal and Pb oxide has been added to the peridotitic silicate (sil#1) starting material. The initial composition of this powder, which has likewise been ground under ethanol for 40 minutes and subsequently been dried in an extractor hood, is given in Table 4.

Table 4: *Initial composition (wt%) of the starting silicate material that was prepared for the reversed experiment H3455.*

	sil#1Pb
sil#1	99.25
Pb_3O_4	0.75

2.1.2 High pressure – high temperature experiments in the multi-anvil apparatus

All experiments have been performed with a multianvil apparatus, namely the 5000 tonne Zwick / Voggenreiter press or the 1000 tonne Hymag press (indicated by capital "Z" or "H" in front of the experiment´s running numbers). Detailed descriptions of the functional principles of these high-pressure devices are presented by, for example, Kawai and Endo (1970), Kawai et al. (1973), Ito et al. (1984), Walker (1990), Rubie (1999), Frost et al. (2004), and Keppler and Frost (2005). The two latter studies provide information on the calibration systematics for the 5000 tonne press and for the 1000 tonne press respectively (Figure 7).

***Figure 7**: Multi-anvil apparatus of the Bayerisches Geoinstitut Bayreuth: **a:** 1000 tonne Hymag Press, **b:** 5000 tonne Press from Zwick and Voggenreiter.*

Each press operates with a two-stage hydraulically-moved anvil system. Whereas the 1000 tonne Hymag press lowers the upper part of the anvil system in order to create a uniaxial force, pressures are reached by lifting the lower part of the outer anvil system when employing the 5000 tonne press from Zwick and Voggenreiter. In both cases the upper and the lower parts of the outer anvil system consist of 3 steel anvils that form a cubic cavity when the system is closed. The high-pressure device contains an inner anvil system, which is comprised of 8 tungsten carbide (WC) cubes whose corners are triangularly truncated in the way that an octahedral cavity arises when assembled. The WC cubes that are used for the 1000 tonne Hymag press and 5000 tonne press from Zwick and Voggenreiter differ from each other by their edge lengths which are 32 mm and 54 mm respectively. The cubes are either covered with Teflon tape that serves as insulation or with cardboard that inhibits the movement of pyrophyllite gaskets, which seal the pressure medium.

The pressure medium itself is located inside the cavity formed by the inner anvil system and consists of a Cr_2O_3-doped MgO octahedron. A typical 18/11 pressure medium (explanations on this notation are given below) is schematically displayed in Figure 8.

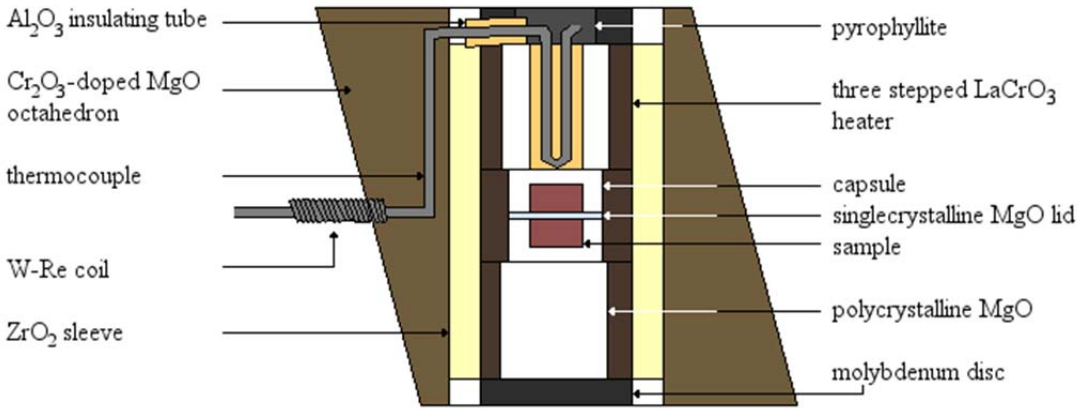

Figure 8: *Schematic illustration showing the inside of a multi-anvil sample assembly.*

The octahedron contains a cylindrical hole which is lined with thermally insulating ZrO_2 typically completed by a ring of MgO at the bottom and top. Into this is inserted a stepped $LaCrO_3$ resistance heater which minimizes thermal gradients in the sample region (Frost et al., 2004). The outer heater parts enclose one hollow and one solid MgO cylinder respectively and the middle part of the stepped heating system accommodates two MgO capsules that are separated by a MgO lid. A molybdenum disc and a molybdenum ring in contact with the solid and hollow MgO cylinders respectively complete the assembly and connect the pressure medium to the truncations of the WC cubes enabling electrical conduction to the heater. All $LaCrO_3$ parts as well as the octahedron and the MgO parts were heated at 1000 °C for 30 to 60 minutes to remove water and organic impurities.

For determinations of the temperatures that prevail during the experiments a thermocouple was located inside the MgO sleeve. It consists of a fourfold perforated aluminium tube in which $W_{25}Re_{75}$ and W_3Re_{97} wires are located that are crossed to form a junction. The wires that emerge from edges of the octahedron are covered with coils of the same type of wire in order to prevent breakage due to friction. The use of the same type of wire is required in order to avoid a secondary EMF (electromagnetic force) (Nishihara et al., 2006).

A complete set up is illustrated in Figure 9. It is separated from the outer anvil system by epoxy sheets which operate as a low-friction surface when the assembly is compressed. Small pieces of copper foil that are bent through cuts in the epoxy sheets ensure electrical conduction to the heater.

Higher pressures can either be achieved by increasing the force applied to the system or by reducing the sizes of the pressure medium and thus by using smaller truncations of the inner anvil system. Several assembly types can therefore be distinguished. They are characterized by the notation OEL/ TEL (octahedral edge length / truncation edge length in millimetre). For this study assemblies of the type 18/11, 18/8 and 10/4 have been used with which pressures of 11, 18, 20, 21 and 23 GPa have been generated over a temperature range of 2342 K to 2911 K. However, in contrast to the 18/11 and 18/8 assemblies the comparatively small 10/4 assembly can only accommodate one capsule instead of two.

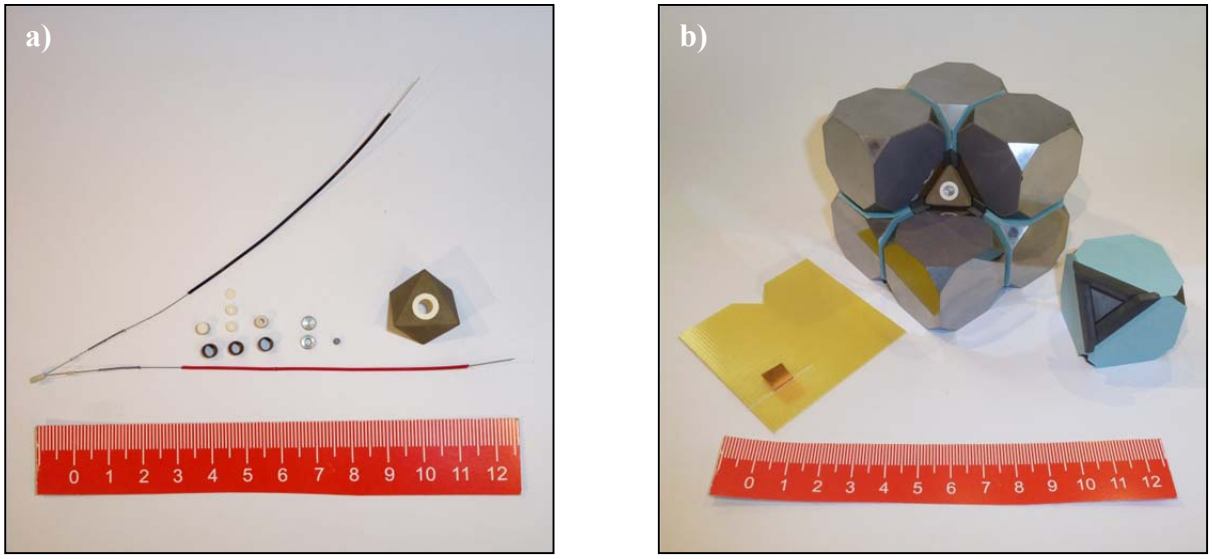

Figure 9a: *Image of all individual parts of a typical 18/11 assembly before its preparation.* ***b:*** *The assembly is placed into the octahedral space that arises when the prepared cubes are assembled. The cubes are either glued with cardboard or with grey Teflon tape. The epoxy sheet (yellow) will finally be attached to the sides of the cube. It exhibits a copper foil that forms part of the electrical heating surface.*

Pressures were increased slowly over a period of 200 to 280 minutes. Maximum pressures were maintained for 1 hour and the subsequent decompression lasted for 850 to 1000 minutes. The heating of the samples was performed in steps of around 100 to 200 K per minute, but the time-intervals were reduced once temperatures exceeded 1773 K. In most cases the samples were held for 10 minutes at 1773 K in order to allow the assembly to stabilize at the high temperatures. Maximum temperatures were maintained for a period of 1 to 3 minutes (Table 5). Finally the experiments were quenched by switching off the electrical power.

The determinations of temperature were based on thermocouple readings and subsequent power-temperature (Watts / K) correlations above 1773 K. The best correlation – that means

the one that was found to be the most stable and that additionally resulted in the highest temperatures as a function of power – was used to derive the temperatures of all experiments. However different power – temperature correlations have been employed when experiments were performed in different presses, at different pressures or when a new consignment of $LaCrO_3$ resulted in minor differences in the composition of the resistance heater. The employment of the correlation that exhibits the highest temperatures is based on the assumption that lower temperatures most likely result from an outward movement of the thermocouple at the extremely high pressures that prevail during the experiments. They are thus not representing the temperatures within the sample region. In order to further account for temperature gradients an error of +/- 100 K has been assumed for all experiments. An example of a typical power-temperature correlation (experiment Z822, 11 GPa, 18/11 assembly) is given in Figure 10.

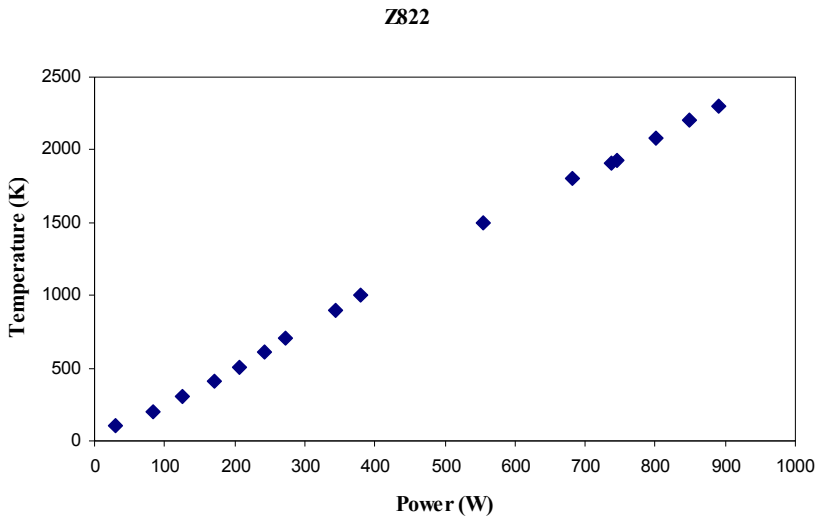

***Figure 10**: Power-temperature correlation for the experiment Z822. Details are given in the text.*

The experiments H3355 to H3407 were conducted with a mixed powder of silicate and metal with a mass ratio of 75/25. In subsequent experiments the individual metal and silicate powders were loaded so that a metal layer was sandwiched between two layers of silicate powder (Figure 11). This approach was found to facilitate the formation of a single large metal sphere. The composition of the metal and silicate powders, the metal/silicate mass ratios and the conditions of the individual experiments are given in Table 5.

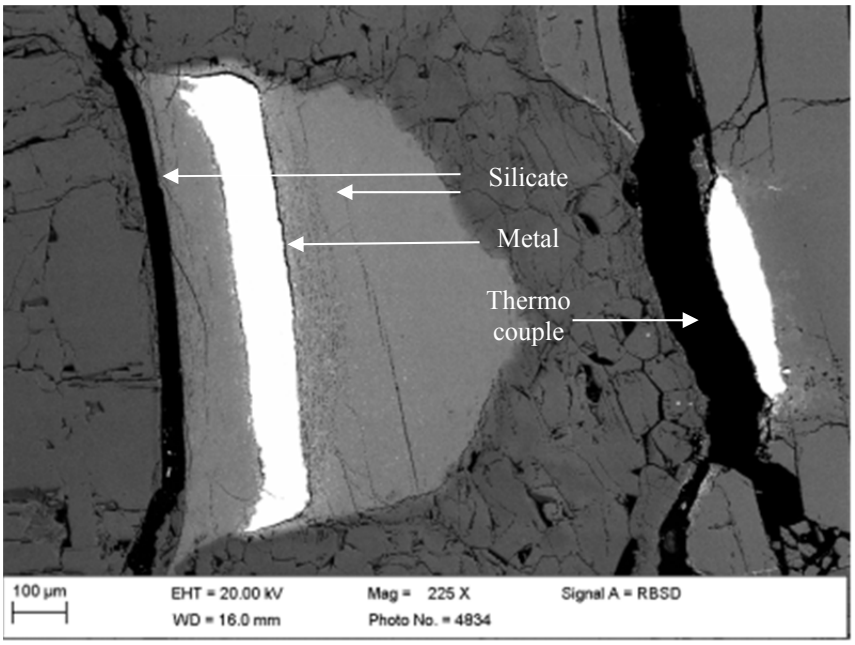

Figure 11: *Sample configuration of high pressure – high temperature multi anvil experiments: Sample H3496, 23 GPa, 2200°C. The temperature was too low to melt the starting materials at 23 GPa. This "failed" experiment enables the initial way of sample loading to be seen: a metal layer (white) is sandwiched between two layers of peridotite powder (grey). The metal/silicate mass ratio is 62:38.*

Table 5: *Experimental conditions of experiments performed in this study. Additional information include the assembly type, the composition (for notation see tables 2, 3 and 4) the metal/silicate mass ratio and the duration of heating.*

Sample	Assembly type	T (K)	Composition (notation see Tables 2, 3, 4)	Metal/silicate mass ratio	Duration of heating (s)
11GPa					
H3355a	18/11	2490	met#2 + sil#1	75:25	120
H3355b	18/11	2490	met#2 + sil#1	75:25	120
H3361a	18/11	2844	met#2b + sil#1	75:25	120
H3361b	18/11	2844	met#2 + sil#1	75:25	120
H3364a	18/11	2570	met#2b + sil#1	75:25	120
H3364b	18/11	2570	met#2b + sil#1	75:25	120
H3367b	18/11	2342	met#2b + sil#1	75:25	120
H3371a	18/11	2773	met#1b + sil#1	75:25	120
H3371b	18/11	2773	met#1a + sil#1	75:25	120
H3372a	18/11	2478	met#1b + sil#1	75:25	140
H3372b	18/11	2478	met#1a + sil#1	75:25	140
H3400a	18/11	2553	met#3 + sil#1	75:25	120
H3400b	18/11	2553	met#3b + sil#1	75:25	120
H3404a	18/11	2777	met#3 + sil#1	75:25	130
H3404b	18/11	2777	met#3b + sil#1	75:25	130
H3439a	18/11	2567	met#3 + sil#1	78:22	197
H3439b	18/11	2567	met#3 + sil#1	67:33	197
H3444a	18/11	2609	met#5a + sil#1	51:49	190
H3444b	18/11	2609	met#5a + sil#1	82:18	190
H3449a	18/11	2560	met#4a + sil#1	50:50	190

Table 5 continued

H3449b	18/11	2560	met#4a + sil#1	66:34	190
H3450a	18/11	2560	met#2a + sil#1	72:28	192
H3455a[*1]	18/11	2562	sil#1Pb + Fe	54:46	195
H3455b[*1]	18/11	2562	sil#1Pb + Fe	40:60	195
H3497a	18/11	2718	met#4a + sil#1	60:40	180
H3497b	18/11	2718	met#5a + sil#1	47:53	180
H3586a	18/8	2609	met#1a + sil#1	74:26	130
H3586b	18/8	2609	met#1a + sil#1	48:52	130
H3704a	18/11	2639	met#4g + sil#2	70:30	120
H3704b	18/11	2639	met#4h + sil#2	52:48	120
H3707a	18/11	2584	met#5h + sil#2	54:46	120
H3707b	18/11	2584	met#5g + sil#2	43:57	120
H3718a	18/11	2658	met#2f + sil#2	65:35	120
H3718b	18/11	2658	met#2h + sil#2	67:33	120
Z798a	18/11	2500	met#5a + sil#1	66:34	190
Z798b	18/11	2500	met#5a + sil#1	61:39	190
Z822a	18/11	2573	met#2a + sil#1	64:36	180
Z822b	18/11	2573	met#1a + sil#1	54:46	180
Z915a	18/11	2641	met#2a + sil#2	41:59	120
Z915b	18/11	2641	met#2g + sil#2	61:39	120
Z916a	18/11	2580	met#5a + sil#2	64:36	120
Z916b	18/11	2580	met#1a + sil#2	48:52	120
Z919a	18/11	2605	met#4a + sil#2	60:40	120
Z919b	18/11	2605	met#4f + sil#2	52:48	120
Z920b	18/11	2580	met#4e + sil#2	57:43	120
Z922a[*2]	18/11	2588	met#5e + sil#2	60:40	120
Z922b[*2]	18/11	2588	met#5f + sil#2	52:48	120
Z926a[*3]	18/11	2668	met#2e + sil#2	52:48	120
Z926b[*3]	18/11	2668	met#2e + sil#2	54:46	120
Z941b	18/11	2752	met#2a + sil#2	56:44	120
Z1000a	18/11	2612	met#3a + sil#2	67:33	120
Z1000b	18/11	2612	met#3a + sil#2	66:34	120
Z1001a	18/11	2636	met#4d + sil#1	86:14	155
Z1002a	18/11	2602	met#3g + sil#2	67:33	120
Z1002b	18/11	2602	met#3h + sil#2	66:34	120
Z1008a	18/11	2614	met#2d + sil#2	80:20	120
Z1008b	18/11	2614	met#3e + sil#2	93:7	120
Z1009b	18/11	2619	met#1b + sil#2	75:25	120
Z1011a	18/11	2605	met#3f + sil#2	69:31	120
Z1011b	18/11	2605	met#1a + sil#2	81:19	120
Z1013a	18/11	2624	met#5c + sil#2	89:11	120
Z1016a	18/11	2607	met#5d + sil#2	74:26	130
Z1016b	18/11	2607	met#4d + sil#2	89:11	130
Z1019a	18/11	2624	met#4c + sil#2	81:19	120
Z1019b	18/11	2624	met#3g + sil#2	68:32	120
Z1043a	18/11	2636	met#3c + sil#2	87:13	120
Z1043b	18/11	2636	met#3c + sil#2	80:20	120
Z1051a	18/11	2626	met#1c + sil#2	89:11	120
Z1051b	18/11	2626	met#1c + sil#2	87:13	120
Z1062a	18/11	2636	met#2c + sil#2	75:25	120
Z1062b	18/11	2636	met#2c + sil#2	73:27	120
18 GPa					
Z852a	18/8	2663	met#5a + sil#1	66:34	145
Z854a	18/11	2740	met#4a + sil#2	64:36	120
Z854b	18/11	2740	met#5a + sil#2	60:40	120
Z858a	18/11	2942	met#5a + sil#2	53:47	120
Z858b	18/11	2942	met#4a + sil#2	54:46	120
Z859a	18/11	2717	met#1a + sil#2	60:40	124

Table 5 continued

Z859b	18/11	2717	met#2a + sil#2	50:50	124
Z865a	18/11	2834	met#2a + sil#2	53:47	60
Z865b	18/11	2834	met#1a + sil#2	60:40	60
Z869b	18/11	2677	met#3 + sil#2	60:40	120
Z878a	18/11	2742	met#3 + sil#2	64:36	120
Z878b	18/11	2742	met#3 + sil#2	68:32	120
Z881a	18/11	2653	met#4a + sil#2	64:36	120
Z881b	18/11	2653	met#3 + sil#2	77:23	120
Z957b	18/11	2603	met#3a + sil#2	69:31	120
20 GPa					
Z929a	18/11	2799	met#1a + sil#2	59:41	90
Z929b	18/11	2799	met#2a + sil#2	59:41	90
21 GPa					
Z949b	18/8	2870	met#2a + sil#1	58:42	90
Z950a	18/8	2904	met#1a + sil#2	46:54	90
Z950b	18/8	2904	met#2a + sil#2	63:37	90
Z969a	18/8	2897	met#3a + sil#2	70:30	90
Z969b	18/8	2897	met#3a + sil#2	72:28	90
Z970a	18/8	2911	met#1a + sil#2	58:42	90
Z970b	18/8	2911	met#1a + sil#2	59:41	90
Z977a	18/8	2893	met#4a + sil#2	76:24	90
Z977b	18/8	2893	met#5a + sil#2	72:28	90
Z980a	18/8	2911	met#5a + sil#2	55:45	100
Z980b	18/8	2911	met#4a + sil#2	70:30	100
23 GPa					
H3518	10/4	2594	met#4a + sil#1	66:34	180
H3536	10/4	2542	met#4a + sil#1	78:22	180
H3581	10/4	2540	met#4a + sil#1	60:40	60
H3606	10/4	2540	met#5a + sil#2	64:36	60
H3629	10/4	2589	met#4a + sil#2	53:47	60

[*1] Reversed experiment

[*2] Composition of samples Z922a and Z922b probably vice versa

[*3] Metal/silicate mass ratios of Z926a and Z926b probably vice versa

2.2 Analytical methods

In a successfully performed experiment, a round metal sphere develops that is surrounded by a silicate matrix (Figure 12). The use of MgO capsules leads to the formation of ferroperriclase crystals near the border of the capsules and occasionally around the metal spheres. Metal and ferropericlase phases were analysed by the electron probe micro-analyser (EPMA), whereas the concentrations of all elements in the silicate were measured with laser ablation inductively coupled plasma mass spectrometry (LA-ICP-MS) (see below).

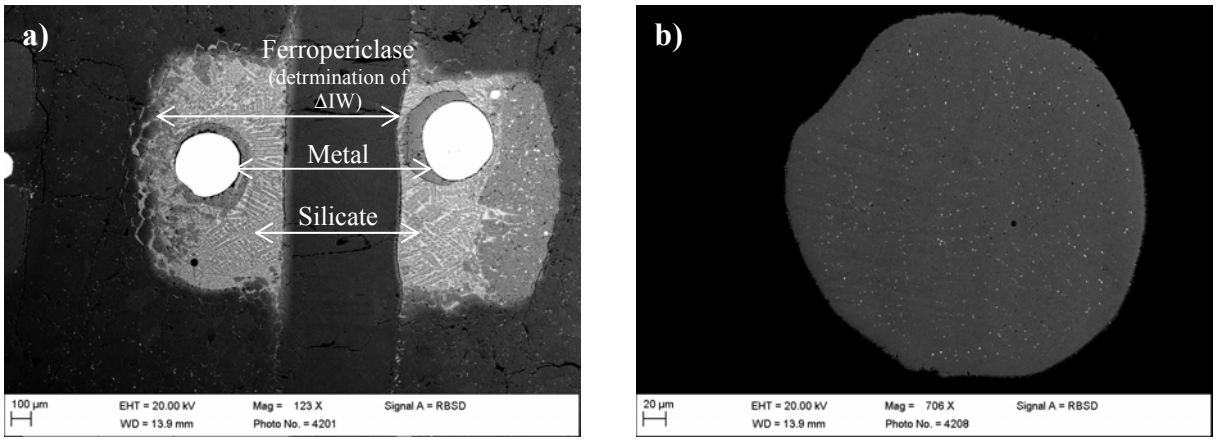

Figure 12a: *Backscattered electron image of sample: H3444a (left) and b (right), 11 GPa, 2609 K, ΔIW = -2.0 / -2.3 respectively, Ag-bearing. Metal spheres (white) are surrounded by a silicate matrix that exhibits elongated skeletal olivine quench crystals. Ferropericlase has formed around the metal spheres and at the borders of the capsules.* ***b)*** *Close-up of the metal phase of sample H3444a that exhibits very tiny (< 1 µm) exsolutions (white) that are enriched in Ag.*

2.2.1 Electron probe micro-analyser (EPMA)

A JEOL JXA-8200 electron probe micro-analyser (EPMA) was employed for all quantitative analyses of the metal and ferropericlase phases. The accelerating voltage and the beam current were set to 15 kV and 15 nA respectively and the peak counting times were fixed at 20 s for every element on the peak position and 10 s for all background measurements.

A range of pure metals, oxides, silicates, as well as an arsenide, a telluride, a phosphate and a boride have been employed as standards for measurements. These are listed against elements that were analysed in Table 6.

All data have been corrected by either the phi-rho-z routine or by the ZAF approach.

Table 6: *Elements that have been analyzed with the electron probe micro-analyser (EPMA) correlated to the standards employed*

Element	Standard	Chemical Formula
Si	Andradite	$Ca_3Fe_2[SiO_4]_3$
Ca	Andradite	$Ca_3Fe_2[SiO_4]_3$
Al	Spinel	$MgAl_2O_4$
Mg	Enstatite	$Mg_2[Si_2O_6]$
Fe	Iron	Fe
O	Periclase	MgO
S	Pyrite	FeS_2
Ni	Nickel	Ni
Co	Cobalt	Co
W	Tungsten	W
Mo	Molybdenum	Mo
Cu	Copper	Cu
Ge	Germanium	Ge
Sn	Tin dioxide	SnO_2
Sb	Antimony	Sb
Pb	Lead telluride	PbTe
Ag	Silver	Ag
Au	Gold	Au
As	Indium arsenide	InAs
P	Apatite	$Ca_5[(PO_4)_3(F,Cl,OH)]$
Measured in case of suspected contamination by impurities		
La	Lanthanum hexaboride	LaB_6
Cr	Chromium	Cr
Re	Rhenium	Re
Zr	Zirconium	Zr

2.2.1.1 Metal phases

When analyzing the metal phases of the experiments a defocused electron beam with a diameter of usually 20 µm was adopted. In some cases, for smaller metal spheres, diameters of 5 or 10 µm have additionally been applied. The number of measurements of the metal phase of each sample ranged between 20 and 77 analyses, depending on the size of the metal spheres.

Occasionally, quenching of the samples led to exsolutions of heavy elements like Ag, Au and Pb, identifiable by small bright round blobs within a grey-toned metal matrix in a backscattered electron image (compare Figure 13a). These exsolutions may be very tiny and uniformly distributed within the metal sphere, however they were also found to reach sizes of more than 1 µm right up to (extremely rarely) > 5 µm and also to occur preferentially at the rim of the metal spheres. When equally distributed and tiny (~1µm) the use of a broad

defocused electron beam together with the combination of numerous analyses was found to facilitate the determination of the bulk composition of the metal phase, since additional calculations that were based on image analyses (see below) led to the same results. If, however, exsolution was concentrated at the rim of the metal spheres determining the bulk metal composition becomes extremely difficult, because analyses of the metal are not statistically uniform and measurements too close to the metal rim may also be contaminated by the surrounding silicate phases.

It was found that reducing the number of elements of interest in the starting metal material as well as lower concentrations inhibited the formation of exsolutions. Because of this observation, the number of elements in the starting metal material was minimized and Ag as well as Pb were probed individually and with lower concentrations as previously described in Section 2.1.1.1.

Samples exhibiting exsolutions exceeding 1 μm in size (Figure 13a) were investigated by image analysis (Chapter 3). In these cases the exsolutions of heavy elements were analysed individually with beam diameters of 1 μm (occasionally 5 μm), as well as the grey metal matrix, where beam diameters ranged from 5 to 20 μm. Due to the small sizes of the exsolutions and additionally due to their limited abundance the number of analyses was restricted to 10 to 31 measurements. The matrix of the metal spheres was similarly analysed 20 to 30 times to prevent that numerous sub-micron exsolutions are incorporated into the analyses.

It was also found that O and Si exsolve in some cases within the metal phases, forming round blobs that appear black in backscattered electron images (Figure 13b). The exsolutions of O and Si usually have sizes ~5 μm in diameter and their formation was found to be facilitated by the presence of and, in particular, increasing S-contents. In contrast to the above mentioned bright exsolutions of heavy elements, these were found to generally be distributed uniformly within the whole metal sphere. Therefore averaged analyses of numerous measurements, performed with a broad defocused electron beam with a diameter of usually 20 μm, provide reliable results as already discussed for the exsolutions of heavy elements (see above).

In both cases (i.e. in metal spheres with exsolutions that are either enriched in heavy elements or in O and Si), occasionally an exsolution free border region formed within the metal phase adjacent to the silicate phase (see Chapter 3). If compositionally different from the rest of the metal phase this region was avoided for bulk metal analyses with a broad

electron beam. When image analyses were required to integrate the exsolutions of the heavy elements into the bulk metal composition, this rim was analysed as part of the metal matrix.

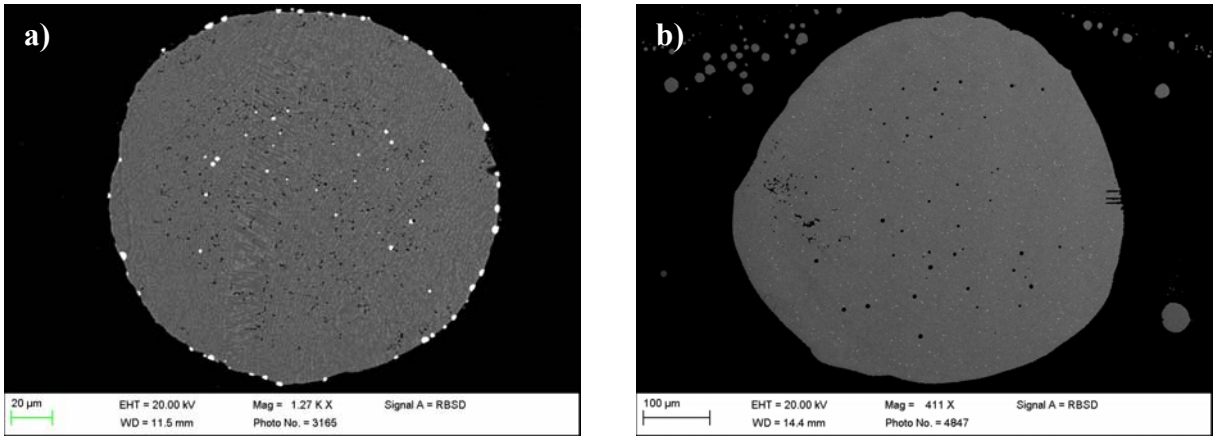

Figure 13a: *Example for the exsolution of heavy elements (white blobs within the grey-toned metal sphere). Sample H3404a, 11 GPa, 2777 K, ΔIW -2.4. The exsolutions are enriched in Au, As, Ag and P and occur mainly around the rim of the metal sphere, which necessitates image analysis to properly determine the bulk metal composition.* ***b)*** *Example of exsolutions of Si and O (black blobs within the grey-toned metal sphere). Sample H3497b, 11 GPa, 2718 K, ΔIW -2.3. The exsolutions are tiny and uniformly distributed within the metal phase enabling the investigation of the bulk metal composition by the use of a broad defocused electron beam.*

2.2.1.2 Ferropericlase

The formation of ferropericlase was induced by the use of poly- and single-crystal MgO-capsules. The crystals were located in the silicate melt usually close to the capsule walls as well as around the metal spheres. Crystals that were surrounded by silicate melt were analysed preferentially in order to ensure equilibrium resulting from sufficient Fe-Mg exchange between ferropericlase and the silicate melt. For the same reason – the achievement of Fe-Mg equilibrium at experimental conditions - the measurements were performed very close to the edges of these crystals. However, due to quenching, a small rim, which is enriched in Fe, was found at the edges of the crystals. This rim can easily be identified on the backscattered images displayed on the electron probe micro-analyser since the higher atomic number of Fe in comparison to Mg results in brighter shades of grey. Analyses of these rims will inevitably lead to errorneous values for the oxygen fugacity, whereas analyses that are

too close to the center of the ferropericlase phases may also not mirror the correct conditions. The Fe enriched rim in all ferropericlase phases has a thickness of approximately 1 μm. The beam diameter used for the analysis was also 1 μm. All analyses were thus performed around 2 μm distant from the crystal´s edge.

Whenever samples lacked ferropericlase crystals in the silicate melt or around metal spheres, the border of the MgO capsules adjacent to the silicate phase of the samples has been analysed instead.

2.2.2 Laser ablation inductively coupled plasma mass spectrometry (LA-ICP-MS)

Due to the low concentrations of the siderophile elements of interest in the silicate melt, quantitative analysis of both major and trace element concentrations in the silicate have been performed with an Elan DRC-e quadrupole mass spectrometer (Perkin Elmer Instruments, Canada) connected to a GeolasPro 193 nm ArF Excimer Laser System (Coherent Inc., USA). All analyses were performed with the help of Dr. Andreas Audétat who additionally provided an Excel-based program for the integration of the signal intensities and the subsequent acquisition of the concentrations of the elements of interest, which was based on the study of Longerich et al. (1996). During the analyses the sample chamber was flushed with helium gas at a rate of 0.4 l/min which was complemented by Ar gas and H_2 gas with rates of 0.95 l/min and 5 ml/min respectively.

The instrument background was measured once before each set of standards and each set of sample measurements with the measuring times on background and signal lasting between 10 s and 40 s.

Because of the often coarse-grained heterogeneous quench structures of the silicate melt a beam diameter of 20 to (normally) 80 μm at a frequency range between 5 – 10 Hz has been employed dependent on the available space between coexisting metal and ferropericlase phases. Spikes were deleted manually by replacing the value at this time by the mean of the neighbouring values. A typical diagram displaying the signal intensities of various elements against time is shown in Figure 14.

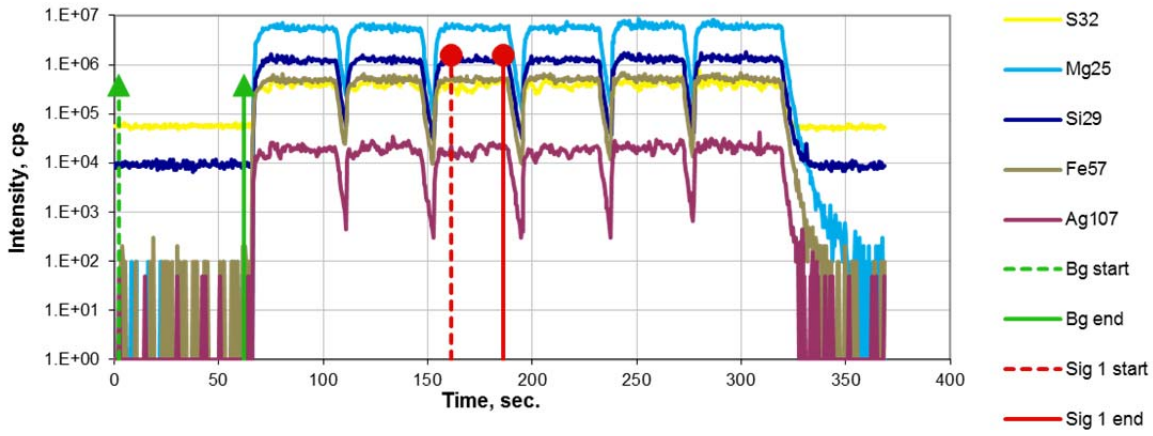

Figure 14: *Example of a typical diagram that shows the signal intensities of - in this case – S, Mg, Si, Fe and Ag obtained from the LA-ICP-MS measurements. The sample has been analyzed 6 times at different spots. While changing the spot the signal intensity drops down significantly. The green arrows at 2 s and 62 s mark the range of the background measurements and red lines indicate the area of the sample measurements that will be integrated. After 309 s the signal of Ag exhibits a spike which was deleted manually when integrating this section.*

The integrated signal intensities were referenced to the external standard NIST SRM 610 that was measured prior to and after all other measurements in the case of all elements except S because the concentration of S in the standard NIST SRM 610 is low and poorly constrained. The concentration of S in the silicate melt has therefore been obtained by using either Afghanite (Seo et al., 2011) or a S-bearing basaltic glass kindly provided by Roman Botcharnikov (Botcharnikov #19; Botcharnikov et al., 2011) as external standards.

The derived element ratios were converted into absolute abundances by normalizing SiO_2, CaO, FeO, Al_2O_3 and MgO to 100 wt%. In contrast to these oxides the concentrations of all other elements have been obtained as pure element ppm abundances. Table A3 in the appendix summarizes the results of the LA-ICP-MS measurements and additionally provides the number of averaged analyses for each sample.

In order to get an estimate of the quality of the measurements, the USGS silicate glass standards BCR-2G (Wilson, 2006a), NKT-1G (Wilson, 2006b) and another S-bearing basaltic glass (Botcharnikov #36; Botcharnikov et al., 2011) have been periodically analyzed as unknowns. The results obtained for MgO, Al_2O_3, SiO_2, CaO, Fe_2O_3, P_2O_5, Co, Mo and S typically agree within less than 10 % uncertainty of the certified/reference values at the most, whereas the contents of other trace elements in the secondary standards are not constrained precisely enough to allow a firm comparison.

2.2.3 Field-emission scanning electron microscopy (FESEM)

As described above, exsolutions of heavy elements such as Pb and Ag occurred during quenching (e.g. Gessmann et al., 1998; O´Neill et al., 1998). Therefore it is important to integrate the concentrations of the elements within these phases into the bulk metal composition. As already mentioned in Section 2.2.1.1 the exsolutions of heavy elements occasionally occurred at the rim of the metal spheres and were then analysed separately from the metal matrix. Subsequent investigations of the bulk metal composition require image analyses based on several backscattered electron images of the corresponding samples.

For this purpose the field-emission scanning electron microscope LEO 1530 Gemini that is connected to the energy dispersive X-ray spectroscopy system Oxford INCA has been employed. The magnification was varied in order to obtain images of the whole metal sphere as well as several close-ups within the metal and was thus dependent on the size of the metal spheres. The electron beam was operated at an EHT (extra high tension) of 20 kV.

3. General results

In the course of this study 104 samples were produced over a pressure and temperature range from 11 GPa to 23 GPa and 2342 K to 2911 K respectively. Elements of interest were the non-volatile siderophile elements Ni, Co, W and Mo and the volatile elements Cu, Sn, Sb, Ge, Pb, Au, As, Ag and P. For each element multiple experiments have been performed at various pressure and temperature conditions.

Additionally the influence of S on the partitioning of all elements has been investigated by performing experiments at 11 GPa with four different S metal concentrations. Besides experiments in which the starting metal material was either free of S or consisted of FeS plus elements of interest, additional experiments have been performed with concentrations of 10 wt% and 20 wt% S in the starting metal material (see Table 2, Chapter 2).

The effect of Si dissolved in the metal phase and associated changes in oxygen fugacity have been investigated for all volatile elements. For this purpose additional experiments have been performed within which the starting metal material consisted of $Fe_{91}Si_9$ or $Fe_{83}Si_{17}$ plus elements of interest (see Table 2, Chapter 2). As will be shown in Chapter 4 it was additionally possible to derive the valence states of the elements of interest in the silicate by investigating how they are influenced by the presence of Si in the metal phase.

As previously described in Chapter 2 successfully performed experiments resulted in the formation of a single large metal sphere surrounded by quenched silicate matrix that exhibits skeletal olivine crystals. Due to the use of MgO capsules ferropericlase formed at the border of the capsules and occasionally around the metal sphere. Figure 15 displays a backscattered electron image of experiment H3444 that was performed at 11 GPa and 2609 K. The experiment was performed with two capsules (left hand side: a; right hand side: b) that were separated by a single crystal MgO lid, the corresponding oxygen fugacity of each sample was determined as -2.0 and -2.3 logarithmic units relative to the iron-wüstite buffer respectively. The white semicircle on the left edge of Figure 15 is part of the thermocouple that was used to determine temperature during the experiment.

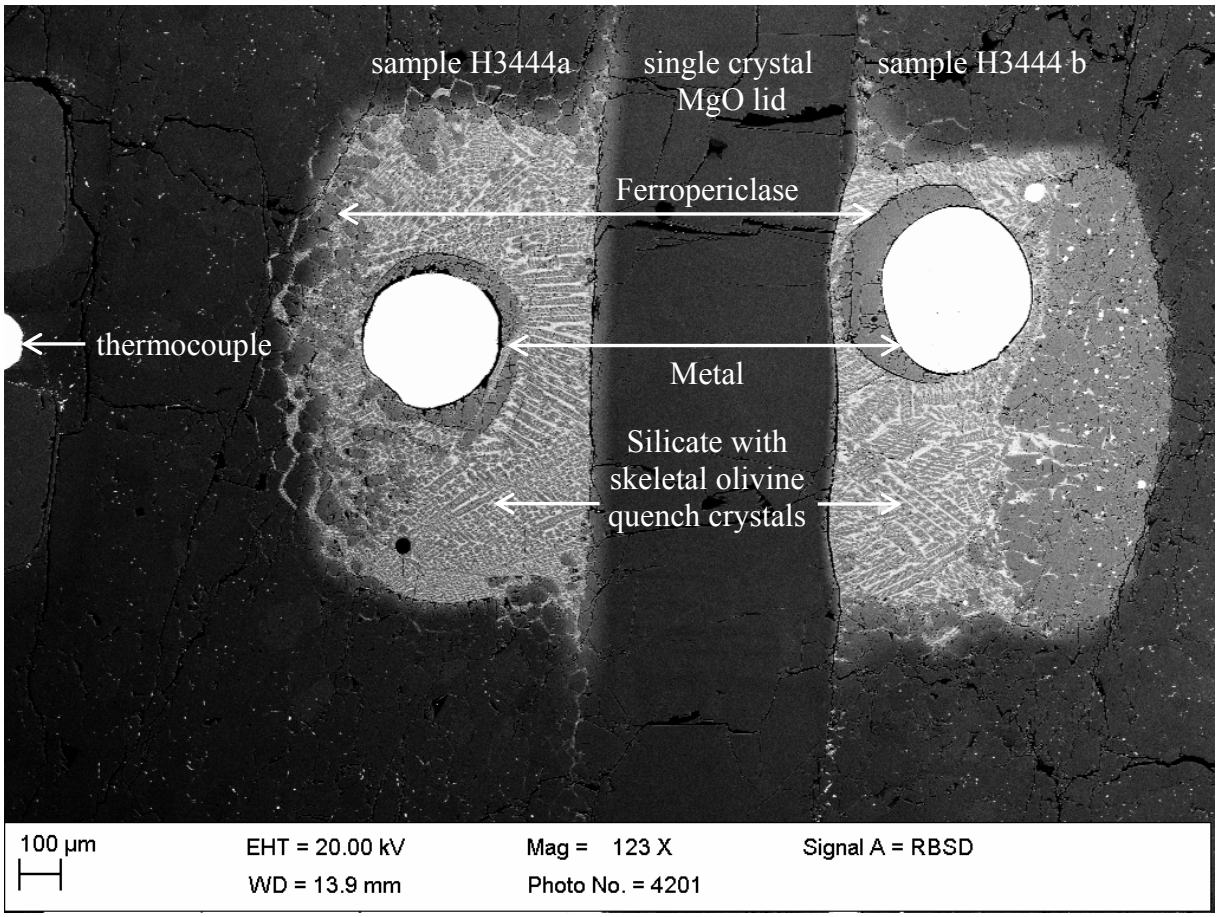

Figure 15: *Backscattered electron image of sample: H3444a (left) and b (right), 11 GPa, 2609 K, ΔIW = -2.0 / -2.3 respectively, Ag-bearing. Metal spheres (white) are surrounded by a silicate matrix that exhibits elongated skeletal olivine quench crystals. Ferropericlase has formed around the metal spheres and at the borders of the capsules.*

Figure 16 displays a more detailed picture of the metal phase of sample H3444a. By varying the contrast, sub-micron and uniformly-distributed exsolutions (white) that are enriched in Ag become visible that can easiliy be taken into account by the use of a broad defocused electron beam when determining bulk metal compositions with the electron probe micro-analyser (see Section 2.2.1.1).

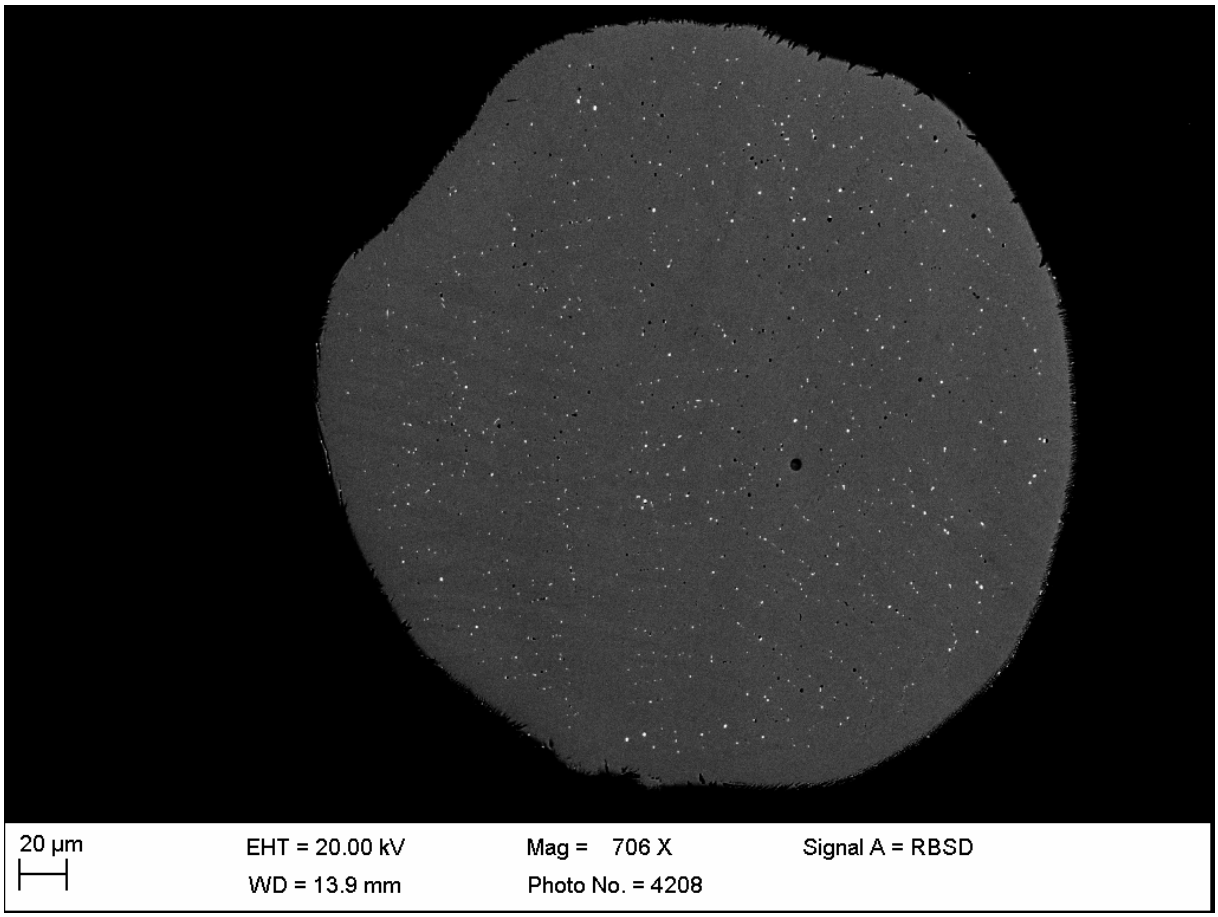

Figure 16: *Backscattered electron image of the metal phase of sample H3444a, 11 GPa, 2609 K, ΔIW = -2.0, Ag bearing. The sub-micron white phases are uniformly distributed exsolutions that are enriched in Ag. When determining the bulk metal composition they can easily be taken into account by analyzing the metal sphere with a broad defocused electron beam.*

In contrast Figure 17 shows the metal phase of sample H3404a that exhibits exsolutions that are enriched in the siderophile elements Ag, Au, As and P and that are not uniformly distributed but are preferentially located around the rim of the metal sphere, which requires image analysis when determining the bulk metal composition.

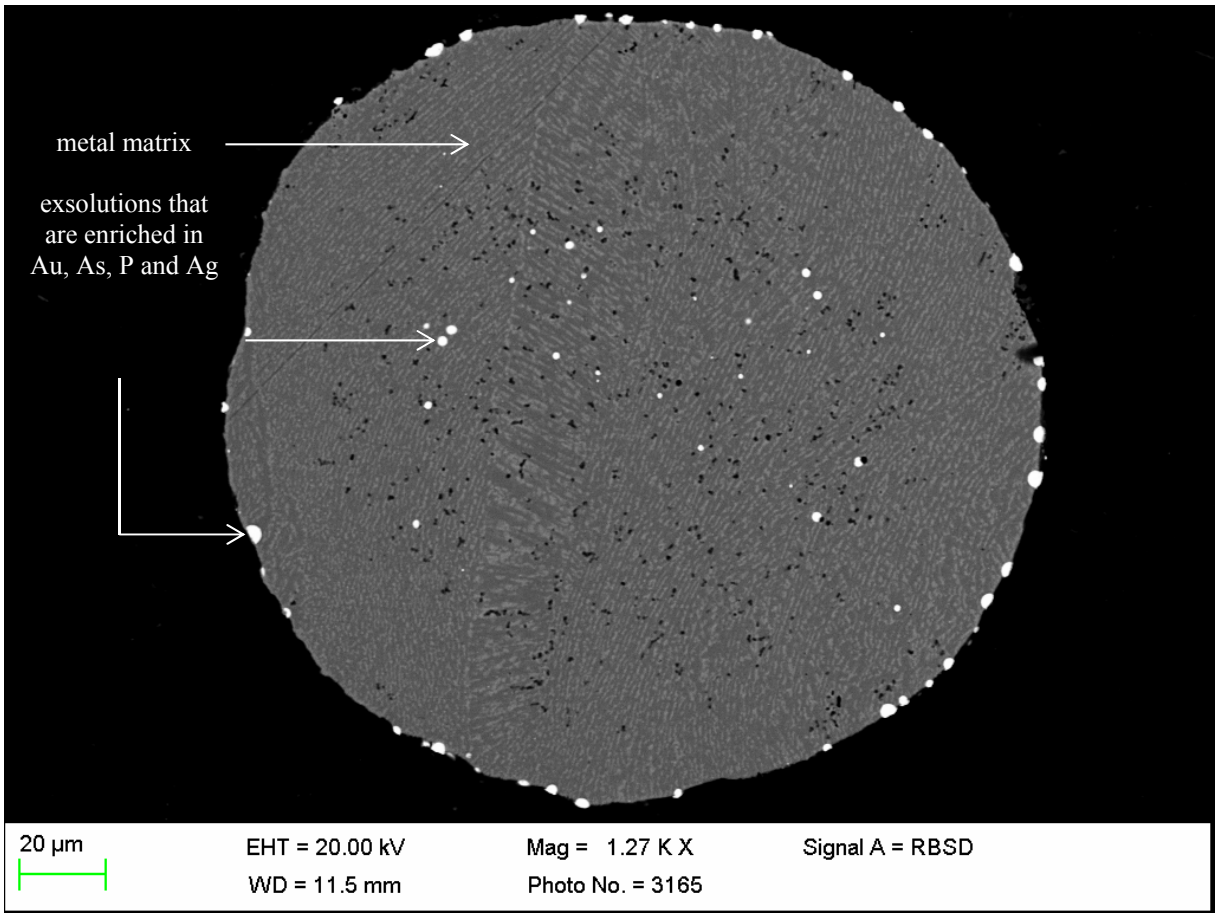

Figure 17: *Backscattered electron image of the metal phase of sample H3404a, 11 GPa, 2777 K, ΔIW -2.4. The white exsolutions are enriched in Au, As, P and Ag and form during quenching (Gessmann et al., 1998; O'Neill et al., 1998). Because of their non-uniform distribution image analyses are necessary when determining the bulk metal composition.*

For the sake of completeness Figure 18 shows exsolutions in the metal phase of sample Z1008b that contain up to 40 wt% and 50 wt% Si and O. Besides Fe, its starting composition contained 5 wt% of FeO, 1 wt% of each of the siderophile elements As and Au and 3 wt% P_2O_5. The backscattered electron image of the metal phase of sample Z1008b has in this case been obtained by employing the electron probe micro-analyser rather than the field-emission scanning electron microscope.

The exsolutions with high concentrations of Si and O are uniformly distributed within the metal sphere rather than being present at the rim of the metal sphere. Therefore the bulk metal composition has been investigated with the electron probe micro-analyser by the use of a broad defocused electron beam as explained above (Section 2.2.1.1).

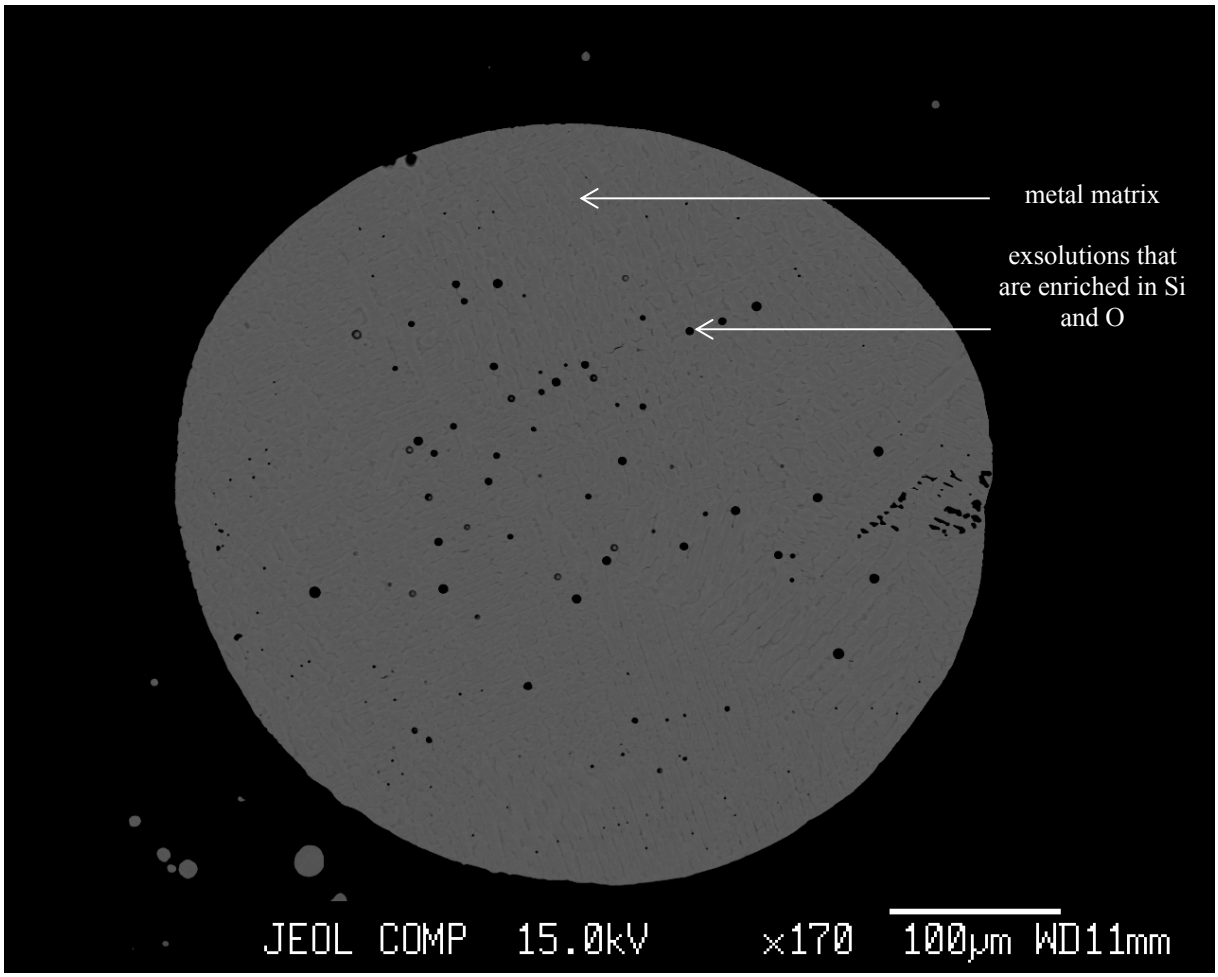

Figure 18: *Backscattered electron image of sample Z1008b, 11 GPa, 2614 K, ΔIW -2.9, P-, As- and Au-bearing. The black round exsolutions within the grey-toned metal matrix are enriched in Si and O. Because they are uniformly distributed the bulk metal composition has been investigated by the electron probe micro-analyser with a broad defocused electron beam.*

Some metal phases that exhibit exsolutions, either of heavy elements or enriched in O and Si, developed an exsolution-free rim adjacent to the surrounding silicate. In the case of O and Si rich exsolutions this has also been observed by Ohtani and Ringwood (1984) and O´Neill et al. (1998). The latter authors argued that in this region the exsolved components migrated to the metal - silicate interface during quenching. If compositional differences between the border region of a metal phase and its interior were observed, this exsolution-free zone was avoided for bulk metal analyses with a broad electron beam. When performing image analysis on metal phases exhibiting exsolutions of heavy elements that are visible around the metal sphere in a backscattered electron image, the rim was taken into account as part of the exsolution-free metal matrix.

Samples H3455a and b resulted from an experiment that was performed at 11 GPa and 2652 K with the element of interest Pb being added to the starting silicate powder rather than to the starting metal powder. A further experiment was performed at the same conditions (11 GPa and 2650 K), but, as usual, Pb was initially hosted by the metal phase (H3449b). As can be read from Table 13, Chapter 5, the exchange coefficients of all three samples agree within error with one another, showing that the choice of metal being the initial host phase of the elements of interest did not influence the outcome of the experiments.

3.1 Data treatment

3.1.1 Metal

The concentrations of all elements in the metal phase of each sample were obtained as mass percentages from the electron probe micro-analyser (EPMA) measurements. The results are displayed in Table A1 in the appendix together with the number of the averaged analyses, the beam diameters and an indication if image analyses have been performed (see below).

For each sample the results of 20 to 77 analyses have been converted into molar values and renormalized and averaged. Errors were obtained as 1 σ standard deviations.

As mentioned above the metal phases occasionally exhibit exsolutions that are enriched in heavy elements (see Figure 17). These have separated from a homogeneous metallic liquid during quenching (Gessmann et al., 1998; O´Neill et al., 1998). When determining liquid metal – liquid silicate partition or exchange coefficients it is thus important to integrate these exsolutions into the bulk metal composition. As mentioned earlier these blobs that are enriched in heavy elements such as Ag and Pb are often uniformly distributed over the whole metal sphere. However occasionally they were found to be enriched at the rim of the metal phase. In these cases exsolutions and metal matrix were analysed separately (see Chapter 2, Section 2.2.1.1).

Subsequent calculations of the bulk metal composition were then based on image analysis, which have been performed using the public domain software ImageJ: Based on several backscattered electron images the areal proportions of exsolved blobs and metal matrix have

been investigated. In agreement with Gessmann et al. (1998) and O´Neill et al. (1998) it has been assumed that the areal proportions are identical to the volumetric fractions of the individual phases. Taking into account these individual proportions and the densities of each phase, calculated as the ratio of the average molar mass and average molar volume, the bulk metal composition has been recalculated in form of mass percentages. Subsequently all values have been converted into renormalized molar abundances.

Errors have been calculated by error propagation taking into account the standard deviations of exsolutions and metal matrix analyses as well as the standard deviations of the image analyses.

3.1.2 Ferropericlase

As with the metal analyses the concentrations of all elements in the ferropericlase phases were obtained as mass percentages. Table A2 in the appendix provides the results of the ferropericlase analyses, the associated errors and the number of the averaged measurements.

In order to obtain reliable concentrations of especially FeO and MgO in the ferropericlase phase the individual results of 15 to 59 analyses have been converted into renormalized molar oxide values and been averaged. The corresponding errors have been calculated as 1 σ standard deviations.

3.1.3 Silicate

Table A3 in the appendix provides the results of the silicate analyses, the associated errors and the number of the averaged measurements. The major element concentrations of the silicate phase have been obtained by the laser ablation inductively coupled plasma mass spectrometry (LAICPMS) as weight percentages of their corresponding oxides, whereas the abundances of the elements of interest were initially received in ppm. The bulk silicate composition has subsequently been converted into renormalized molar oxide values.

Typically 4 to 6 analyses were averaged. As for the metal and ferropericlase analyses, errors have been calculated as 1 σ standard deviations.

3.2 Primary calculations

3.2.1 Partition and exchange coefficients

There are two ways of describing the liquid metal – liquid silicate partitioning behaviour of siderophile elements: either in form of a partition coefficient $D^{met\text{-}sil}$ or by an exchange coefficient K_D^{M-Fe}.

As shown in equation [3] partition coefficients $D^{met\text{-}sil}$ are defined as the molar ratio of the concentration of an element *M* in the metal phase to its concentration in the silicate phase. In the silicate phase the molar abundance of the element of interest *M* refers to an one cation based oxide, which necessitates assumptions about the valence *n* of the element of interest *M* (see below):

$$D^{met-sil} = \frac{X_M^{met}}{X_{MO_{\frac{n}{2}}}^{sil}} \qquad [3]$$

However partitioning can also be understood as an exchange reaction that involves Fe and FeO:

$$MO_{\frac{n}{2}}^{sil} + \frac{n}{2}\, Fe^{met} = M^{met} + \frac{n}{2}\, FeO^{sil} \qquad [4]$$

Exchange coefficients K_D^{M-Fe} can be defined by the respective mole fractions of each phase with respect to the valence *n* of the element *M* as follows:

$$K_D^{M-Fe} = \frac{X_M^{met} \left(X_{FeO}^{sil}\right)^{\frac{n}{2}}}{X_{MO_{\frac{n}{2}}}^{sil} \left(X_{Fe}^{met}\right)^{\frac{n}{2}}} = \frac{D_M^{met-sil}}{\left(D_{Fe}^{met-sil}\right)^{\frac{n}{2}}}$$

[5]

Contrary to the equilibrium constant *K* the exchange coefficient K_D^{M-Fe} does not include the activities of the individual components. K_D^{M-Fe}-values can thus be understood simply as a normalization of the partition coefficient $D^{met\text{-}sil}$ of element *M* to the partition coefficient of Fe with the latter being raised to the power of half of the valence of the element *M*. Equation [5] once more clarifies the importance of knowledge of the valence state of the element *M*.

By normalizing partition coefficients to that for Fe, the liquid metal – liquid silicate partitioning behaviour can be described independently of oxygen fugacity, thus simplifying the comparison of results from different data sets.

How partition and exchange coefficients depend thermodynamically on pressure and temperature as well as on the composition of the metal phase which will be shown in detail in Chapters 4 to 6.

3.2.2 Oxygen fugacity relative to the iron-wüstite buffer

A critical parameter of all partitioning experiments is the oxygen fugacity of the sample, which can be computed relative to the iron-wüstite buffer from the composition of ferropericlase in the sample due to the equilibrium:

$$2\,Fe + O_2 = 2\,FeO$$

[6]

Calculations were based on the following equation that has been derived by Mann et al. (2009):

$$\Delta IW = 2\log\left(\frac{X_{FeO}^{fp}}{X_{Fe}^{met}}\right) + \frac{2\,W_{FeMg}^{fp}\left(1 - X_{FeO}^{fp}\right)^2}{R\,T\ln(10)} \quad [7]$$

The definition of the Margueles interaction parameter W_{FeMg}^{fp} was adopted from Frost (2003) as:

$$W_{FeMg}^{fp} = 11000 + 0.011\,P \quad [8]$$

In equation [7] X_{FeO}^{fp} and X_{Fe}^{met} stand for the mole fractions of FeO in ferropericlase and Fe in metal respectively, *R* is the gas constant and *T* denotes the temperature in K. The calculation of the Margueles interaction parameter W_{FeMg}^{fp} involves pressure (P) in bar. Equation [7] is based on the equilibrium constant of equation [6] and furthermore assumes the validity of Raoult´s Law for the metal, thus implying a value of 1 for the activity coefficient of Fe in the metal phase. Uncertainties on *ΔIW* were calculated by error propagation taking into account the standard derivations of the metal and ferropericlase values as well as uncertainties of 1 GPa and 100 K on the pressure and temperature values respectively that were reached during the experiments.

In the case of S-bearing samples the mole fraction of Fe in the metal phase was reduced by the value of the mole fraction of S, that means by the amount of Fe necessary to form FeS. Oxygen fugacities have not been calculated for samples in which the metal phase contained a higher mole fraction of S than of Fe.

4. The dependence of volatile element partitioning on oxygen fugacity and Si contents of the Fe metal: Implications for the valence states of volatile elements in the silicate liquid

4.1 Introduction

Recent core formation models are based on multistage core formation scenarios in which pressure and temperature change through time. In addition the composition of the accreting matter is believed to have varied from initially reduced to more oxidized at the end of the Earth´s accretion. Linked with the composition of the accreting material is the oxidation state of the Earth meaning that oxygen fugacity additionally varied over the time of accretion.

As already introduced in the first Chapter, Wade and Wood (2005) incorporated an increase in oxygen fugacity of two logarithmic units into their continuous core formation model. As a result, the abundances of the elements Ni, Co, W and V in the Earth´s mantle could be explained when the temperatures of core formation at the base of a magma ocean are fixed along the peridotitic liquidus. However Wade and Wood (2005) argued that the main mechanism that caused the Earth´s mantle to oxidize is the crystallization of perovskite rather than the addition of oxidized material to the accreting Earth alone. According to the authors magnesium silicate perovskite is capable of incorporating Al^{3+} and Fe^{3+} instead of Mg^{2+} and Si^{4+}. This substitution mechanism is enhanced by the disproportionation of Fe^{2+} into Fe^{3+} and native Fe (Frost et al. 2004). Subsequently the produced Fe can be extracted to the Earth´s core and thus cause an increase in the oxidation state of the mantle, but it has been shown by Frost et al. (2008) that this mechanism is only efficient in the late stages of accretion, when the amount of accreting Fe metal is too low to cause the disproportionation reaction to be reversed. Frost et al. (2008) furthermore showed that the metal – silicate partitioning behaviour of Si predicts significant dissolution of Si into the Earth´s core which results in increased FeO contents and with it oxidation of the Earth´s mantle due to the exchange reaction:

$$SiO_2^{sil} + 2Fe^{met} = Si^{met} + 2FeO^{sil} \quad [9]$$

In the study of Rubie et al. (2011) the oxidation state of the Earth´s mantle is increased by varying the material that accreted to the growing Earth and also by the reaction displayed in equation [9]. Here the first 60 – 70 wt% of the Earth was composed of highly-reduced material, which was complemented by the later addition of more oxidized material. The authors found that the abundances of Ni, Co and W in the Earth´s mantle can only be explained in the case of some extent of disequilibrium between the cores of late impactors and the Earth´s mantle. In the course of their investigations Rubie et al. (2011) found the Earth´s core to contain 8 wt% Si together with 5 wt% Ni, 0.5 wt % O and 2 wt% S.

As shown by the above studies, the investigation of the metal – silicate partitioning behaviour of siderophile elements can constrain the conditions that prevailed during the formation of the Earth´s core. It is thus important to investigate the dependence of siderophile element partitioning on oxygen fugacity, which in addition can provide information about the valence state *n* of the element of interest *M* when dissolved in silicate liquid.

Knowledge of elemental valences in turn is crucial when the partitioning behaviour of element *M* is described by an exchange coefficient K_D^{M-Fe}. The latter facilitates the comparison of partitioning data that were obtained at various oxygen fugacity conditions, since K_D^{M-Fe} is a normalization of the partition coefficient $D^{met\text{-}sil}$ of the element of interest *M* to the partition coefficient $D^{met\text{-}sil}$ of Fe with the latter being raised to the power of half of the valence of the element of interest in the silicate phase (see Chapter 3, equation 5). Furthermore K_D^{M-Fe} values are used to extrapolate experimental partitioning data to higher pressures and temperatures that are assumed in most core formation models.

To date the generalized approach of determining valence states from partitioning experiments is based on an oxidation reaction of the element *M*:

$$MO_{\frac{n}{2}}^{sil} = M^{met} + \frac{n}{4} O_2 \qquad [10]$$

The equilibrium constant of equation [10] is defined as:

$$K = \frac{a_M^{met} \left(f_{O_2}\right)^{\frac{n}{4}}}{a_{MO_{\frac{n}{2}}}^{sil}} = \frac{X_M^{met} \gamma_M^{met} \left(f_{O_2}\right)^{\frac{n}{4}}}{X_{MO_{\frac{n}{2}}}^{sil} \gamma_{MO_{\frac{n}{2}}}^{sil}}$$

[11]

The conversion into logarithmic values leads to:

$$\log K = \log \frac{X_M^{met}}{X_{MO_{\frac{n}{2}}}^{sil}} + \log \frac{\gamma_M^{met}}{\gamma_{MO_{\frac{n}{2}}}^{sil}} + \frac{n}{4} \log fO_2$$

[12]

Together with the definition of the partition coefficient $D^{met\text{-}sil}$ as the ratio of the molar concentration of the element *M* in the metal phase to its molar concentration in the silicate phase and the assumption that the activities of the individual components remain constant at isobaric and isothermal conditions, equation [12] can be rearranged to the following expression that gives the dependence of the partitioning behaviour of an element *M* on oxygen fugacity which is expressed relative to the iron-wüstite buffer:

$$\log D = -\frac{n}{4} \Delta IW + const. \qquad [13]$$

In a diagram of logarithmic partition coefficient values against logarithmic oxygen fugacity expressed relative to the iron-wüstite buffer the slope of the corresponding regression line equals one quarter of the valence of the element of interest *M* in the silicate phase. Equation [13] also shows that the metal – silicate partitioning behaviour of an element with a high valence state is more strongly affected by changes in oxygen fugacity than the partitioning behaviour of low-valence elements.

By employing this approach a number of studies have addressed the valence state of mostly refractory siderophile elements:

Capobianco et al. (1994) determined a valence of 1+ for Ag and Sn based on solubility experiments in a gas mixing furnace at 1293 °C and partitioning experiments at 1260 °C respectively. These authors could not completely exclude the presence of a zero-valence Ag-species in the silicate melt. Gessmann et al. (1999) investigated the partitioning behaviour of Ni, Co, Mn, Cr, V and Si between liquid metal and magnesiowüstite at pressures and

temperatures of 9 – 18 GPa and 2200 °C respectively. This study showed that Co, Mn and V are divalent, Si is tetravalent and that Ni and Cr have valence states of 1.5+ and 2.5+ respectively. The mixed valences of Ni and Cr are, according to the authors, most likely caused by non-ideal mixing behaviour of these elements in the metal and/or magnesiowüstite phase, meaning that the corresponding activity coefficients might not be constant over the experimental range of condition. The investigations of Capobianco et al. (1999) that were based on experiments performed at 1 atm and at oxygen fugacity between -1.3 and +3.8 logarithmic units relative to the iron-wüstite buffer led to the conclusion that Ge is present as GeO_2 in the silicate. Mann et al. (2009) determined the liquid metal – liquid silicate partitioning behaviour of a wide range of elements at pressures and temperatures between 2 – 24 GPa and 2023 – 2873 K respectively. The results indicate a 1+ valence state for In, the elements Zn, Ga, Mn and Cr were found to be divalent, V and Si had valence states of 3+ and 4+ respectively, whereas Nb and Ta both exhibited a 5+ valence state. Kegler et al. (2009) report that Cu has a valence of 0.76+ in the silicate phase of partitioning experiments that were performed at 0.5 GPa and 1350 °C. The investigations of the partitioning behaviour of Ge at comparatively low pressures of 0.5 GPa and temperatures of 1350 °C by Kegler and Holzheid (2011) resulted in a valence of 2+ for Ge within an oxygen fugacity range of -0.9 to -2.7 logarithmic units relative to the iron wüstite buffer which is in disagreement with the results of Capobianco (1999) of a GeO_2 species in the silicate phase (see above). Therefore Kegler and Holzheid (2011) argue for a change in the valence state of Ge close to the iron-wüstite buffer. Siebert et al. (2011) characterized the siderophile elements Ni, Co, Mn, Cr and Zn as divalent and V, Ga and Ge as trivalent. The elements Mo and W exhibited valence states of 4.1+ and 4.4+ respectively and P, As and Nb had a valence of 5+. The liquid metal – liquid silicate partitioning behaviour of highly siderophile elements has been investigated by Mann et al. (2012). The authors determined a valence of 2+ for the elements Ru, Rh, Re and 1+ for Pt and Pd.

When determining valence states, oxygen fugacity is often decreased by adding Si to the Fe metal. But as will be shown below Si can affect the partitioning behaviour and with it the determination of valence states. In the framework of this study it was found that the presence of Si in the metal phase significantly lowers the partition coefficients of all elements studied (compare Section 4.3). Thus the amount of Si and its interaction with the element of interest *M* have to be taken into account when determining valence states on the basis of experiments that exhibit significant amounts of Si in the metal phase, the procedure of which is explained in detail further below.

To date the effects of Si on the metal-silicate partition coefficients of siderophile elements have been investigated for a wide range of non-volatile elements, namely Ni, Co, Mo, W, V, Cr and Nb, by Tuff et al. (2011). The metal – silicate partitioning experiments of their study were performed at 1.5 GPa and 6 GPa at temperatures of 1923 K and 2123 K. Tuff et al. (2011) found that the partitioning of Ni, Co, Mo, W and V is affected by increasing Si contents in the metal by lowering their metal-silicate partition coefficients. On the other hand the partitioning of Cr and Nb was found to not depend on the presence of Si in the metal. Thus if Si contributes to the Earth´s core density deficit the elements Ni, Co, Mo, W and V behave more lithophile than in the case of a Si-free metal what means that these elements were extracted from the Earth´s mantle to a lesser extent than in the case of a pure Fe metal. Tuff et al. (2011) conclude that if Si is present in the liquid metal that formed the Earth´s core the pressures that prevailed during core formation are 5 GPa lower than the estimated pressures that are derived from studies based on a Si-free metallic liquid.

It is thus important to understand the effect of Si, when dissolved in liquid Fe, on the partitioning behaviour of siderophile elements because many studies have shown that Si might be the main abundant light element in the Earth`s core that contributes to its density deficit (e.g. Rubie et al., 2011; Fischer et al., 2012; Fischer et al., 2013; Siebert et al., 2013). In order to quantify the abundances of Si and O in the Earth´s core Ricolleau et al. (2011) have recently performed high pressure metal – silicate partitioning experiments of these two elements. The authors found that O becomes more siderophile with increasing oxygen fugacity, pressures and temperatures. In the case of Si the same tendency has been observed for pressure and temperature, but its siderophility increases with decreasing oxygen fugacity. By incorporating their results into a continuous core formation model Ricolleau et al. (2011) conclude that the Earth´s core cannot contain more than 2.5 wt% O while the Si abundance might lie between 1 and 11 wt% and that several combinations of Si and O contents could explain the Earth´s core density deficit. However Tsuno et al. (2013) clarified that at high temperatures O dissolved in the liquid Fe metal leads to an increase on the siderophile behaviour of Si. In contrast to low temperature conditions O and Si are not any longer mutually exclusive as has been assumed by previous studies (e.g. O´Neill et al., 1998). If equilibration between the core forming metal and the silicate Earth took place at pressures ad temperatures of 45 – 55 GPa and > 3300 K respectively similar concentrations of both Si and O can account for and even exceed the Earth´s core density deficit. In the latter case a Si and O rich layer might have formed in the upper region of the outer core that in turn could enrich the base of the lower mantle in SiO_2 and FeO concentrations when temperatures decrease.

4.2 Methods

All experiments as well as the analyses of the metal, ferropericlase and silicate phases have been performed according to the routines described in Chapter 2. For the investigation of the effect of fO_2 and the amount of Si in the metal phase on the liquid metal – liquid silicate partitioning behaviour of volatile elements, high pressure – high temperature experiments have been performed at 11 GPa and approximately 2600 K in the multi anvil apparatus. In this study the liquid metal – liquid silicate partitioning behaviours of the volatile elements Sn and Pb and the moderately volatile elements Ag, Cu, Ge, Sb, As, Au and P have been investigated. The determinations of the effects of changing fO_2 and the Si contents in the metal phase on the partitioning behaviour also enabled the valence states of the elements to be determined.

The partitioning of an element *M* between liquid metal and liquid silicate can be described by a molar partition coefficient $D^{met\text{-}sil}$:

$$D^{met-sil} = \frac{X_M}{X_{MO_{\frac{n}{2}}}} \qquad [14]$$

where *n* denotes the valence of the element of interest in the silicate phase. The partitioning of the element *M* between liquid metal and liquid silicate can furthermore be expressed by an exchange reaction that involves Fe:

$$\frac{n}{2}\, Fe^{met} + MO_{\frac{n}{2}}^{sil} = \frac{n}{2}\, FeO^{sil} + M^{met} \qquad [15]$$

From this equation, the equilibrium constant *K* is defined as:

$$K = \frac{X_M^{met}\, \gamma_M^{met} \left(X_{FeO}^{sil}\, \gamma_{FeO}^{sil}\right)^{\frac{n}{2}}}{X_{MO_{\frac{n}{2}}}^{sil}\, \gamma_{MO_{\frac{n}{2}}}^{sil}\, \left(X_{Fe}^{met}\, \gamma_{Fe}^{met}\right)^{\frac{n}{2}}} \qquad [16]$$

In equation [16] X denotes the molar fractions of components in the individual phases, γ are the activity coefficients and n is the valence of the element of interest M. The equilibrium constant K can further be simplified by assuming that the activity coefficients in the silicate phase remain constant over the narrow range of silicate compositions in our experiments. Incorporating this assumption, the expression for K becomes:

$$K = \frac{X_M^{met}\,\gamma_M^{met}\left(X_{FeO}^{sil}\right)^{\frac{n}{2}}}{X_{MO_{\frac{n}{2}}}^{sil}\,\left(X_{Fe}^{met}\,\gamma_{Fe}^{met}\right)^{\frac{n}{2}}} \qquad [17]$$

At chemical equilibrium the Gibbs free energy change ΔG^0 can be related to the equilibrium constant K as follows:

$$\Delta G^0 = -RTlnK \qquad [18]$$

Together with the definition of the partition coefficient, the equilibrium constant K and the assumptions that the activity coefficients of the oxides in the silicate phase are constant and may be neglected, equation [18] can be rearranged to

$$\log D^{met-sil} = \frac{-\Delta G^0}{RT\ln(10)} - \log(\gamma_M^{met}) - \frac{n}{2}\log\left(X_{FeO}^{sil}\right) + \frac{n}{2}\log(X_{Fe}^{met}\,\gamma_{Fe}^{met}) \qquad [19]$$

The activities of Fe and the element of interest M in the metal phase have been calculated employing the ε-model as formulated by Ma et al. (2001). The general expression for calculating activities of Fe (solvent: 1) and of any solute i among a number of N solutes in Fe-bearing metallic solutions is given by equation [20] and [21] respectively.

$$ln\gamma_1 = \sum_{i=2}^{N} \varepsilon_i^i \left(X_i + ln(1 - X_i)\right) - \sum_{j=2}^{N-1} \sum_{k=j+1}^{N} \varepsilon_j^k X_j X_k \left(1 + \frac{ln(1 - X_j)}{X_j} + \frac{ln(1 - X_k)}{X_k}\right)$$
$$+ \sum_{i=2}^{N} \sum_{\substack{k=2 \\ (k \neq i)}}^{N} \varepsilon_i^k X_i X_k \left(1 + \frac{ln(1 - X_k)}{X_k} - \frac{1}{1 - X_i}\right)$$
$$+ \frac{1}{2} \sum_{j=2}^{N-1} \sum_{k=j+1}^{N} \varepsilon_j^k X_j^2 X_k^2 \left(\frac{1}{1 - X_j} + \frac{1}{1 - X_k} - 1\right)$$
$$- \sum_{i=2}^{N} \sum_{\substack{k=2 \\ (k \neq i)}}^{N} \varepsilon_i^k X_i^2 X_k^2 \left(\frac{1}{1 - X_i} + \frac{1}{1 - X_k} + \frac{X_i}{2(1 - X_i)^2} - 1\right)$$

[20]

$$ln\gamma_i = ln\gamma_i^0 - \varepsilon_i^i \, ln(1 - X_i) - \sum_{\substack{k=2 \\ (k \neq i)}}^{N} \varepsilon_i^k X_k \left(1 + \frac{ln(1 - X_k)}{X_k} - \frac{1}{1 - X_i}\right)$$
$$+ \sum_{\substack{k=2 \\ (k \neq i)}}^{N} \varepsilon_i^k X_k^2 X_i \left(\frac{1}{1 - X_i} + \frac{1}{1 - X_k} + \frac{X_i}{2(1 - X_i)^2} - 1\right)$$

[21]

The interaction parameter ε_i^k describes the influence on the activity of a given element i as a function of the concentration of another element *k* dissolved in Fe metal. The parameter γ_i^o is the activity of the element *i* at infinite dilution and *X* is the mole fraction of the individual components in Fe metal. Equations [20] and [21] have been solved for a three-component system with Fe (solvent) and Si and the element of interest *M* being solutes:

$$ln\gamma_{Fe} = \varepsilon_{Si}^{Si} \left(X_{Si} + ln(1 - X_{Si})\right) + \varepsilon_M^M \left(X_M + ln(1 - X_M)\right)$$
$$+ \varepsilon_M^{Si} X_{Si} X_M \left(1 - \frac{1}{1 - X_M} - \frac{1}{1 - X_{Si}}\right)$$
$$- \frac{\varepsilon_M^{Si}}{2} X_{Si}^2 X_M^2 \left(\frac{3}{1 - X_M} + \frac{3}{1 - X_{Si}} + \frac{X_{Si}}{(1 - X_{Si})^2} + \frac{X_M}{(1 - X_M)^2} - 3\right)$$

[22]

$$ln\gamma_M = ln\gamma_{Fe} + ln\gamma_M^0 - \varepsilon_M^M \, ln(1 - X_M) - \varepsilon_M^{Si} \, X_{Si} \left(1 + \frac{ln(1 - X_{Si})}{X_{Si}} - \frac{1}{1 - X_M}\right) + \varepsilon_M^{Si} \, X_{Si}^2 \, X_M \left(\frac{1}{1 - X_M} + \frac{1}{1 - X_{Si}} + \frac{X_M}{2(1 - X_M)^2} - 1\right)$$

[23]

By the use of these equations the partition coefficient $D^{met\text{-}sil}$ values have been recalculated on the assumption of a constant ΔG^0 value within the suite of isobaric and isothermal experiments in this study. ΔG^0 has initially been calculated for an experiment whose starting metal was free of Si and FeO components. According to the Steelmaking Data Sourcebook an interaction parameter ε_i^k equals the interaction parameter ε_k^i. However in the Steelmaking Data Sourcebook mass related e_i^k values are listed which can be converted into interaction parameter values ε_i^k by employing equation [24] in which M_k denotes the molar mass of element *k*:

$$e_i^k = 0.00434 \left[\left(\varepsilon_i^k - 1\right) \frac{55.85}{M_k} + 1\right]$$

[24]

When available the values for the activities at infinite dilution and the individual interaction parameters ε_i^k were derived from the values given in the Steelmaking Data Sourcebook in order to calculate $ln\gamma_M$ and $ln\gamma_{Fe}$ (equations [22] and [23]). If the values were not available for certain elements they were set to zero. However because the terms ε_M^M, ε_{Si}^{Si} and γ_M^0 in equations [22] and [23] have no significant compositional dependence they are essentially constant at given pressure and temperature. If unknown and thus set to zero they can therefore be added to the ΔG^0 term and they simply become part of the refinement of ΔG^0, which we continue to refer to as ΔG^0 for simplicity. Table 7 summarizes the values obtained from the Steelmaking Data Sourcebook that are used in the calculations of this study.

Table 7: *Summary of interaction parameter values* $\boldsymbol{\varepsilon_i^k}$ *and activity coefficients at infinite dilution* $\boldsymbol{\gamma_i^0}$ *that were used to calculate the activity coefficients of Fe and the element of interest M in the metal. All values were derived from the Steelmaking Data Sourcebook (see text).*

	Cu	**Ag**	**Au**	**Pb**	**Sn**	**Ge**	**Sb**	**As**	**P**	**Si**
$\boldsymbol{\gamma_M^0}$	8.58	200	-	837	2.58	-	-	-	-	-
$\boldsymbol{\varepsilon_M^M}$	-5.38	-18.73	-	-	-0.29	1.80	-	-	7.35	12.43

These values however refer to a temperature of 1873 K. Temperature corrections have been performed following Tuff et al. (2011).

$$\varepsilon_i^j\ (T) = \frac{1873}{T}\ \varepsilon_i^j\ (1873) \qquad [25]$$

The individual interaction parameters ε_{Si}^M were fitted by minimizing the sum of the weighted deviation between experimentally determined and calculated log $D^{met-sil}$ values. The sum of the weighted deviations was calculated by employing equation [26] where $\delta \log D^{met-sil^{(exp)}}$ denotes the error on the experimentally investigated logarithmic exchange coefficients as calculated by error propagation:

$$\sigma = \sum \sqrt{\left(\frac{\left(D^{met-sil^{(calc)}} - D^{met-sil^{(exp)}} \right)}{\left(\frac{100\ \delta\ D^{met-sil^{(exp)}}}{D^{met-sil^{(exp)}}} \right)^2} \right)^2} \qquad [26]$$

The quantification of the ε_M^{Si} values has been performed for different possible valence states and subsequently the individual deviations as calculated by equation [26] have been compared. The lowest value of σ obtained represents the best fit between the calculated (equation [19]) and experimental $D^{met\text{-}sil}$ values.

In order to give some comparability between different elements the deviations obtained by equation [26] have been normalized to the number of experiments and to the calculated

logarithmic $D^{met\text{-}sil}$ value of the experiment that has initially been employed to estimate ΔG^0. This normalized residual function will during the further procedure be abbreviated with *NR*.

The derived interaction parameter values ε_M^{Si} likewise refer to a temperature of 1873 K comparable to the mass related interaction parameters e_i^j in the Steelmaking Data Sourcebook. As mentioned above temperature corrections were performed following Tuff et al. (2011) employing equation [25].

4.3 Results

For each element Table 8 summarizes the experimental conditions, the experimentally determined as well as the calculated partition coefficient values $D^{met-sil}$, the exchange coefficient values K_D^{M-Fe} that were calculated on the basis of the derived valence states for the individual elements and the oxygen fugacity relative to the IW buffer. Uncertainties that were obtained by error propagation are given for the last digit(s).

Table 8: *Summary of experimental conditions, experimental and recalculated partition coefficient values $D^{met\text{-}sil}$, exchange coefficients, Si metal contents (mole fractions) and oxygen fugacity relative to the IW buffer. Pressures and temperatures are given in GPa and K respectively. Values in brackets represent uncertainties for the last digit(s) that were obtained via error propagation.*

Exp.	P	T	D_{Sn}^{exp}	D_{Sn}^{calc}	K_D^{Sn-Fe}	D_{Sb}^{exp}	D_{Sb}^{calc}	K_D^{Sb-Fe}	D_{Ge}^{exp}	D_{Ge}^{calc}	K_D^{Ge-Fe}	X_{Si}^{met}	ΔIW
H3707a	11	2641	198 (44)	198	2.4 (5)	7778 (1849)	7774	21 (6)	1231 (257)	1231	15 (3)	-	-2.2 (2)
H3707b	11	2641	643 (83)	643	0.11 (3)	14906 (4137)	14906	0.14 (7)	4833 (1261)	4833	0.8 (3)	0.210 (3)	-4.7 (4)
H3718a	11	2658	228 (48)	173	3.0 (7)	19884 (4972)	6611	61 (18)	2192 (478)	1093	29 (7)	-	-2.1 (2)
H3718b	11	2658	864 (218)	1445	0.8 (2)	52724 (18934)	47163	5 (2)	7183 (2082)	6209	7 (2)	0.0766 (8)	-3.7 (2)
Z926a	11	2668	202 (58)	187	2.4 (8)	15383 (4876)	7035	43 (16)	1864 (603)	1149	23 (8)	-	-2.4 (4)
Z926b	11	2668	315 (118)	222	3 (1)	12855 (4961)	8367	32 (13)	2302 (726)	1297	25 (8)	-	-2.2 (2)

Exp.	P	T	D_{Cu}^{exp}	D_{Cu}^{calc}	K_D^{Cu-Fe}	D_{Pb}^{exp}	D_{Pb}^{calc}	K_D^{Pb-Fe}	D_{Ag}^{exp}	D_{Ag}^{calc}	K_D^{Ag-Fe}	X_{Si}^{met}	ΔIW
H3707a	11	2641	33 (4)	33	8 (1)	-	-	-	-	-	-	-	-2.2 (2)
H3707b	11	2641	136 (16)	136	8 (1)	-	-	-	-	-	-	0.210 (3)	-4.7 (4)
H3718a	11	2658	32 (3)	32	7.6 (8)	-	-	-	-	-	-	-	-2.1 (2)
H3718b	11	2658	75 (9)	74	7.3 (9)	-	-	-	-	-	-	0.0766 (8)	-3.7 (2)
Z926a	11	2668	32 (4)	33	7 (1)	-	-	-	-	-	-	-	-2.4 (4)
Z926b	11	2668	38 (4)	35	8.5 (9)	-	-	-	-	-	-	-	-2.2 (2)
Z919a	11	2605	-	-	-	26 (13)	26	1.1 (5)	-	-	-	-	-2.4 (2)
H3704a	11	2639	-	-	-	57 (56)	46	0.2 (2)	-	-	-	0.205 (2)	-4.5 (3)
H3704b	11	2639	-	-	-	56 (29)	56	0.4 (2)	-	-	-	0.118 (1)	-3.8 (3)
Z919b	11	2605	-	-	-	20 (16)	20	1.1 (9)	-	-	-	-	-2.1 (2)
Z920b	11	2580	-	-	-	24 (18)	24	1.1 (8)	-	-	-	-	-2.3 (3)
H3444a	11	2609	-	-	-	-	-	-	23 (17)	23	5 (3)	-	-2.03 (8)
H3444b	11	2609	-	-	-	-	-	-	23 (9)	25	5 (2)	-	-2.3 (3)
Z915a	11	2584	-	-	-	-	-	-	31 (16)	31	3 (2)	0.114 (1)	-4.2 (6)
Z915b	11	2584	-	-	-	-	-	-	44 (49)	32	2 (2)	0.259 (2)	-4.7 (3)
Z916a	11	2580	-	-	-	-	-	-	23 (17)	24	5 (4)	-	-2.5 (3)
Z922a	11	2588	-	-	-	-	-	-	25 (14)	23	5 (3)	-	-2.5 (4)
Z922b	11	2588	-	-	-	-	-	-	21 (10)	21	5 (2)	-	-1.97 (9)

Table 8 continued

Exp.	P	T	D_{Au}^{exp}	D_{Au}^{calc}	K_D^{Au-Fe}	D_{As}^{exp}	D_{As}^{calc}	K_D^{As-Fe}	D_P^{exp}	$D_P^{calc}*$	$K_D^{P-Fe}*$	X_{Si}^{met}	ΔIW
Z1000b	11	2612	6811 (2238)	6811	212 (70)	20779 (11537)	20772	4 (2)	52 (7)	52	0.009 (1)	-	-2.7 (3)
Z1002b	11	2602	12741 (5701)	12384	130 (59)	83490 (22516)	83490	0.9 (3)	531 (289)	361	0.006 (3)	0.043 (2)	-3.5 (2)
Z1008b	11	2614	13289 (5078)	5132	524 (203)	58510 (15328	10328	18 (6)	144 (53)	29	0.04 (2)	-	-2.9 (7)
Z1011a	11	2605	7266 (3578)	3370	455 (226)	32250 (12136)	3480	32 (13)	129 (51)	9	0.13 (5)	-	-2.1 (3)
Z1019b	11	2624	5218 (3828)	5557	10 (8)	13898 (5747)	7293	0.002 (1)	379 (101)	379	0.00007 (2)	0.214 (3)	-4.8 (4)
Z1000a	11	2612	3329 (3802)	6025	117 (139)	2335 (3937)	12306	1 (1)	26 (8)	38	0.006 (5)	-	-2.7 (4)
Z1002a	11	2602	8060 (3356)	8060	26 (12)	-	-	-	-	-	-	0.158 (3)	-4.5 (1)

* D_P^{calc} values and K_D^{P-Fe} values are calculated based on the assumption of a 5^+ valence state. For details see text.

4.3.1 Metal – Silicate partition coefficients $D^{met\text{-}sil}$

Experimental data have been compared to literature data sets when available. In previous studies partition coefficients have often been calculated on the basis of mass and additionally the method of determining oxygen fugacity shows differences between individual studies. Therefore these parameters have been recalculated from the analytical results that have been published by the individual authors. Out of a given data set comparable experiments have been carefully selected on the basis of similar experimental conditions as well as consistency between the composition of metal and silicate phases and the capsule material. However due to the limited amount of experimental partitioning studies for volatile elements, the results have additionally been compared to data that were obtained in experiments with slightly different compositions and capsule material, when other conformable investigations were not available.

The experimental and recalculated results (equation [19]) are shown in Figures 19a – 27a together with comparable experimental data from the literature. In these plots logarithmic partition coefficient values of the individual elements have been plotted against logarithmic oxygen fugacity relative to the iron-wüstite buffer. Half-filled symbols represent experiments from literature datasets that were conducted in graphite capsules. For each element studied the fitted partitioning trend matches the experimental observations very well. Concerning the data points from the literature one should note that in contrast to the suite of isobaric and isothermal experiments of this study, previous results have often been determined at different pressure and temperature conditions as indicated in Figures 19a to 27a.

Figures 19b – 27b show the normalized residual functions (*NR*) for various valence states of the individual elements. The lowest value represents the best fit and thus indicates the valence of the element of interest in the silicate phase.

The derived interaction parameters ε_{Si}^{M} of each element refer to a temperature of 1873 K. Temperature corrections were performed employing equation [25].

4.3.1.1 Monovalent elements copper and silver

The comparison of the summed and normalized deviations (*NR*) between experimental and recalculated partition coefficient values shows a clear minimum at a valence state of 1+ in the silicate phase for the element Cu (Figure 19b). The partitioning of copper is thus little affected by changes in oxygen fugacity that might have occurred during accretion of the Earth. The interaction parameter ε_{Cu}^{Si} was determined to be 0.73. This relatively small interaction parameter testifies to a small influence of the metal Si content on the partitioning behavior of this element – in other words the siderophility of Cu is hardly affected by the presence of Si in the metal. The results for the volatile element Cu are compared with data from Corgne et al. (2008), Wood et al. (2008) and Righter et al. (2010) in Figure 19a. Agreement between the dataset of this study and those from the literature was found for the latter two publications, whereas the first one results in slightly lower logarithmic partition coefficient values. This might be caused by different pressure and temperature conditions as well as by the fact that the experiments of Corgne et al. (2008) were performed in C-capsules. It is well known that the presence of C - another element that possibly accounts for the Earth´s core density deficit (e.g. Poirier, 1994) - in the metallic liquid can influence the partitioning behaviour of siderophile elements (e.g. Mann et al., 2009). From the Steelmaking Data Sourcebook a positive interaction parameter between C and Cu can be derived, that implies that C in the Fe-rich metal causes a decrease in siderophility for the element Cu.

Similar results have been obtained for the siderophile element Ag. The normalized residual function *NR* shows a minimum at a valence of 1+ with an interaction parameter ε_{Si}^{Ag} of 6.42. When comparing the experimental data for Ag to the work of Wheeler et al. (2011) it was found that the results are not in good agreement with one another. This might be caused by the fact that the experiments of Wheeler et al. (2011) have been performed at lower pressures and temperatures of 2 GPa and 2273 K respectively (see Chapter 5). However the observations of this study are in perfect agreement with the derivations of Capobianco et al (1994) that were based on solubility experiments of Ag in a gas mixing furnace at 1566 K. The latter authors could not exclude a possible contribution of a zero-valence Ag species in the silicate phase. The comparison of the *NR* values obtained for various valence states in this study indeed shows a minimum at a valence of 1+, yet similarly the difference in *NR* values between a 1+ valence and a zero-valence species is not very distinct. All experimental and recalculated data of this study, the results of Wheeler et al. (2011) and the deviation trend between experimental and recalculated data are shown in Figures 20a and 20b.

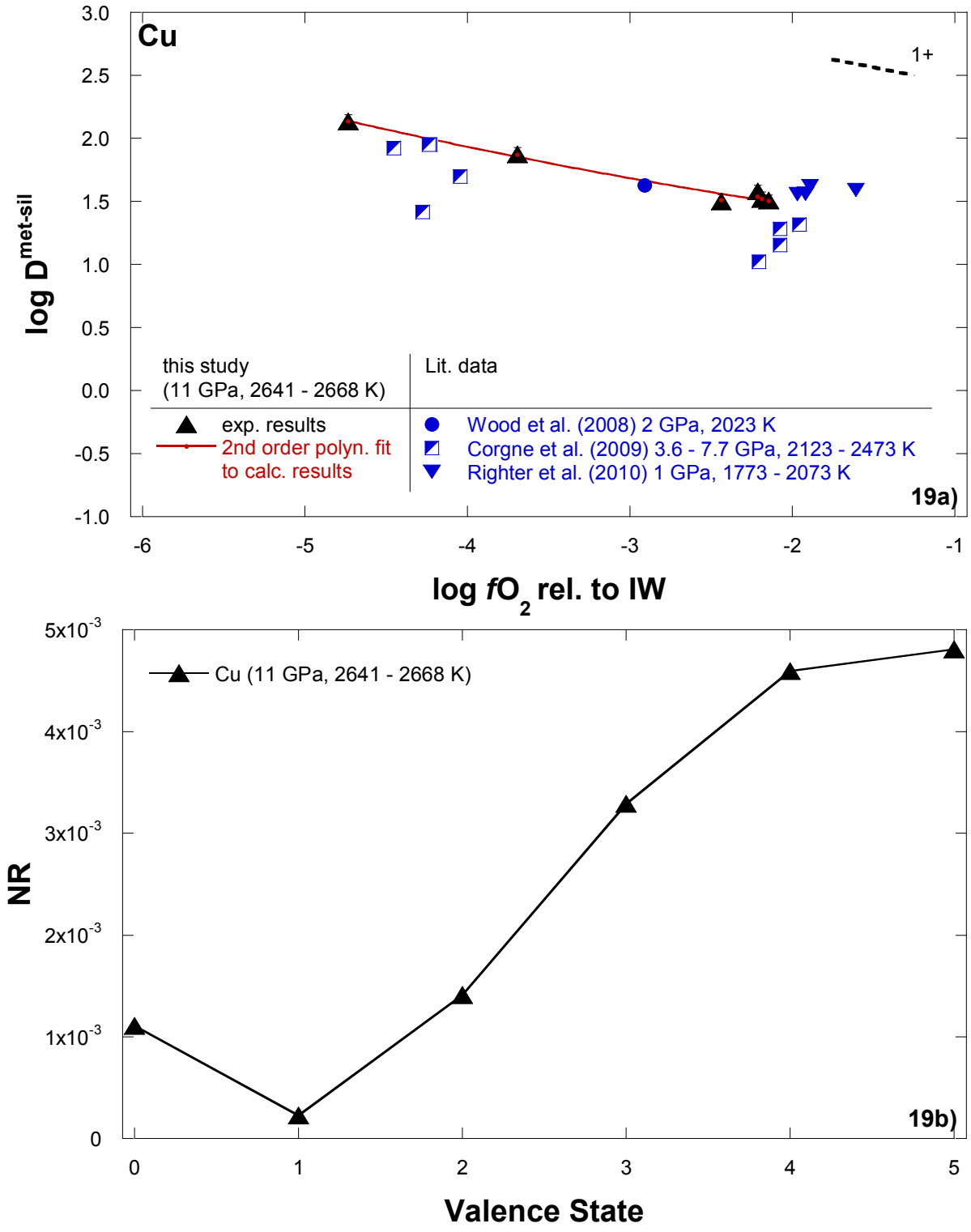

Figure 19a: *Logarithmic partition coefficient values of the experimental data of this study, a second order polynomial fit to the recalculated results and literature data have been plotted against oxygen fugacity relative to the IW buffer for the element Cu. Errors on the logarithmic partition coefficients of Cu do not exceed the symbol size. Half-filled symbols denote experiments that were performed in C-capsules. The dotted line represents the partitioning trend for a 1+ cation without the effect of Si.* ***b:*** *The values of the normalized residual function NR (see equation [26] and text) plotted against possible valence states of the element Cu.*

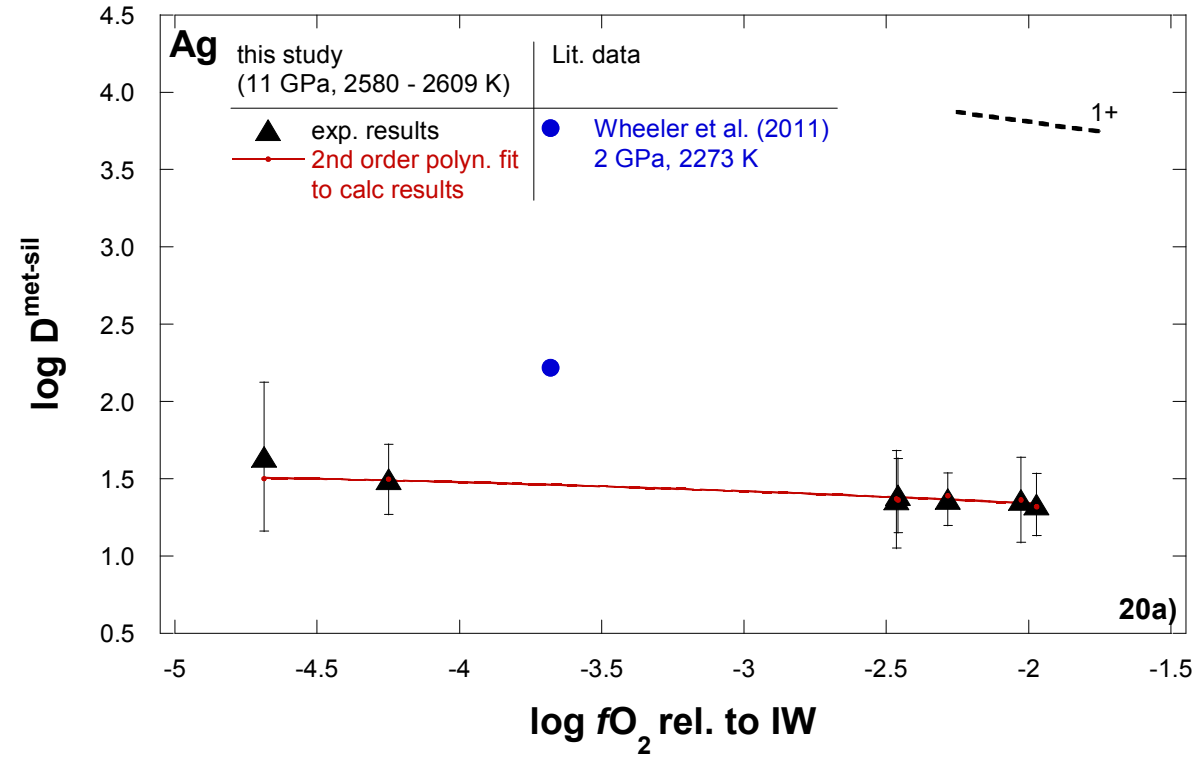

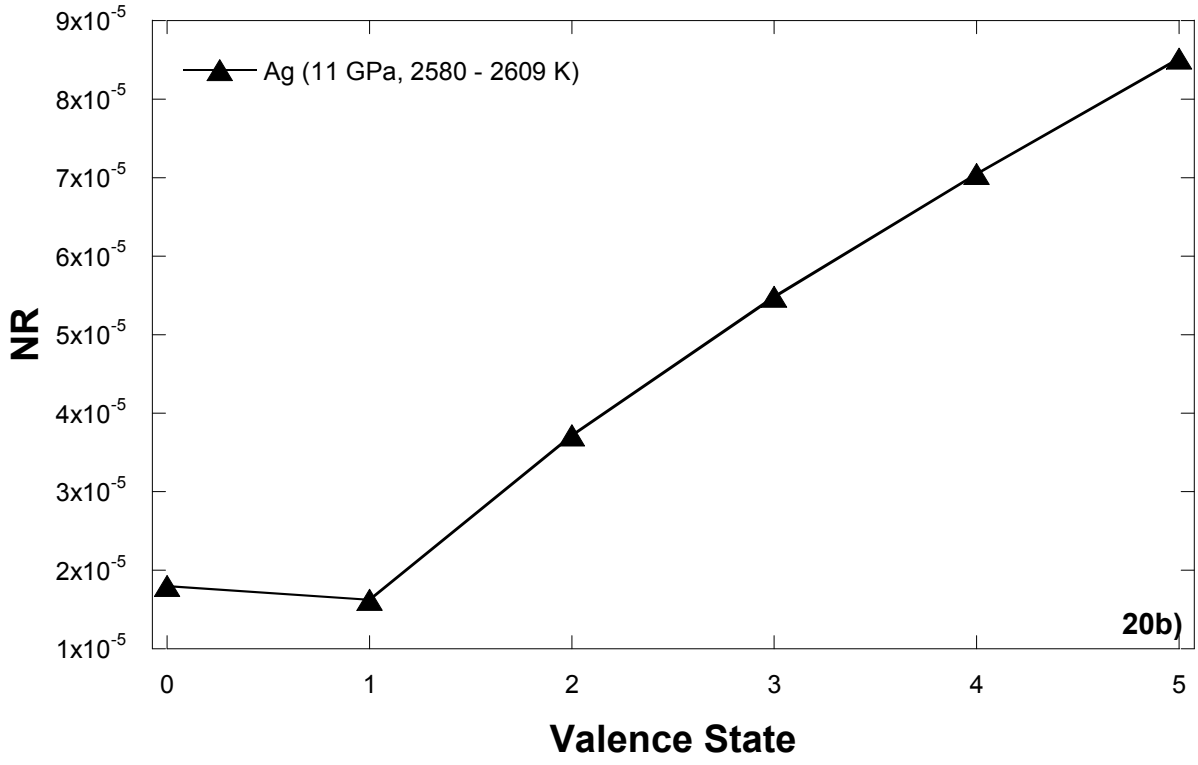

Figure 20a: *Logarithmic partition coefficient values of the experimental data of this study, a second order polynomial fit to the recalculated results and literature data have been plotted against oxygen fugacity relative to the IW buffer for the element Ag. The dotted line represents the partitioning trend for a 1+ cation without the effect of Si.* ***b:*** *The values of the normalized residual function NR (see equation [26] and text) plotted against possible valence states of the element Ag.*

4.3.1.2 Divalent elements lead and gold

Minimum deviations of the experimentally determined partition coefficients from the calculated ones were found for the divalent state for the volatile element Pb as displayed in Figure 21b. The interaction parameter ε_{Pb}^{Si} was determined to be 11.30.

The experimental partitioning data of Pb are shown in Figure 21a together with the data that has been recalculated from the analytical results given by Lagos et al. (2008), Wood et al. (2008), Wood and Halliday (2010), Ballhaus et al. (2013) and Bouhifd et al. (2013). Perfect agreement was found between the results of this study and those of Wood et al. (2008), Wood and Halliday (2010) and Ballhaus et al. (2013). However large discrepancies have been found when comparing the data to the results of Lagos et al. (2008) and Bouhifd et al. (2013). The offset of the partition coefficient values from Lagos et al. (2008) is possibly caused by their use of C-capsules that results in an influence of C in the metal phase on the partitioning behaviour of Pb. From the Steelmaking Data Sourcebook a positive interaction parameter between C and Pb can be derived, that implies that C in the Fe-rich metal causes a decrease in siderophility for the element Pb. Additionally the pressures and temperatures of the experiments of Lagos et al. (2008) were significantly lower than in this study. For the investigations of Bouhifd et al. (2013) the Fe–C–Ni–Si–S metal system was employed. However, the datapoint shown in Figure 21a denotes an experiment the metal phase of which contained negligible amounts of C, Ni and S. Pressures and temperatures were 8 GPa and 2373 K respectively. Slight differences exist in the starting silicate composition which was chosen to be similar to a CI-chondritic composition rather than the peridotitic composition employed in this study.

In the case of Au the values of the normalized residual functions *NR* are almost constant in the cases of valences from zero to 2+ (compare Figure 22b). However the deviation of the calculated from the experimental $D^{met\text{-}sil}$ values becomes minimum at a valence of 2+. The corresponding ε_{Au}^{Si} value is 17.00. The results for the element Au are displayed in Figure 22a.

Borisov and Palme (1996) investigated the solubility of Au in silicate melts rather than performing partitioning experiments between metal and silicate. The experiments were performed in a vertical tube furnace at 1 atm and temperatures between 1573 K and 1753 K. Combined with a thermodynamic description of the activity of Au in Fe metal, partition coefficients of Au were calculated for temperatures of 1623 K and 3000 K at an oxygen fugacity of IW -2. The results of respectively 2.5 x 10^7 and 2.4 x 10^6 are several orders of

magnitude higher than the observations of this study which is probably caused by the huge difference in applied pressures.

Solubility experiments of Au have additionally been conducted by Brenan and McDonough (2009). The latter authors furthermore performed four partitioning experiments between metal and silicate. However the experimental conditions of Brenan and McDonough (2009) and the experiments of this study differ strongly: The experiments of Brenan and McDonough (2009) were performed in C-capsules rather than in MgO capsules. The composition of the silicate phase was chosen to be basaltic in contrast to the peridotitic composition employed in this study and additionally the experiments of Brenan and McDonough (2009) were conducted at comparatively lower pressures of 2 GPa. The results of $D^{met\text{-}sil}$ from this study and from Brenan and McDonough (2009) differ by around 1 logarithmic unit. All results are displayed in Figure 22a.

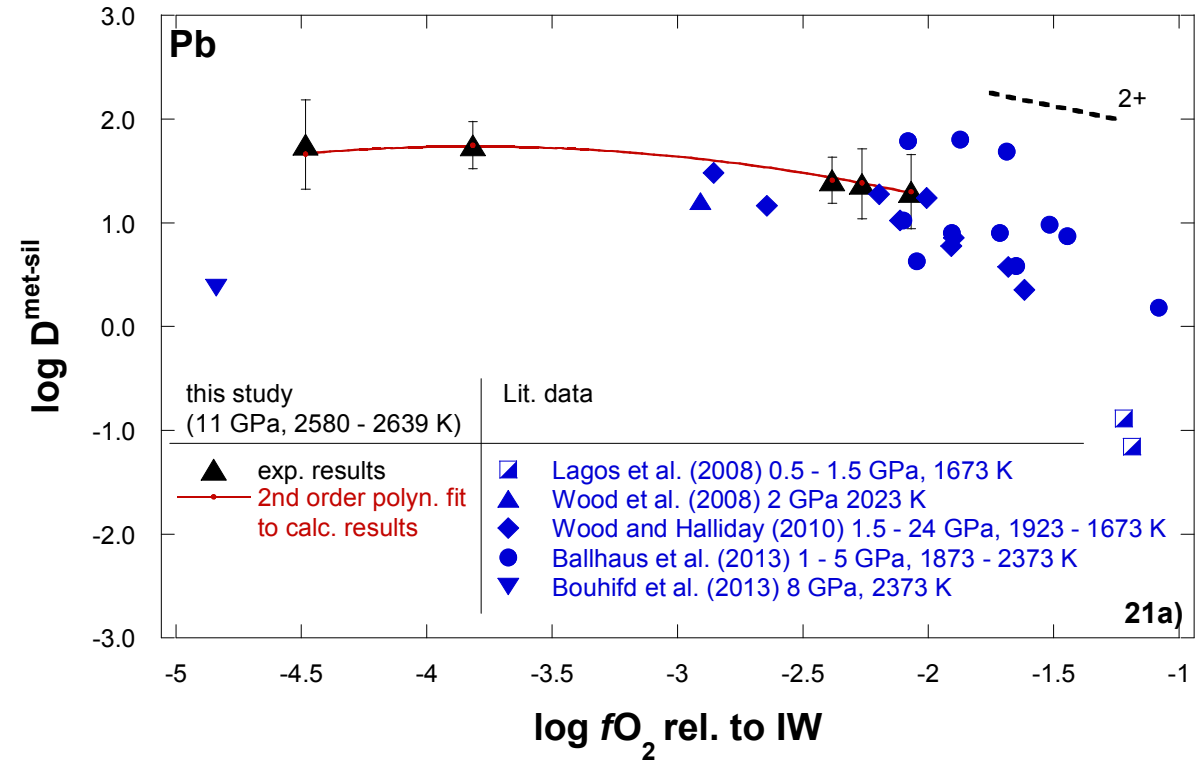

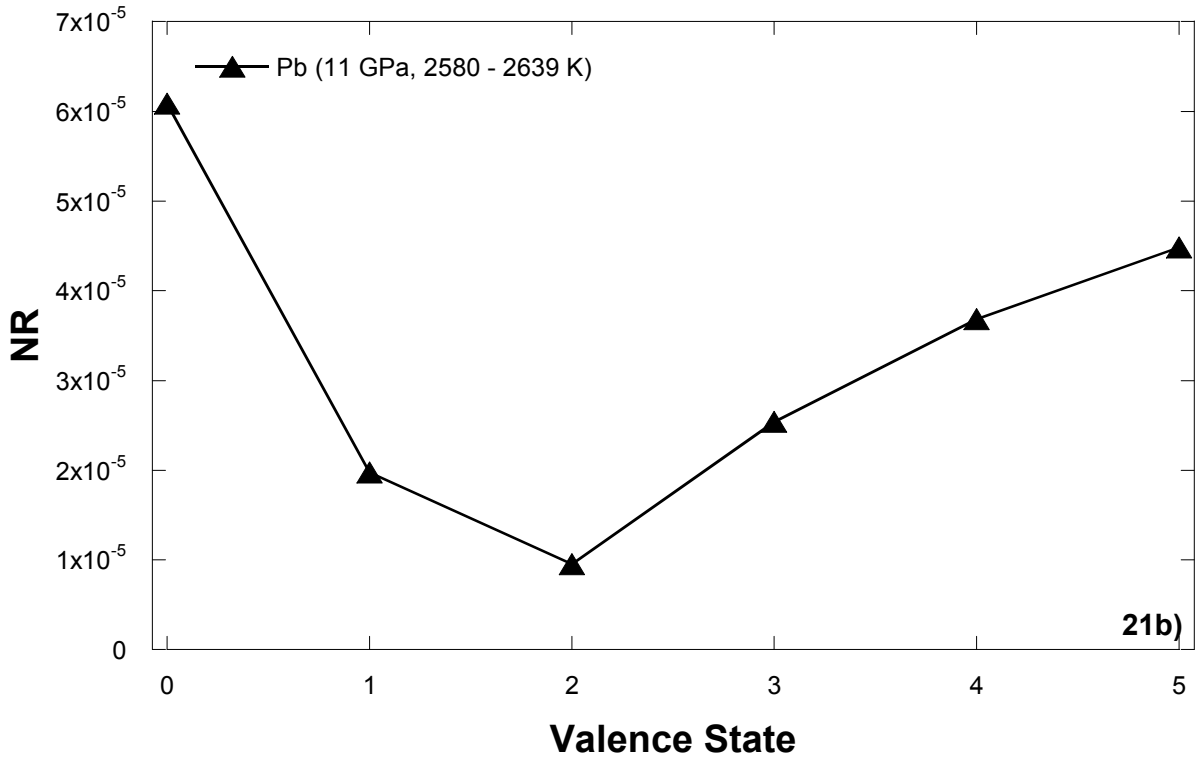

Figure 21a: *Logarithmic partition coefficient values of the experimental data of this study, a second order polynomial fit to the recalculated results and literature data have been plotted against oxygen fugacity relative to the IW buffer for the element Pb. Half-filled symbols denote experiments that were performed in C-capsules. The dotted line represents the partitioning trend for a 2+ cation without the effect of Si.* ***b:*** *The values of the normalized residual function NR (see equation [26] and text) plotted against possible valence states of the element Pb.*

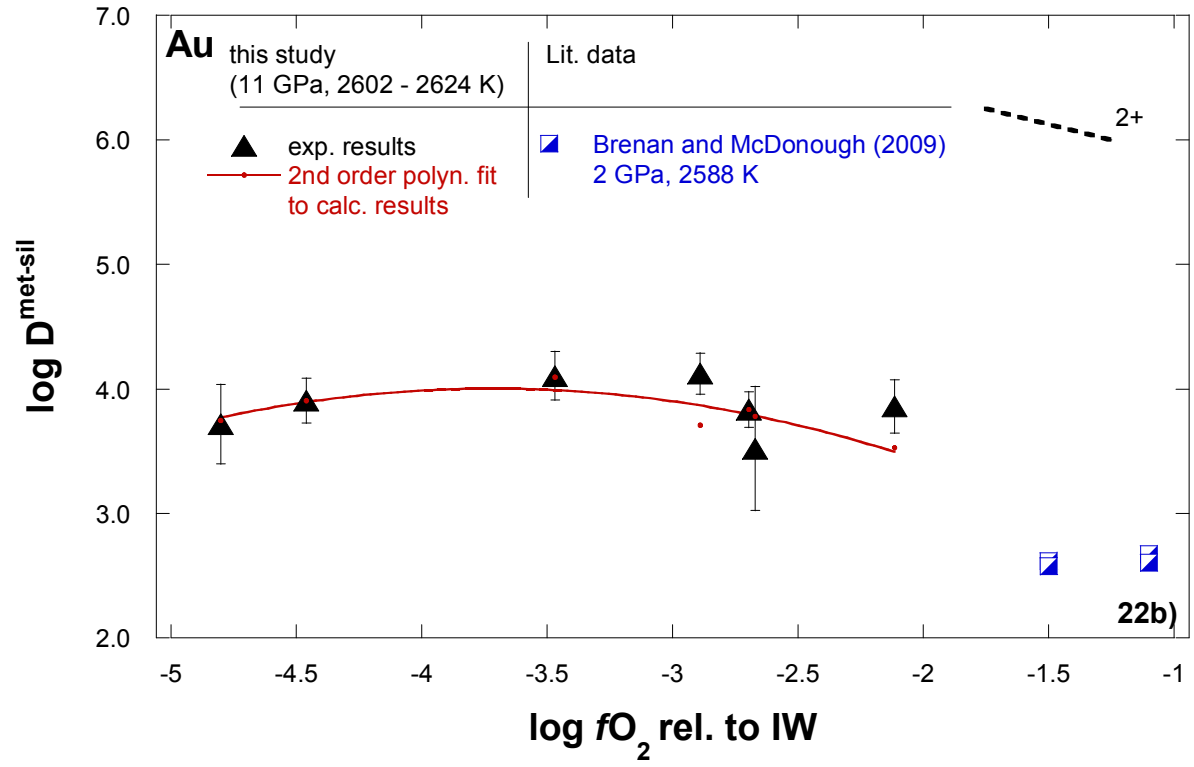

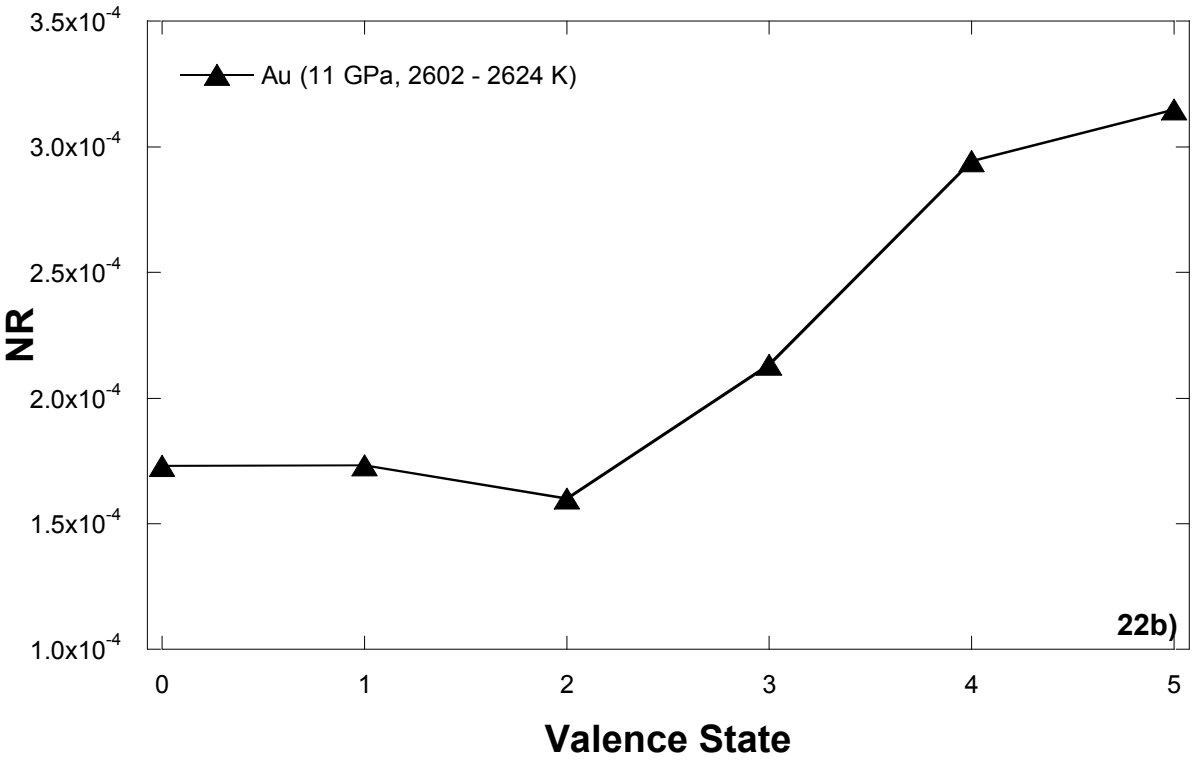

Figure 22a: *Logarithmic partition coefficient values of the experimental data of this study, a polynomial fit to the recalculated results and literature data have been plotted against oxygen fugacity relative to the IW buffer for the element Au. Half-filled symbols denote experiments that were performed in C-capsules. The dotted line represents the partitioning trend for a 2+ cation without the effect of Si.* ***b:*** *The values of the normalized residual function NR (see equation [26] and text) plotted against possible valence states of the element Au.*

4.3.1.3 Trivalent elements tin and germanium

In two cases a valence of 3+ was determined, namely for the elements Sn and Ge. The corresponding interaction parameters ε_{Sn}^{Si} and ε_{Ge}^{Si} have values of 17.79 and 16.58 respectively. The values of the normalized residual function *NR* for various valence states of Sn and Ge are displayed in Figures 23b and 24b respectively. The experimental and calculated results are shown in Figures 23a and 24a together with a variety of literature data (see below).

The results of the partitioning behaviour of Sn are in quite good agreement with the data published by Righter et al. (2010) and Ballhaus et al. (2013). In particular the data given by Ballhaus et al. (2013) match the fitted trend of the partition coefficients obtained in this study when extrapolated to higher oxygen fugacity.

The liquid metal – liquid silicate partitioning behaviour of Ge has been compared to the results of Siebert et al. (2011), Righter et al. (2011) and Kegler et al. (2011). The results of the first two studies lie on the extrapolation of the partitioning behaviour trend obtained in this study towards higher oxygen fugacity. The $D^{met\text{-}sil}$ values that have been recalculated from the analytical results of Kegler et al. (2011) are slightly higher than those of this study, probably due to the use of basaltic silicate starting material and lower pressure and temperature conditions of 0.5 GPa and 1623 K respectively.

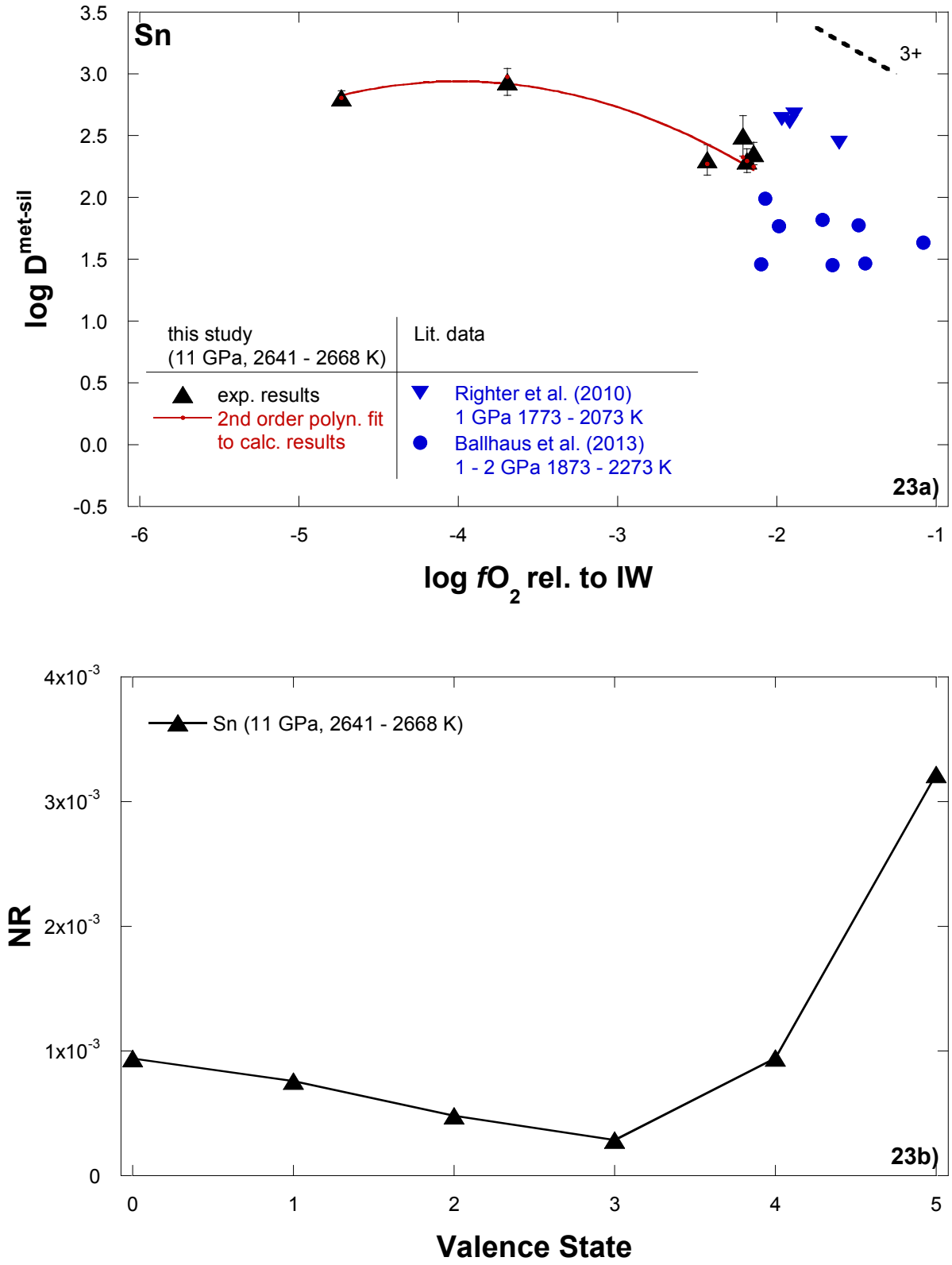

Figure 23a: *Logarithmic partition coefficient values of the experimental data of this study, a second order polynomial fit to the recalculated results and literature data have been plotted against oxygen fugacity relative to the IW buffer for the element Sn. The dotted line represents the partitioning trend for a 3+ cation without the effect of Si.* ***b:*** *The values of the normalized residual function NR (see equation [26] and text) plotted against possible valence states of the element Sn.*

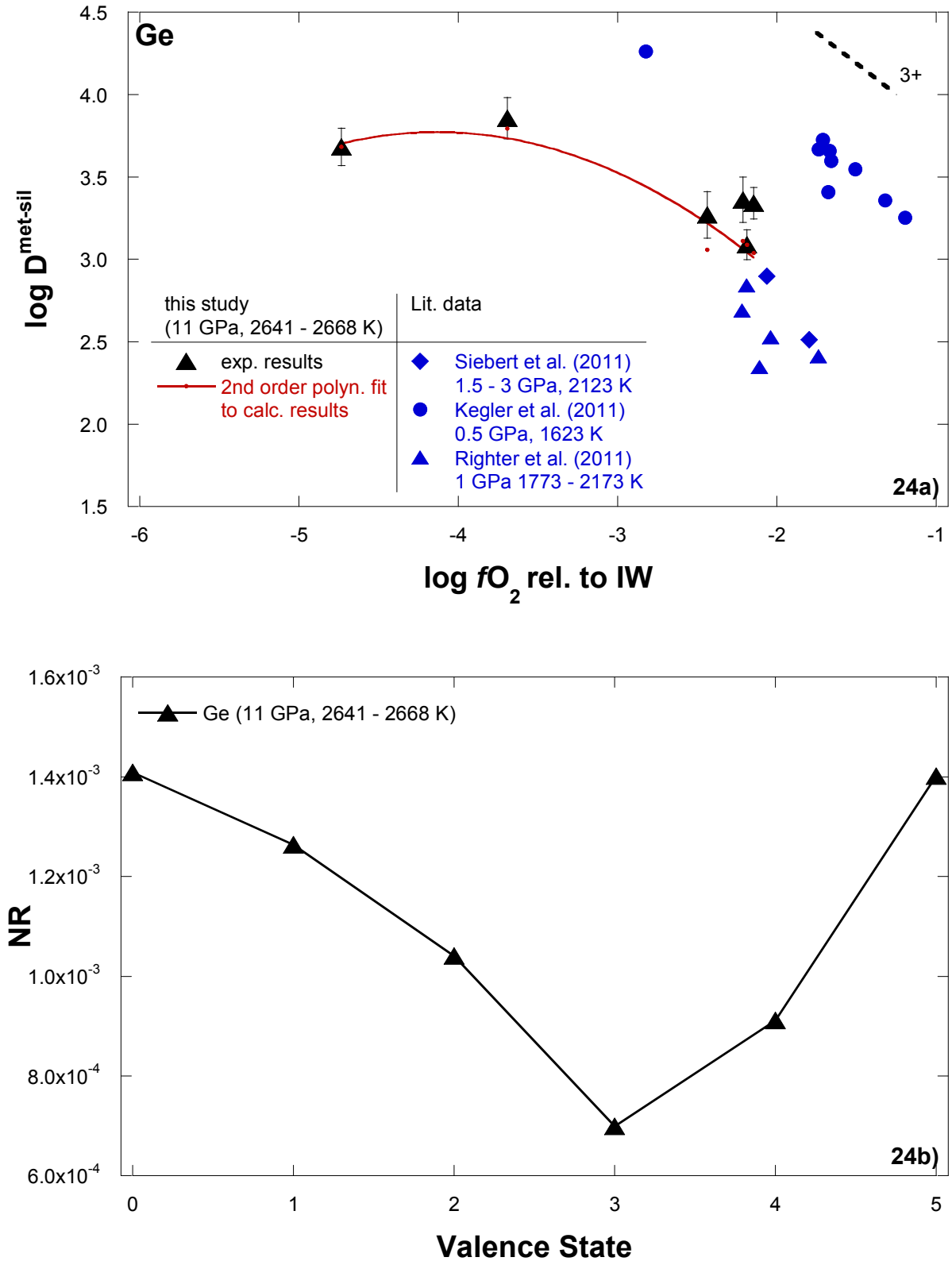

Figure 24a: *Logarithmic partition coefficient values of the experimental data of this study, a second order polynomial fit to the recalculated results and literature data have been plotted against oxygen fugacity relative to the IW buffer for the element Ge. The dotted line represents the partitioning trend for a 3+ cation without the effect of Si.* ***b:*** *The values of the normalized residual function NR (see equation [26] and text) plotted against possible valence states of the element Ge.*

4.3.1.4 Tetravalent element antimony

Of the elements investigated in this study Sb was found to have a valence of 4+ in the silicate phase (compare Figure 25b). The interaction between the Si content of the metal and Sb in the metal phase results in an interaction parameter value, ε_{Sb}^{Si} of 28.51.

A broad investigation of the metal – silicate partitioning behaviour of Sb has been performed by Righter et al. (2009). Of their experiments ten were conducted in MgO capsules and only two of those exhibited negligible amounts of S in the metal phase. These two results have been recalculated and compared to the results of this study. Pressures and temperatures were 1.5 GPa and 1873 and 2073 K respectively. The results diverge strongly from the observations of this study which might have the following reasons: The silicate compositions of the experiments from Righter et al. (2009) were basaltic and rhyolitic rather than the peridotitic composition of the silicate phase in this study. Moreover one of the compared experiments exhibited high amounts of Pd in the metal phase (22.5 mole%) Finally the experiments of Righter et al. (2009) were conducted at comparatively low pressures and temperatures (see above). The experimental and calculated partition coefficients as well as those that were derived from the study of Righter et al. (2009) are shown in Figure 25a.

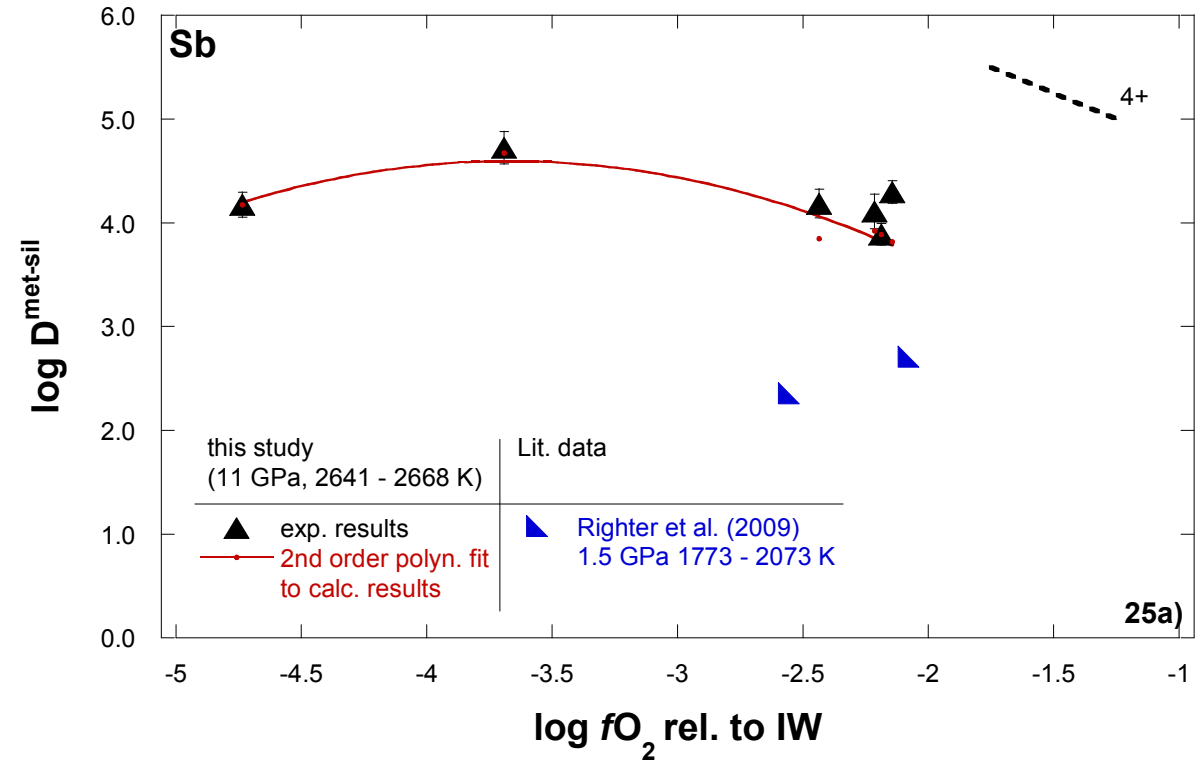

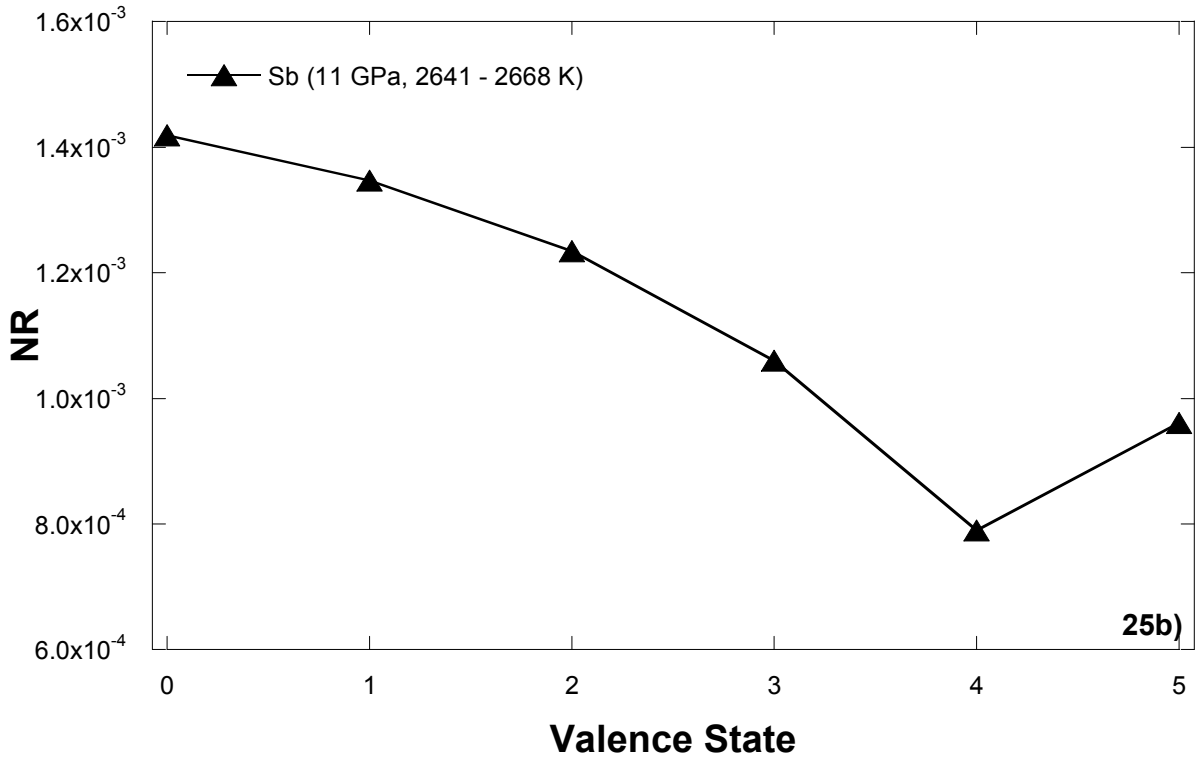

Figure 25a: *Logarithmic partition coefficient values of the experimental data of this study, a second order polynomial fit to the recalculated results and literature data have been plotted against oxygen fugacity relative to the IW buffer for the element Sb. The dotted line represents the partitioning trend for a 4+ cation without the effect of Si. b: The values of the normalized residual function NR (see equation [26] and text) plotted against possible valence states of the element Sb.*

4.3.1.5 Pentavalent element arsenic

Arsenic is present in form of As_2O_5 in the silicate phase (Figure 26b). The influence of Si in the metal phase on its partitioning behaviour has been fitted to give $\varepsilon_{As}^{Si} = 43.47$. However in the case of As the recalculated results do not completely match the experimental observations. Several LA-ICP-MS measurements failed in detecting the concentration of As in the silicate phase, because of which the obtained partition coefficients represent maximum values. Further experiments will be necessary to verify the observations of this study.

Only a single experiment from the study of Siebert et al. (2011) was suitable for comparing the metal – silicate partitioning behaviour of As. It is in perfect agreement with the results of this study as can be seen in Figure 26a.

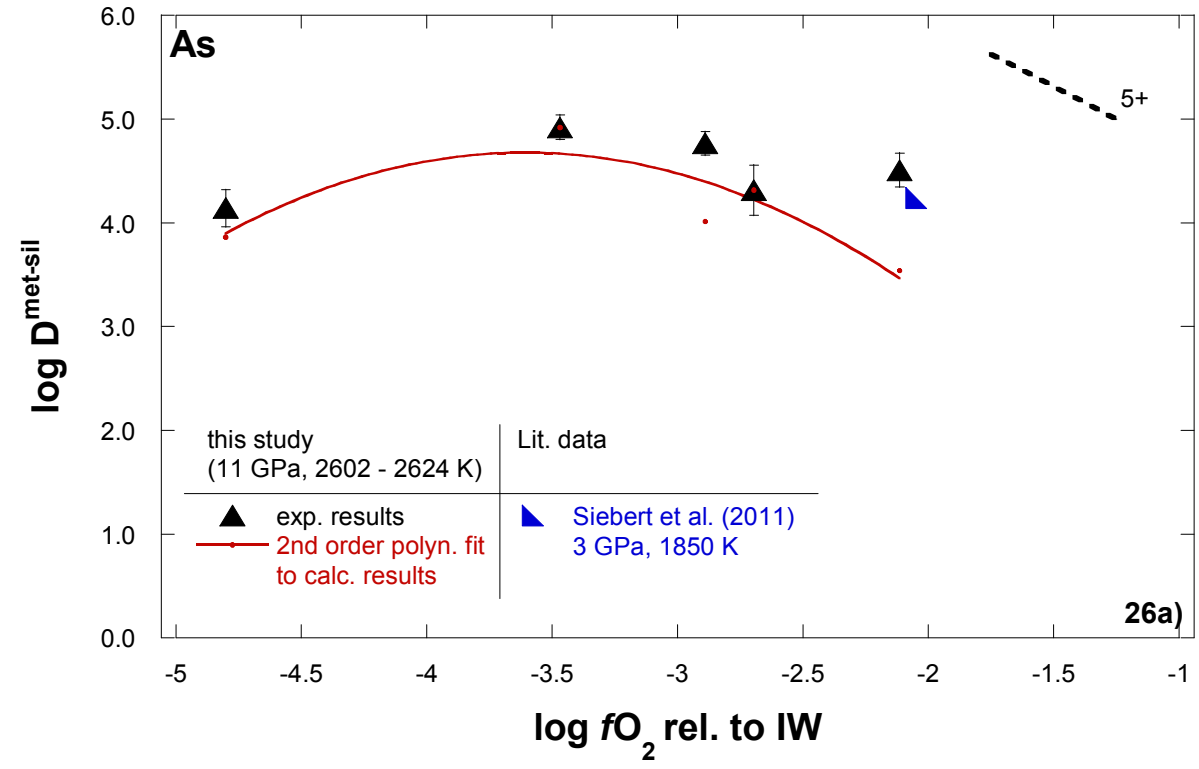

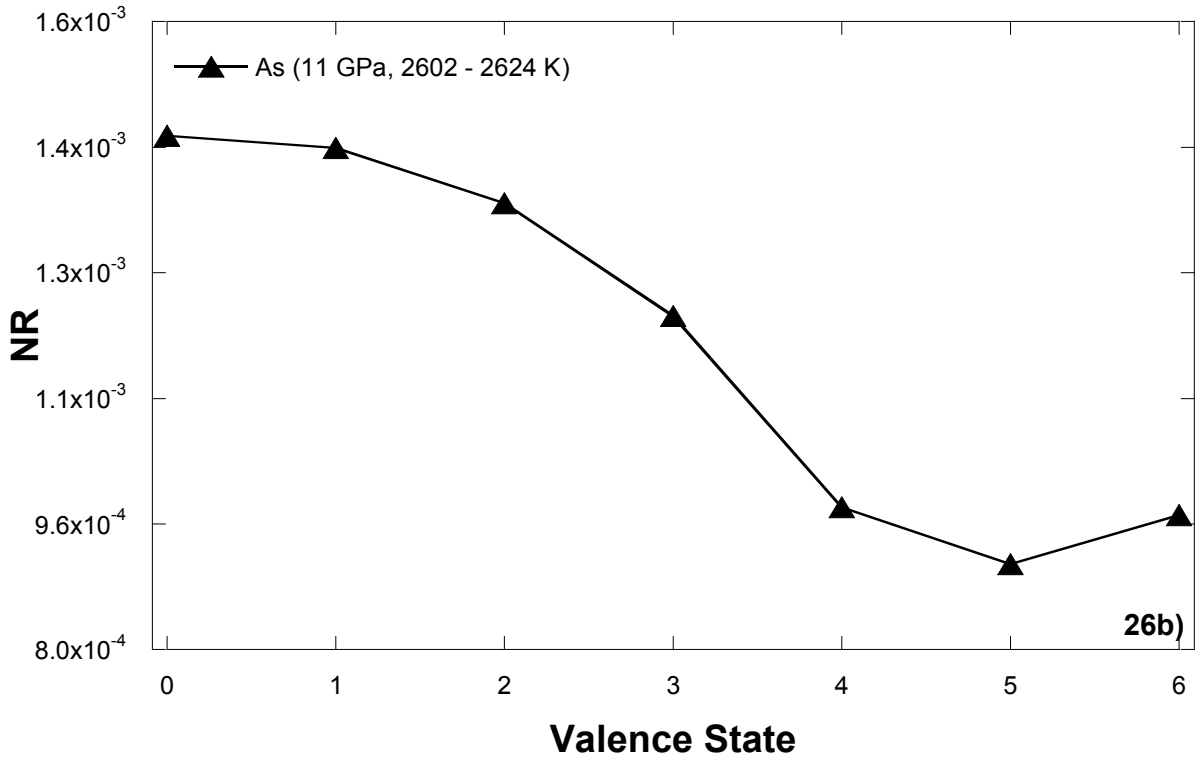

Figure 26a: *Logarithmic partition coefficient values of the experimental data of this study, a second order polynomial fit to the recalculated results and literature data have been plotted against oxygen fugacity relative to the IW buffer for the element As. The dotted line represents the partitioning trend for a 5+ cation without the effect of Si. b: The values of the normalized residual function NR (see equation [26] and text) plotted against possible valence states of the element As.*

4.3.1.6 Special case: phosphorus

Unfortunately the results of the dependence of the liquid metal – liquid silicate partitioning behaviour on oxygen fuagcity and Si metal contents are unreliable for the element P. The investigations of this study lead to a chemically unrealistic valence of 6+ (Figure 27b) and an interaction parameter ε_P^{Si} of 34.02. Moreover during the preparation of the starting material the incorporation of P_2O_5 into the starting metal composition was hindered by its strong hygroscopic behaviour. More experiments are necessary to better characterize the influence of Si on the partitioning of P and to derive its valence state in the silicate phase.

During the further procedure P will therefore be treated as a 5+ cation following the results of Siebert et al. (2011). The corresponding interaction parameter ε_P^{Si} for a valence of 5+ yields a value of 26.82. The experimentally determined and recalculated data (for P^{5+}) are shown in Figure 27a together with a suite of data sets from various authors. If extrapolated to higher oxygen fugacity values the partitioning trend for P is in good agreement with the results given by Ballhaus et al. (2013), Righter et al. (2010), Righter et al. (2011) and Siebert et al. (2011).

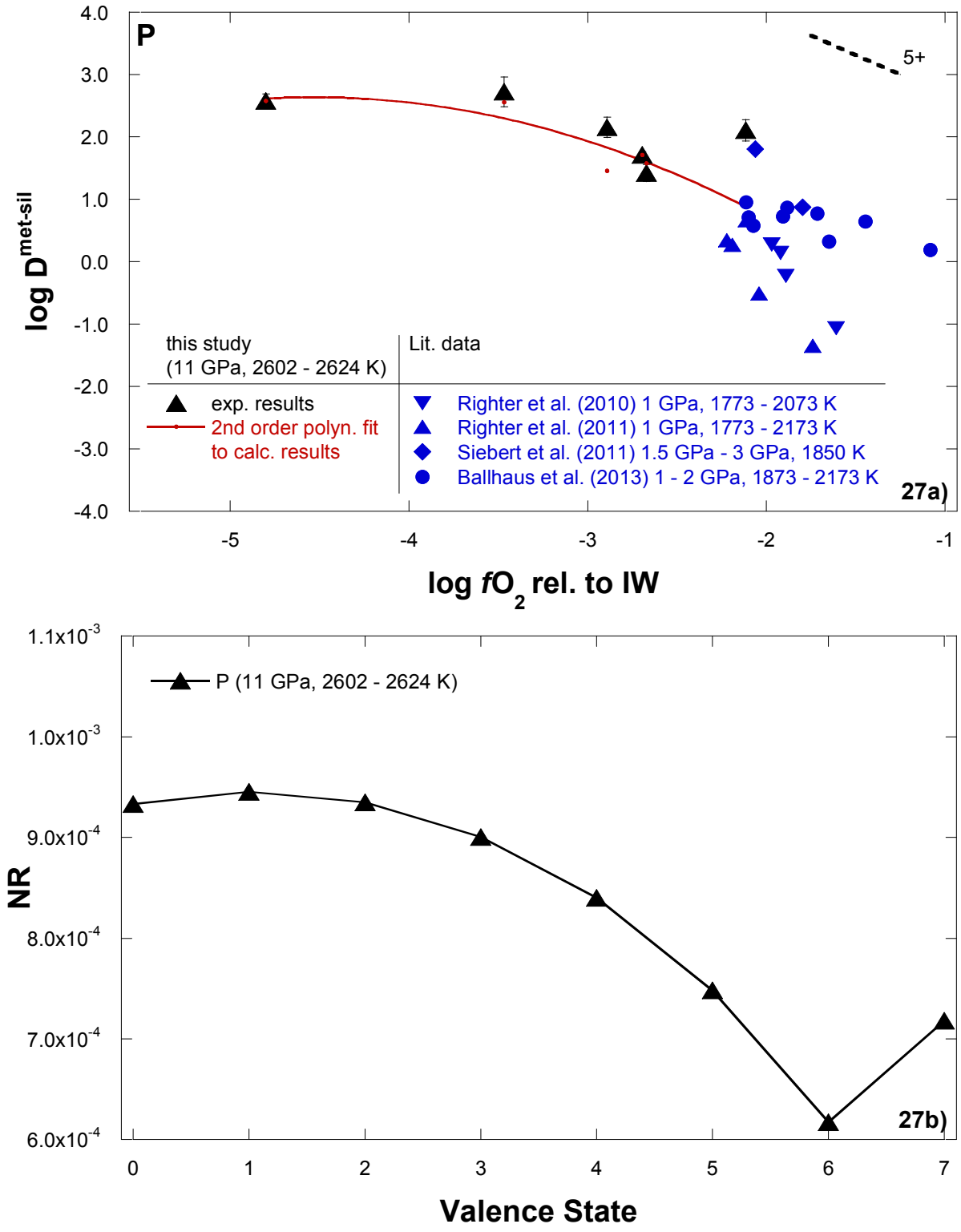

Figure 27a: *Logarithmic partition coefficient values of the experimental data of this study, a second order polynomial fit to the recalculated results and literature data have been plotted against oxygen fugacity relative to the IW buffer for the element P. One should note that fitting was based on a P^{5+} cation as derived by Siebert et al. (2011). For details see text The dotted line represents the partitioning trend for a 5+ cation without the effect of Si.* ***b:*** *The values of the normalized residual function NR (see equation [26] and text) plotted against possible valence states of the element P.*

4.3.2 Exchange coeffcients K_D^{M-Fe}

The effect of Si on the partitioning behaviour of the volatile elements of this study can be clarified by expressing the partitioning in form of an exchange coefficient K_D^{M-Fe} as defined in equation 5, Chapter 3. In Figure 28 the experimentally determined logarithmic exchange coefficient values are plotted against the molar fraction of Si in the metal phase of the partitioning experiments in order to illustrate the dependence of Si metal contents on the partitioning behaviour. The calculations of K_D^{M-Fe} values are based on the valence states that were determined in the course of this study. In the case of P a 5+ valence state was assumed following the results of Siebert et al. (2011). Dotted lines represent linear regressions to the experimental data.

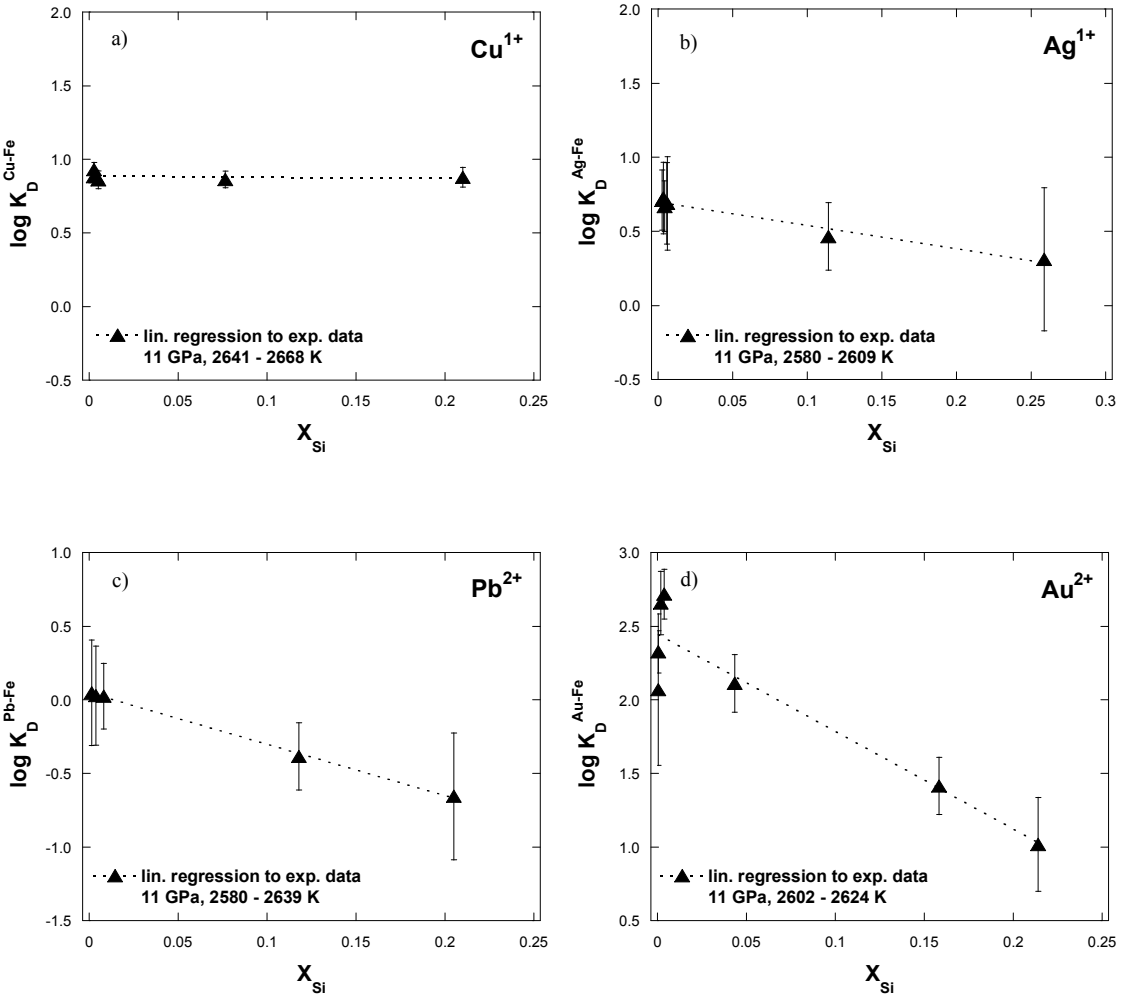

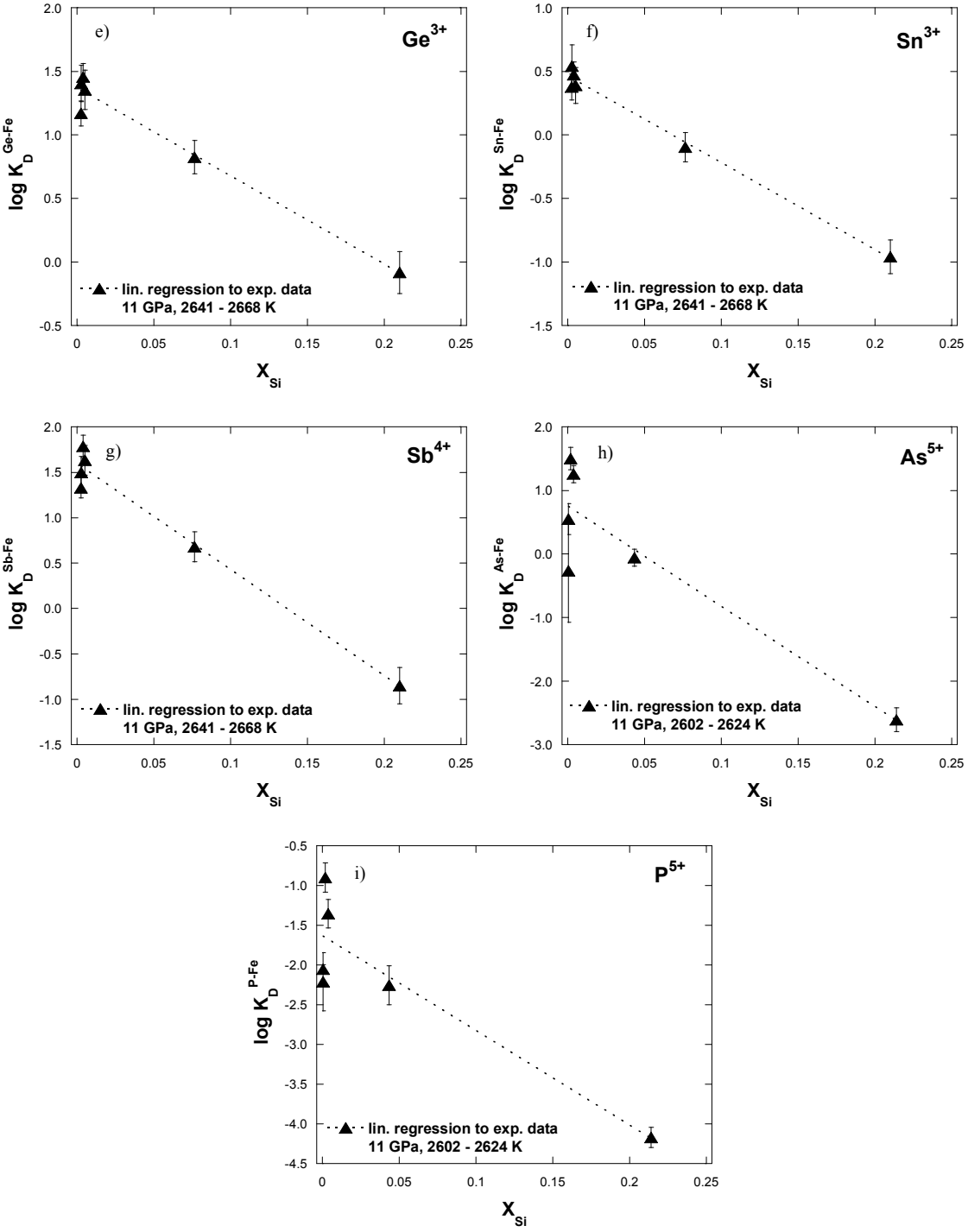

Figure 28: *The effect of Si metal contents on the logarithmic exchange coefficients K_D^{M-Fe} for the volatile elements* ***a:*** *Cu,* ***b:*** *Ag,* ***c:*** *Pb,* ***d:*** *Au,* ***e:*** *Sn,* ***f:*** *Ge,* ***g:*** *Sb,* ***h:*** *As and* ***i:*** *P. Valence states for the calculation of K_D^{M-Fe} values have been adopted from the derivations of this study except for P. Here a valence of 5+ was assumed following the results of Siebert et al. (2011). Si was found to lower the logarithmic exchange coefficients for each element studied.*

4.4 Summary and conclusions

The deviations of the experimental data from the calculated $D^{met\text{-}sil}$ values have been compared for different valence states of the elements of interest in form of the normalized residual function *NR* (see equation [26] and text). The lowest value that was obtained represents the best fit of the experimental results to the recalculated values. The valence states and interaction parameters that have been determined are summarized in Table 9.

In the case of P the determination of its valence state was not possible. More experiments are needed to better constrain this parameter.

Table 9 additionally lists interaction parameters ε_{Si}^{M} derived from the Steelmaking Data Sourcebook. In this study it was found that increasing Si contents reduce the siderophility of Pb, whereas the value derived from the Steelmaking Data Sourcebook predicts the opposite. In all other cases, that means for Cu, Sn and P, the result of increasing Si contents of the metal leading to reduced partition coefficients is the same, but the absolute values of the individual interaction parameters are different.

Table 9: *Summary of the derived valence states and interaction parameters* $\boldsymbol{\varepsilon_{Si}^{M}}$ *of this study and from the Steelmaking Data Sourcebook. All interaction parameters correspond to a temperature of 1873 K (compare Section 4.2 Methods).*

Element	Valence State	Interaction Parameter ε_{M}^{Si} (1873 K) This study	Interaction Parameter ε_{M}^{Si} (1873 K) Steelmaking Data Sourcebook
Cu	1+	0.73	3.64
Ag	1+	6.42	-
Au	2+	17.00	-
Pb	2+	11.30	-11.26
Sn	3+	17.79	7.2
Ge	3+	16.58	-
Sb	4+	28.51	-
As	5+	43.47	-
P	5+	26.82	11.95
(P	6+	34.02)	

In Figure 29 the derived interaction parameters ε_{Si}^{M} are plotted against their corresponding valence states. Higher valence states indicate that the element of interest is more strongly effected by changes in oxygen fugacity with lower fO_2 leading to an increase in siderophility. This means that Sn and Ge will be affected more strongly by changes in oxygen fugacity in

comparison to Au regardless of the Si content in the metal, because these three elements exhibit very similar interaction parameter values ε_{Si}^{M}.

However for elements that exhibit the same valence state, higher ε-values indicate a stronger influence of Si in the metal phase on the partitioning behaviour by decreasing the partition coefficient values to a greater extent.

Within the suite of the elements investigated in this study this means that Pb tends to become relatively less lithophile than Au. The same conclusion can be referred for the element pairs Cu - Ag and P^{5+} - As respectively.

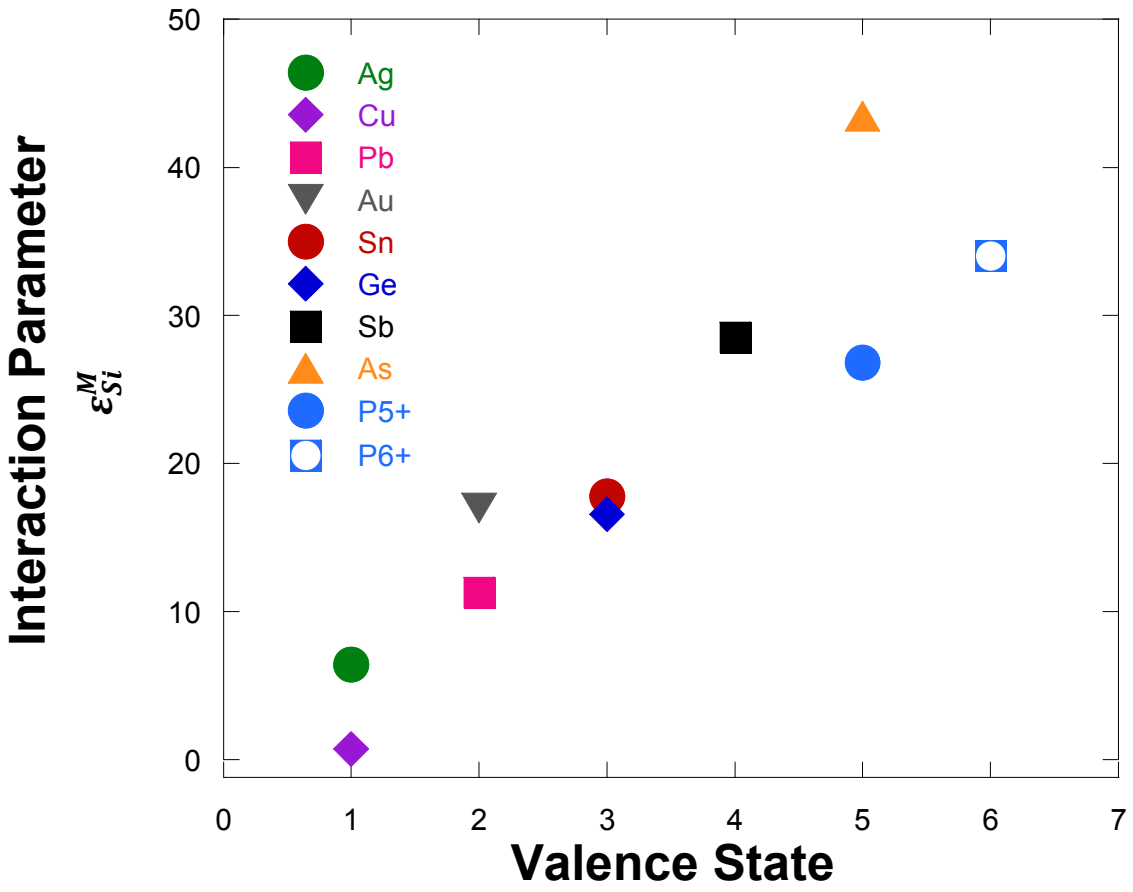

Figure 29: *The derived valence states for all elements studied are shown together with their corresponding interaction parameter values.*

In summary it was found that for each element studied the interaction of Si with these counteracts the effect of low fO_2 which normally results in increased siderophile behaviour. This shows that reducing conditions in the early stages of core formation do not necessarily result in complete or even strong depletion of siderophile elements when Si is present as a light element in the metal phase.

5. The dependence of volatile element partitioning on pressure, temperature and the Si- and S-content of the metal

5.1 Introduction

5.1.1 Pressure and temperature

Experimental studies have demonstrated that the abundances of many siderophile elements in the Earth´s mantle, regardless of being classified as volatile or refractory, cannot be explained by low pressure – low temperature metal – silicate partitioning experiments (e.g. Walter et al., 2000; Rubie et al., 2007; Kegler et al., 2008; Mann et al., 2009). In fact an overabundance of most elements in the Earth´s mantle is observed terming this issue the "excess siderophile element problem" (Chapter 1, Figure 6). A solution to this problem was first provided by Li and Agee (1996), who showed that the partition coefficients of Ni and Co decrease with increasing pressure. Based on these results, the absolute abundances of Ni and Co in the Earth´s mantle could be explained by a core formation event at a pressure of 28 GPa, which corresponds to a magma ocean depth of 750 km. Furthermore the authors found that Ni partitioning is more strongly effected by increasing pressure than Co partitioning. According to Li and Agee (1996) at 28 GPa the partition coefficients converge, thus explaining the chondritic relative abundances of Ni and Co in the Earth´s mantle (see also Chapters 1 and 6). Subsequent investigations on the effects of pressure as well as of temperature and composition of silicate and metal phases have supported the idea of a high pressure and also high temperature core formation scenario. However, the pressure and temperature conditions estimated to account for the depletions of elements in the Earth´s mantle cover a wide range as illustrated in Table 1, Chapter 1.

As previously discussed in Chapter 1, a number of core formation models that are based on metal – silicate partitioning data have confirmed the theory of equilibration between the core-forming Fe-rich metal and the silicate mantle at high pressures and temperatures. In addition, as described in detail in Chapter 4, these core formation models place constraints on other important parameters such as oxygen fugacity and the degree of equilibration between the Earth´s core and mantle: It has been shown that the oxygen fugacity in the Earth´s mantle most likely changed over a range of around two logarithmic units from initially reduced to

more oxidized at the later stages of accretion (e.g. Wade and Wood, 2005; Wood et al., 2006; Corgne et al., 2008; Rubie et al., 2011). According to Rubie et al. (2011) changes in oxygen fugacity over time can be caused by the accretion of relatively reduced material in the early stages of Earth´s growth, followed by the addition of oxidized material, that means matter that is enriched in oxygen and perhaps volatile elements, in the later stages of accretion. These authors furthermore find evidence for a significant degree of disequilibrium between the metal that was added late to the Earth and the mantle. Disequilibrium was also proposed by Rudge et al. (2010) who argued for only 36 wt% of the core having been in equilibrium with the mantle.

However to date most of the investigations of the pressure and temperature dependences of siderophile elements that can be incorporated into core formation models have been focused primarily on refractory elements and precise determinations of metal – silicate partitioning behaviour are still lacking for the volatile element group. Among the few experimental studies that address the effects of pressure and temperature on the partitioning behaviour of volatile elements is the work of Corgne et al. (2008), who, in addition to other refractory elements, investigated the metal – silicate partitioning of the volatile elements Mn, Ga, Cu and Zn at pressures between 3.6 and 7.7 GPa and temperatures between 2123 and 2473 K. They showed that increasing temperatures reduce the partition coefficients for the element Zn whereas the opposite in the case for all other elements studied. Changes in pressure only effected the partitioning behaviour of the two volatile elements Ga and Mn, where increasing pressure resulted in decreased and increased siderophility respectively. The authors favored the idea that core formation, involving equilibration in a magma ocean at high pressures, can explain the abundances of Ga, Mn and Zn in the Earth´s mantle rather than depletions being the result of volatility alone. Mann et al. (2009) emphasized that core formation must have involved a deep magma ocean with this conclusion basing on the study of the liquid metal – liquid silicate partitioning behaviour of the volatile elements Mn, Ga, In and Zn. The experiments of Mann et al. (2009) have been performed between 2 - 24 GPa and 2023 – 2873 K at oxygen fugacity ranging between -1.3 to -4.2 logarithmic units relative to the iron-wüstite buffer. The authors find that pressures > 30 to 60 GPa are necessary to explain the chondritic element ratios of Ga/Mn and In/Zn. Siebert et al. (2011) studied the partitioning behaviour of the volatile elements As, Ge, P, Zn, Ga and Mn at a pressure and temperature range of 0.5 – 18 GPa and 1873 – 2873 K respectively. Additionally the effect of silicate melt composition on metal – silicate partitioning behavior was constrained by varying the silicate composition from basaltic to peridotitic. Increasing temperature was found to result in increased

siderophile behaviour for Mn and Zn, whereas the partition coefficients of Ge and As are decreased. The partitioning behaviour of Ga and P was hardly effected by temperature. With increasing pressure the elements Ga and As became less siderophile, while the metal –silicate partitioning of all other volatile elements did not exhibit a pressure dependence. Including several refractory elements the authors were able to find a single stage core formation solution with pressures between 32 and 42 GPa and temperatures between 3000 and 3200 K that can effectively account for the Earth´s mantle abundances of the elements Ni, Co, Cr, Mn, Zn, W and Mo, but not for V, Nb, Ge, Ga, As and P. Even when applying a continuous core formation model in which oxygen fugacity is increased with time the abundances of Ge and Ga still remain unexplainable within the framework of the experimental investigations of Siebert et al. (2011). The authors emphasize the necessity of studying the effects of light elements on the metal – silicate partitioning behaviour of volatile elements to further constrain the conditions that prevailed during the accretion of the Earth and the segregation of the core-forming metal from the silicate Earth´s mantle. Contrasting conclusions about the mechanism that resulted in the volatile element budget of the Earth´s mantle have recently been published by Ballhaus et al. (2013). The partitioning behaviour of a wide range of volatile elements, namely Pb, P, Rb, Cs, Sn, Zn, In, Cd and Tl, was investigated by performing metal-silicate partitioning experiments at 1 – 5 GPa and 1773 – 2373 K. Ballhaus et al. (2013) found that the partitioning of none of the elements studied depends significantly on pressure within the experimental pressure range. Increasing temperature resulted in an increase of siderophility for the elements Pb, P, Cd, Tl and Zn, whereas the partition coefficients of Sn and In remained constant over the temperature range covered in this study. Rb and Cs were found to be lithophile at all experimental conditions. Ballhaus et al. (2013) did not find a solution that satisfactorily explains the abundances of the studied volatile elements in the Earth´s mantle based on metal – silicate equilibration in a deep magma ocean. Instead the authors conclude that the moderately volatile element inventory of the Earth´s mantle was mainly delivered by a late accretionary component after core formation was terminated. In particular the latter study implies a final addition of 2.5% volatile rich material delivering up to 90% of the Earth´s Pb. Several other studies additionally investigated the liquid metal – liquid silicate partitioning of single volatile elements, e.g. Sb by Righter et al. (2009), Au by Brenan and McDonough (2009), Pb by Wood and Halliday (2010), P by Righter et al. (2010) and Ge by Righter et al. (2011) and Kegler et al. (2011).

In order to better compare the individual results of the pressure and temperature dependences of volatile element partitioning all studies that have been mentioned above

together with several other investigations are summarized in Table 10. Here authors are correlated with their investigated elements. Red plus (+) or minus (–) signs indicate whether the particular element becomes more or less siderophile with increasing temperature. By contrast blue plus (+) or minus (–) signs respectively show if increasing pressure results in increased or decreased siderophility of the individual volatile elements. One should note that if the pressure dependence exhibits the opposite algebraic sign in comparison to the temperature dependence, the latter can be reversed at very high pressures, because the pressure and temperature dependences are coupled as can be seen in equation [33], Section 5.2.1.

Table 10: *Summary of studies that investigated the pressure and / or temperature dependence of volatile elements. Red plus or minus signs indicate whether the siderophility of a particular element is increased or decreased by increasing temperature respectively. Blue plus or minus signs respectively denote whether increasing pressure causes an increase or a decrease of metal – silicate partition coefficients. Purple shaded columns mark volatile elements the pressure- and temperature dependent partitioning of which is also investigated within the course of this study. N.e. stands for "no effect".*

Volatile elements →	**P**	**S**	**V**	**Mn**	**Cu**	**Zn**	**Ga**	**Ge**	**As**	**Ag**	**Cd**	**In**	**Sn**	**Sb**	**Au**	**Tl**	**Pb**
Publications ↓	**increasing temperature** leads to increased (+) or decreased (–) siderophility: **increasing pressure** leads to increased (+) or decreased (–) siderophility:																
Walker et al. (1993)	+							–									
Ohtani et al. (1997)	 –		+ +	+ +													
Gessmann et al. (1998)			+	+													
Gessmannn et al. (1999)			**n.e.**	**n.e.**													
Gessmann et al. (2000)			+ +	+ +													
Danielson et al. (2005)															+ –		
Wade and Wood (2005)			+ **n.e.**	+ –													
Holzheid et al. (2007)					–			–									
Corgne et al. (2008)				+ +	– **n.e.**	– **n.e.**	+ –										
Lagos et al. (2008)																	–
Wood et al. (2008)																+	+
Brenan and McDonough (2009)															– **n.e.**		
Kegler et al. (2009)					– –												
Mann et al. (2009)			+ **n.e.***	+ **n.e.**		**n.e.** –	**n.e.** –					**n.e.** –					

Table 10 continued

Righter et al. (2009)														– –			
Wood et al. (2009)			+ –														
Righter et al. (2010)	+		+	+	–	+	–						–				
Wood and Halliday (2010)																	+ +
Righter et al. (2011)								–									
Siebert et al. (2011)	**n.e.** **n.e.**		+ **n.e.**	+ **n.e.**		+ **n.e.**	**n.e.** –	– **n.e.**	– –								
Wheeler et al. (2011)										**n.e.**							
Ballhaus et al. (2013)	+ **n.e.**					+ **n.e.**					+ **n.e.**	**n.e.** **n.e.**	**n.e.** **n.e.**			+ **n.e.**	+ **n.e.**
Bouhifd et al. (2013)																	+ –
Boujibar et al. (2014)		– +															
Siebert et al. (2013)			+ **n.e.**														

*above 6 GPa

5.1.2 S-content of the Fe metal

It has been explained in Chapter 1, Section 1.7 and shown in Chapter 4 that the nature and concentration of light elements in the core-forming metallic melt can significantly influence the partitioning behaviour of siderophile elements. In this Chapter it will be shown that also S can cause major changes in the partition coefficients of volatile elements that could change their absolute and relative abundances in the mantle. To study the effect of S on the metal – silicate partitioning of volatile elements is of particular importance, because it has been proposed by several authors that the Earth´s core contains up to 2 wt% S (Dreibus and Palme, 1996; McDonough, 2003). Moreover it has been argued by O´Neill (1991) that significant amounts of S have been added to the Earth in its final stages of growth, which was extracted to the Earth´s core in the form of the "Hadean matte" – a Fe-Ni-S-O liquid – with the result of chalcophile (S-loving) elements being particularly depleted. Recently Boujibar et al. (2014) investigated the metal – silicate partitioning behaviour of S at high pressures and temperatures. When these results are incorporated into core formation models the authors find indications for both: The Earth´s S abundances might either be established by metal –silicate equilibration in a magma ocean or by the addition of a late veneer.

A few studies have exclusively investigated the effects of S in the metal phase on partitioning including the early studies of Jana and Walker (1997) and of Gaetani and Grove (1997). Both studies were focused on refractory elements, yet also provide results for the volatile elements Ge, W, P, Au and Cu. Jana and Walker (1997) showed that Ge, P and Au become less siderophile with increasing S content in the metal. The authors could not explain the abundances of the studied elements in the Earth´s mantle by the contribution of S in the metal phase alone. However one should note that their experiments were conducted at comparably low pressures of 1 – 5 GPa and that the experiments were performed in graphite capsules which is known to influence the partitioning of siderophile elements due to dissolution of C in the metal phase during the experiment. On the basis of experiments with variable S contents that were conducted at 1 atm and 1623 K Gaetani and Grove (1997) could also not satisfactorily explain the mantle abundance of Cu. The influence of increasing S contents in the metal on the partitioning behaviour of Pb and Tl based on experiments performed at 2 GPa and 1650 to 2158 K was studied by Wood et al. (2008). Increasing the S content from 0 to 35 wt% resulted in increased partition coefficient values for both elements. The authors argue that a late extraction of 0.1 % sulphide to the Earth´s core through a

partially molten mantle can satisfy both the concentration and isotopic signature of Pb and Tl. Recently Bouhifd et al (2013) investigated the partitioning behaviour of U and Pb between a CI like silicate melt and different Fe rich metal phases in the system Fe-C-Ni-Si-S at a pressure and temperature range between 3 and 8 GPa and 2073 and 2373 K respectively. The investigations of Bouhifd et al. (2013) showed that both elements become more siderophile if the concentration of S in the metal phase is enhanced. Bouhifd et al. (2013) found that either high pressure – high temperature equilibration in a deep magma ocean or the additions of a late accretionary component that exhibits > 30 wt% S in the metal phase can account for the depletion of Pb in the Earth´s mantle. Lately the high pressure – high temperature partitioning of a wide range of elements (Cu, In, Tl, Pb, Ag, Mn, Zn, Cr, Co, Ni, Sb and Cd) between sulphide (FeS) and an anhydrous basaltic melt in graphite capsules has been investigated by Kiseeva et al. (2013). The authors argue for a simple relationship between the FeO content of the silicate phase and the sulphide - silicate partition coefficients of the elements of interest. A detailed description of the approach of constraining the sulphide - silicate partitioning behaviour as proposed by Kiseeva et al. (2013) follows at the end of Section 5.2.

Table 11 summarizes the results of the S dependent partitioning behaviour of volatile elements of the above mentioned publications as well as several other studies that partly incorporated S bearing phases into their set of partitioning experiments (e.g. Mann et al., 2009). Plus signs (+) indicate that the particular element becomes more siderophile with increasing S content of the metal phase and vice versa for minus signs (–).

Table 11: *Summary of experimental studies that investigated the influence of S on the partitioning behaviour of volatile elements. Green plus or minus signs respectively indicate whether increasing S-contents of the metal phase cause an increase or decrease of a particular element. Purple shaded columns mark volatile elements the S-dependent partitioning of which is also investigated within the course of this study. N.e. stands for "no effect".*

Volatile elements →	**P**	**K**	**V**	**Mn**	**Zn**	**Ga**	**Ge**	**Ag**	**In**	**Sb**	**Au**	**Tl**	**Pb**
Publications ↓	**increasing S-content of the metal** leads to increased **(+)** or decreased **(–)** siderophility												
Jana and Walker (1997)	–						–				–		
Ohtani et al. (1997)			**n.e.**	**n.e.**									
Chabot and Drake (1999)		+											
Lagos et al. (2008)													+
Wood et al. (2008)												+	+
Mann et al. (2009)			+	+	**n.e.**	+			**n.e.**				
Righter et al. (2009)										+			
Wood and Halliday (2010)													+
Wheeler et al (2011)								–					
Bouhifd et al. (2013)													+

5.1.3 Si-content of the metal

In Chapter 4 the effect of Si dissolved in the metal on the partitioning of the volatile elements Cu, Ag, Pb, Au, Sn, Ge, Sb, As and P has been extensively studied. The results relate to the investigations of this Chapter since the derived valence states are used to calculate the concentrations of the oxides of the elements of interest in the silicate phase and more importantly to formulate exchange coefficient values K_D^{M-Fe}. In the course of the calculations of this Chapter the derived interaction parameter values ε_{Si}^{M} of Chapter 4 have been refined facilitated by several other additional experiments.

5.2 Methods

5.2.1 This study

The volatile elements Ag, Cu, Au, Pb, Sn, Ge, Sb, As and P were chosen for investigations of liquid metal – liquid silicate partitioning behaviour at pressures and temperatures between 11 and 23 GPa and 2400 – 2800 K. Furthermore experiments at 11 GPa were performed in order to quantify the effect of variable S-contents in the metal phase. The experiments, the determination of temperatures and the analysis of metal, ferropericlase and silicate phases were performed following the routines that are described in Chapter 2. Partition coefficients as well as exchange coefficients and oxygen fugacities have been calculated employing equations [3], [5] and [7] (Chapters 3). The determinations incorporate molar values for both: the native element of interest in the metal phase and the oxide values (based on one cation) of the element of interest in the silicate phase. The formulation of the oxides and the final calculations of K_D^{M-Fe} values are based on the valence states that have been derived in Chapter 4.

As described in Chapter 4 the partitioning of any element of interest *M* between liquid metal and liquid silicate can be described by formulating an exchange reaction that involves Fe and FeO:

$$\frac{n}{2}\,Fe^{met} + MO_{\frac{n}{2}}^{sil} = \frac{n}{2}\,FeO^{sil} + M^{met} \qquad [27]$$

The equilibrium constant of this equation is defined as:

$$K = \frac{X_M^{met}\,\gamma_M^{met}\left(X_{FeO}^{sil}\,\gamma_{FeO}^{sil}\right)^{\frac{n}{2}}}{X_{MO_{\frac{n}{2}}}^{sil}\,\gamma_{MO_{\frac{n}{2}}}^{sil}\,\left(X_{Fe}^{met}\,\gamma_{Fe}^{met}\right)^{\frac{n}{2}}} \qquad [28]$$

X and *γ* denote the molar fractions of the individual phases and their corresponding activity coefficients respectively. The parameter *n* is the valence of the element of interest in the silicate phase. In concordance with the assumptions made in Chapter 4 the equilibrium

constant *K* can be simplified by assuming that the activity coefficients in the silicate phase remain constant over the narrow range of silicate compositions in our experiments. Employing the definition of the exchange coefficient K_D^{M-Fe} (equation [5], Chapter 3) the expression for K reduces to:

$$K = K_D^{M-Fe} \frac{\gamma_M^{met}}{(\gamma_{Fe}^{met})^{\frac{n}{2}}} \quad [29]$$

At chemical equilibrium *K* is related to the Gibbs free energy change of the standard state, the temperature (in K) and the gas constant R as follows:

$$-\Delta G^0 = RT\ lnK \quad [30]$$

The combination of equations [29] and [30] together with a conversion from the natural to the common logarithm leads to an expression for logarithmic K_D^{M-Fe}:

$$\log K_D^{M-Fe} = \frac{-\Delta G^0}{RT \ln(10)} - \frac{\ln(\gamma_M)}{\ln(10)} + \frac{\frac{n}{2}\ln(\gamma_{Fe})}{\ln(10)} \quad [31]$$

Finally the Gibbs free energy change of the standard state -ΔG^0 can be described with the help of expressions for the enthalpy, entropy and volume change at standard state conditions:

$$-\Delta G^o = \Delta H^0 - T\Delta S^0 + P\Delta V \quad [32]$$

Incorporating equation [32] into equation [31] leads to the following expression of $\log K_D^{M-Fe}$ in which *a*, *b* and *c* denote constants that are correlated to the entropy, enthalpy and the volume change respectively:

$$\log K_D^{M-Fe} = a + \frac{b}{T} + \frac{c\ P}{T} - \frac{\ln(\gamma_M)}{\ln(10)} + \frac{\frac{n}{2}\ln(\gamma_{Fe})}{\ln(10)} \quad [33]$$

The activities of Fe and the element of interest *M* in the metal phase have been calculated employing the ε-model as formulated by Ma et al. (2001). The general expressions for calculating activities of Fe (solvent: 1) and of any solute *i* among a number of *N* solutes in Fe-bearing metallic solutions are given by equations [34] and [35] respectively.

$$ln\gamma_1 = \sum_{i=2}^{N} \varepsilon_i^i \left(X_i + ln(1-X_i)\right) - \sum_{j=2}^{N-1}\sum_{k=j+1}^{N} \varepsilon_j^k X_j X_k \left(1 + \frac{ln(1-X_j)}{X_j} + \frac{ln(1-X_k)}{X_k}\right) + \sum_{i=2}^{N}\sum_{\substack{k=2 \\ (k\neq i)}}^{N} \varepsilon_i^k X_i X_k \left(1 + \frac{ln(1-X_k)}{X_k} - \frac{1}{1-X_i}\right) + \frac{1}{2}\sum_{j=2}^{N-1}\sum_{k=j+1}^{N} \varepsilon_j^k X_j^2 X_k^2 \left(\frac{1}{1-X_j} + \frac{1}{1-X_k} - 1\right) - \sum_{i=2}^{N}\sum_{\substack{k=2 \\ (k\neq i)}}^{N} \varepsilon_i^k X_i^2 X_k^2 \left(\frac{1}{1-X_i} + \frac{1}{1-X_k} + \frac{X_i}{2(1-X_i)^2} - 1\right)$$

[34]

$$ln\gamma_i = ln\gamma_i^0 - \varepsilon_i^i\, ln(1-X_i) - \sum_{\substack{k=2 \\ (k\neq i)}}^{N} \varepsilon_i^k X_k \left(1 + \frac{ln(1-X_k)}{X_k} - \frac{1}{1-X_i}\right) + \sum_{\substack{k=2 \\ (k\neq i)}}^{N} \varepsilon_i^k X_k^2 X_i \left(\frac{1}{1-X_i} + \frac{1}{1-X_k} + \frac{X_i}{2(1-X_i)^2} - 1\right)$$

[35]

The interaction parameter ε_i^k describes the influence on the activity of a given solute *i* as a function of the concentration of another solute all dissolved in Fe metal. The parameter γ_i^o is the activity of *i* at infinite dilution and *X* are the mole fractions of the individual components in Fe metal. In the framework of this study the effects of pressure, temperature and of Si- and S- contents of the metal phase on the partitioning behaviour of volatile elements have been quantified. Equations [34] and [35] were thus solved for a quarternary system with the solvent Fe (1) and the three solutes S, Si and the element of interest *M*. The expressions for the calculations of $ln\gamma_{Fe}$ and $ln\gamma_M$ are given in equations [36] and [37] respectively.

$$
\begin{aligned}
ln\gamma_{Fe} = {} & \varepsilon_{Si}^{Si}\,(X_{Si} + \ln(1 - X_{Si})) + \varepsilon_{S}^{S}\,(X_S + \ln(1 - X_S)) + \varepsilon_{M}^{M}\,(X_M + \ln(1 - X_M)) \\
& - \varepsilon_{Si}^{S}\,X_{Si}\,X_S\left(1 + \frac{\ln(1 - X_{Si})}{X_{Si}} + \frac{\ln(1 - X_S)}{X_S}\right) \\
& - \varepsilon_{Si}^{M}\,X_{Si}\,X_M\left(1 + \frac{\ln(1 - X_{Si})}{X_{Si}} + \frac{\ln(1 - X_M)}{X_M}\right) \\
& - \varepsilon_{S}^{M}\,X_S\,X_M\left(1 + \frac{\ln(1 - X_S)}{X_S} + \frac{\ln(1 - X_M)}{X_M}\right) \\
& + \varepsilon_{Si}^{S}\,X_{Si}\,X_S\left(1 + \frac{\ln(1 - X_S)}{X_S} - \frac{1}{1 - X_{Si}}\right) \\
& + \varepsilon_{Si}^{M}\,X_{Si}\,X_M\left(1 + \frac{\ln(1 - X_M)}{X_M} - \frac{1}{1 - X_{Si}}\right) \\
& + \varepsilon_{S}^{Si}\,X_S\,X_{Si}\left(1 + \frac{\ln(1 - X_{Si})}{X_{Si}} - \frac{1}{1 - X_S}\right) \\
& + \varepsilon_{S}^{M}\,X_S\,X_M\left(1 + \frac{\ln(1 - X_M)}{X_M} - \frac{1}{1 - X_S}\right) \\
& + \varepsilon_{M}^{Si}\,X_M\,X_{Si}\left(1 + \frac{\ln(1 - X_{Si})}{X_{Si}} - \frac{1}{1 - X_M}\right) \\
& + \varepsilon_{M}^{S}\,X_M\,X_S\left(1 + \frac{\ln(1 - X_S)}{X_S} - \frac{1}{1 - X_M}\right) \\
& + \frac{1}{2}\,\varepsilon_{Si}^{S}\,X_{Si}^2\,X_S^2\left(\frac{1}{1 - X_{Si}} + \frac{1}{1 - X_S} - 1\right) \\
& + \frac{1}{2}\,\varepsilon_{Si}^{M}\,X_{Si}^2\,X_M^2\left(\frac{1}{1 - X_{Si}} + \frac{1}{1 - X_M} - 1\right) \\
& + \frac{1}{2}\,\varepsilon_{S}^{M}\,X_S^2\,X_M^2\left(\frac{1}{1 - X_S} + \frac{1}{1 - X_M} - 1\right) \\
& - \varepsilon_{Si}^{S}\,X_{Si}^2\,X_S^2\left(\frac{1}{1 - X_{Si}} + \frac{1}{1 - X_S} + \frac{X_{Si}}{2(1 - X_{Si})^2} - 1\right) \\
& - \varepsilon_{Si}^{M}\,X_{Si}^2\,X_M^2\left(\frac{1}{1 - X_{Si}} + \frac{1}{1 - X_M} + \frac{X_{Si}}{2(1 - X_{Si})^2} - 1\right) \\
& - \varepsilon_{S}^{Si}\,X_S^2\,X_{Si}^2\left(\frac{1}{1 - X_S} + \frac{1}{1 - X_{Si}} + \frac{X_S}{2(1 - X_S)^2} - 1\right) \\
& - \varepsilon_{S}^{M}\,X_S^2\,X_M^2\left(\frac{1}{1 - X_S} + \frac{1}{1 - X_M} + \frac{X_S}{2(1 - X_S)^2} - 1\right) \\
& - \varepsilon_{M}^{Si}\,X_M^2\,X_{Si}^2\left(\frac{1}{1 - X_M} + \frac{1}{1 - X_{Si}} + \frac{X_M}{2(1 - X_M)^2} - 1\right) \\
& - \varepsilon_{M}^{S}\,X_M^2\,X_S^2\left(\frac{1}{1 - X_M} + \frac{1}{1 - X_S} + \frac{X_M}{2(1 - X_M)^2} - 1\right) \qquad [36]
\end{aligned}
$$

$$ln\gamma_M = ln\gamma_{Fe} + ln\gamma_M^0 - \varepsilon_M^M \ln(1-X_M) - \varepsilon_M^{Si} X_{Si}\left(1 + \frac{\ln(1-X_{Si})}{X_{Si}} - \frac{1}{1-X_M}\right) - \varepsilon_M^S X_S\left(1 + \frac{\ln(1-X_S)}{X_S} - \frac{1}{1-X_M}\right) + \varepsilon_M^{Si} X_{Si}^2 X_M\left(\frac{1}{1-X_M} + \frac{1}{1-X_{Si}} + \frac{X_M}{2(1-X_M)^2} - 1\right) + \varepsilon_M^S X_S^2 X_M\left(\frac{1}{1-X_M} + \frac{1}{1-X_S} + \frac{X_{Si}}{2(1-X_M)^2} - 1\right)$$

[37]

According to the Steelmaking Data Sourcebook an interaction parameter ε_i^k equals the interaction parameter ε_k^i. One should note that the Steelmaking Data Sourcebook provides mass related e_i^k values that can be converted into interaction parameter values ε_i^k by employing equation [38] in which M_k denotes the molar mass of element *k*:

$$e_i^k = 0.00434\left[\left(\varepsilon_i^k - 1\right)\frac{55.85}{M_k} + 1\right]$$

[38]

When available the values for the activities at infinite dilution and the individual interaction parameters ε_i^k were derived from the values given in the Steelmaking Data Sourcebook. If the values were not available for certain elements they were set to zero. Table 12 summarizes the values that are used in this study.

Table 12: *Summary of interaction parameter values* $\boldsymbol{\varepsilon_i^k}$ *and activity coefficients at infinite dilution* $\boldsymbol{\gamma_i^0}$ *that were used to calculate the activity coefficients of Fe and the element of interest M in the metal with regards to equations [36] to [37]. All values were derived from the Steelmaking Data Sourcebook.*

	Cu	**Ag**	**Au**	**Pb**	**Sn**	**Ge**	**Sb**	**As**	**P**
$\boldsymbol{\gamma_M^0}$	8.58	200	-	837	2.58	-	-	-	-
$\boldsymbol{\varepsilon_M^M}$	-5.38	-18.73	-	-	-0.29	1.80	-	-	7.35

$\boldsymbol{\varepsilon_{Si}^{Si}}$	12.43
$\boldsymbol{\varepsilon_S^S}$	-5.66
$\boldsymbol{\varepsilon_{Si}^S}$	9.16

Temperature corrections were performed following Tuff et al. (2011):

$$\varepsilon_i^j\ (T) = \frac{1873}{T}\ \varepsilon_i^j\ (1873) \qquad [39]$$

The interaction parameters ε_{Si}^M and ε_S^M as well as the constants *a*, *b* and *c* were fitted simultaneously by minimizing the sum of the weighted deviation between experimentally determined and calculated log K_D^{M-Fe} values. The summarized weighted deviations were calculated by employing equation [40] where $\delta \log K_D^{M-Fe(exp)}$ denotes the error on the experimentally investigated logarithmic exchange coefficients as calculated by error propagation:

$$\sigma = \sum \sqrt{\left(\frac{\left(log\ K_D^{M-Fe(calc)} - \log K_D^{M-Fe(exp)} \right)}{\left(\frac{100\ \delta \log K_D^{M-Fe(exp)}}{log K_D^{M-Fe(exp)}} \right)^2} \right)^2} \qquad [40]$$

Uncertainties on the expressions for logarithmic K_D^{M-Fe}values are derived from the average deviation between experimentally determined logarithmic K_D^{M-Fe}values and those that were calculated from the fitted parameters employing equation [41]. *N.* stands for the number of experiments.

$$\pm \log K_D^{M-Fe} = \frac{\sum \sqrt{\left(log K_D^{M-Fe(calc)} - log K_D^{M-Fe(exp)} \right)^2}}{N.} \qquad [41]$$

5.2.2 Parameterization of the sulphide – silicate partitioning behaviour as proposed by Kiseeva et al. (2013)

As mentioned above Kiseeva et al. (2013) investigated the high pressure – high temperature partitioning of a wide range of elements (Cu, In, Tl, Pb, Ag, Mn, Zn, Cr, Co, Ni, Sb and Cd)

between sulphide (FeS) and an anhydrous basaltic melt. The authors argue for a simple relationship between the FeO content of the silicate phase and the sulphide-silicate partition coefficients of the individual elements. Kiseeva et al. (2013) consider an exchange reaction that involves two sulphides and the valence *n* of the element of interest *M* in the silicate phase when parameterizing the partitioning behaviour:

$$MO_{\frac{n}{2}} + \frac{n}{2}\, FeS = MS_{\frac{n}{2}} + \frac{n}{2}\, FeO \qquad [42]$$

The authors assume that the activity coefficient ratio of $\frac{\gamma MS_{\frac{n}{2}}^{sulph}}{\gamma\, MO_{\frac{n}{2}}^{sil}}$ is constant for experiments at constant pressure and temperature, that the activity of FeS equals 1 and that the activity of FeO in the silicate phase is also constant because it was found by O´Neill and Eggins (2002) that γ_{FeO}^{sil} is only very little effected by composition. Taking into account these assumptions and defining a sulphide-metal partition coefficient as the molar ratio of the concentration of the element of interest *M* in the sulphide phase over its concentration in the silicate phase the equilibrium constant *K* becomes:

$$K = D_M^{sulph-sil} * \left(X_{FeO}^{sil}\right)^{\frac{n}{2}} \qquad [43]$$

Logarithmic $D_M^{sulph-sil}$ values are thus related to the FeO content of the silicate phase as shown in equation [44]:

$$logD_M^{sulph-sil} = A + \frac{n}{2}\log X_{FeO}^{sil} \qquad [44]$$

However these assumptions are only valid if the effect of S on the partitioning behaviour is investigated close to the FeS composition. For lower concentrations of S in the metal phase the activity of FeS needs to be corrected. To a first approximation it can be equated with the molar fraction of FeS in the metal phase. For this study equation [44] was thus expanded to the following expression:

$$\log D^{sulph-sil} = A + \frac{n}{2}\log X_{FeO}^{sil} - \frac{n}{2}\log X_{FeS}^{sulph} \quad [45]$$

It was found that this equation (or the "enhanced Kiseeva et al. (2013) approach") is not capable of reproducing partition coefficients of S-bearing samples if S-free experiments are taken into account when fitting the data. If S-free experiments are neglected this approach is capable of reproducing partition coefficients in the compositional metal region close to FeS, but does not match the observed partition coefficient values if the S-contents of the metal phase is lower. An example is shown for the element Cu in Section 5.3.1.1, Figure 31 a and b.

Although the ε-approach that will be used to parameterize partitioning in this study (see above) is established for iron alloys rather than for sulphides, it will be shown that this approach is sufficient for describing partitioning even if the S content of the metal phase is varied from pure Fe metal to FeS. The calculated exchange coefficient values matched the experimentally determined values in almost all cases as can be seen in Section 5.3 Results.

5.3 Results

For each element Table 13 summarizes the experimentally determined as well as the recalculated (equation [33]) exchange coefficient values K_D^{M-Fe}. Additionally the values for the Gibbs free energy change $-\Delta G^0$ and the molar fractions of Fe, Si, S and the element of interest *M* in the metal phase are given. Pressure, temperature and oxygen fugacity relative to the iron-wüstite buffer are also displayed. Uncertainties that were obtained by error propagation are given for the last digit(s).

Experimental data have been compared to literature data sets when available. In order to ensure comparability between the individual results the exchange coefficient values have been recalculated from the published results according to the criteria described in Chapter 3. Out of a given data set comparable experiments have been carefully selected on the basis of similar experimental conditions including agreement between the composition of metal and silicate phases and the capsule´s material. Because of this not all studies listed in Tables 10 and 11

have been used for comparison. On the other hand, results of two studies that did not derive a complete pressure, temperature or S trend, namely Kegler et al. (2011) and Kiseeva et al. (2013), could be compared to the results of this study. However due to the limited amount of experimental partitioning studies for volatile elements, the results have additionally been compared to data that was based on experiments with slightly different composition and capsule material, when other conformable investigations were not available.

A significant effect of pressure on the partitioning of the studied elements has not been observed for any element, while the partitioning of several elements is sensitive to temperature. Increasing S contents are capable of changing the exchange coefficient values significantly to both higher and lower values. The interaction parameters ε_{Si}^{M} which have been derived in Chapter 4 have been refined by the incorporation of several additional experiments. As will be shown further below the results do not significantly change.

The following Section provides detailed results for every element. In each case the pressure and / or temperature dependences are illustrated by plotting the experimentally investigated logarithmic exchange coefficients K_D^{M-Fe} minus the activity terms of equation [33] against inverse temperature. The calculated pressure and / or temperature dependences are shown by solid lines. Equation [46] displays the relationship between the calculated pressure and temperature dependences and the modified exchange coefficient values.

$$\log K_D^{M-Fe} + \frac{\ln(\gamma_M)}{\ln(10)} - \frac{\frac{n}{2}\ln(\gamma_{Fe})}{\ln(10)} = \log K_D^{M-Fe} - activity\ terms = a + \frac{b}{T} + \frac{c\,P}{T} \qquad [46]$$

Secondly the experimentally determined logarithmic exchange coefficient values have been plotted against inverse temperature. The ranges of inverse temperature (x-axis) and logarithmic exchange coefficient values (y-axis) have been expanded in order to be able to compare the results of this study with comparable literature data. Finally the parameterization of the S-dependent partitioning of each element is demonstrated by a diagram of logarithmic exchange coefficients against the S content of the metal phase. Dotted lines represent a linear regression line to the calculated results.

In the case of Cu two other diagrams illustrate the results of the parameterization of the S-dependent partitioning behaviour based on the “enhanced Kiseeva et al. (2013) approach” (see above).

The individual results Sections are ordered by increasing valence states as derived in Chapter 4.

Table 13: *Summary of the results of experimental and calculated* K_D^{M-Fe} *values and the Gibbs free energy change* $-\Delta G^0$ *for each element studied. X denote the molar fractions of Fe, Si, S and the element of interest in the metal phase. Pressures and temperatures are given in GPa and K respectively, oxygen fugacity is expressed relative to the iron-wüstite buffer. When determining* fO_2 *in the case of S-bearing samples the Fe content of the metal phase was corrected by subtracting the amount of Fe equal to the amount of S (formation of FeS). Uncertainties that were obtained by error propagation are given for the last digit(s).*

Copper Experiment	P (GPa)	T (K)	ΔIW	$-\Delta G^0$ [J/mole]	K_D^{Cu-Fe} (exp)	K_D^{Cu-Fe} (calc)	X_{Fe}^{met}	X_{Si}^{met}	X_S^{met}	X_{Cu}^{met}
H3355a	11	2490	-2.18 (8)	76417	7.8 (6)	8.6	0.9481	0.0011		0.0196
H3355b	11	2490	-2.02 (9)	76417	6 (3)	8.0	0.9383	0.0055		0.0009
H3361b	11	2844	-2.3 (2)	77563	8 (8)	7.0	0.9245	0.0014		0.0242
H3450a	11	2560	-2.4 (4)	76644	8.0 (6)	8.0	0.9655	0.0011		0.0118
H3707a	11	2641	-2.2 (2)	76906	8 (1)	7.6	0.9687	0.0026		0.0117
H3707b	11	2641	-4.7 (4)	76906	8 (1)	7.5	0.7551	0.2101		0.0119
H3718a	11	2658	-2.1 (2)	76961	7.6 (8)	7.5	0.9490	0.0041		0.0121
H3718b	11	2658	-3.7 (2)	76961	7.3 (9)	7.2	0.8941	0.0766		0.0091
Z822a	11	2573	-2.2 (1)	76686	7.7 (8)	7.9	0.9456	0.0078		0.0122
Z926a	11	2668	-2.4 (4)	76994	7 (1)	7.4	0.9459	0.0052		0.0126
Z926b	11	2668	-2.2 (2)	76994	8.5 (9)	7.7	0.9473	0.0028		0.0196
Z941b	11	2752	-2.5 (4)	77265	7.5 (8)	7.1	0.9559	0.0044		0.0125
Z859b	18	2717	-2.1 (2)	77152	6.7 (6)	7.2	0.9450	0.0079		0.0118
Z865b	18	2834	-2.4 (6)	77531	5.4 (4)	6.8	0.9530	0.0081		0.0127
Z929b	20	2799	-2.5 (5)	77418	7.7 (5)	6.9	0.9583	0.0041		0.0124
Z949b	21	2870	-2.0 (1)	77647	5.1 (6)	6.6	0.9312	0.0186		0.0119
Z950b	21	2904	-2.37 (3)	77757	6.0 (5)	6.5	0.9548	0.0121		0.0124
Z1062b	11	2636	-0.9 (3)	76890	13 (2)	14.9	0.5526	0.0006	0.3699	0.0137
Z1062a	11	2636	-1.6 (7)	76890	11 (2)	15.3	0.5616	0.0000	0.3834	0.0142
Z1008a	11	2614	-	76819	21 (2)	20.6	0.4090	0.0027	0.5113	0.0235
H3361a	11	2844	-2.0 (3)	77563	4 (1)	9.2	0.7749	0.0001	0.1403	0.0311
H3364-1	11	2570	-1.8 (3)	76676	7 (2)	11.7	0.7749	0.0001	0.1546	0.0365
H3364-2	11	2570	-1.8 (3)	76676	9 (2)	10.9	0.7741	0.0000	0.1758	0.0106
H3367b	11	2342	-1.6 (2)	75938	8 (2)	13.6	0.7783	0.0001	0.1647	0.0208

Table 13 continued

Silver Experiment	P (GPa)	T (K)	ΔIW	$-\Delta G^0$ [J/mole]	K_D^{Ag-Fe} (exp)	K_D^{Ag-Fe} (calc)	X_{Fe}^{met}	X_{Si}^{met}	X_S^{met}	X_{Ag}^{met}
H3400a	11	2553	-1.89 (6)	115564	5 (4)	5.1	0.9668	0.0001		0.0057
H3404a	11	2777	-2.4 (2)	127255	3.0 (6)	7.3	0.9528	0.0001		0.0037
H3439a	11	2567	-2.08 (8)	116295	1 (2)	4.9	0.9671	0.0004		0.0011
H3439b	11	2567	-1.8 (1)	116295	2 (3)	5.0	0.9092	0.0003		0.0019
H3444a	11	2609	-2.03 (8)	118487	5 (3)	5.3	0.9781	0.0060		0.0033
H3444b	11	2609	-2.3 (3)	118487	5 (2)	5.3	0.9809	0.0045		0.0030
H3497b	11	2718	-2.3 (2)	124176	2 (1)	6.2	0.9840	0.0055		0.0011
Z798a	11	2500	-2.2 (1)	112798	5 (2)	4.3	0.9803	0.0067		0.0028
Z798b	11	2500	-2.04 (7)	112798	4 (2)	4.4	0.9830	0.0013		0.0029
Z915a	11	2584	-4.3 (6)	117182	3 (2)	2.9	0.8825	0.1142		0.0015
Z915b	11	2584	-4.7 (3)	117182	2. (2)	1.4	0.7369	0.2588		0.0012
Z916a	11	2580	-2.5 (3)	116973	5 (4)	5.0	0.9842	0.0064		0.0028
Z922a	11	2588	-2.5 (4)	117391	5 (3)	5.2	0.9907	0.0035		0.0026
Z922b	11	2588	-1.97 (9)	117391	5 (2)	5.2	0.9835	0.0027		0.0024
Z852a	18	2663	-2.6 (5)	110058	0.5 (4)	3.3	0.9744	0.0114		0.0004
Z858a	18	2942	-2.5 (5)	124619	4 (2)	5.5	0.9714	0.0121		0.0029
Z869b	18	2677	-2.5 (3)	110789	3 (6)	3.6	0.8930	0.0079		0.0027
Z878a	18	2742	-2.4 (1)	114181	3 (5)	4.0	0.9491	0.0077		0.0030
Z881b	18	2653	-2.39 (8)	109536	3 (8)	3.4	0.9155	0.0082		0.0031
Z977b	21	2893	-2.3 (2)	117241	4 (2)	4.0	0.9726	0.0207		0.0025
Z980a	21	2911	-2.2 (2)	118181	4 (2)	4.3	0.9749	0.0134		0.0031
H3606	23	2540	-2.3 (2)	95605	0.4 (2)	1.6	0.9524	0.0296		0.0003
H3400b	11	2553	-1.66 (6)	115564	9 (7)	8.4	0.8281	0.0001	0.1422	0.0096
H3404b	11	2777	-2.2 (2)	127255	9 (8)	11.9	0.8186	0.0001	0.1432	0.0105
Z1013a	11	2624	-	119270	26 (3)	26.4	0.4648	0.0001	0.4810	0.0024
Z1016a	11	2607	-	118383	31 (8)	31.7	0.4219	0.0007	0.5345	0.0022

Table 13 continued

Gold Experiment	P (GPa)	T (K)	ΔIW	-ΔG^0 [J/mole]	K_D^{Au-Fe} (exp)	K_D^{Au-Fe} (calc)	X_{Fe}^{met}	X_{Si}^{met}	X_S^{met}	X_{Au}^{met}
H3400a	11	2553	-1.89 (6)	133912	763 (323)	548.5	0.9668	0.0001		0.0056
H3404a	11	2777	-2.4 (2)	134707	157 (35)	341.2	0.9528	0.0001		0.0065
H3439a	11	2567	-2.08 (8)	133962	2415 (868)	528.0	0.9671	0.0004		0.0054
H3439b	11	2567	-1.8 (1)	133962	1291 (605)	528.9	0.9092	0.0003		0.0047
Z1000a	11	2612	-2.7 (4)	134122	122 (141)	477.0	0.9557	0.0005		0.0043
Z1000b	11	2612	-2.7 (4)	134122	220 (72)	476.2	0.9566	0.0006		0.0048
Z1002a	11	2602	-4.5 (1)	134086	27 (12)	27.6	0.8151	0.1583		0.0064
Z1002b	11	2602	-3.4 (2)	134086	135 (61)	234.6	0.9244	0.0434		0.0035
Z1008b	11	2614	-2.9 (7)	134129	545 (209)	448.8	0.9618	0.0039		0.0031
Z1011a	11	2605	-2.1 (3)	134097	474 (234)	473.5	0.9639	0.0019		0.0022
Z1019b	11	2624	-4.8 (4)	134164	11 (8)	8.8	0.7721	0.2141		0.0015
Z869b	18	2677	-2.5 (3)	134352	274 (97)	367.7	0.8930	0.0079		0.0048
Z878a	18	2742	-2.4 (1)	134583	173 (68)	324.1	0.9491	0.0077		0.0043
Z878b	18	2742	-2.4 (3)	134583	347 (140)	331.8	0.9515	0.0062		0.0041
Z881b	18	2653	-2.39 (8)	134267	490 (343)	384.5	0.9155	0.0082		0.0046
Z957b	18	2603	-2.9 (6)	134090	476 (120)	483.1	0.9607	0.0009		0.0050
Z969a	21	2897	-2.5 (3)	135133	338 (118)	248.8	0.9478	0.0062		0.0052
Z969b	21	2897	-2.5 (4)	135133	571 (245)	259.5	0.9487	0.0034		0.0048
H3400b	11	2553	-1.66 (6)	133912	471 (313)	518.2	0.8281	0.0001	0.1422	0.0043
H3404b	11	2777	-2.2 (2)	134707	75 (58)	324.1	0.8186	0.0001	0.1432	0.0022
Z1043a	11	2636	-1.3 (4)	134207	125 (41)	388.7	0.6093	0.0001	0.3629	0.0028
Z1043b	11	2636	-1.4 (4)	134207	404 (158)	393.6	0.6211	0.0001	0.3390	0.0025

Lead Experiment	P (GPa)	T (K)	ΔIW	-ΔG^0 [J/mole]	K_D^{Pb-Fe} (exp)	K_D^{Pb-Fe} (calc)	X_{Fe}^{met}	X_{Si}^{met}	X_S^{met}	X_{Pb}^{met}
H3355a	11	2490	-2.18 (8)	98614	2 (2)	1.2	0.9481	0.0011		0.0033
H3355b	11	2490	-2.02 (9)	98614	1 (1)	1.2	0.9383	0.0055		0.0029
H3361b	11	2844	-2.3 (2)	98614	1 (1)	1.3	0.9245	0.0014		0.0026

Table 13 continued

H3449a	11	2560	-1.9 (2)	98614	2 (1)	1.2	0.9742	0.0022		0.0025
H3449b	11	2560	-1.94 (5)	98614	1 (1)	1.2	0.9736	0.0029		0.0021
H3455a	11	2562	-1.8 (1)	98614	0.6 (6)	1.2	0.9795	0.0006		0.0017
H3455b	11	2562	-2.0 (2)	98614	0.3 (3)	1.2	0.9895	0.0001		0.0019
H3497a	11	2718	-2.3 (3)	98614	1.5 (7)	1.2	0.9811	0.0074		0.0014
H3704a	11	2639	-4.5 (3)	98614	0.2 (2)	0.2	0.7845	0.2050		0.0012
H3704b	11	2639	-3.8 (3)	98614	0.4 (2)	0.5	0.8796	0.1180		0.0004
Z919a	11	2605	-2.4 (2)	98614	1.1 (5)	1.2	0.9864	0.0082		0.0010
Z919b	11	2605	-2.1 (2)	98614	1.1 (9)	1.2	0.9907	0.0015		0.0011
Z920b	11	2580	-2.3 (3)	98614	1.1 (8)	1.2	0.9871	0.0039		0.0008
Z854a	18	2740	-2.3 (2)	98643	1.0 (3)	1.1	0.9460	0.0148		0.0009
Z858b	18	2942	-2.4 (3)	98643	1 (1)	1.2	0.9684	0.0128		0.0013
Z881a	18	2653	-2.5 (4)	98643	1.0 (5)	1.1	0.9671	0.0137		0.0009
Z977a	21	2893	-2.3 (7)	98656	1.2 (6)	1.1	0.9697	0.0251		0.0011
Z980b	21	2911	-2.3 (3)	98656	1.1 (5)	1.1	0.9656	0.0220		0.0010
H3518	23	2594	-2.6 (3)	98664	0.8 (4)	1.1	0.9646	0.0186		0.0013
H3536	23	2542	-2.4 (7)	98664	2 (1)	1.1	0.9704	0.0111		0.0016
H3581	23	2540	-2.1 (2)	98664	1.0 (3)	1.2	0.9608	0.0087		0.0010
H3629	23	2589	-2.3 (3)	98664	1.4 (4)	1.0	0.9482	0.0246		0.0011
Z1001a	11	2636	-	98614	1.7 (5)	1.7	0.4325	0.0024	0.5237	0.0010
H3361a	11	2844	-2.0 (3)	98614	1.0 (7)	1.3	0.7749	0.0001	0.1403	0.0023
H3364-1	11	2570	-1.8 (3)	98614	1.3 (9)	1.3	0.7749	0.0001	0.1546	0.0030
H3364-2	11	2570	-1.8 (3)	98614	2 (1)	1.3	0.7741	0.0000	0.1758	0.0033
H3367b	11	2342	-1.6 (2)	98614	0.9 (7)	1.3	0.7783	0.0001	0.1647	0.0030
Z1016b	11	2607	-	98614	1.6 (7)	1.8	0.4190	0.0006	0.5518	0.0012
Z1019a	11	2624	0.8 (2)	98614	1.0 (8)	1.6	0.4893	0.0005	0.4508	0.0004

Tin Experiment	**P (GPa)**	**T (K)**	**ΔIW**	**$-\Delta G^0$** [J/mole]	**K_D^{Sn-Fe} (exp)**	**K_D^{Sn-Fe} (calc)**	**X_{Fe}^{met}**	**X_{Si}^{met}**	**X_S^{met}**	**X_{Sn}^{met}**
H3355a	11	2490	-2.18 (8)	36426	2.3 (3)	2.8	0.9481	0.0011		0.0036

Table 13 continued

H3355b	11	2490	-2.02 (9)	36426	1.6 (7)	2.6	0.9383	0.0055		0.0032
H3361b	11	2844	-2.3 (2)	37657	1 (2)	2.6	0.9245	0.0014		0.0051
H3450a	11	2560	-2.4 (4)	36669	3.4 (5)	2.8	0.9655	0.0011		0.0042
H3707a	11	2641	-2.2 (2)	36951	2.7 (6)	2.7	0.9687	0.0026		0.0032
H3707b	11	2641	-4.7 (4)	36951	0.12 (4)	0.1	0.7551	0.2101		0.0038
H3718a	11	2658	-2.1 (3)	37010	3.3 (8)	2.6	0.9490	0.0041		0.0045
H3718b	11	2658	-3.7 (2)	37010	0.9 (2)	1.0	0.8941	0.0766		0.0046
Z822a	11	2573	-2.2 (2)	36714	2.5 (4)	2.5	0.9456	0.0078		0.0049
Z926a	11	2668	-2.4 (4)	37045	2.7 (9)	2.6	0.9459	0.0052		0.0045
Z926b	11	2668	-2.2 (2)	37045	4 (2)	2.6	0.9473	0.0028		0.0049
Z941b	11	2752	-2.5 (4)	37337	2.1 (3)	2.5	0.9559	0.0044		0.0045
Z859b	18	2717	-2.1 (2)	45707	4.0 (7)	3.6	0.9450	0.0079		0.0047
Z865b	18	2834	-2.4 (6)	46114	3.1 (5)	3.4	0.9530	0.0081		0.0044
Z929b	20	2799	-2.5 (5)	48418	4.0 (9)	4.0	0.9583	0.0041		0.0041
Z949b	21	2870	-2.0 (2)	49878	4 (1)	3.5	0.9312	0.0186		0.0044
Z950b	21	2904	-2.4 (3)	49996	2.5 (7)	3.7	0.9548	0.0121		0.0040
Z1062b	11	2636	-0.9 (3)	36934	0.38 (8)	0.4	0.5526	0.0006	0.3699	0.0037
Z1062a	11	2636	-1.6 (7)	36934	0.4 (1)	0.4	0.5616	0.0000	0.3834	0.0044
Z1008a	11	2614	-	36857	0.15 (7)	0.2	0.4090	0.0027	0.5113	0.0026
H3361a	11	2844	-2.0 (3)	37657	0.6 (2)	1.4	0.7749	0.0001	0.1403	0.0058
H3364-1	11	2570	-1.8 (3)	36704	0.8 (1)	1.3	0.7749	0.0001	0.1546	0.0061
H3364-2	11	2570	-1.8 (3)	36704	0.9 (2)	1.2	0.7741	0.0000	0.1758	0.0067
H3367b	11	2342	-1.6 (2)	35911	1.0 (2)	1.2	0.7783	0.0001	0.1647	0.0066

Germanium Experiment	**P (GPa)**	**T (K)**	**ΔIW**	**$-\Delta G^0$** [J/mole]	K_D^{Ge-Fe} **(exp)**	K_D^{Ge-Fe} **(calc)**	X_{Fe}^{met}	X_{Si}^{met}	X_S^{met}	X_{Ge}^{met}
H3355a	11	2490	-2.18 (8)	59350	17 (2)	17.1	0.9481	0.0011		0.0077
H3355b	11	2490	-2.02 (9)	59350	11 (7)	16.2	0.9383	0.0055		0.0065
H3361b	11	2844	-2.3 (2)	67787	5 (8)	17.1	0.9245	0.0014		0.0116
H3450a	11	2560	-2.4 (4)	61018	0.15 (6)	17.2	0.9655	0.0011		0.0062

Table 13 continued

H3707a	11	2641	-2.2 (2)	62949	15 (3)	16.9	0.9687	0.0026		0.0051
H3707b	11	2641	-4.7 (4)	62949	0.8 (3)	0.9	0.7551	0.2101		0.0056
H3718a	11	2658	-2.1 (3)	63354	29 (7)	16.6	0.9490	0.0041		0.0054
H3718b	11	2658	-3.7 (2)	63354	7 (2)	6.7	0.8941	0.0766		0.0054
Z822a	11	2573	-2.2 (2)	61328	15 (4)	15.8	0.9456	0.0078		0.0079
Z926a	11	2668	-2.4 (4)	63592	23 (8)	16.4	0.9459	0.0052		0.0046
Z926b	11	2668	-2.2 (2)	63592	25 (8)	16.9	0.9473	0.0028		0.0049
Z941b	11	2752	-2.5 (4)	65594	8 (2)	16.6	0.9559	0.0044		0.0071
Z859b	18	2717	-2.1 (2)	64760	14 (8)	15.9	0.9450	0.0079		0.0069
Z865b	18	2834	-2.4 (6)	67549	21 (4)	15.9	0.9530	0.0081		0.0072
Z929b	20	2799	-2.5 (5)	66715	34 (6)	16.6	0.9583	0.0041		0.0066
Z949b	21	2870	-2.0 (2)	68407	14 (5)	14.2	0.9312	0.0186		0.0066
Z950b	21	2904	-2.4 (3)	69217	11 (3)	15.3	0.9548	0.0121		0.0069
Z1062b	11	2636	-0.9 (3)	62830	0.28 (7)	0.3	0.5526	0.0006	0.3699	0.0049
Z1062a	11	2636	-1.6 (7)	62830	0.35 (8)	0.2	0.5616	0.0000	0.3834	0.0065
Z1008a	11	2614	-	62305	0.01 (1)	0.0	0.4090	0.0027	0.5113	0.0005
H3361a	11	2844	-2.0 (3)	67787	1.9 (5)	4.7	0.7749	0.0001	0.1403	0.0094
H3364-1	11	2570	-1.8 (3)	61256	2.4 (6)	3.5	0.7749	0.0001	0.1546	0.0080
H3364-2	11	2570	-1.8 (3)	61256	2.9 (9)	2.8	0.7741	0.0000	0.1758	0.0084
H3367b	11	2342	-1.6 (2)	55822	3.3 (9)	2.7	0.7783	0.0001	0.1647	0.0075

Antimony Experiment	**P (GPa)**	**T (K)**	**ΔIW**	**$-\Delta G^0$** [J/mole]	**K_D^{Sb-Fe} (exp)**	**K_D^{Sb-Fe} (calc)**	**X_{Fe}^{met}**	**X_{Si}^{met}**	**X_S^{met}**	**X_{Sb}^{met}**
H3355a	11	2490	-2.18 (8)	64445	14 (2)	21.9	0.9481	0.0011		0.0029
H3355b	11	2490	-2.02 (9)	64445	3 (4)	20.0	0.9383	0.0055		0.0027
H3361b	11	2844	-2.3 (2)	73607	2 (5)	21.9	0.9245	0.0014		0.0042
H3450a	11	2560	-2.4 (4)	66257	1.7 (9)	22.0	0.9655	0.0011		0.0004
H3707a	11	2641	-2.2 (2)	68353	21 (6)	21.3	0.9687	0.0026		0.0043
H3707b	11	2641	-4.7 (4)	68353	0.14 (7)	0.1	0.7551	0.2101		0.0068
H3718a	11	2658	-2.1 (3)	68793	61 (18)	20.7	0.9490	0.0041		0.0054

Table 13 continued

H3718b	11	2658	-3.7 (2)	68793	5 (2)	4.4	0.8941	0.0766		0.0036
Z822a	11	2573	-2.2 (2)	66594	0.8 (3)	19.1	0.9456	0.0078		0.0003
Z926a	11	2668	-2.4 (4)	69052	43 (16)	20.2	0.9459	0.0052		0.0032
Z926b	11	2668	-2.2 (2)	69052	32 (13)	21.2	0.9473	0.0028		0.0035
Z941b	11	2752	-2.5 (4)	71226	9 (2)	20.6	0.9559	0.0044		0.0067
Z859b	18	2717	-2.1 (2)	70320	11 (9)	19.2	0.9450	0.0079		0.0064
Z865b	18	2834	-2.4 (6)	73349	1.0 (5)	19.3	0.9530	0.0081		0.0002
Z929b	20	2799	-2.5 (5)	72443	37 (9)	20.8	0.9583	0.0041		0.0059
Z949b	21	2870	-2.0 (2)	74280	10 (5)	15.8	0.9312	0.0186		0.0061
Z950b	21	2904	-2.4 (3)	75160	7 (3)	17.9	0.9548	0.0121		0.0057
Z1062b	11	2636	-0.9 (3)	68224	2.3 (9)	0.4	0.5526	0.0006	0.3699	0.0050
Z1062a	11	2636	-1.6 (7)	68224	1.7 (4)	0.4	0.5616	0.0000	0.3834	0.0055
Z1008a	11	2614	-	67655	0.06 (3)	0.1	0.4090	0.0027	0.5113	0.0026
H3361a	11	2844	-2.0 (3)	73607	3 (2)	6.3	0.7749	0.0001	0.1403	0.0059
H3364-1	11	2570	-1.8 (3)	66516	2 (1)	4.8	0.7749	0.0001	0.1546	0.0049
H3364-2	11	2570	-1.8 (3)	66516	8 (5)	3.8	0.7741	0.0000	0.1758	0.0069
H3367b	11	2342	-1.6 (2)	60615	7 (3)	3.7	0.7783	0.0001	0.1647	0.0045

Arsenic Experiment	**P (GPa)**	**T (K)**	**ΔIW**	**$-\Delta G^0$** [J/mole]	**K_D^{As-Fe} (exp)**	**K_D^{As-Fe} (calc)**	**X_{Fe}^{met}**	**X_{Si}^{met}**	**X_S^{met}**	**X_{As}^{met}**
H3400a	11	2553	-1.89 (6)	47724	7 (3)	9.4	0.9668	0.0001		0.0105
H3404a	11	2777	-2.4 (2)	48624	7 (2)	8.2	0.9528	0.0001		0.0132
H3439b	11	2567	-1.8 (1)	47780	1 (1)	9.3	0.9092	0.0003		0.0067
Z1000b	11	2612	-2.7 (4)	47961	5 (3)	8.9	0.9566	0.0006		0.0070
Z1002b	11	2602	-3.5 (2)	47921	1.2 (4)	2.2	0.9244	0.0434		0.0062
Z1008b	11	2614	-2.9 (7)	47969	24 (8)	8.0	0.9618	0.0039		0.0077
Z1011a	11	2605	-2.1 (3)	47933	42 (17)	8.6	0.9639	0.0019		0.0048
Z1019b	11	2624	-4.8 (4)	48009	0.003 (1)	0.0	0.7721	0.2141		0.0044
Z869b	18	2677	-2.5 (3)	72060	6 (4)	19.9	0.8930	0.0079		0.0102
Z878a	18	2742	-2.4 (1)	72322	4 (2)	18.9	0.9491	0.0077		0.0094

Table 13 continued

Z878b	18	2742	-2.4 (3)	72322	37 (10)	19.7	0.9515	0.0062		0.0093
Z881b	18	2653	-2.39 (8)	71964	48 (13)	20.1	0.9155	0.0082		0.0093
Z957b	18	2603	-2.9 (6)	71763	22 (5)	26.7	0.9607	0.0009		0.0089
Z969a	21	2897	-2.5 (3)	83161	21 (7)	26.4	0.9478	0.0062		0.0075
Z969b	21	2897	-2.5 (4)	83161	17 (4)	28.6	0.9487	0.0034		0.0080
H3400b	11	2553	-1.66 (6)	47724	2 (1)	7.5	0.8281	0.0001	0.1422	0.0077
H3404b	11	2777	-2.2 (2)	48624	0.7 (6)	6.6	0.8186	0.0001	0.1432	0.0031
Z1043a	11	2636	-1.3 (4)	48057	1.9 (6)	6.4	0.6093	0.0001	0.3629	0.0089
Z1043b	11	2636	-1.4 (4)	48057	6 (2)	6.3	0.6211	0.0001	0.3390	0.0076

Phosphorus Experiment	**P (GPa)**	**T (K)**	**ΔIW**	**$-\Delta G^0$** [J/mole]	K_D^{P-Fe} **(exp)**	K_D^{P-Fe} **(calc)**	X_{Fe}^{met}	X_{Si}^{met}	X_S^{met}	X_P^{met}
H3400a	11	2553	-1.89 (6)	-99380	0.007 (5)	0.0090	0.9668	0.0001		0.0049
H3404a	11	2777	-2.4 (2)	-99640	0.020 (3)	0.0124	0.9528	0.0001		0.0137
H3439a	11	2567	-2.08 (8)	-99397	0.09 (3)	0.0090	0.9671	0.0004		0.0079
H3439b	11	2567	-1.8 (1)	-99397	0.03 (1)	0.0091	0.9092	0.0003		0.0069
Z1000a	11	2612	-2.7 (4)	-99449	0.006 (5)	0.0089	0.9557	0.0005		0.0240
Z1000b	11	2612	-2.7 (4)	-99449	0.009 (1)	0.0089	0.9566	0.0006		0.0249
Z1002b	11	2602	-3.5 (2)	-99437	0.006 (3)	0.0038	0.9244	0.0434		0.0143
Z1008b	11	2614	-2.9 (7)	-99451	0.04 (2)	0.0089	0.9618	0.0039		0.0121
Z1011a	11	2605	-2.1 (3)	-99441	0.13 (5)	0.0091	0.9639	0.0019		0.0137
Z1019b	11	2624	-4.8 (4)	-99463	0.00007 (2)	0.0001	0.7721	0.2141		0.0039
Z869b	18	2677	-2.5 (3)	-99524	0.04 (1)	0.0087	0.8930	0.0079		0.0211
Z878a	18	2742	-2.4 (1)	-99600	0.08 (2)	0.0098	0.9491	0.0077		0.0213
Z878b	18	2742	-2.4 (3)	-99600	0.14 (3)	0.0101	0.9515	0.0062		0.0201
Z881b	18	2653	-2.39 (8)	-99496	0.06 (1)	0.0082	0.9155	0.0082		0.0238
Z957b	18	2603	-2.9 (6)	-99438	0.037 (9)	0.0089	0.9607	0.0009		0.0209
Z969a	21	2897	-2.5 (3)	-99779	0.04 (1)	0.0129	0.9478	0.0062		0.0192
Z969b	21	2897	-2.5 (4)	-99779	0.028 (7)	0.0133	0.9487	0.0034		0.0232
H3400b	11	2553	-1.66 (6)	-99380	0.0005 (6)	0.0016	0.8281	0.0001	0.1422	0.0026

Table 13 continued

H3404b	11	2777	-2.2 (2)	-99640	0.005 (2)	0.0023	0.8186	0.0001	0.1432	0.0158
Z1043a	11	2636	-1.3 (4)	-99477	0.0001 (1)	0.0001	0.6093	0.0001	0.3629	0.0001
Z1043b	11	2636	-1.4 (4)	-99477	0.00016 (9)	0.0002	0.6211	0.0001	0.3390	0.0002

5.3.1 Monovalent elements copper and silver

5.3.1.1 Copper

The parameterization of the metal – silicate partitioning behaviour of the volatile element Cu resulted in ε_{Si}^{M} and ε_{S}^{M} values of 0.73 and -2.58 respectively. The partitioning of Cu was found to be insensitive to changes in pressure. Increasing temperature however leads to decreased siderophility. The constants *a* and *b* (equation [33]) were found to be 0.17 and 3571 respectively. The temperature trend is shown in Figure 30a. The general trend of increasing temperature leading to decreasing siderophility of Cu is in agreement with the observations of Corgne et al. (2008), Kegler et al. (2009) and Righter et al. (2010). In agreement with this study Corgne et al. (2008) also showed that the partitioning of Cu is not affected by pressure. However, Kegler et al. (2009) and Righter et al. (2010) reported a negative pressure dependence (Table 10).

In Figure 30b the experimental results of the logarithmic exchange coefficient values K_D^{Cu-Fe} of this study and of Corgne et al. (2008) and Righter et al. (2010) are plotted against inverse temperature. Perfect agreement was found between the absolute values obtained in this study and by Righter et al. (2010). Differences between the results of this study and the results of the investigations made by Corgne et al. (2008) might be rooted in the use of graphite capsules by the latter authors, which necessitates corrections for the activities of Cu dissolved into the metal phase. From the Steelmaking Data Sourcebook a positive interaction parameter between C and Cu can be derived, that implies that C in the Fe-rich metal causes a decrease in siderophility for the element Cu.

Figure 30c shows the effect of increasing S contents of the metal phase on Cu partitioning. Logarithmic exchange coefficients change only slightly over the range of experimentally investigated conditions. An increase from 0 to 0.5 mole% S in the metal phase leads to an increase in siderophility of only half a logarithmic unit. The data of this study has been compared to the recalculated results of Wood et al. (2008) and Kiseeva et al. (2013). Differences between the results of this study and the results of the investigations made by Kiseeva et al. (2013) might be caused by the lower temperatures of the latter study. According to equation [41] a very small uncertainty on the fit for Cu of ± log K_D^{M-Fe} = 0.07 was found.

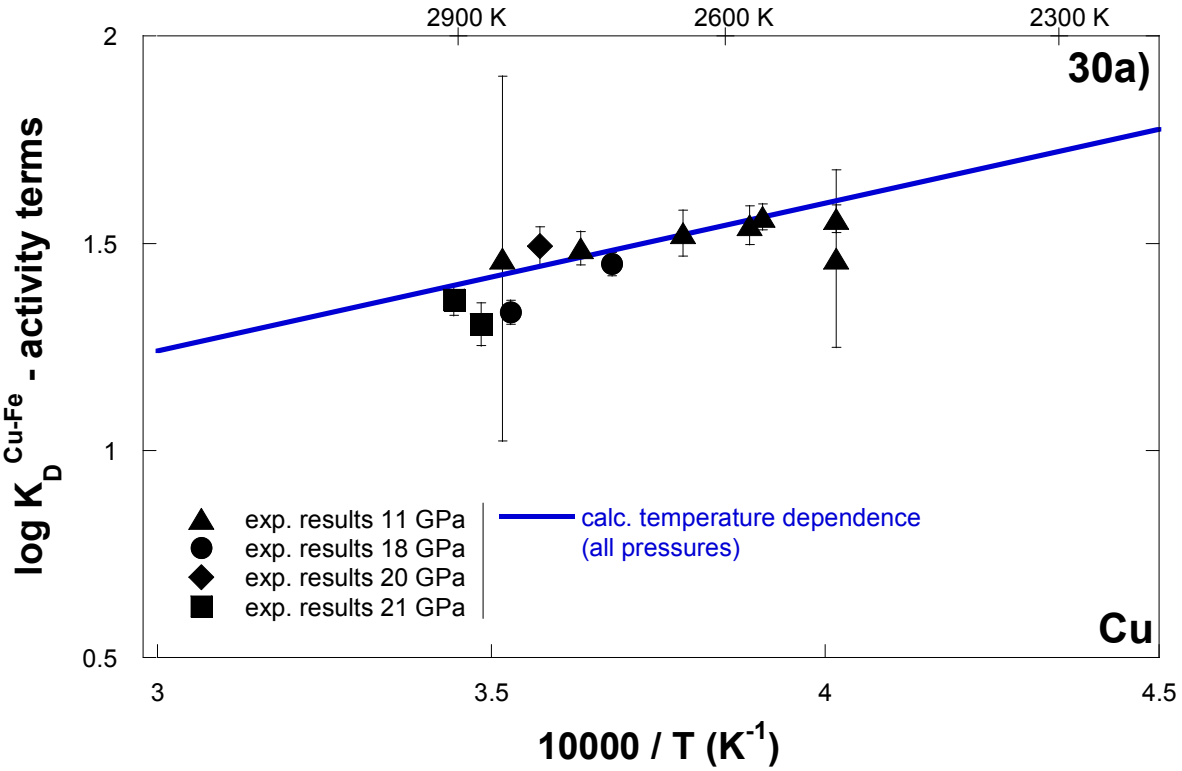
2900 K
2600 K
2300 K
30a)
log K_D^{Cu-Fe} - activity terms
2
1.5
1
0.5
exp. results 11 GPa
exp. results 18 GPa
exp. results 20 GPa
exp. results 21 GPa
calc. temperature dependence
(all pressures)
Cu
3
3.5
4
4.5
10000 / T (K^{-1})

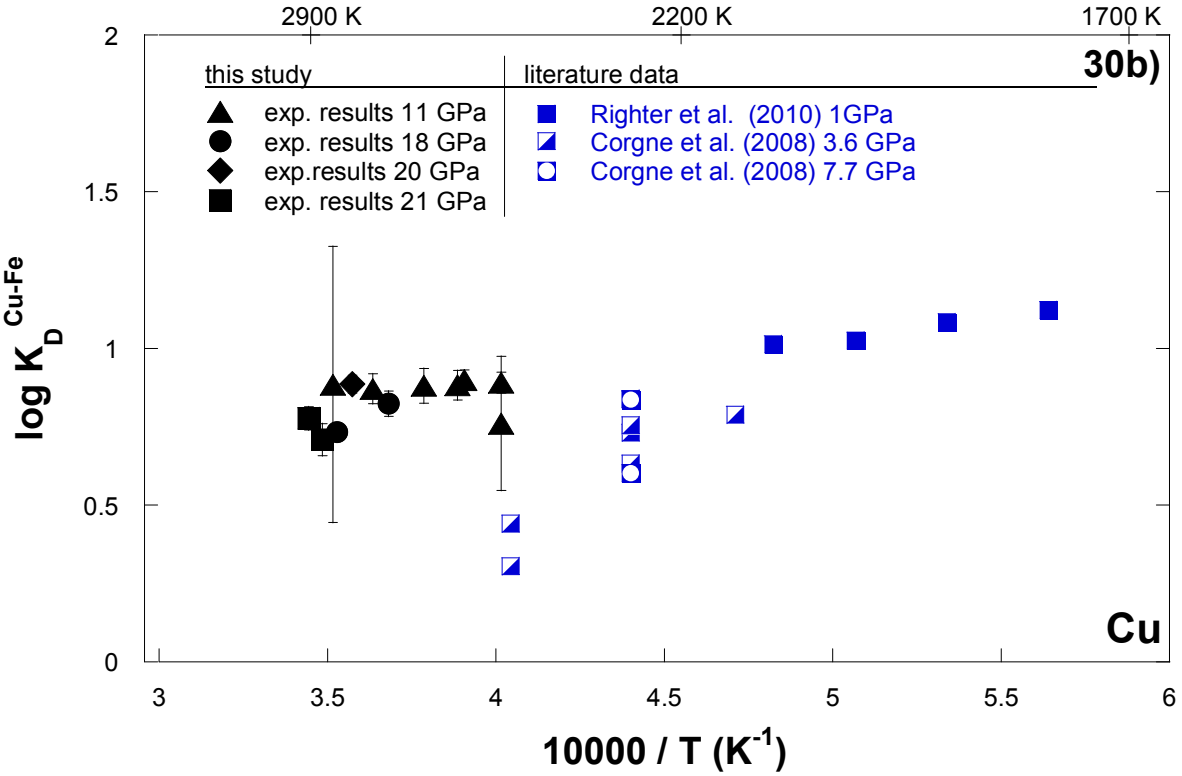
2900 K
2200 K
1700 K
30b)
this study
literature data
exp. results 11 GPa
exp. results 18 GPa
exp.results 20 GPa
exp. results 21 GPa
Righter et al. (2010) 1GPa
Corgne et al. (2008) 3.6 GPa
Corgne et al. (2008) 7.7 GPa
log K_D^{Cu-Fe}
2
1.5
1
0.5
0
Cu
3
3.5
4
4.5
5
5.5
6
10000 / T (K^{-1})

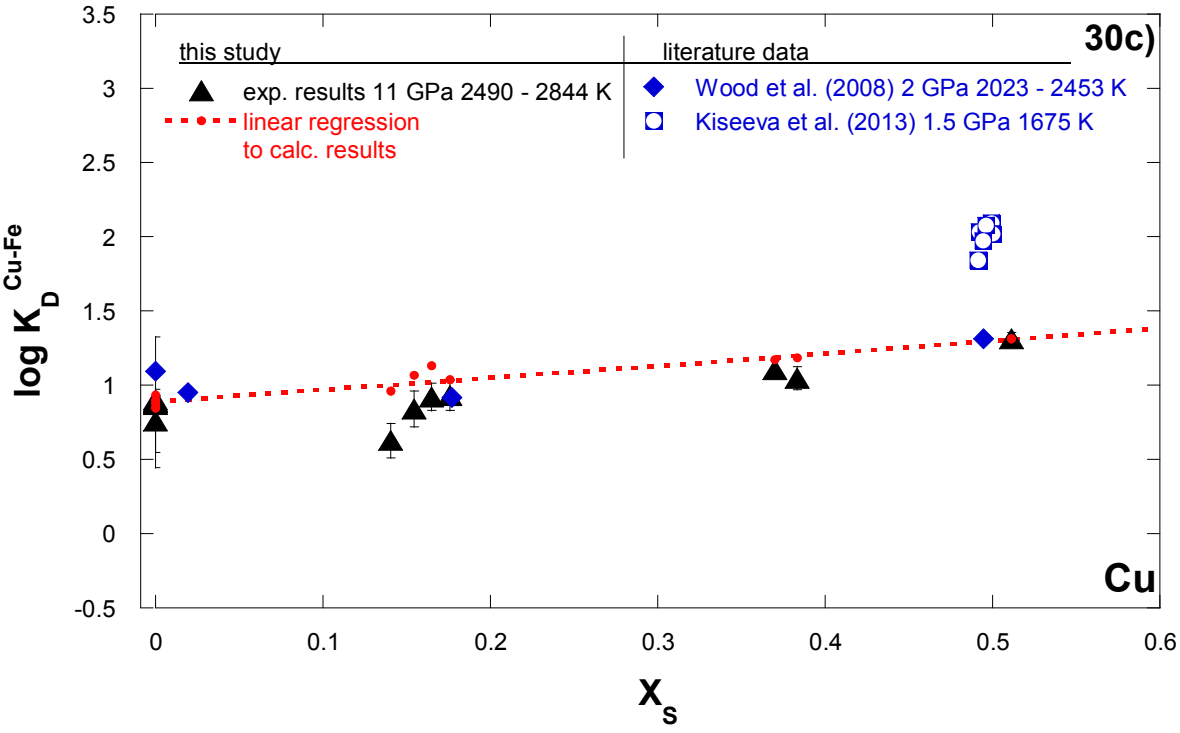

Figure 30a: *The temperature dependence of the partitioning behaviour of Cu. Experimentally determined logarithmic exchange coefficients minus the activity terms for Fe and Cu (equation [46]) are plotted against inverse temperature. The solid line represents the calculated temperature dependence of Cu partitioning.* ***b:*** *Comparison between the results of this study and the recalculated results from literature data sets for Cu. Experimentally obtained logarithmic exchange coefficient values are plotted against inverse temperature.* ***c:*** *The dependence of the metal – silicate partitioning of Cu on the S-content of the metal (mole fractions). The red dotted line represents a linear regression to the recalculated results for a fitted* ε_S^{Cu} *value of -2.58. Unfilled symbols in b) and c) denote experiments that were conducted in graphite capsules.*

As mentioned earlier the epsilon approach is established for trace elements in iron alloys. At very high S concentrations however the metal phase becomes a sulphide. Kiseeva et al. (2013) proposed that the partitioning behaviour of siderophile elements between liquid sulphide and liquid silicate can be parameterized by correlating the logarithmic partition coefficients $D^{met\text{-}sil}$ to the FeO content of the silicate phase (Section 5.2.2). However this approach has been solely designed for isobaric and isothermal experiments because of which the number of experiments was reduced. It was found that the "enhanced Kiseeva et al. (2013) approach" is not capable of reproducing partition coefficients of S-bearing samples if S-free experiments are incorporated into the fit. This can be seen in Figure 31a: In this diagram logarithmic partition coefficients are plotted against molar FeS contents of the metal or sulphide phase. Constant *a* in equation [45] equals -8.25. The calculated values only match with the experimental data in the case of S-free experiments. The results of the S-bearing samples

however are missed by 10 orders of magnitude. This changes when S-free experiments are neglected for fitting the experimental data as can be seen in Figure 31b. Now, as predicted by Kiseeva et al. (2013) the calculated partition coefficients are in perfect agreement with the experimental findings in the case of pure FeS. Constant a of equation [45] has a value of 2.57. However, the experimental data of experiments with lower concentrations of S in the metal phase are still not well reproduced by this approach.

In summary it is confirmed that the approach published by Kiseeva et al. (2013) is capable of parameterizing sulphide – silicate partition coefficients. For metal phases with S-concentrations up to 20 mole% however it was found that this approach does not produce good results. Instead it has been found that the ε-approach works perfectly even if the metal phase of the experiments was completely replaced by FeS. Therefore the complete parameterization of the influence of S on the partitioning behaviour of siderophile elements in this study was based on the ε-approach.

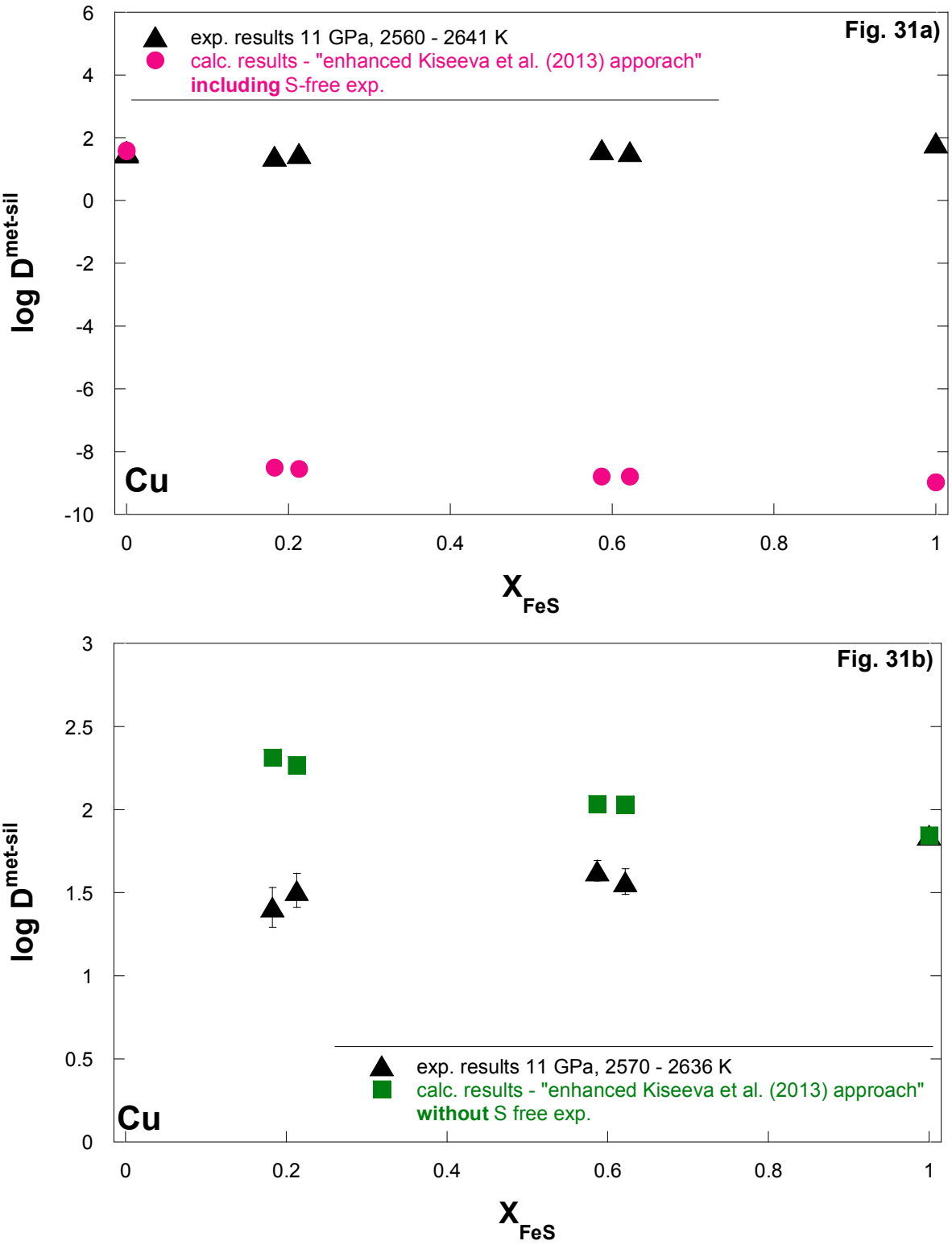

Figure 31: *Experimental and calculated logarithmic partition coefficients for the element Cu are plotted against the molar fraction of FeS in the experiments. The calculated data points have been obtained by employing the "enhanced Kiseeva et al. (2013) approach" as given in equation [45].* ***a:*** *All experiments – S-free up to pure FeS – have been taken into account when fitting the data.* ***b:*** *S-free experiments have been neglected when fitting the data.*

5.3.1.2 Silver

The pressure and temperature dependent partitioning behaviour of Ag is best described by neglecting constant *b* of equation [33]. The constants *a* and *c* were found to be 2.73 and -84 respectively. The siderophility of Ag thus increases with increasing temperature and decreases with increasing pressure. In good agreement with Chapter 4 the interaction parameter between Si and Ag was refined to be 6.75. Increasing S contents lead to an increase in siderophility, corresponding to an ε_S^{Ag} value of -4.07. The uncertainty on the fit for Ag is 0.17 logarithmic units.

The data of this study have been compared to the datasets of Wheeler et al. (2011) and Kiseeva et al. (2013). Within the error bars the results of this study and those from the first publication are in agreement although Wheeler et al. did not observe any effect of temperature on the metal – silicate partitioning of Ag. The exchange coefficient values derived from the dataset of Kiseeva et al. (2013) were again found to exceed the observations of this study by around half a logarithmic unit. According to the results of this study this might be caused by a difference in pressure.

The pressure and temperature dependent partitioning behaviour of Ag, the comparison to literature and the influence of S on the metal – silicate partitioning are displayed in Figures 32a, 32b and 32c respectively.

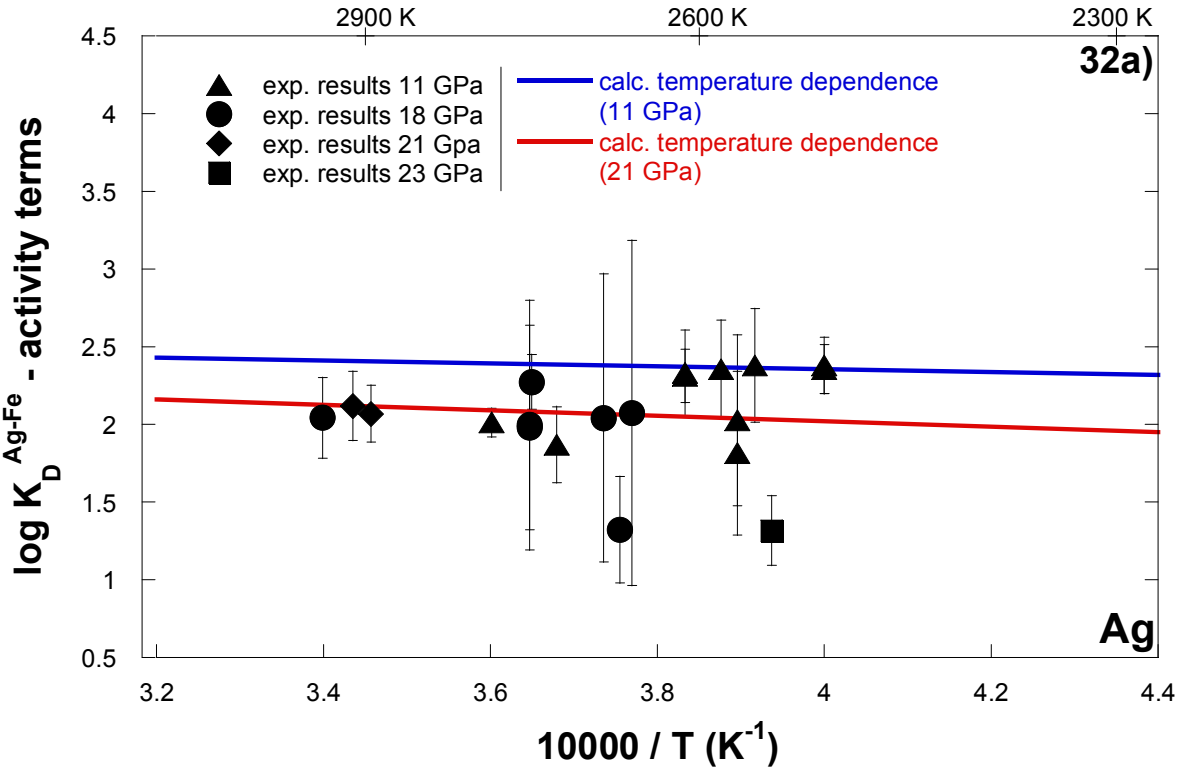
2900 K
2600 K
2300 K
32a)
exp. results 11 GPa
exp. results 18 GPa
exp. results 21 Gpa
exp. results 23 GPa
calc. temperature dependence (11 GPa)
calc. temperature dependence (21 GPa)
log K_D^Ag-Fe - activity terms
Ag
10000 / T (K^-1)

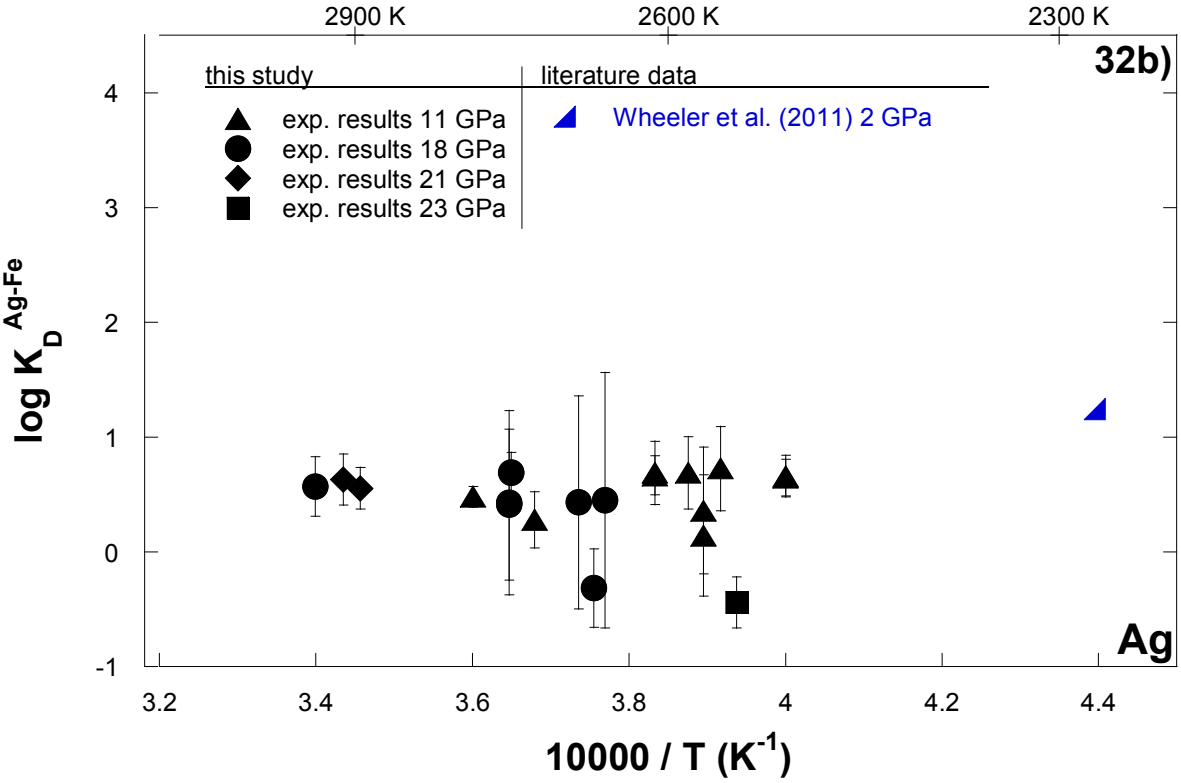
2900 K
2600 K
2300 K
32b)
this study
literature data
exp. results 11 GPa
exp. results 18 GPa
exp. results 21 GPa
exp. results 23 GPa
Wheeler et al. (2011) 2 GPa
log K_D^Ag-Fe
Ag
10000 / T (K^-1)

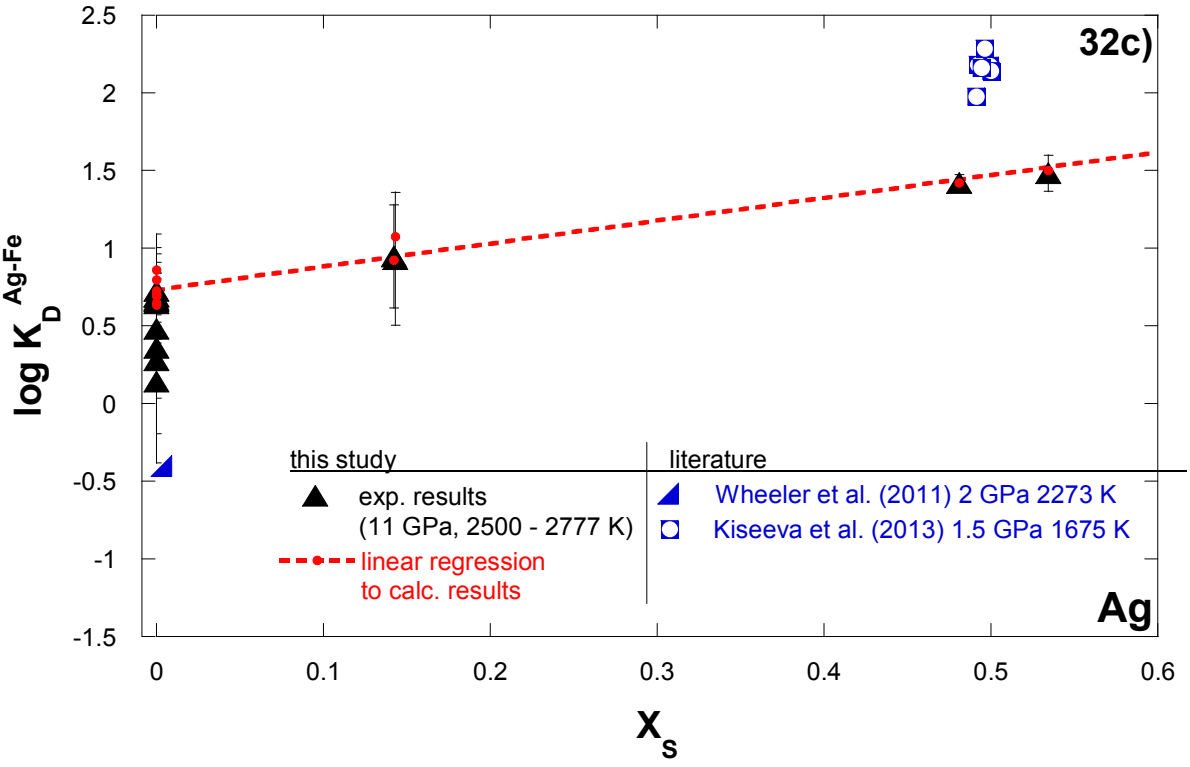

Figure 32a: *The pressure and temperature dependences of the partitioning behaviour of Ag. Experimentally determined logarithmic exchange coefficients minus the activity terms for Fe and Ag (equation [46]) are plotted against inverse temperature. The solid lines represent the calculated temperature dependence of Ag partitioning at 11 GPa and 21 GPa.* ***b:*** *Comparison between the results of this study and the recalculated results from literature datasets for Ag. Experimentally obtained logarithmic exchange coefficient values are plotted against inverse temperature.* ***c:*** *The dependence of the metal – silicate partitioning of Ag on the S-content of the metal (mole fractions). The red dotted line represents a linear regression to the recalculated results for a fitted* ε_S^{Ag} *value of -4.07. Unfilled symbols denote experiments that were conducted in graphite capsules.*

5.3.2 Divalent elements lead and gold

5.3.2.1 Lead

In agreement with the investigations of Ballhaus et al. (2013) no pressure dependence was found for the metal – silicate partitioning behaviour of Pb (see Table 10). However previous studies found that increasing temperature leads to increased siderophility of Pb. In the course of this study a negative effect of temperature on the metal silicate partitioning of Pb has been

observed over the experimental range of conditions. The constants *a* and *b* (equation [33]) have values of 0.22 and 5149 respectively. The results are shown in Figure 33a.

However as can be seen in Figure 33b the absolute exchange coefficient values for Pb obtained in this study are in perfect agreement with the results of Wood and Halliday (2010). The experiments performed by Lagos et al. (2008) were conducted in graphite capsules, which possibly explains the mismatch between the latter study and this one since according to the Steelmaking Data Sourcebook that C dissolved in the metal decreases the siderophility of Pb.

The addition of S to the metal phase slightly increases the partitioning behaviour of Pb which is in perfect agreement with the observations of Lagos et al. (2008), Wood et al. (2008), Wood and Halliday (2010) and Bouhifd et al. (2013) (compare Table 11). The derived interaction parameter ε_S^{Pb} equals -0.6. The logarithmic exchange coefficient values K_D^{Pb-Fe} of the S-bearing samples are shown in Figure 33c together with comparable experimental results of Wood et al. (2008), Kiseeva et al. (2013) and Bouhifd et al. (2013). The different datasets are in very good agreement with one another.

In concordance with the results of Chapter 4 the interaction of Si with Pb has been refined to ε_{Si}^{Pb} = 10.59. Uncertainties on logarithmic exchange coefficient values are ± 0.1 logarithmic units.

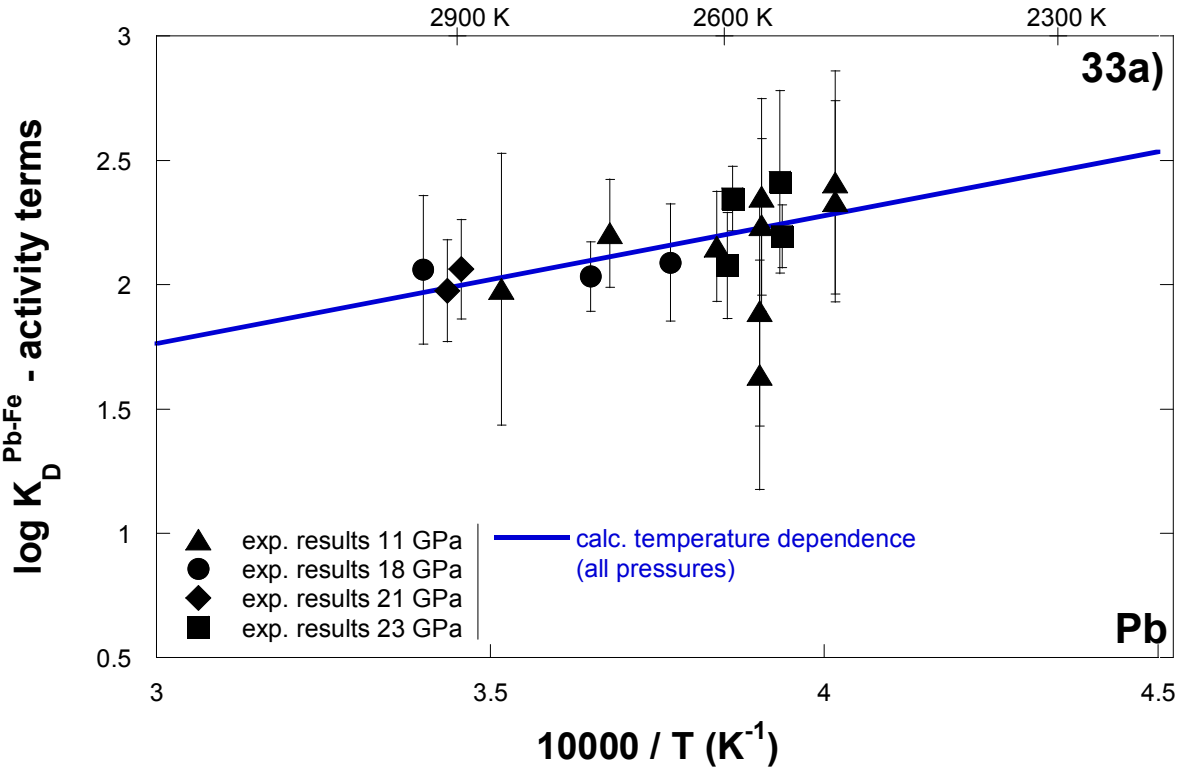
2900 K
2600 K
2300 K
33a)
log K_D^Pb-Fe - activity terms
exp. results 11 GPa
exp. results 18 GPa
exp. results 21 GPa
exp. results 23 GPa
calc. temperature dependence
(all pressures)
Pb
10000 / T (K^-1)

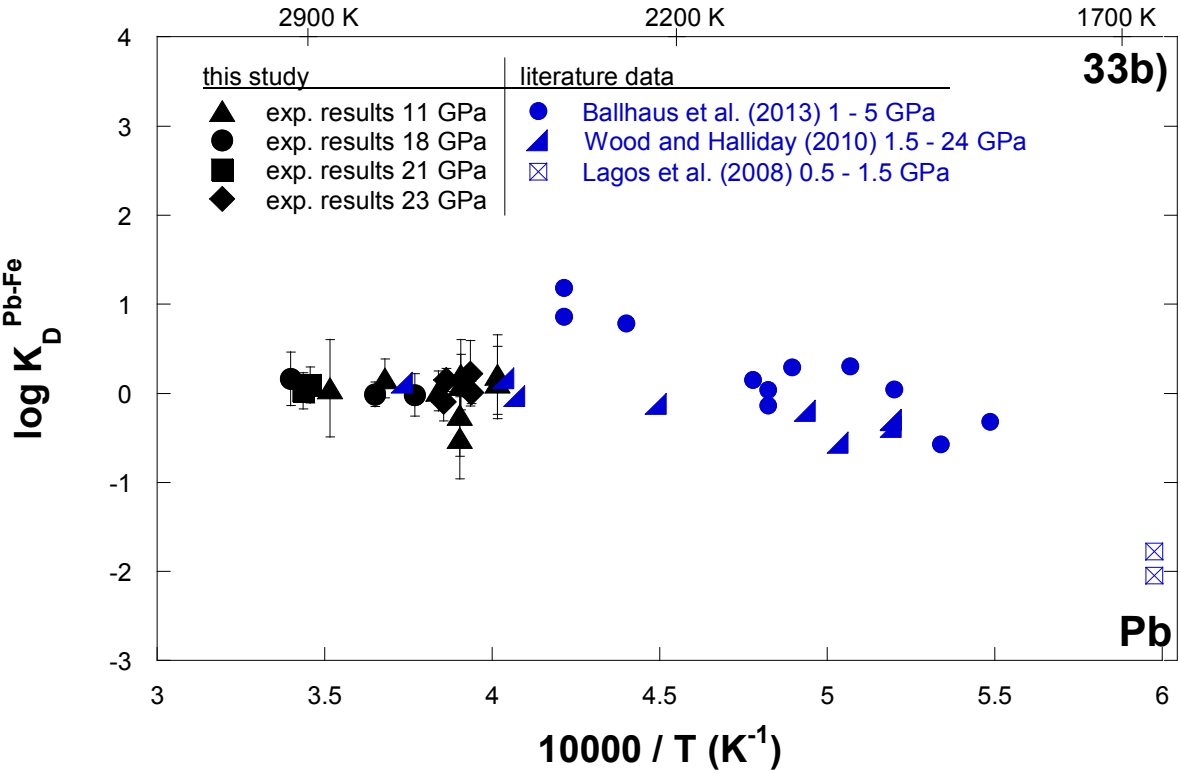
2900 K
2200 K
1700 K
33b)
this study
literature data
exp. results 11 GPa
exp. results 18 GPa
exp. results 21 GPa
exp. results 23 GPa
Ballhaus et al. (2013) 1 - 5 GPa
Wood and Halliday (2010) 1.5 - 24 GPa
Lagos et al. (2008) 0.5 - 1.5 GPa
log K_D^Pb-Fe
Pb
10000 / T (K^-1)

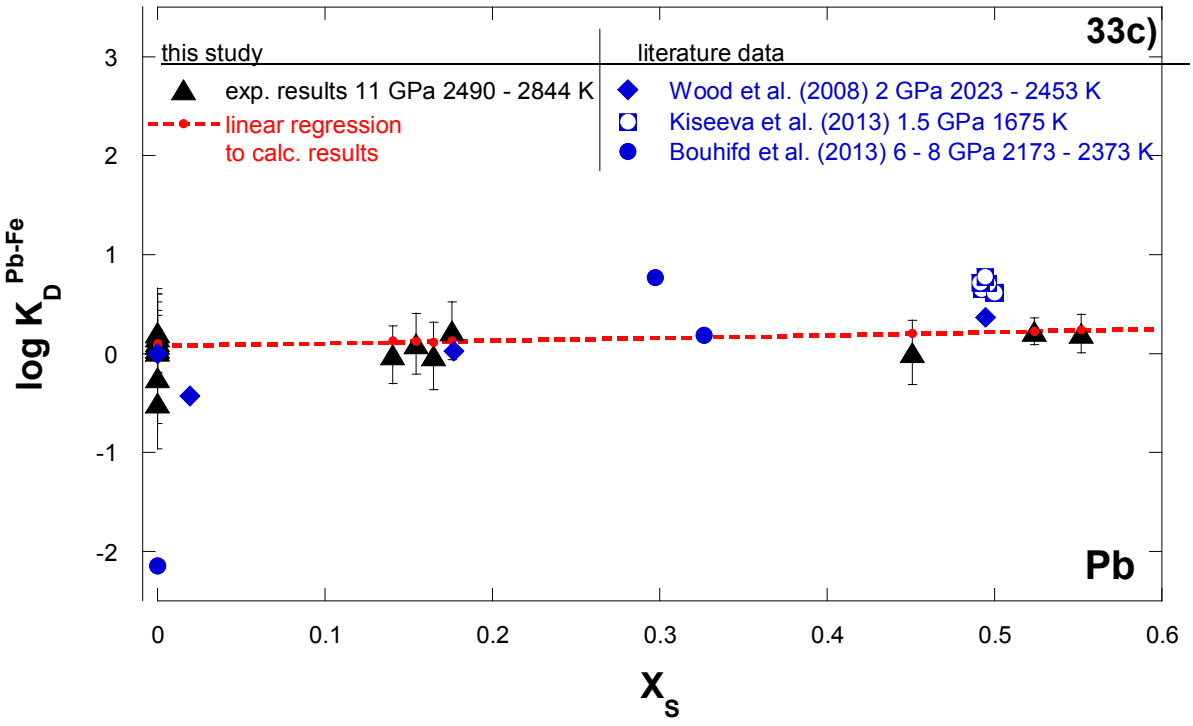

Figure 33a: *The temperature dependence of the partitioning behaviour of Pb. Experimentally determined logarithmic exchange coefficients minus the activity terms for Fe and Pb (equation [46]) are plotted against inverse temperature. The solid line represents the calculated temperature dependence of Pb partitioning.* ***b:*** *Comparison between the results of this study and the recalculated results from literature datasets for Pb. Experimentally obtained logarithmic exchange coefficient values are plotted against inverse temperature.* ***c:*** *The dependence of the metal – silicate partitioning of Pb on the S-content of the metal (mole fractions). The red dotted line represents a linear regression to the recalculated results for a fitted* ε_S^{Pb} *value of -0.60. Unfilled symbols in b) and c) denote experiments that were conducted in graphite capsules.*

5.3.2.2 Gold

Similar to the partitioning behaviour of Pb, the liquid metal – liquid silicate partitioning behaviour of the highly siderophile element Au was found to be independent of pressure but slightly affected by temperature such that increasing temperatures cause a decrease in partition or exchange coefficients. Values of 0.19 and 6521 have been derived for the constants *a* and *b* of equation [33] respectively. In Figure 34a the temperature dependence of the partitioning of Au is demonstrated. Here logarithmic exchange coefficient values, K_D^{Au-Fe}, that have been corrected for the activity terms of equation [33] and the calculated temperature

dependence of the partitioning behaviour of Au are plotted against inverse temperature. The observations of a negative temperature dependence and an insensitivity on pressure are in perfect agreement with the partitioning trends given by Brenan and McDonough (2009), yet contrary to the trends reported by Danielson et al. (2005) (compare Table 10). The results of the partitioning experiments of Brenan and McDonough (2009) and this study are plotted against inverse temperature in Figure 34b. The absolute values of $\log K_D^{Au-Fe}$ are similar. However, contrary to the experiments of this study, Brenan and McDonough (2009) used graphite capsules in their experiments and the silicate composition was basaltic rather than peridotitic.

The results of the effect of S on the liquid metal – liquid silicate partitioning of Au are shown in Figure 34c. Sulphur hardly changes the exchange coefficient values of Au. The ε_S^{Au} value of 0.49 is the smallest S dependence of all elements studied. Increasing S contents slightly lower the partition or exchange coefficients of Au as it has also been proposed by Jana and Walker (1997) (Table 11).

By incorporating several more experiments into the fitting during the procedure of which the constants *a* and *b* and the interaction parameters ε_S^{Au} and ε_{Si}^{Au} have been fitted simultaneously the interaction of Si with Au has been refined to a higher value of ε_{Si}^{Au}= 23.06 instead of 17.

Uncertainties for the fitted logarithmic exchange coefficients have been calculated by equation [41] to ± 0.23.

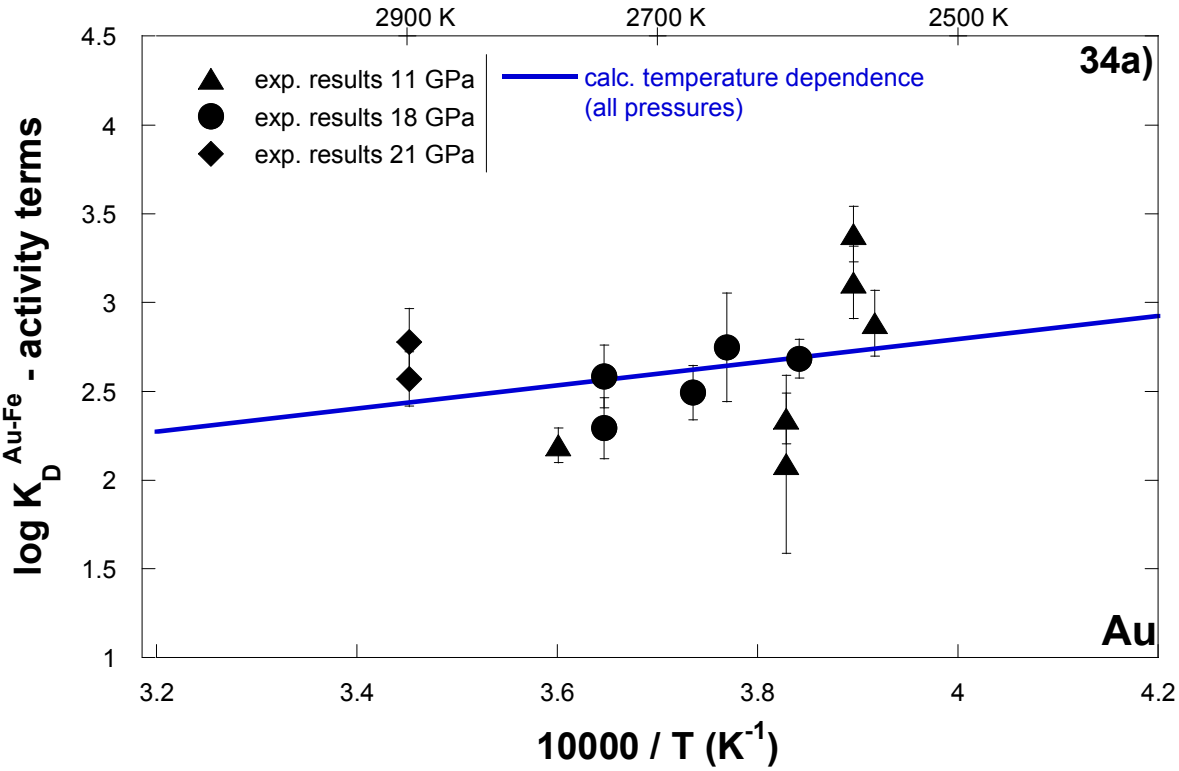
2900 K
2700 K
2500 K
34a)
exp. results 11 GPa
exp. results 18 GPa
exp. results 21 GPa
calc. temperature dependence
(all pressures)
log K_D^Au-Fe - activity terms
Au
10000 / T (K^-1)

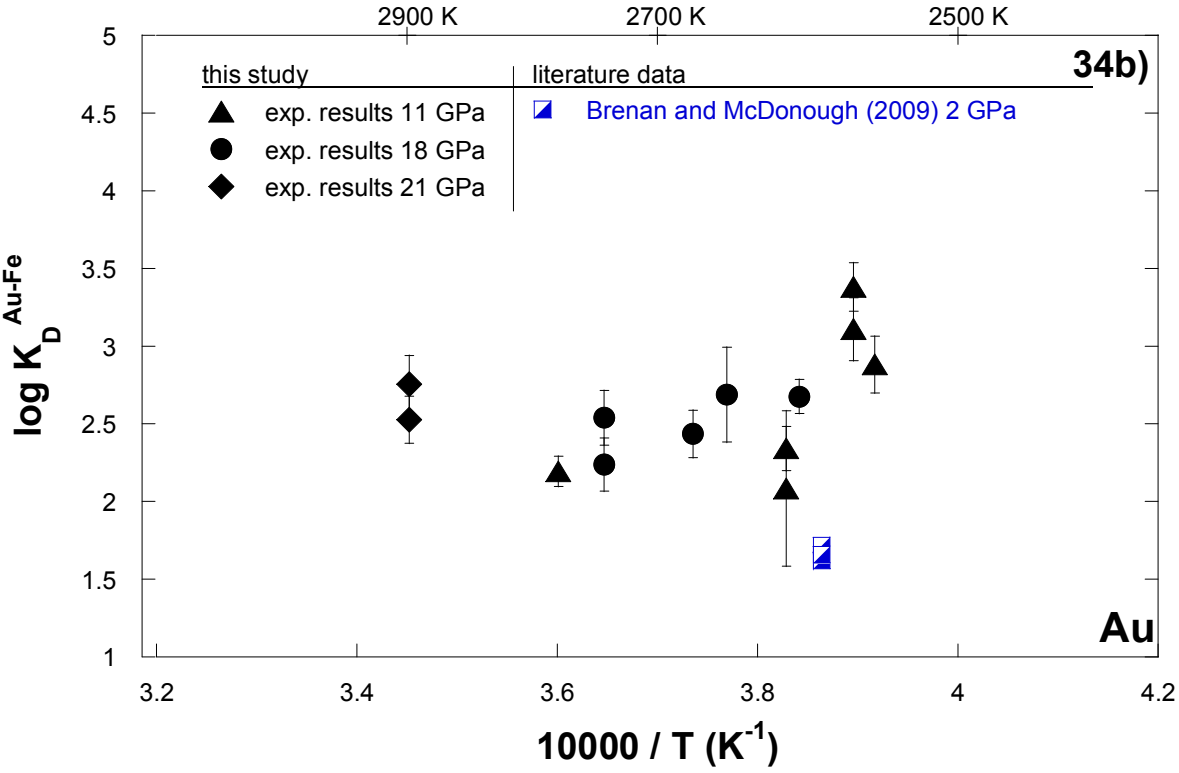
2900 K
2700 K
2500 K
34b)
this study
literature data
exp. results 11 GPa
exp. results 18 GPa
exp. results 21 GPa
Brenan and McDonough (2009) 2 GPa
log K_D^Au-Fe
Au
10000 / T (K^-1)

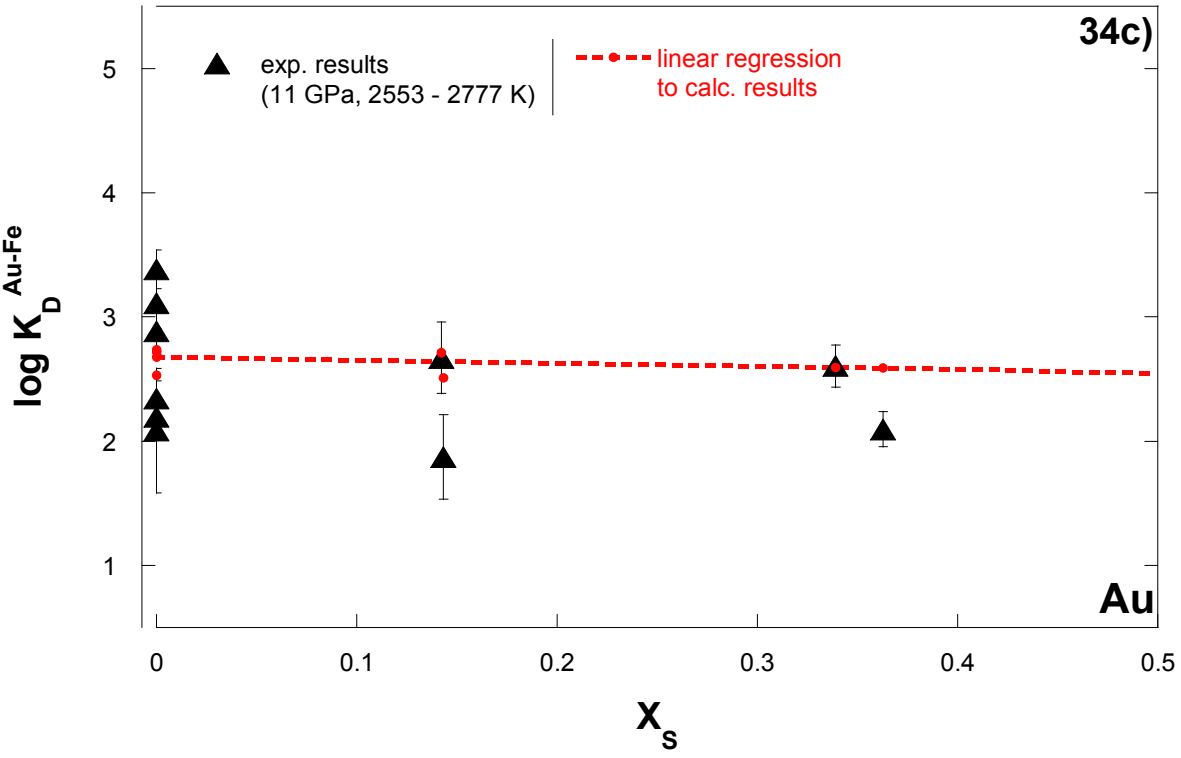

Figure 34a: *The temperature dependence of the partitioning behaviour of Au. Experimentally determined logarithmic exchange coefficients minus the activity terms for Fe and Au (equation [46]) are plotted against inverse temperature. The solid line represents the calculated temperature dependence of Au partitioning.* ***b:*** *Comparison between the results of this study and the recalculated results from literature datasets for Au. Experimentally obtained logarithmic exchange coefficient values are plotted against inverse temperature. Experiments of Brenan and McDonough (2009) were performed in graphite capsules.* ***c:*** *The dependence of the metal – silicate partitioning of Au on the S-content of the metal (mole fractions). The red dotted line represents a linear regression to the recalculated results for a fitted* ε_S^{Au} *value of 0.49.*

5.3.3 Trivalent elements tin and germanium

5.3.3.1 Tin

Parameterizing the effects of pressure, temperature and Si- and S-contents in the metal on the liquid metal – liquid silicate partitioning behaviour of Sn resulted in *a*, *b* and *c* values of 0.18, 753 and 63 respectively, ε_S^{Sn} equals 6.34 and ε_{Si}^{Sn} is 17.79 (equation [33]). The interaction parameter between Si and Sn is still in agreement with the result that was obtained

in Chapter 4 based on less experiments. The uncertainty on the fit that corresponds to equation [41] is only ±0.09 logarithmic units.

In agreement with the observations of Ballhaus et al. (2013) and Righter et al. (2010) (compare Table 10) the pressure dependence of the liquid metal – liquid silicate partitioning of Sn was found to be almost insignificant, whereas increasing temperatures result in slightly lower exchange coefficient values (Figure 35a). This observation is confirmed when comparing the experimental data of this study with the results of Righter et al. (2010) and Ballhaus et al. (2013) which were conducted at lower temperatures and show comparatively higher K_D^{Sn-Fe} values (Figure 35b).

Increasing S contents of the metal result in decreased exchange coefficient values (Figure 35c) as shown by the interaction parameter value ε_S^{Sn} = 6.34. The latter has been derived individually because the simultaneous parameterization of the constants *a*, *b* and *c* and the ε_{Si}^{Sn}- and ε_S^{Sn} values did not result in a satisfying reproduction of the exchange coefficients of S-bearing samples. Five experiments from the dataset of Righter et al. (2009), performed in MgO capsules, have been compared to the results of this study. These experiments contained either a basaltic or rhyolitic silicate composition. The recalculated logarithmic exchange coefficient values K_D^{Sn-Fe} are significantly different from the observations of this study.

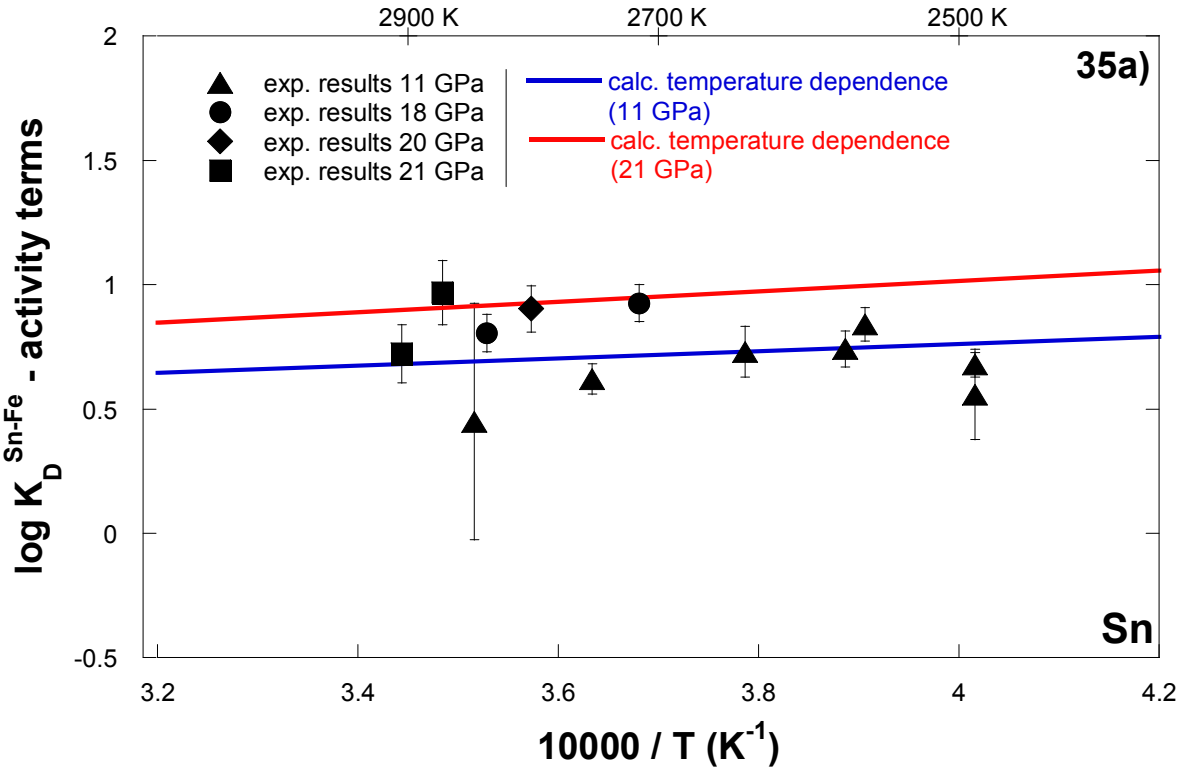
2900 K
2700 K
2500 K
35a)
exp. results 11 GPa
exp. results 18 GPa
exp. results 20 GPa
exp. results 21 GPa
calc. temperature dependence (11 GPa)
calc. temperature dependence (21 GPa)
log K_D Sn-Fe - activity terms
Sn
10000 / T (K-1)

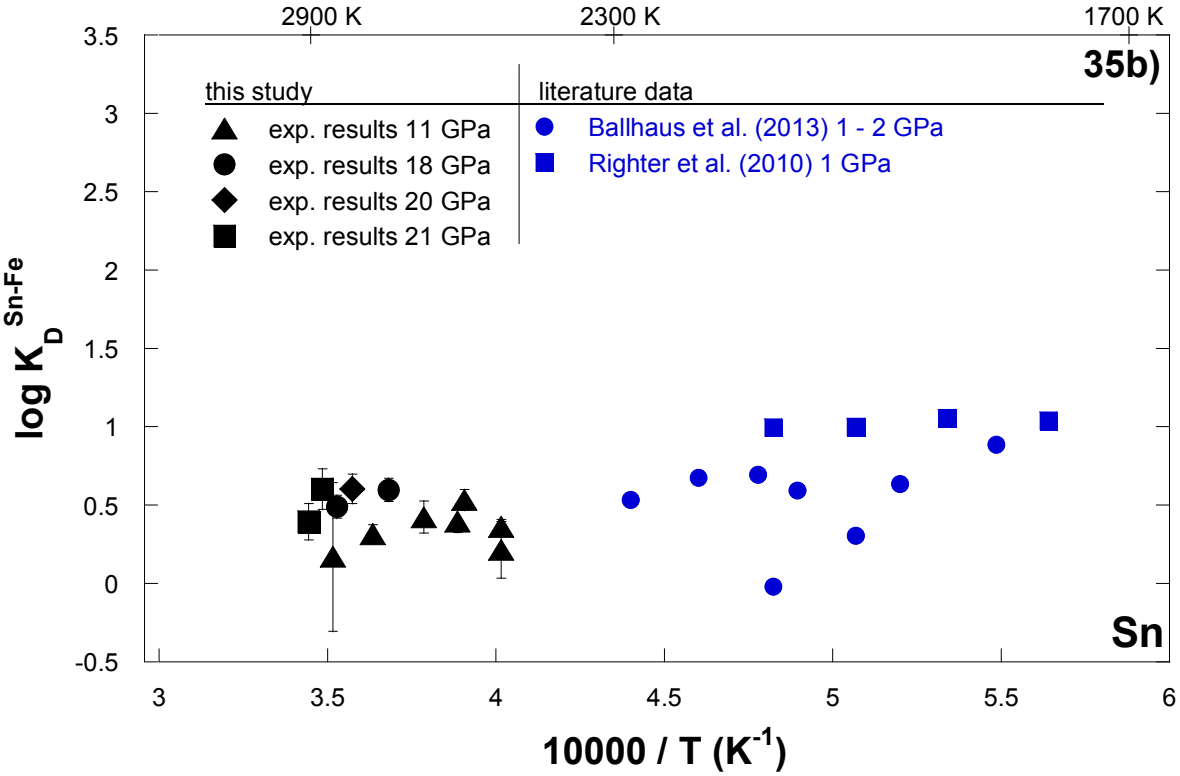
2900 K
2300 K
1700 K
35b)
this study
exp. results 11 GPa
exp. results 18 GPa
exp. results 20 GPa
exp. results 21 GPa
literature data
Ballhaus et al. (2013) 1 - 2 GPa
Righter et al. (2010) 1 GPa
log K_D Sn-Fe
Sn
10000 / T (K-1)

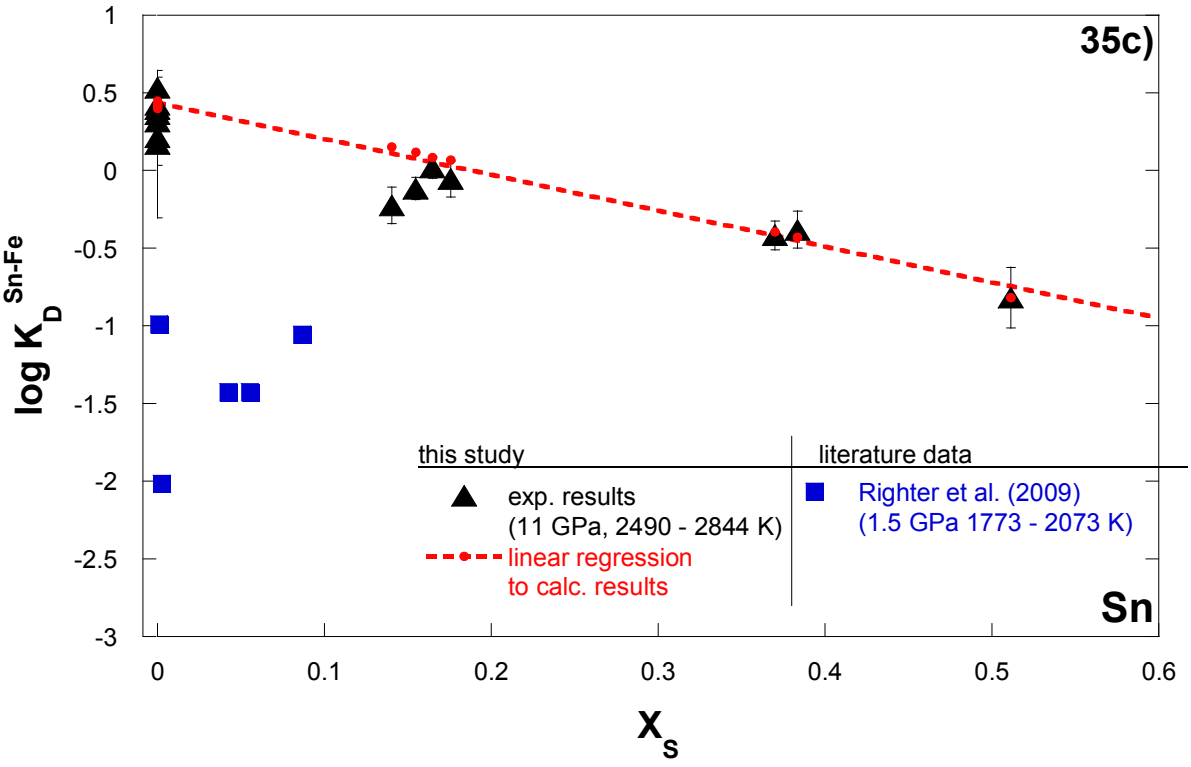

Figure 35a: *The pressure and temperature dependences of the partitioning behaviour of Sn. Experimentally determined logarithmic exchange coefficients minus the activity terms for Fe and Sn (equation [46]) are plotted against inverse temperature. The solid lines represent the calculated temperature dependence of Sn partitioning at 11 GPa and 21 GPa.* ***b:*** *Comparison between the results of this study and the recalculated results from literature data sets for Sn. Experimentally obtained logarithmic exchange coefficient values are plotted against inverse temperature.* ***c:*** *The dependence of the metal – silicate partitioning of Sn on the S-content of the metal (mole fractions). The red dotted line represents a linear regression to the recalculated results for a fitted* ε_S^{Sn} *value of 6.34.*

5.3.3.2 Germanium

Within the experimental range of pressures and temperatures in this study the moderately volatile element Ge exhibits neither a pressure nor a temperature dependence on its liquid metal – liquid silicate partitioning behaviour (Figure 36a). Constant *a* in equation [33] was fitted to 1.24.

These observations find support when comparing the results of this study to the results published by Righter et al. (2011) and Siebert et al. (2011) (Figure 36b). Although conducted at lower temperatures and variable pressures all logarithmic K_D^{Ge-Fe} values are within one

order of magnitude which contradicts the observations of several studies that proposed that increasing temperature results in increasing siderophility of Ge (Table 10).

A possible explanation for the slightly higher values that were obtained by Kegler et al. (2011) might be that the silicate composition of the latter study was basaltic rather than the peridotitic composition that was chosen for the investigations of this study.

The partitioning behaviour of Ge is strongly dependent on S contents in the metal phase which is mirrored by a high ε_S^{Ge} value of 13.04. Increasing S contents significantly lower the siderophility of Ge – a trend that has also been observed by Jana and Walker (1997) (Table 11). As can be seen in Figure 36c the logarithmic exchange coefficients of Ge decrease by 3 orders of magnitude within the experimentally investigated range of S contents. The refitted value of ε_{Si}^{Ge} equals 16.76 instead of 16.58 as derived in Chapter 4. Uncertainties on the fit that correspond to equation [41] were calculated to ± 0.24 logarithmic units.

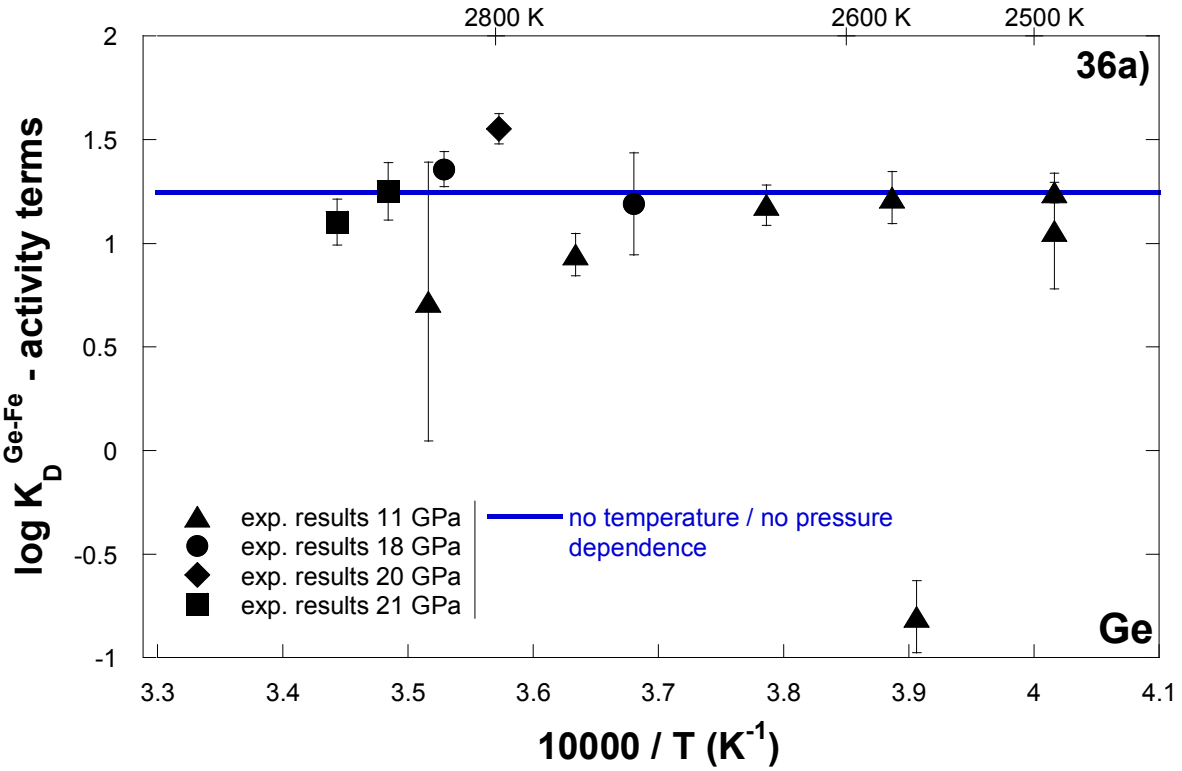
2800 K
2600 K
2500 K
36a)
log K_D^{Ge-Fe} - activity terms
exp. results 11 GPa
exp. results 18 GPa
exp. results 20 GPa
exp. results 21 GPa
no temperature / no pressure dependence
Ge
10000 / T (K^{-1})

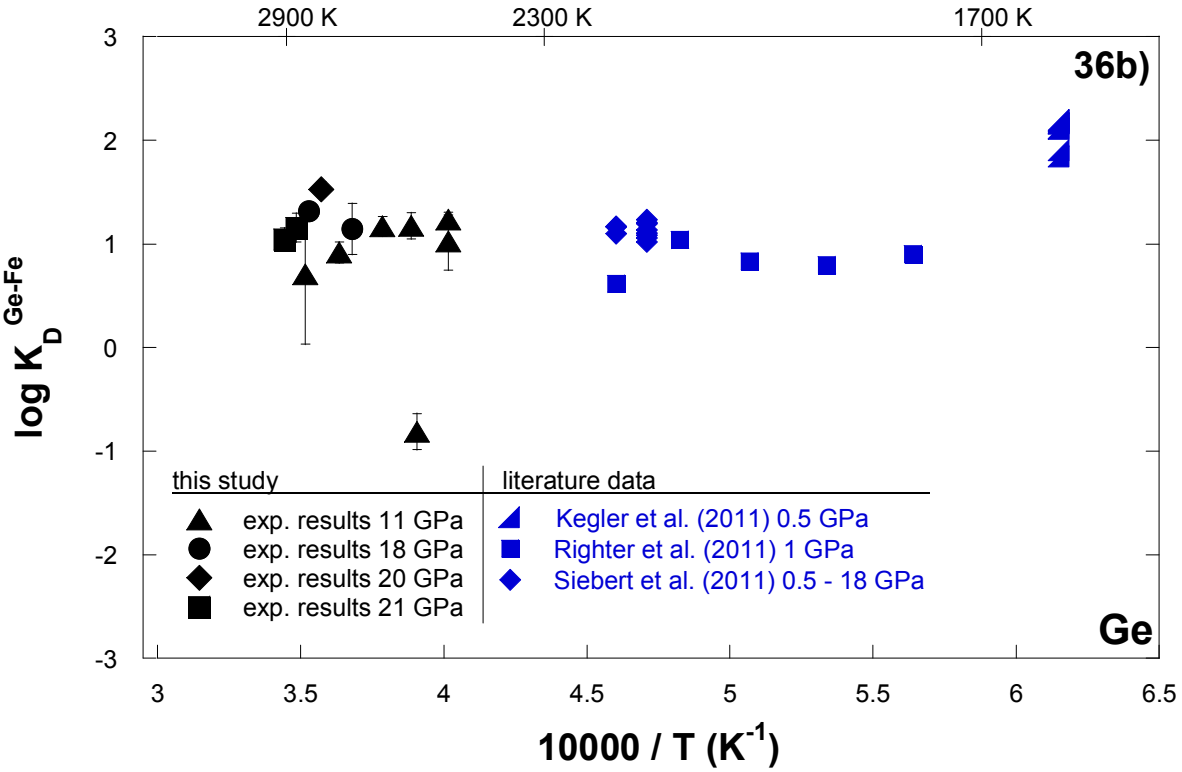
2900 K
2300 K
1700 K
36b)
log K_D^{Ge-Fe}
this study
exp. results 11 GPa
exp. results 18 GPa
exp. results 20 GPa
exp. results 21 GPa
literature data
Kegler et al. (2011) 0.5 GPa
Righter et al. (2011) 1 GPa
Siebert et al. (2011) 0.5 - 18 GPa
Ge
10000 / T (K^{-1})

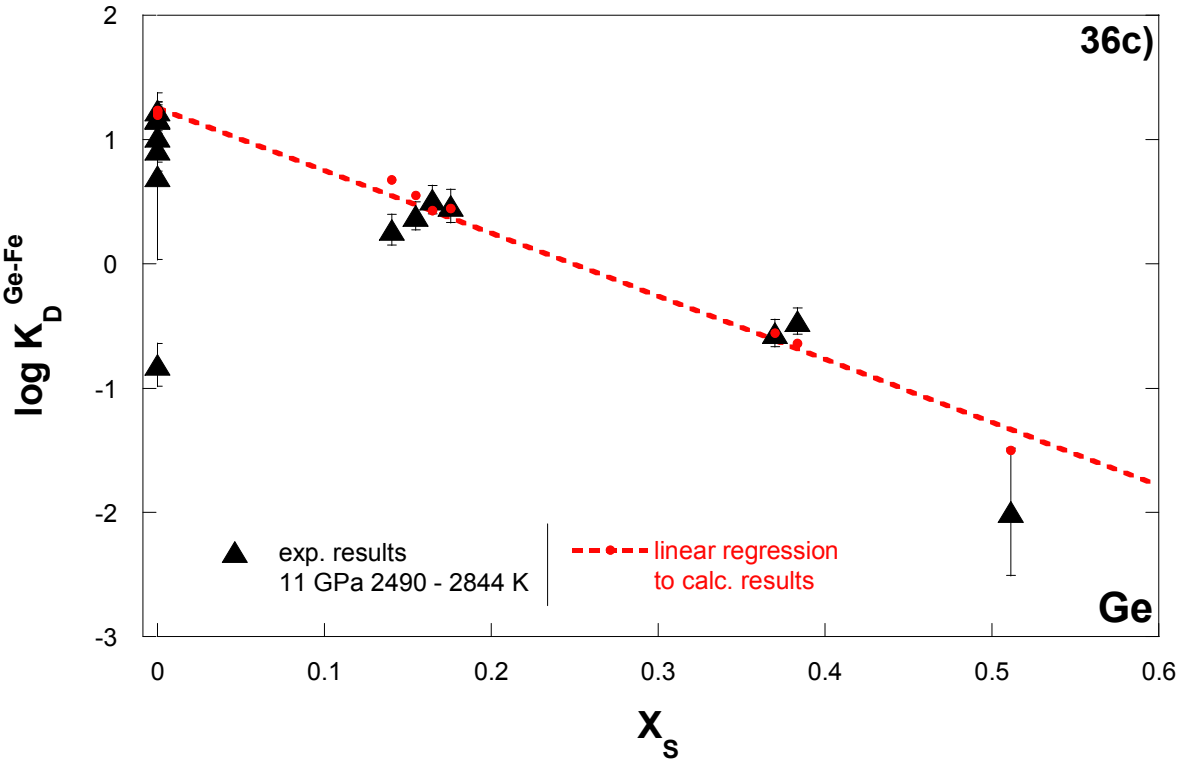

Figure 36a: *The pressure and temperature dependence of the partitioning behaviour of Ge. Experimentally determined logarithmic exchange coefficients minus the activity terms for Fe and Ge (equation [46]) are plotted against inverse temperature.* ***b:*** *Comparison between the results of this study and the recalculated results from literature data sets for Ge. Experimentally obtained logarithmic exchange coefficient values are plotted against inverse temperature.* ***c:*** *The dependence of the metal – silicate partitioning of Ge on the S-content of the metal (mole fractions). The red dotted line represents a linear regression to the recalculated results for a fitted* $\boldsymbol{\varepsilon_S^{Ge}}$ *value of 13.04.*

5.3.4 Tetravalent element antimony

The liquid metal – liquid silicate partitioning behaviour of Sb was found to be independent of pressure and temperature over the experimental range of conditions. Constant a (equation [33]) is 1.35. The experimental logarithmic exchange coefficient values K_D^{Sb-Fe} minus the activity terms of equation [46] are shown in Figure 37a.

As can be seen in Figure 37b the results of this study are similar to the results obtained by Righter et al. (2009) although the silicate compositions used in the latter study was basaltic or

rhyolitic. The authors however report that both increasing temperature and pressure reduce the siderophility of Sb.

In agreement with the observations of Righter et al. (2009) increasing S contents were found to decrease the logarithmic exchange coefficient values of Sb (Figure 37c). Over the experimentally investigated range of S contents the exchange coefficient values dropped down by two orders of magnitude. The interaction parameter between S and Sb exhibits a value of 12.95.

Like derived in Chapter 4 Si influences the partitioning of Sb by lowering its siderophility, the interaction parameter ε_{Si}^{Sb} retained its value of 28.51. Uncertainties on the logarithmic exchange coefficient values for Sb have been calculated to ± 0.45 logarithmic units.

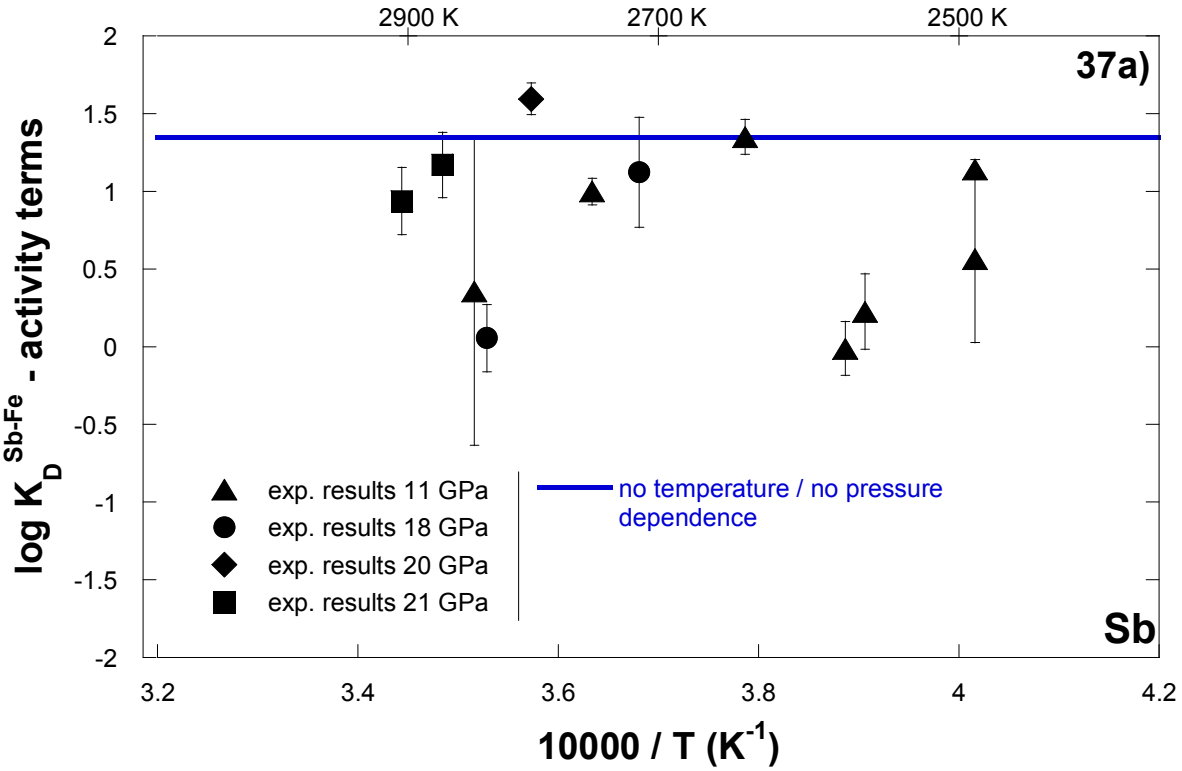
2900 K
2700 K
2500 K
37a)
log K_D^{Sb-Fe} - activity terms
exp. results 11 GPa
exp. results 18 GPa
exp. results 20 GPa
exp. results 21 GPa
no temperature / no pressure dependence
Sb
10000 / T (K^{-1})

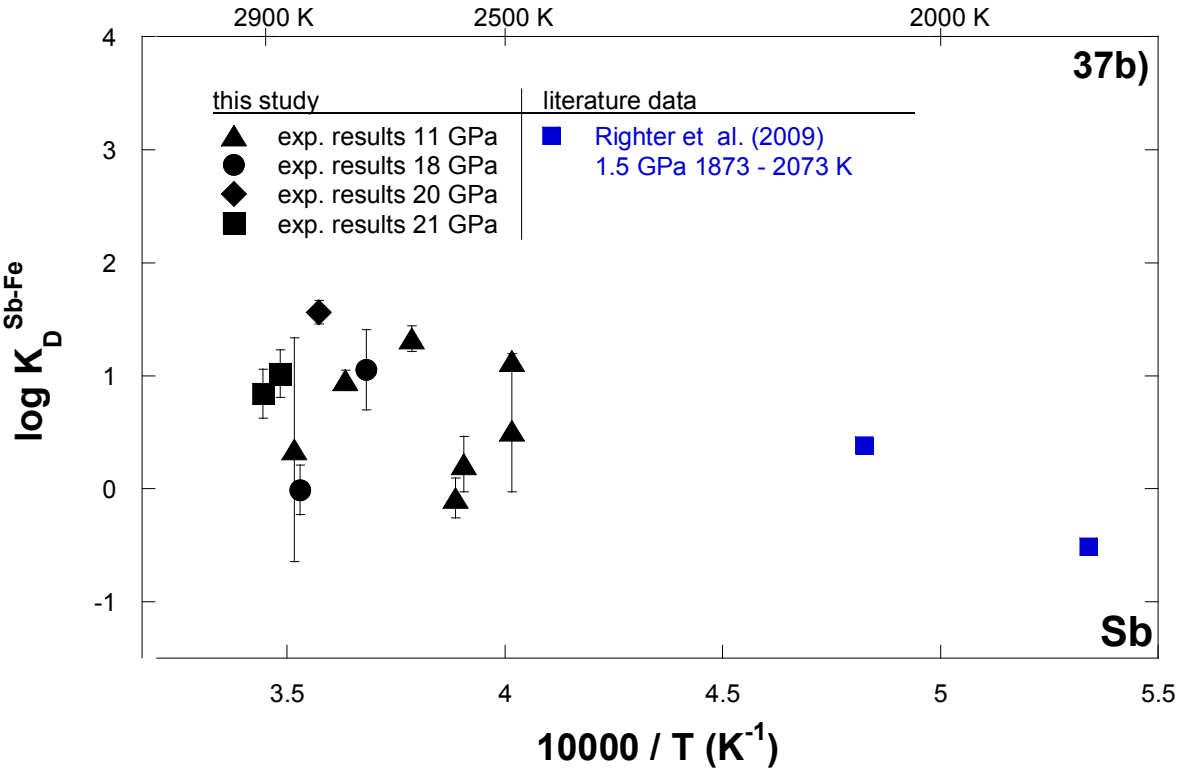
2900 K
2500 K
2000 K
37b)
this study
literature data
exp. results 11 GPa
exp. results 18 GPa
exp. results 20 GPa
exp. results 21 GPa
Righter et al. (2009)
1.5 GPa 1873 - 2073 K
log K_D^{Sb-Fe}
Sb
10000 / T (K^{-1})

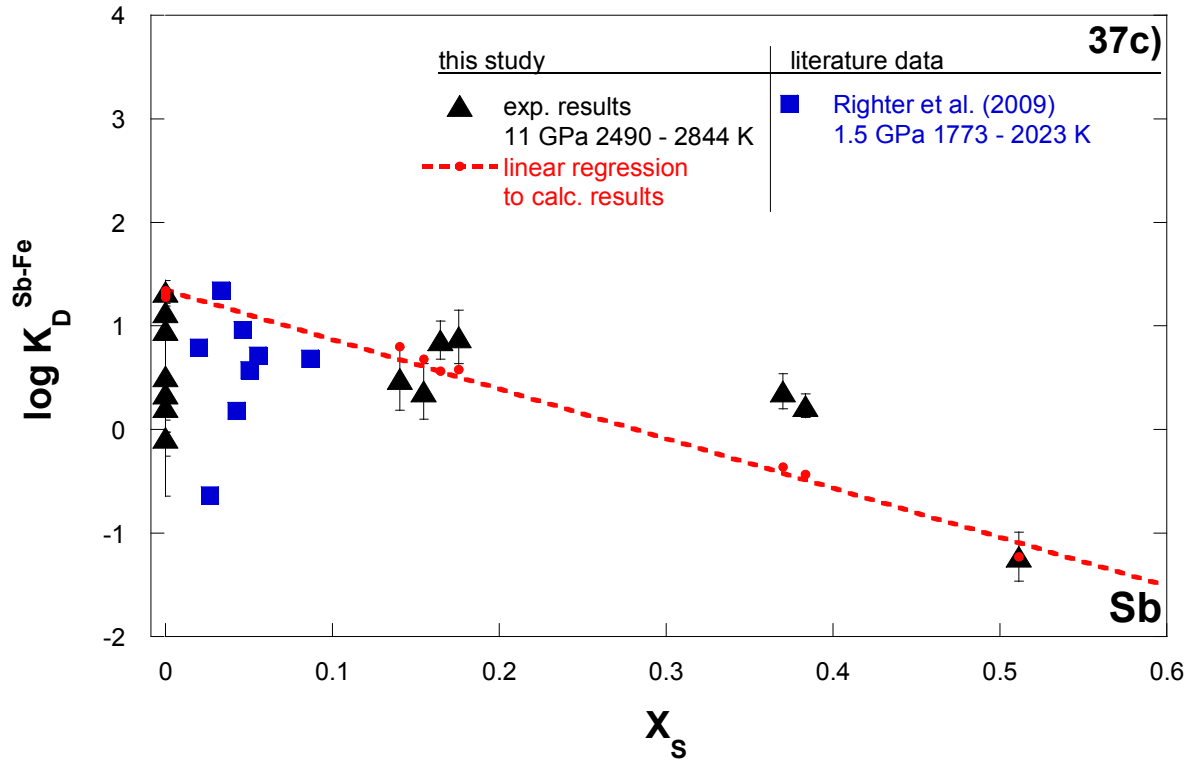

Figure 37a: *The pressure and temperature insensitivity of the partitioning behaviour of Sb. Experimentally determined logarithmic exchange coefficients minus the activity terms for Fe and Sb (equation [46]) are plotted against inverse temperature.* ***b:*** *Comparison between the results of this study and the recalculated results from literature datasets for Sb. Experimentally obtained logarithmic exchange coefficient values are plotted against inverse temperature.* ***c:*** *The dependence of the metal – silicate partitioning of Sb on the S-content of the metal (mole fractions). The red dotted line represents a linear regression to the recalculated results for a fitted* ε_S^{Sb} *value of 12.95.*

5.3.5 Pentavalent elements arsenic and phosphorus

5.3.5.1 Arsenic

The siderophility of the volatile element As was found to increase with pressure, constants *a* and *c* of equation [33] are 0.21 and 178 respectively. The logarithmic exchange coefficients minus the activity terms for Fe and As (equation [46]) are plotted against inverse temperature in Figure 38a.

Although Siebert et al. (2011) find that both increasing temperature and pressure results in decreased siderophile behaviour of As the logarithmic exchange coefficient values of the experiments performed by the latter authors are partly in agreement with the results obtained by this study as can be seen in Figure 38b.

The partitioning behaviour of As is weakly effected by the addition of S to the metal phase as can be seen in Figure 38c. The parameterization was performed separately and led to an ε_S^{As} value of 2.64. However the fit does not reproduce the data very well. More experiments are necessary to better constrain the influence of S on the metal – silicate partitioning of As.

Taking all available experiments into account the ε_{Si}^{As} value of 43.47 as derived in Chapter 4 remained constant.

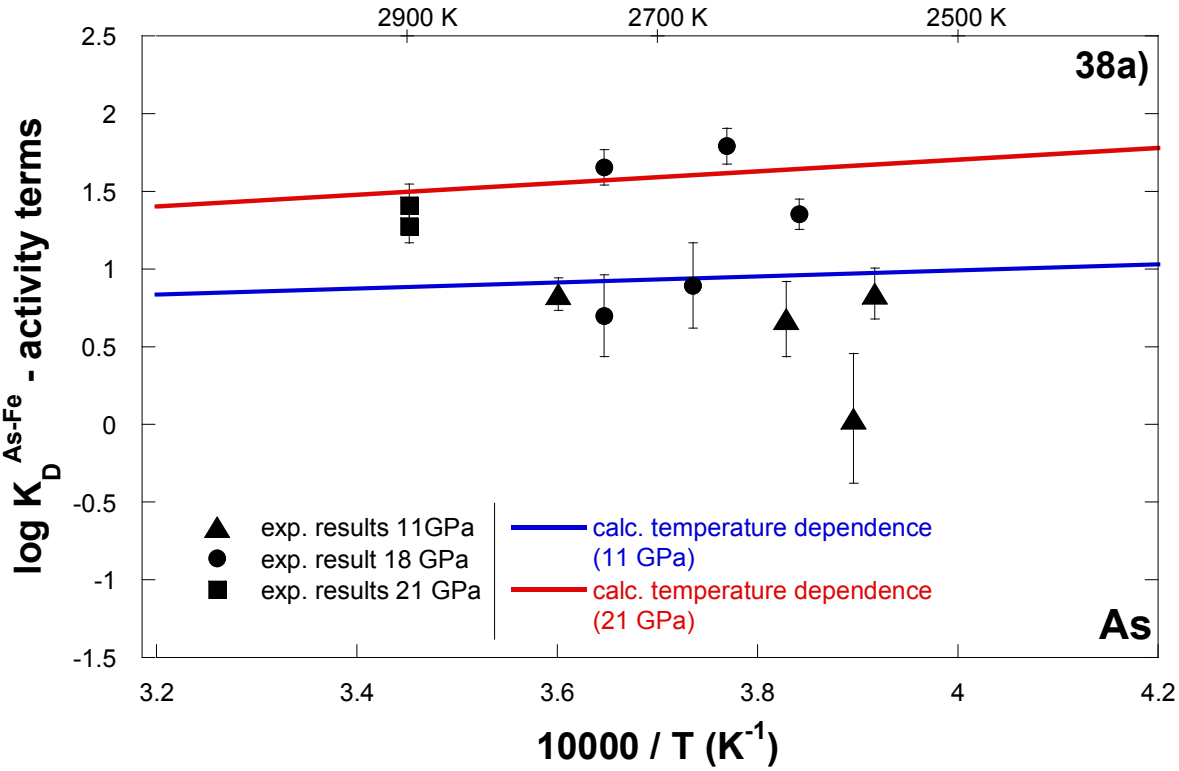
2900 K
2700 K
2500 K
38a)
log K_D^{As-Fe} - activity terms
exp. results 11GPa
exp. result 18 GPa
exp. results 21 GPa
calc. temperature dependence (11 GPa)
calc. temperature dependence (21 GPa)
As
10000 / T (K^{-1})

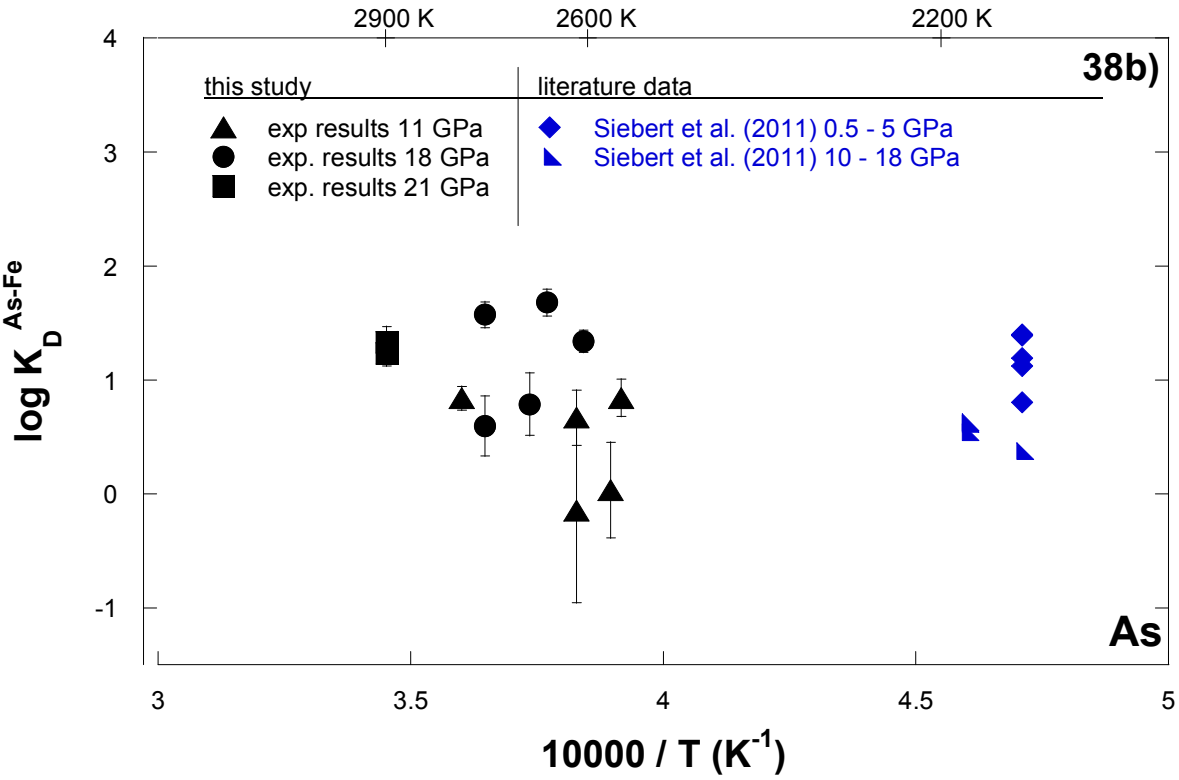
2900 K
2600 K
2200 K
38b)
this study
literature data
exp results 11 GPa
exp. results 18 GPa
exp. results 21 GPa
Siebert et al. (2011) 0.5 - 5 GPa
Siebert et al. (2011) 10 - 18 GPa
log K_D^{As-Fe}
As
10000 / T (K^{-1})

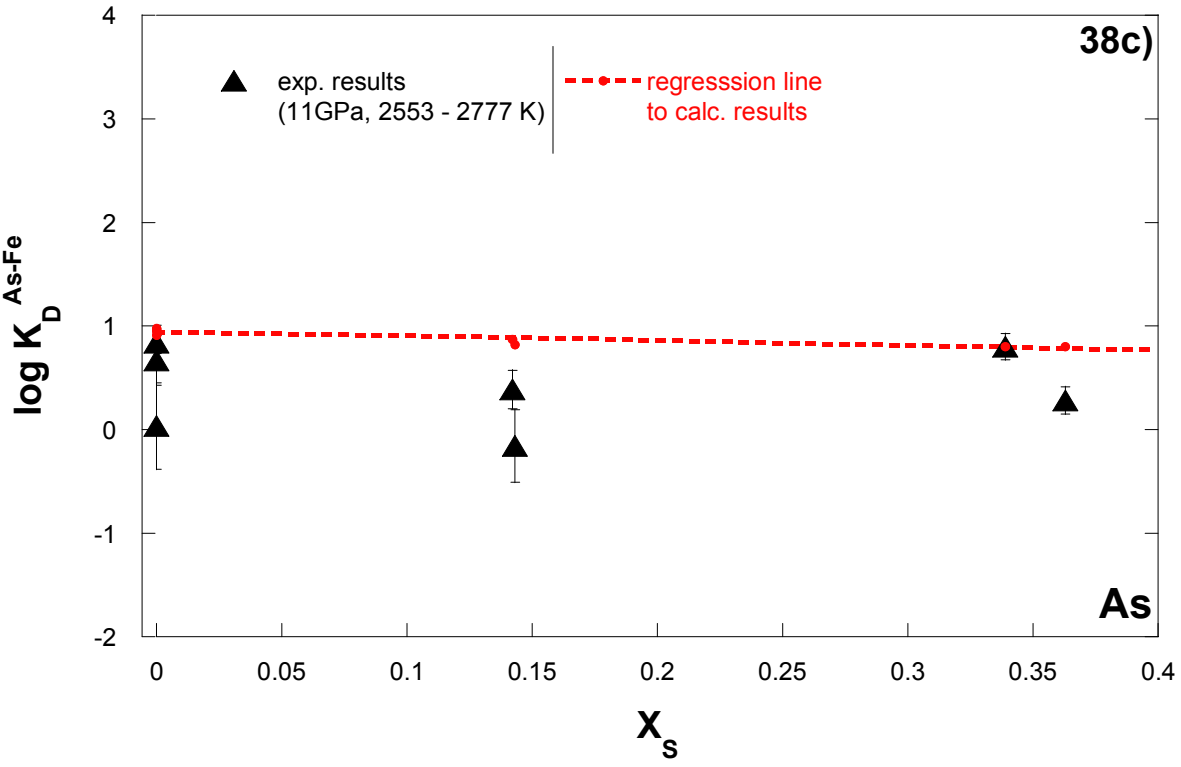

Figure 38a: *The pressure and temperature dependence of the partitioning behaviour of As. Experimentally determined logarithmic exchange coefficients minus the activity terms for Fe and As (equation [46]) are plotted against inverse temperature.* ***b:*** *Comparison between the results of this study and the recalculated results from literature datasets for As. Experimentally obtained logarithmic exchange coefficient values are plotted against inverse temperature.* ***c:*** *The dependence of the metal – silicate partitioning of As on the S-content of the metal (mole fractions). The red dotted line represents a linear regression to the recalculated results for a fitted* $\boldsymbol{\varepsilon_S^{As}}$ *value of 2.64.*

5.3.5.2 Phosphorus

Phosphorus is the only element investigated in this study that exhibits a negative *b* value when parameterizing its metal – silicate partitioning behaviour meaning that increasing temperatures result in increasing siderophility of P. This observation is in perfect agreement with the results of Walker et al. (1993), Righter et al. (2010) and Ballhaus et al. (2013) as illustrated in Table 10. The corresponding parameters to equation [33] are: *a*: -0.06, *b*: -5036, ε_{Si}^{As}: 26.82 and ε_S^{As}: 15.77. No pressure dependence has been found. The temperature dependence of the liquid metal – liquid silicate partitioning of P is shown in Figure 39a in which logarithmic exchange coefficients minus the activity terms of equation [33] are plotted against inverse temperature.

The comparison of the results of this study with recalculated literature data is displayed in Figure 39b. The data is in agreement with the results of Righter et al. (2010), Ballhaus et al. (2013) and Siebert et al. (2011). In particular the results of Righter et al. (2010) support the observation that decreasing temperatures result in reduced exchange coefficient values.

Within the framework of this study P is the element that is effected the most by the addition of S to the metal phase, which is reflected by its high interaction parameter ε_S^P of 15.77. Similar to Ge the logarithmic exchange coefficient values for P are decreased by more than 3 logarithmic units over the range of investigated S concentrations as can be seen in Figure 39c. Uncertainties on the fit correspond to ± 0.47 logarithmic units.

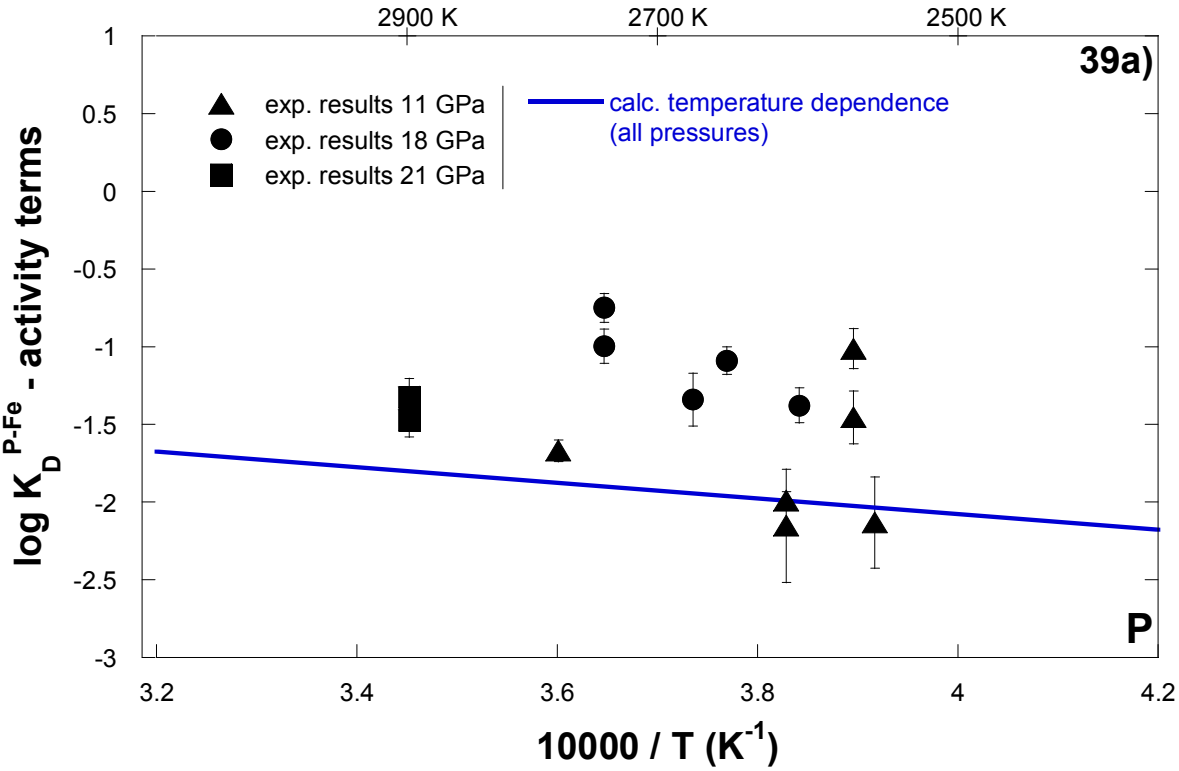
2900 K
2700 K
2500 K
39a)
exp. results 11 GPa
exp. results 18 GPa
exp. results 21 GPa
calc. temperature dependence
(all pressures)
log K_D^P-Fe - activity terms
P
10000 / T (K^-1)

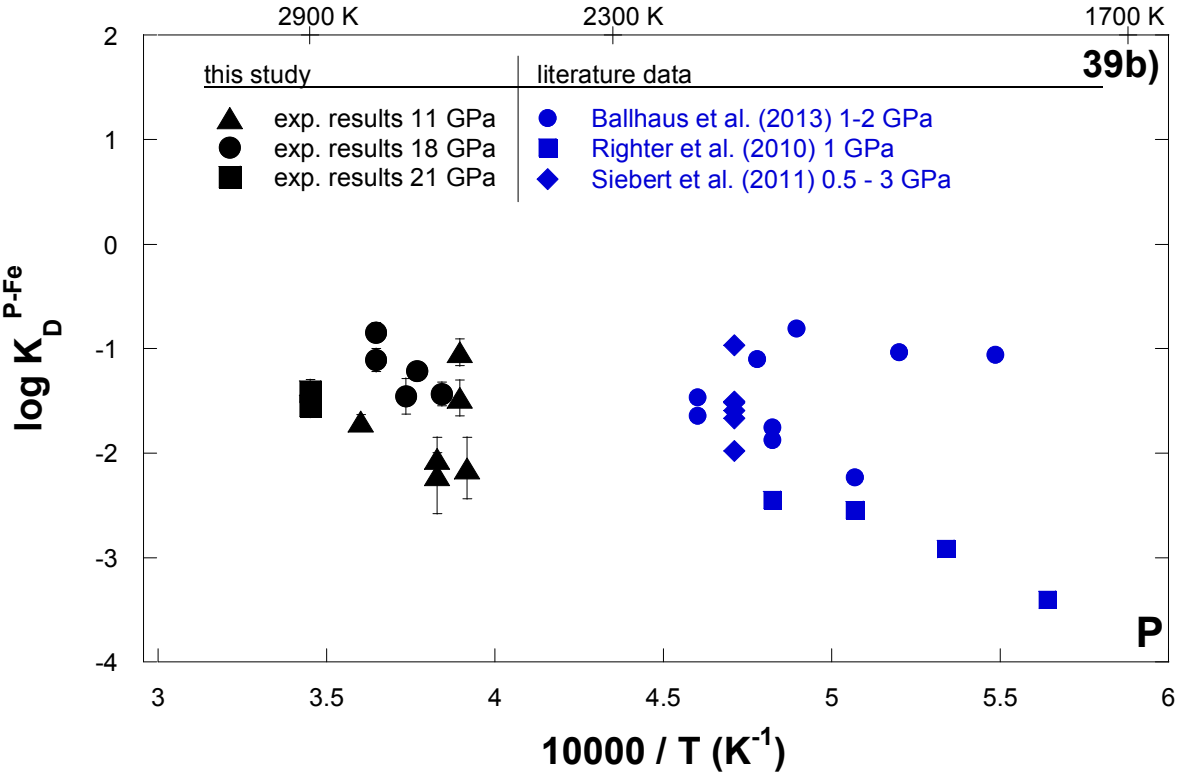
2900 K
2300 K
1700 K
39b)
this study
literature data
exp. results 11 GPa
exp. results 18 GPa
exp. results 21 GPa
Ballhaus et al. (2013) 1-2 GPa
Righter et al. (2010) 1 GPa
Siebert et al. (2011) 0.5 - 3 GPa
log K_D^P-Fe
P
10000 / T (K^-1)

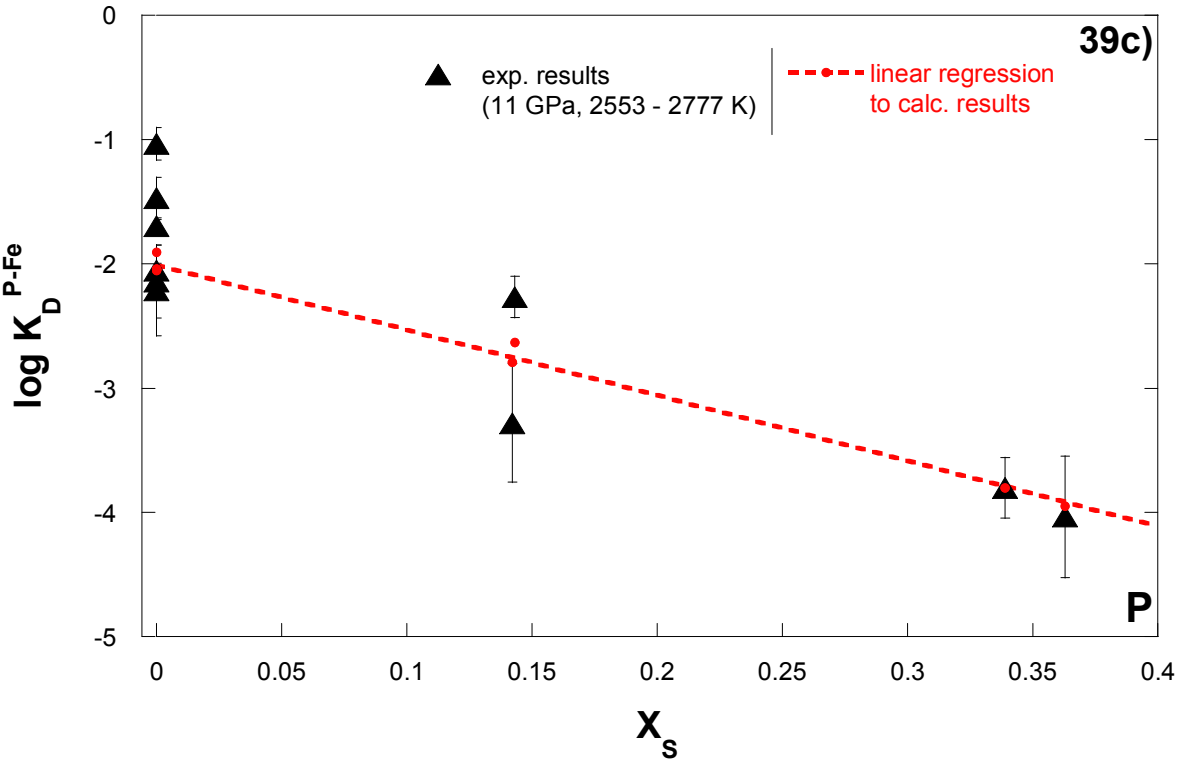

Figure 39a: *The temperature dependence of the partitioning behaviour of P. Experimentally determined logarithmic exchange coefficients minus the activity terms for Fe and P (equation [46]) are plotted against inverse temperature. The solid line represents the calculated temperature dependence of P partitioning.* ***b:*** *Comparison between the results of this study and the recalculated results from literature datasets for P. Experimentally obtained logarithmic exchange coefficient values are plotted against inverse temperature.* ***c:*** *The dependence of the metal – silicate partitioning of P on the S-content of the metal (mole fractions). The red dotted line represents a linear regression to the recalculated results for a fitted* ε_S^P *value of 15.77.*

5.4 Summary and implications

The liquid metal – liquid silicate partitioning behaviour has been parameterized for a wide range of volatile elements, namely Cu, Ag, Pb, Au, Sn, Ge, Sb, As and P. In particular the effects of pressure, temperature, Si- and S-contents have been parameterized. In general it was found that the partitioning behaviour of most elements studied is affected insignificantly by pressure, but is partly sensitive to temperature. Increasing S-contents of the metal phase cause an increase in siderophility for the elements Ag, Cu and Pb and vise versa for Au, Sn, Ge, Sb, As and P with Ge, Sb and P being influenced to the greatest extent.

The results of this study are in very good agreement with the results that were obtained from literature datasets. Only minor differences were found which might be the result of different capsule material, silicate composition or applied pressures and temperatures.

Table 14 shows the fitted parameters *a*, *b*, *c*, ε_{Si}^{M} and ε_{S}^{M} that were derived in this study for each of the volatile elements. By employing equation [33] exchange coefficient values can now be derived for specified pressure, temperature and metal compositions. Additionally the uncertainty on calculated $\log K_D^{M-Fe}$ values is given. One should note that the interaction parameters ε_i^k are valid for a given temperature of 1873 K and thus need to be corrected to the temperature of interest by the use of equation [39].

Table 14: *Summary of fitted parameters that correspond to equation [33]. Uncertainties on* $log\, K_D^{M-Fe}$ *are obtained by employing equation [41].*

Element	a	b	c	ε_{Si}^{M} (1873 K)	ε_{S}^{M} (1873 K)	Uncertainty on log K_D^{M-Fe}
Ag	2.73	-	-84	6.75	-4.07	0.17
Cu	0.17	3571	-	0.73	-2.58	0.07
Au	0.19	6521	-	23.06	0.49	0.23
Pb	0.22	5149	-	10.59	-0.60	0.10
Sn	0.18	753	63	17.79	6.34	0.09
Ge	1.24	-	-	16.76	13.04	0.24
Sb	1.35	-	-	28.51	12.95	0.45
As	0.21	-	178	43.47	2.64	0.41
P	-0.06	-5036	-	26.82	15.77	0.47

Table 15 compares the interaction parameters ε_{Si}^{M} and ε_{S}^{M} that have been derived in this study with those derived from the massrelated e-values in the Steelmaking Data Sourcebook. In the cases of Pb (ε_{Si}^{Pb}), Au (ε_{S}^{Au}) and Sn (ε_{S}^{Sn}) the opposite effect of Si or S on the partitioning of these elements was observed.

Table 15: *Comparison between the interaction parameters derived in this study with those derived from the Steelmaking Data Sourcebook. All values refer to a temperature of 1873 K.*

Element	ε_{Si}^{M} (1873 K) This study	ε_{Si}^{M} (1873 K) Steelmaking Data Sourcebook	ε_{S}^{M} (1873 K) This study	ε_{S}^{M} (1873 K) Steelmaking Data Sourcebook
Ag	6.75	-	-4.07	-
Cu	0.73	3.64	-2.58	-2.34
Au	23.06	-	0.49	-0.25
Pb	10.59	-11.26	-0.60	-42.03
Sn	17.79	7.2	6.34	-3.28
Ge	16.76	-	13.04	3.89
Sb	28.51	-	12.95	0.68
As	43.47	-	2.64	-5.66
P	26.82	11.95	15.77	4.92

The parameterization of the partitioning behaviour of volatile elements was used to derive constraints about the conditions that prevailed during core formation of the Earth by incorporating the results into a core formation model:

The bulk Earth composition is assumed to be similar to CI chondrites except for volatile element depletion. By employing a mass balance equation that takes into account the mass fractions of the Earth´s mantle and core, McDonough (2003) calculated the concentrations of elements in the Earth´s core based on their known mantle and CI chondrite abundances. However as mentioned in Chapter 1 volatile elements are depleted relative to CI chondrites because they most likely failed to condense at the high temperatures in the inner part of the Solar System (Palme and O´Neill, 2003). The degree of volatility however is still under debate. Pairs of elements, namely Cu-Au, Cu-As, Ag-Sb and Sn-Pb, have been incorporated individually into a simplified core formation model in order to model their partitioning behaviour. The elements of each pair have, according to Lodders (2003), similar condensation temperatures and should therefor be affected to the same extent by volatility, because of which any assumptions about volatilization can be avoided. One should note however that the results of the element pair Cu – As are probably in error because the partitioning behaviour of As has been parameterized with a comparatively high error of almost half a logarithmic unit (exchange coefficient values). However because the ratio of the core – mantle partition coefficients of these element pairs changes with different degree of volatilization, the ratio of the mantle concentrations has been used as the constraining parameter. Table 16 summarizes

the mantle and core abundances of the volatile elements that have been used to model the relative but not the absolute abundances of elements with similar condensation temperatures.

Table 16: *Element pairs that have been incorporated into a single stage core formation model. Given are the 50% condensation temperatures of each element, the respective mantle and core abundances and the corresponding mantle ratio that has been used as constraining parameter.*

Element (Pairs shaded similarly	50% Condensation temperature (Lodders, 2003)	Mantle abundance (ppm) (McDonough, 2003)	Core abundance (ppm) (McDonough, 2003)	Mantle ratio
Cu	1037 K	30	125	Cu / Au
Au	1060 K	0.001	0.5	30000
Cu	1037 K	30	125	Cu / As
As	1065 K	0.05	5	600
Ag	996 K	0.008	0.15	Ag / Sb
Sb	979 K	0.006	0.13	1.33
Pb	727 K	0.15	0.4	Pb / Sn
Sn	704 K	0.13	0.5	1.15

Assuming a single stage core formation scenario it has then been modeled how the ratio of the mantle abundances of the volatile elements changes with pressure and temperature, which can also be understood as an average of a continuous core formation scenario. For a given pressure the temperature was fixed at the peridotitic liquidus as given by Liebske et al. (2012). The Earth´s core was assumed to contain 85.5 wt% Fe and 5.2 wt % Ni. The evolution of the mantle abundance ratio with increasing pressure (and with it increasing temperature) is shown in Figure 40 a-d for each element pair. It was found that the relative abundances of Cu/As, Cu/Au and Pb/Sn are matched at 5 GPa, 12 GPa and 21 GPa respectively. No satisfying solution was found for the element pair Ag/Sb. In this cases the individual elements become more and more fractionated with increasing pressure. However one should note that the extrapolation to very high pressures involves high uncertainties on the derived partition coefficient values, because of which the solution for a pressure regime that can explain the relative mantle abundances of the above mentioned elements might be expanded. In particular it can be seen in Figure 40 b-d that a wide range of pressures leads to ratios of Cu/As, Ag/Sb and Sn/Pb that are very close to the ratios of these elements in the Earth´s mantle.

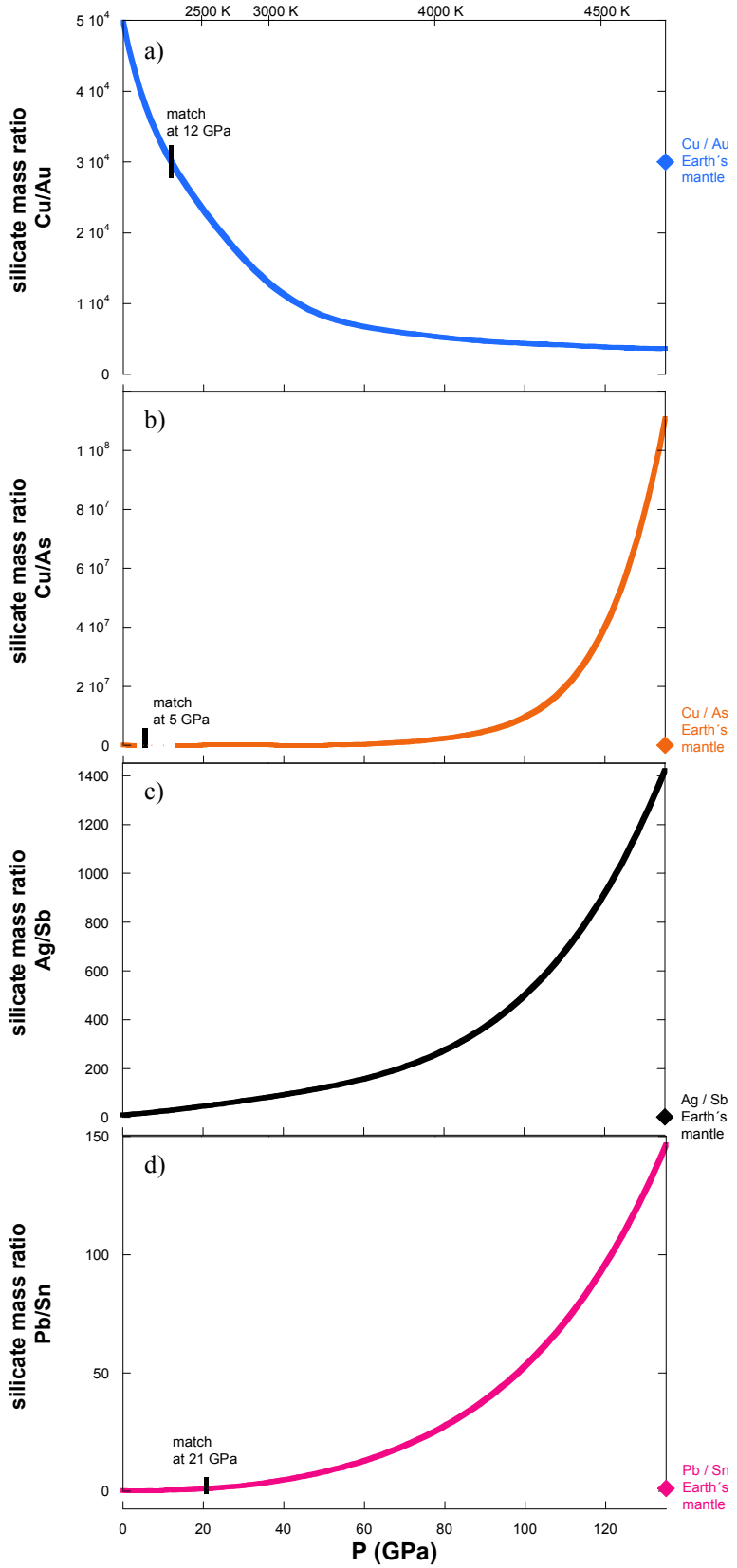

Figure 40: *The silicate mass ratio of a) Cu/Au, b) Cu/As, c) Ag/Sb, d) Pb/Sn is plotted against increasing pressure. The temperature is fixed at the peridotitic liquidus (Liebske et al. (2012). Pressures of 12, 5 and 21 GPa can respectively explain the ratio of the mantle abundances of Cu /Au, Cu/As and Pb/Sn. No solution was found for the element pair Ag/Sb.*

In a second approach the influence of S on the partitioning behaviour has been taken into account. It has been mentioned earlier that the Earth´s core might contain up to 2 wt% S (Dreibus and Palme, 1996; McDonough, 2003). However it has been argued by O´Neill (1991) that a late S-rich accretionary component, the hadean matte, might have influenced the extraction of siderophile elements from the Earth´s mantle to its core. Therefore it has been calculated for increasing pressure the amount of S that is necessary to produce the mantle ratio of the individual element pairs. The metal phase consisted of Fe, S and the element of interest and the temperature was again fixed at the peridotitic liquidus as derived from Liebske et al. (2012). An intersection of the trends for two element pairs was found between 2 GPa and 9 GPa with S-contents ranging from 2 wt% to 12 wt%. More precisely, the solutions for the element pairs Cu – Au and Cu - As intersect at 7 GPa and 4.5 wt% S, Cu/Au and Ag/Sb have the same solution at 2 GPa and 9 wt% S and the trends for Cu/As and Ag/Sb intersect at 9 GPa and 12 wt% S. No solution at any pressure was found to explain the relative abundance of Sn and Pb in the Earth´s mantle. The results are shown in Figure 41.

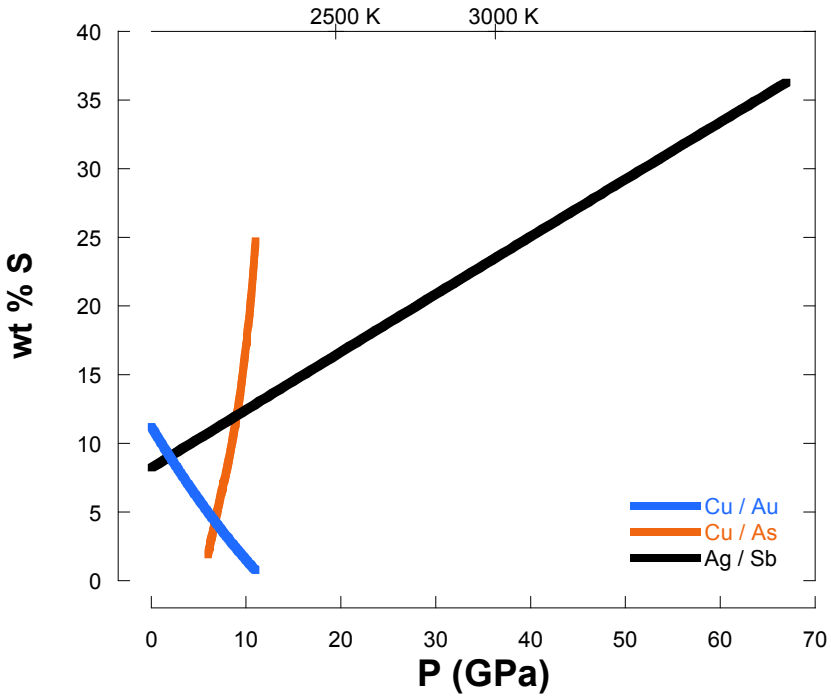

Figure 41: *The concentration of S in the metal phase, necessary to match the relative abundance of the volatile element pairs Cu/Au, Cu/As and Ag/Sb, is plotted against increasing pressure.*

In a third step the combined influence of Si and S has been modeled for each volatile element pair. McDonough (2003) proposed that the Earth´s core contains 85.5 wt% Fe and

5.2 wt% Ni. Therefore this model was designed in the way that the combination of S- and Si-metal contents did not exceed the remaining 9.3 wt %. As before the temperature was fixed at the peridotitic liquidus (Liebske et al., 2012). For increasing pressure the individual concentrations of S and Si in the metal phase that can explain the relative mantle abundance of each volatile element pair were calculated. The results are shown in Figure 42 a – d. While no unique solution was found it can still be seen that the mantle ratio of every element pair can be explained by a combination of Si and S, which has not been the case if only pressure and temperature or pressure, temperature and S has been taken into account (see above). The elements Cu, As and Au all have similar condensation temperatures (Table 16). It was found that < 1wt% S and Si can explain the relative abundances of all three elements between 6 – 9 GPa. In general the amount of Si always exceeds the concentration of S.

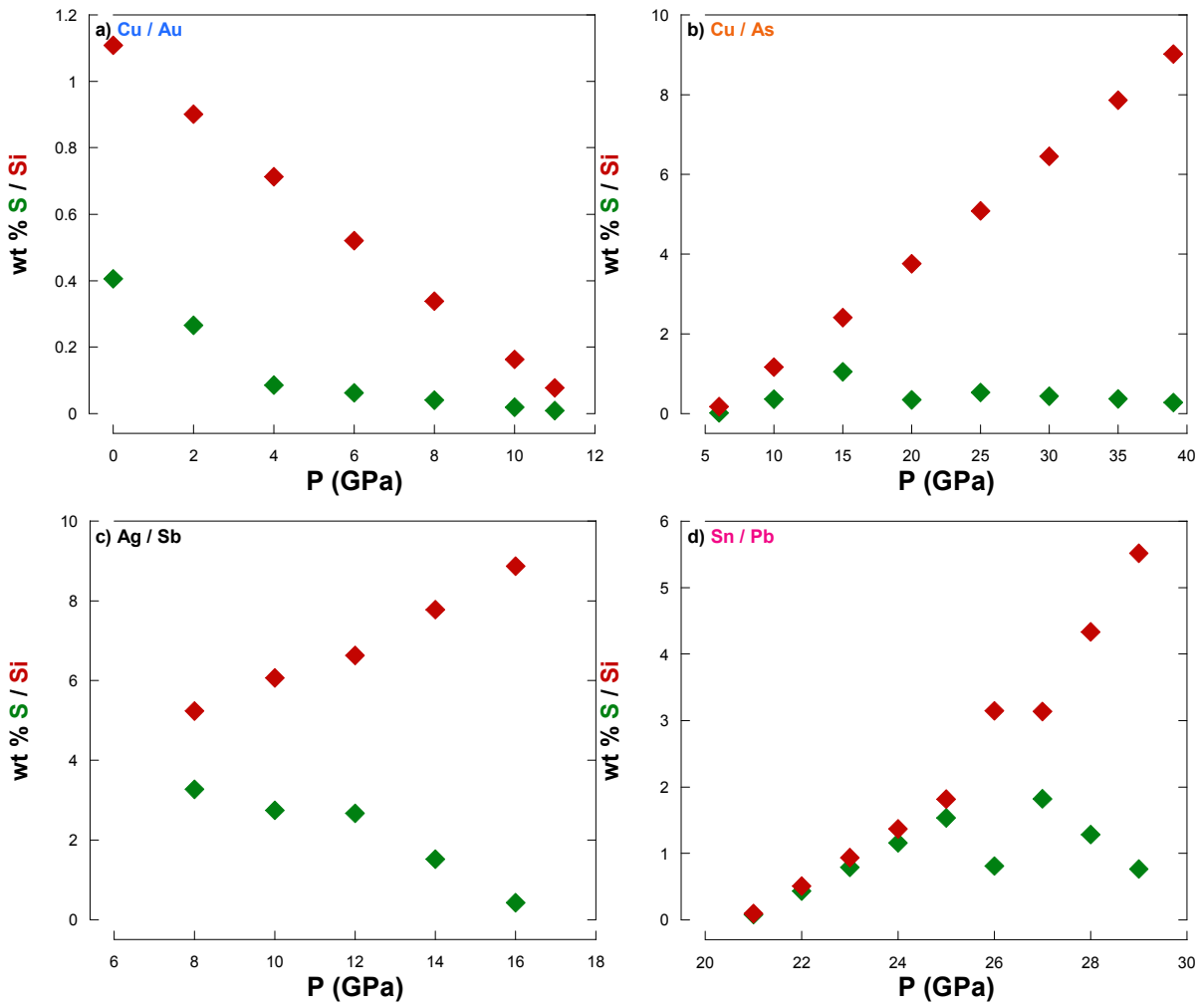

Figure 42: *The concentrations of S and Si in the metal phase, necessary to match the mantle abundance ratio of a) Cu/Au, b) Cu/As, c) Ag/Sb and d) Sn/Pb, are plotted against increasing pressure.*

In summary it was found that only the combination of Si and S provides an explanation for the relative mantle abundances of individual element pairs. However more complex continuous and heterogeneous core formation models need to be considered to provide better constraints on the conditions that prevailed during core formation. Moreover it will be helpful to also incorporate the influence of other light elements, such as O, and variable silicate compositions.

6. The dependence of non-volatile element partitioning on pressure, temperature and S-content of the metal

6.1 Introduction

As discussed in Chapters 1 and 5, the abundances of siderophile elements in the Earth´s mantle are too high to be explained by metal – silicate equilibration at low pressures and moderately temperatures (e.g. Ringwood, 1966; Jagoutz et al., 1979; Jones and Drake, 1986; Newsom, 1990; Murthy, 1991; Walter et al., 2000; Rubie et al., 2007). It has furthermore been shown that increasing temperatures alone are not capable of yielding the observed abundances of siderophile elements in the Earth´s mantle. A solution to this so called "excess siderophile element problem" was found in 1996 by Li and Agee (1996). The latter authors performed metal – silicate partitioning experiments in a multi anvil apparatus at pressures between 2 and 20 GPa and a temperature of 2273 K. The elements investigated were Ni and Co, two refractory siderophile elements that are known to be depleted to the same extent in the Earth´s mantle, thus requiring similar partition coefficients (Palme and O´Neill, 2003). As can be seen in Figure 43a and c, at low pressures the partition coefficients of Ni and Co differ by more than one order of magnitude. However with increasing pressures both elements become less siderophile and in particular Ni becomes less siderophile to a greater extent than Co. Li and Agee (1996) found that the extrapolation of the experimentally determined pressure dependences resulted in an intersection between 28 and 42 GPa, depending on whether the partition coefficient ratio D_{Ni}/D_{Co} of 1.1 is interpreted as the result of equilibration at the base of a magma ocean or as an average of partition coefficient ratios from the top to the bottom of the – in this case deeper – magma ocean (compare Figure 43b). These pressures correspond to a magma ocean depth of 750 to 1100 km.

The experiments that were performed by Li and Agee (1996) produced a metal phase with significant amounts of S (26.96 – 29.69 wt %). Sulphur is known to have an effect on the metal – silicate partitioning behaviour (e.g. Peach, 1993; Jana and Walker, 1997; Kiseeva et al., 2013; this work) and so Li and Agee (1996) compared their results for Ni and Co partitioning between silicate and a S-bearing metal alloy to the results that were obtained by Thibault and Walter (1995) that were based on S-free experiments. As can be seen in Figure 43c the partitioning data for Ni and Co in a S-bearing and a S-free system differ only slightly,

thus the results of Li and Agee (1996) are applicable to core formation scenarious without the necessity of constraining the amount of S that contributes to the Earth´s core.

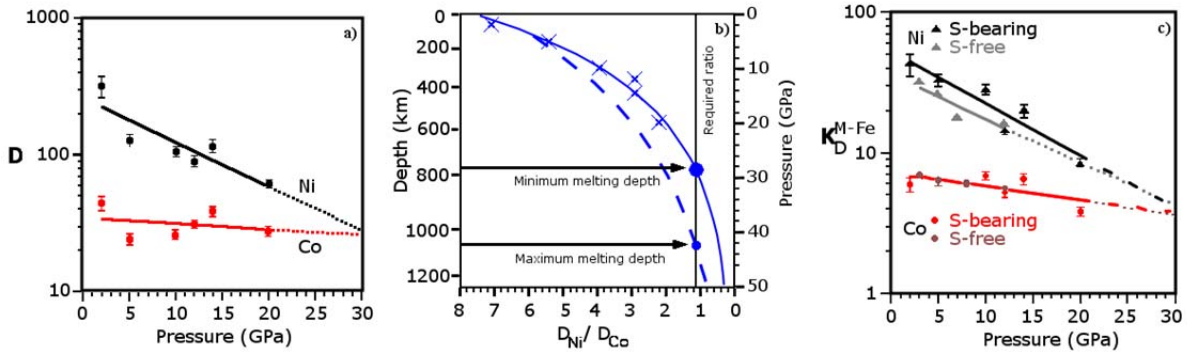

Figure 43a-c: *Modified after Li and Agee (1996).* ***a)*** *Partition coefficients for Ni and Co are plotted against pressure. At low pressures D_{Ni} and D_{Co} differ by more than one order of magnitude, yet the partitioning trends converge at higher pressures.* ***b)*** *The experimental partition coefficient ratio between D_{Ni} and D_{Co} is plotted against pressure. Vertical line indicates the Earth´s near chondritic D_{Ni}/D_{Co} ratio. Within the errors diagram b) shows in another way that pressure between 28 and 42 GPa can account for the mantle depletions of Ni and Co, depending on whether the partition coefficient ratio was established by equilibration at the base of the magma ocean (solid line) or is an average of partition coefficient ratios from the top to the (deeper) bottom of the magma ocean (dotted line).* ***c)*** *The study of Li and Agee was based on a S-bearing metallic phase. However S does not influence the partitioning behaviour of Ni and Co proving that the derived conclusions of high pressure – high temperature equilibration are valid (grey and purple data points are from Thibault and Walter (1995)).*

Subsequently there have been further investigations by Gessmann and Rubie (1998) and Chabot et al. (2005) which additionally investigated the influence of temperature on Ni and Co partitioning. According to these authors increasing temperatures cause a decrease in siderophility for both elements. It has been mentioned several times that Wade and Wood (2005) investigated a continuous core formation model in which oxygen fugacity is increased over two logarithmic units during the time of Earth´s accretion. The results of their model were based on experiments of the metal – silicate partitioning behaviour of Ni and Co as well as V, Mn and Si. Kegler et al. (2008) studied the partitioning of Ni and Co at 1 atm – 25 GPa and 1570 – 2573 K. The starting materials consisted of a FeCoNi alloy and in most cases a basaltic silicate phase. In two experiments the silicate composition was peridotitic. In general the pressure trend of the partitioning of Ni and Co according to the results of Kegler et al. (2008) and of Li and Agee (1996) are in agreement with one another. Both studies find a decrease in partition coefficient values or in the case of Kegler et al. (2008) a decrease in

exchange coefficient values for both elements. However Kegler et al. (2008) argued for two different pressure regimes. Their results indicate that the slopes of the regressions of Ni and Co are much steeper at low pressures up to 5 GPa than at pressures above 5 GPa. The authors can explain the abundances of Ni and Co in the Earth´s mantle by high pressure equilibration at 35 GPa in the case of Co and 45 – 50 GPa in the case of Ni. The required ratio of the partition coefficients of Ni and Co of almost 1 is reached at even higher pressures of 55 GPa, but at these conditions the absolute abundances of Ni and Co in the Earth´s mantle could not be explained. In summary Kegler et al. (2008) conclude that a single stage core formation scenario is unrealistic, a theory that to date is accepted by most scientists (e.g. Wade and Wood, 2005; Schönbächler et al., 2010; Rubie et al., 2011).

Recently the experimental pressure range for the determination of the partitioning of Ni and Co has been extended to pressures of 35 to 74 GPa by Siebert et al. (2012) employing the laser-heated diamond anvil cell. Temperatures between 3100 and 4400 K have been achieved. The results support the previously derived pressure trend for Ni and Co of decreasing partition coefficients with increasing pressures. The authors show that the mantle abundances of Ni and Co are the result of metal – silicate equilibration in a deep magma ocean at a maximum pressure of 60 GPa.

It has been discussed in detail in Chapter 1 that the parameterization of the liquid metal – liquid silicate partitioning behaviour of W is important because the Hf-W decay system with Hf being lithophile and W being siderophile can provide information on the timing of core formation (Jacobsen, 2005; Kleine et al., 2005; Kleine et al., 2009) and on the degree of equilibration (Rudge et al., 2010; Nimmo et al., 2010). Several studies have already provided metal – silicate partitioning data for W. Among these are the publications of Cottrell et al. (2009 and 2010), Righter et al. (2010), Siebert et al. (2011), Wade et al. (2012) and Ballhaus et al. (2013) with which the results of this study will be compared in Section 6.3. With the exception of Cottrell et al (2009 and 2010) all of these studies showed that increasing temperature causes the siderophility of W to decrease. Siebert et al. (2011) and Wade et al (2012) furthermore found that increasing pressure by contrast results in decreased siderophility of W as has been reported earlier by Cottrell et al. (2009 and 2010), although only for pressures above 4 GPa.

Another refractory element that has been depleted by core formation processes is Mo. Its metal – silicate partitioning behaviour has been studied by Righter et al. (2010), Siebert et al. (2011) and Wade et al. (2012) with partly different outcomes. Both Siebert et al. (2011) and

Wade et al. (2012) found that increasing pressure reduces the siderophility of Mo. Increasing temperature however led to lower partition or exchange coefficient values according to Righter et al. (2010) and Siebert et al. (2011), whereas the opposite was found by Wade et al. (2012).

In Chapter 5 it has been discussed on the basis of previous investigations and the results of this study that S needs to be considered when investigating liquid metal –liquid silicate partitioning of siderophile elements. The above mentioned study of Wade et al. (2012) investigated the partitioning of both W and Mo with experimental pressures and temperatures ranging between 1.5 - 24 GPa and 1803 – 2073 K respectively. The Fe metal has in some cases been modified by the addition of FeS or $FeSi_2$ and the silicate composition was based on the system anorthite-diopside-forsterite. Taking into account interaction parameters in order to correct the activities of W and Mo in a S-bearing metal phase and including their results on the partitioning behaviour of both elements Wade et al. (2012) employed a core formation model that showed that the abundances of the refractory elements W and Mo in the Earth´s mantle can be explained if S is added solely during the final 20% of accretion.

It has been mentioned earlier that the partitioning of Ni and Co between metal and silicate phases is hardly effected by the presence of S in the metal phase (Li and Agee, 1996). This has been confirmed by Jana and Walker (1997) who also showed that the siderophility of both Ni and Co only decreases moderately with increasing S-content of the metal phase. Additional studies (Li and Agee, 2001 and Kiseeva et al., 2013) exhibit some metal – silicate partitioning experiments with S being an additive to the metal phase. Their results, more precisely the corresponding exchange coefficient values, will be compared to the findings of this study in section 6.3.

6.2 Methods

The liquid metal – liquid silicate partitioning of the refractory elements Ni, Co, W and Mo has been investigated at pressures between 11 and 21 GPa and temperatures of 2478 – 2911 K. In order to additionally quantify the effect of S in the metal phase of the samples the S concentrations in the metal phase of the starting material have been varied from a S-free system up to FeS. The experimental and analytical methods followed the routines described in

Chapter 2 and partition and exchange coefficients have been calculated employing equations [3] and [5] (Chapter 3). Following the results of Wade et al. (2012) the elements W and Mo were treated as hexavalent and tetravalent cations in the silicate phases respectively. Ni and Co were assumed to be present as divalent cations as it has already been proposed by Holzheid et al. (1994).

As described in Chapter 5 partitioning is described by an exchange reaction that involves Fe and FeO:

$$\frac{n}{2}\,Fe^{met} + MO_{\frac{n}{2}}^{sil} = \frac{n}{2}\,FeO^{sil} + M^{met} \qquad [47]$$

The parameterization of the liquid metal – liquid silicate partitioning behaviour of non-volatile elements follows the procedures that have been described in Chapter 5 (equations [28] to [33]). In agreement with the parameterization of the partitioning behaviour of volatile elements also the partitioning of the non-volatile elements Ni, Co, W and W has been quantified in form of the following expression for logarithmic exchange coefficient values:

$$\log K_D^{M-Fe} = a + \frac{b}{T} + \frac{c\,P}{T} - \frac{\ln(\gamma_M)}{\ln(10)} + \frac{\frac{n}{2}\ln(\gamma_{Fe})}{\ln(10)} \qquad [48]$$

The aim of this Chapter is the quantification of the effects of pressure, temperature and S content of the metal phase on the partitioning behaviour of Ni, Co, W and Mo. Therefore the calculation of the activities of Fe and the element of interest in the metal phase is based on a ternary system similar to that described in Chapter 4. Equations [34] and [35] were solved for the three components Fe, *M* and S, where *M* is the element of interest:

$$\begin{aligned} ln\gamma_{Fe} = {} & \varepsilon_S^S\left(X_S + ln(1 - X_S)\right) + \varepsilon_M^M\left(X_M + ln(1 - X_M)\right) \\ & + \varepsilon_M^S\,X_S\,X_M\left(1 - \frac{1}{1 - X_M} - \frac{1}{1 - X_S}\right) \\ & - \frac{\varepsilon_M^S}{2}\,X_S^2\,X_M^2\left(\frac{3}{1 - X_M} + \frac{3}{1 - X_S} + \frac{X_{Si}}{(1 - X_S)^2} + \frac{X_M}{(1 - X_M)^2} - 3\right) \end{aligned} \qquad [49]$$

$$ln\gamma_M = ln\gamma_{Fe} + ln\gamma_M^0 - \varepsilon_M^M \, ln(1 - X_M) - \varepsilon_M^S \, X_S \left(1 + \frac{ln(1 - X_S)}{X_S} - \frac{1}{1 - X_M}\right) + \varepsilon_M^S \, X_S^2 \, X_M \left(\frac{1}{1 - X_M} + \frac{1}{1 - X_S} + \frac{X}{2(1 - X_M)^2}\right) - 1$$

[50]

Here X is the molar fraction of the components, γ_M^0 denotes the activity of the element of interest at infinite dilution and ε denotes the interaction of components with one another, where $\varepsilon_i^j = \varepsilon_j^i$. Temperature corrections are performed employing equation [39], Chapter 5. Table 17 summarizes the values of γ_M^0, ε_S^S and ε_M^M that were taken from the Steelmaking Data Sourcebook with the interaction parameters being calculated from the mass related e_i^k values by employing equation [38], Chapter 5. If the values were not available for certain elements they were set to zero.

Table 17: *Summary of interaction parameter values $\boldsymbol{\varepsilon_i^k}$ and activity coefficients at infinite dilution $\boldsymbol{\gamma_i^0}$ that were used to calculate the activity coefficients of Fe and the element of interest M in the metal using equations [49] and [50]. All values are from the Steelmaking Data Sourcebook.*

	Ni	**Co**	**W**	**Mo**
$\boldsymbol{\gamma_M^0}$	0.66	0.55	1	1
$\boldsymbol{\varepsilon_M^M}$	0.0007	0.00509	-	0.0121
$\boldsymbol{\varepsilon_S^S}$	-5.66			

Except for replacing equations [36] and [37] (Chapter 5) by equations [49] and [50] respectively, the parameters a, b, c and ε_M^S were obtained following the procedure given in Chapter 5. All parameters were solved by minimizing the sum of the derivations between calculated and experimental logarithmic exchange coefficient values employing equation [40] (Chapter 5). Uncertainties on the expressions for logarithmic K_D^{M-Fe} values are derived from the average deviation between experimentally determined and calculated logarithmic K_D^{M-Fe} values employing equation [41], Chapter 5.

6.3 Results

Liquid metal – liquid silicate partitioning has been studied for the non-volatile elements Ni, Co, W and Mo at a pressure and temperature range of 11 to 21 GPa and 2478 to 2911 K. The S content of the starting metal was varied between zero and 20 wt%. Table 19 lists the experimental conditions of each experiment as well as the measured and recalculated exchange coefficient values K_D^{M-Fe} that were obtained by the parameterization of the data of this study (see below). The values for the Gibbs free energy change $-\Delta G^0$ and the molar fractions of Fe, S and the element of interest *M* in the metal phase are also listed. Uncertainties that were obtained by error propagation are given for the last digit(s).

The partitioning behaviour of non-volatile elements is significantly better studied than the partitioning behaviour of volatile elements. For this reason the results obtained in this study can be better compared to existing data sets. It was possible to select several experiments from literature studies that were performed at very similar conditions. The previously published data have been recalculated and incorporated into the parameterization of the partitioning behaviour of Ni, Co, Mo and W with the aim of better constraining the pressure and temperature dependences. The selected experiments were performed in the same type of capsules (MgO), used the same silicate composition (peridotitic) and were free of Si or S in the metal phase. The selected samples from the literature are listed in Table 18.

Table 18: *Summary of experiments from the literature that have been used to better constrain the pressure and temperature dependences of Ni, Co and W. Agreement between capsule material and silicate composition was presupposed. The metal phases needed to be free of Si and S.*

	Kegler et al. (2008) sample, P, T	**Siebert et al. (2011) sample, P, T**	**Siebert et al. (2012) sample, P, T**	**Wade and Wood (2012) sample, P, T**
Ni	PPC1: 3.5 GPa, 2073 K PHP1: 5 GPa, 2373 K	52: 1.5 GPa, 2123 K 139: 3 GPa, 2123 K	X1-4: 50 GPa, 3700 K	
Co	PPC1: 3.5 GPa, 2073 K PHP1: 5 GPa, 2373 K	52: 1.5 GPa, 2123 K 139: 3 GPa, 2123K	X1-4: 50 GPa, 3700 K	
Mo		52: 1.5 GPa, 2123 K 139: 3 GPa, 2123K		755: 24 GPa, 2473 K 758: 24 GPa, 2673 K
W				755: 24 GPa, 2473 K 758: 24 GPa, 2673 K

As in Chapter 5 the following Section provides a detailed look on the results for each studied element separately. In each case the pressure and / or temperature dependences are illustrated by plotting the experimentally investigated logarithmic exchange coefficients K_D^{M-Fe} minus the activity terms of equation [48] against inverse temperature. The calculated pressure and / or temperature dependences are shown by green and black lines according to whether literature data was incorporated into the fit or not. Equation [51] displays the relationship between the calculated pressure and temperature dependences and the modified exchange coefficient values.

$$\log K_D^{M-Fe} + \frac{\ln(\gamma_M)}{\ln(10)} - \frac{\frac{n}{2}\ln(\gamma_{Fe})}{\ln(10)} = \log - activity\ terms = a + \frac{b}{T} + \frac{c\ P}{T} \qquad [51]$$

In a second diagram experimentally determined logarithmic exchange coefficient values have been plotted against inverse temperature. The range of inverse temperatures (x-axis) and logarithmic exchange coefficient values (y-axis) has been expanded in order to be able to compare the results of this study with additional literature data that are based on experiments conducted at similar conditions yet not necessarily exactly the same. Finally the parameterization of the S-dependent partitioning of each element is demonstrated by a diagram of logarithmic exchange coefficients against increasing S contents of the metal phase. Dotted green and red lines represent a linear regression line to the calculated results according to whether the parameterization of the partitioning behaviour of the particular experiments involved the literature data points as given in Table 18 or not.

Table 19: *Summary of experimental conditions, values of the Gibbs free energy change $-\Delta G^0$ and of the experimentally obtained and recalculated exchange coefficient values that were obtained from the parameterization of the experimental results of this study alone. Additionally the molar fractions of Fe, S and the element of interest (Ni, Co, Mo, W) are given. Errors were obtained by error propagations and are given in parenthesis for the last digit.*

				Ni						Co					
Sample	P (GPa)	T (K)	ΔIW	$-\Delta G^0$ (J/mole)	K_D^{Ni-Fe} (exp)	K_D^{Ni-Fe} (calc)	X_{Fe}^{met}	X_S^{met}	X_{Ni}^{met}	$-\Delta G^0$ (J/mole)	K_D^{Co-Fe} (exp)	K_D^{Co-Fe} (calc)	X_{Fe}^{met}	X_S^{met}	X_{Co}^{met}
H3371b	11	2773	-2.4 (2)	55977	14 (3)	13.4	0.9070		0.0244	34576	6 (1)	6.6	0.9070		0.0264
H3372b	11	2478	-2.11 (5)	50064	10 (1)	17.3	0.9457		0.0115	33955	4.9 (4)	8.0	0.9457		0.0166
H3586b	11	2609	-2.3 (1)	52690	22 (4)	15.3	0.9457		0.0122	34231	9.8 (6)	7.3	0.9457		0.0195
H3586a	11	2609	-2.2 (3)	52690	19 (8)	15.3	0.9389		0.0153	34231	9 (3)	7.3	0.9389		0.0234
Z822b	11	2573	-2.1 (1)	51968	16 (2)	15.8	0.9356		0.0125	34155	8.1 (7)	7.5	0.9356		0.0192
Z916b	11	2580	-2.2 (1)	52109	12 (4)	15.7	0.9508		0.0125	34170	7 (1)	7.5	0.9508		0.0186
Z1011b	11	2605	-2.7 (5)	52610	28 (5)	15.4	0.9205		0.0168	34222	11 (2)	7.3	0.9205		0.0240
Z859a	18	2717	-2.1 (3)	54854	16 (1)	15.5	0.9259		0.0123	34458	6.8 (4)	6.8	0.9259		0.0185
Z865a	18	2834	-2.8 (5)	57199	16 (4)	14.2	0.9332		0.0131	34705	8 (1)	6.4	0.9332		0.0193
Z929a	20	2799	-2.5 (6)	56498	15 (1)	14.9	0.9453		0.0128	34631	6.4 (4)	6.5	0.9453		0.0190
Z950a	21	2904	-2.0 (3)	58602	10 (2)	14.0	0.9343		0.0124	34852	5.2 (8)	6.1	0.9343		0.0188
Z970a	21	2911	-2.8 (8)	58742	12 (2)	13.9	0.9377		0.0128	34867	5.8 (7)	6.1	0.9377		0.0192
Z970b	21	2911	-2.2 (2)	58742	14 (1)	13.9	0.9357		0.0130	34867	7.2 (6)	6.1	0.9357		0.0196
Z1009b	11	2605	-2.1 (6)	52610	23 (4)	15.6	0.7354	0.1999	0.0193	34222	8 (1)	6.7	0.7354	0.1999	0.0212
H3371a	11	2478	-1.9 (2)	50064	15 (1)	17.5	0.7521	0.1782	0.0216	33955	6.6 (6)	7.3	0.7521	0.1782	0.0225
H3372a	11	2626	-1.8 (1)	53031	15.2 (7)	15.2	0.8146	0.1071	0.0189	34267	5.9 (3)	6.9	0.8146	0.1071	0.0199
Z1051a	11	2626	-1.4 (4)	53031	19 (5)	15.5	0.5995	0.3440	0.0204	34267	6.0 (8)	6.1	0.5995	0.3440	0.0090
Z1051b	11	2619	-1.1 (4)	52890	26 (5)	15.7	0.5803	0.3568	0.0199	34252	7 (1)	6.1	0.5803	0.3568	0.0088

				Mo						W					
Sample	P (GPa)	T (K)	ΔIW	$-\Delta G^0$ (J/mole)	K_D^{Mo-Fe} (exp)	K_D^{Mo-Fe} (calc)	X_{Fe}^{met}	X_S^{met}	X_{Mo}^{met}	$-\Delta G^0$ (J/mole)	K_D^{W-Fe} (exp)	K_D^{W-Fe} (calc)	X_{Fe}^{met}	X_S^{met}	X_W^{met}
H3371b	11	2773	-2.4 (2)	36485	6 (3)	4.8	0.9070		0.0212	-63473	0.05 (2)	0.064	0.9070		0.0128
H3372b	11	2478	-2.11 (5)	35105	0.7 (2)	5.1	0.9457		0.0040	-63334	0.017 (6)	0.046	0.9457		0.0033
H3586b	11	2609	-2.3 (1)	35718	3 (1)	5.1	0.9457		0.0049	-63396	0.018 (6)	0.054	0.9457		0.0038
H3586a	11	2609	-2.2 (3)	35718	4 (2)	5.0	0.9389		0.0065	-63396	0.01 (1)	0.054	0.9389		0.0050
Z822b	11	2573	-2.1 (1)	35550	5 (1)	5.1	0.9356		0.0049	-63379	0.05 (1)	0.052	0.9356		0.0049
Z916b	11	2580	-2.2 (1)	35582	3 (2)	5.1	0.9508		0.0049	-63382	0.03 (1)	0.052	0.9508		0.0045

Table 19 continued

Z1011b	11	2605	-2.7 (5)	36485	6 (3)	5.1	0.9205		0.0065	-63473	0.06 (3)	0.064	0.9205		0.0058
Z859a	18	2717	-2.1 (3)	36223	7 (1)	5.1	0.9259		0.0050	-63447	0.09 (3)	0.060	0.9259		0.0048
Z865a	18	2834	-2.8 (5)	36771	5 (2)	5.1	0.9332		0.0050	-63502	0.07 (3)	0.068	0.9332		0.0047
Z929a	20	2799	-2.5 (6)	36607	5 (1)	5.1	0.9453		0.0050	-63485	0.05 (1)	0.065	0.9453		0.0046
Z950a	21	2904	-2.0 (3)	37098	3 (1)	5.1	0.9343		0.0047	-63535	0.09 (3)	0.072	0.9343		0.0045
Z970a	21	2911	-2.8 (8)	37131	3.5 (7)	5.1	0.9377		0.0049	-63538	0.08 (2)	0.072	0.9377		0.0046
Z970b	21	2911	-2.2 (2)	37131	4 (1)	5.1	0.9357		0.0049	-63538	0.09 (3)	0.072	0.9357		0.0046
Z1009b	11	2605	-2.1 (6)	35699	3 (2)	3.4	0.7354	0.1999	0.0093	-63394	0.010 (5)	0.012	0.7354	0.1999	0.0034
H3371a	11	2478	-1.9 (2)	35105	1.7 (3)	3.5	0.7521	0.1782	0.0102	-63334	0.016 (3)	0.011	0.7521	0.1782	0.0044
H3372a	11	2626	-1.8 (1)	35798	3.9 (5)	3.9	0.8146	0.1071	0.0174	-63404	0.024 (3)	0.024	0.8146	0.1071	0.0061
Z1051a	11	2626	-1.4 (4)	35798	2.8 (9)	2.8	0.5995	0.3440	0.0088	-63404	0.004 (1)	0.004	0.5995	0.3440	0.0020
Z1051b	11	2619	-1.1 (4)	35765	4 (1)	2.8	0.5803	0.3568	0.0096	-63401	0.003 (2)	0.004	0.5803	0.3568	0.0012

6.3.1 Divalent elements nickel and cobalt

6.3.1.1 Nickel

The exchange coefficients for the refractory element Ni decrease very slightly with increasing temperature. If literature data are included into the fit the observed effect is much more distinct. The parameterization of all Ni results showed that its partitioning behaviour is insensitive to changes in pressures regardless of literature data (with peridotitic silicate composition) is incorporated into the fit or not. In both cases the partitioning behaviour of Ni can be explained by the effect of temperature changes alone - an observation that is different to previous results that reported that increasing pressures reduce the siderophility of Ni (e.g. Li and Agee, 1996; Siebert et al., 2013). Moreover, unlike Kegler et al. (2008), no evidence for a difference in the partitioning behaviour of Ni below and above 5 GPa was found.

As can be seen in Figure 44a adding other literature data into the fit causes significant changes in the outcome. However the parameterization of the partitioning data of Ni clearly benefits from the addition of other data points as can be seen in Figure 44b: Although conducted at slightly different conditions a clear temperature trend is shown with increasing temperature significantly reducing the exchange coefficient values. Although no pressure dependence was found the data of this study is in very good agreement to literature results.

It is furthermore observed that S hardly effects the partitioning behaviour of Ni. In Figure 44c logarithmic exchange coefficients are plotted against increasing S content of the metal phase. Green and red dotted lines represent a linear regression to the calculated results according to whether literature as given in Table 18 was included in the parameterization of Ni partitioning or not. The temperature effect is included in the fit. The observations are in good agreement with the results of Li and Agee (1996, 2001). The exchange coeffiecients obtained from Kiseeva et al. (2013) are higher than the values obtained in this study, most likely because the experiments of Kiseeva et al. (2013) were performed at much lower pressure and temperature. Equations [52] and [53] show the parameterization of the liquid metal – liquid silicate partitioning behaviour of Ni for this study and including literature according to Table 18 respectively.

$$\log K_D^{Ni-Fe}\,(this\ study) = 1.05 + \frac{21}{T} - \frac{\ln(\gamma_M)}{\ln(10)} + \frac{\ln(\gamma_{Fe})}{\ln(10)} \quad (\pm 0.1)$$

with ε_S^{Ni} = -0.05 [52]

$$\log K_D^{Ni-Fe}\,(this\ study + lit.) = -1.06 + \frac{5824}{T} - \frac{\ln(\gamma_M)}{\ln(10)} + \frac{\ln(\gamma_{Fe})}{\ln(10)} \quad (\pm 0.11)$$

with ε_S^{Ni} = -0.05 [53]

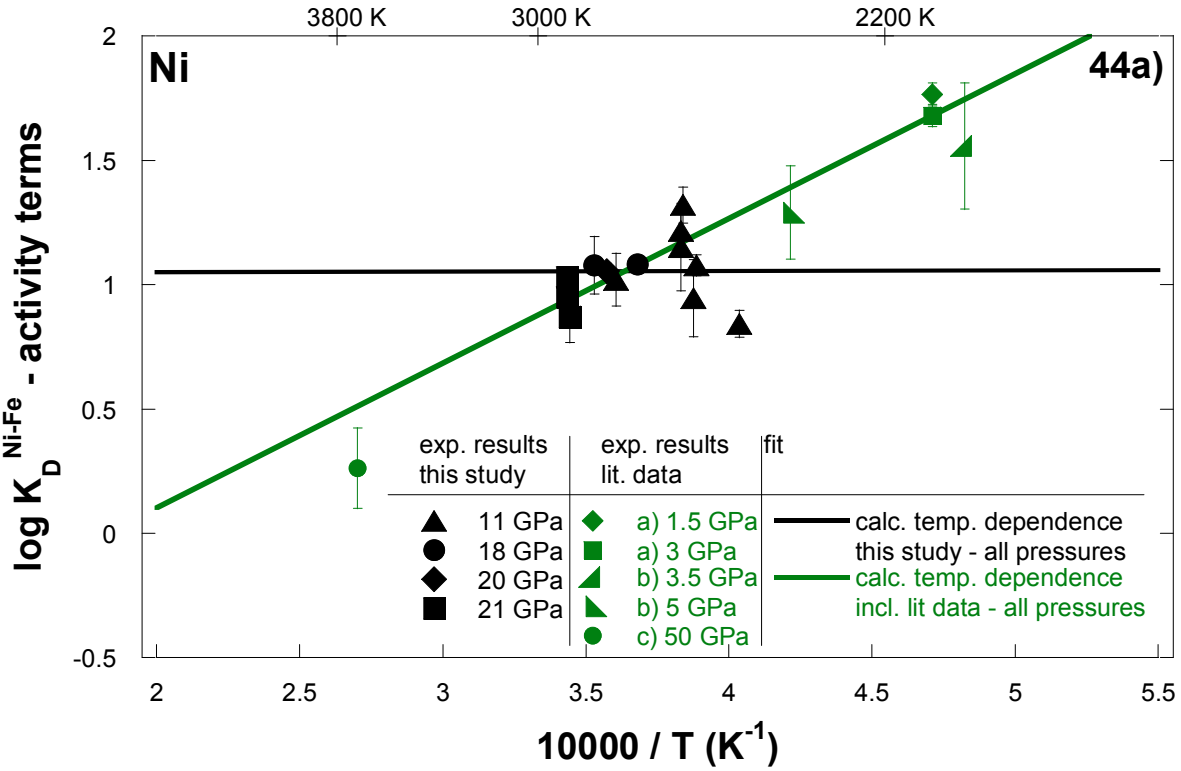
3800 K
3000 K
2200 K
Ni
44a)
log K_D Ni-Fe - activity terms
exp. results this study
exp. results lit. data
fit
11 GPa
18 GPa
20 GPa
21 GPa
a) 1.5 GPa
a) 3 GPa
b) 3.5 GPa
b) 5 GPa
c) 50 GPa
calc. temp. dependence this study - all pressures
calc. temp. dependence incl. lit data - all pressures
10000 / T (K-1)

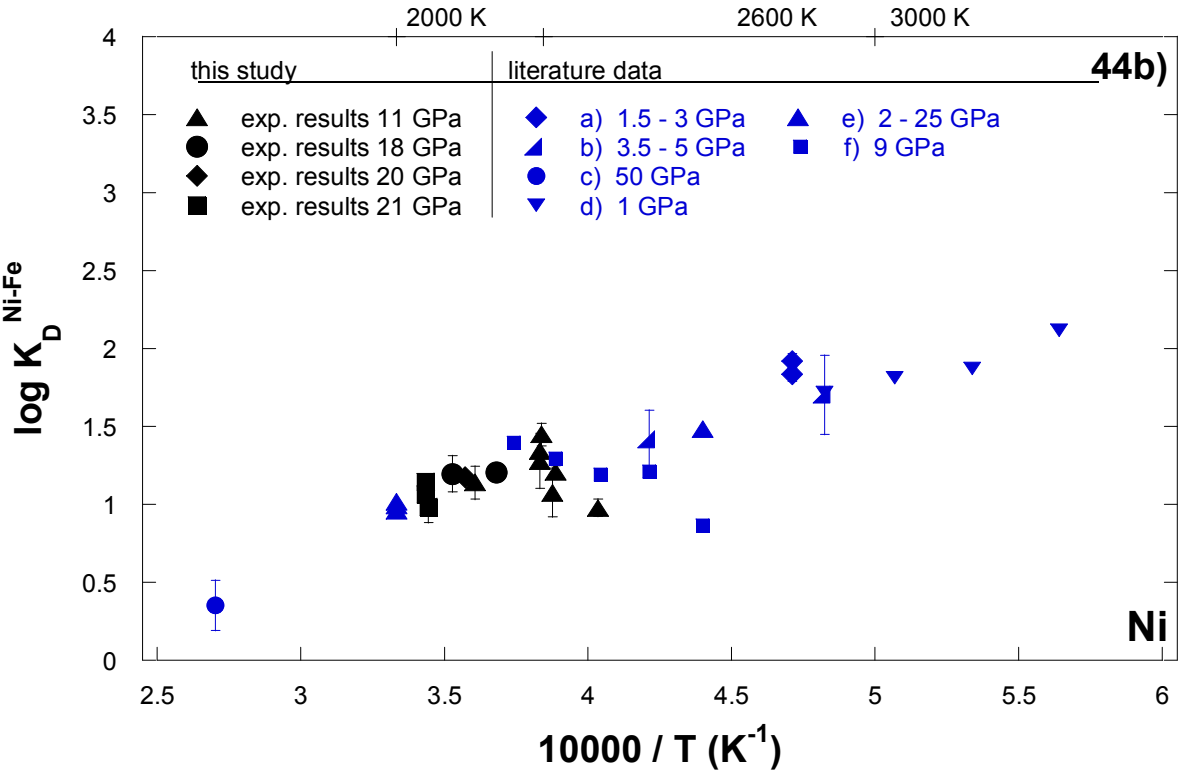
2000 K
2600 K
3000 K
44b)
this study
literature data
exp. results 11 GPa
exp. results 18 GPa
exp. results 20 GPa
exp. results 21 GPa
a) 1.5 - 3 GPa
b) 3.5 - 5 GPa
c) 50 GPa
d) 1 GPa
e) 2 - 25 GPa
f) 9 GPa
log K_D Ni-Fe
Ni
10000 / T (K-1)

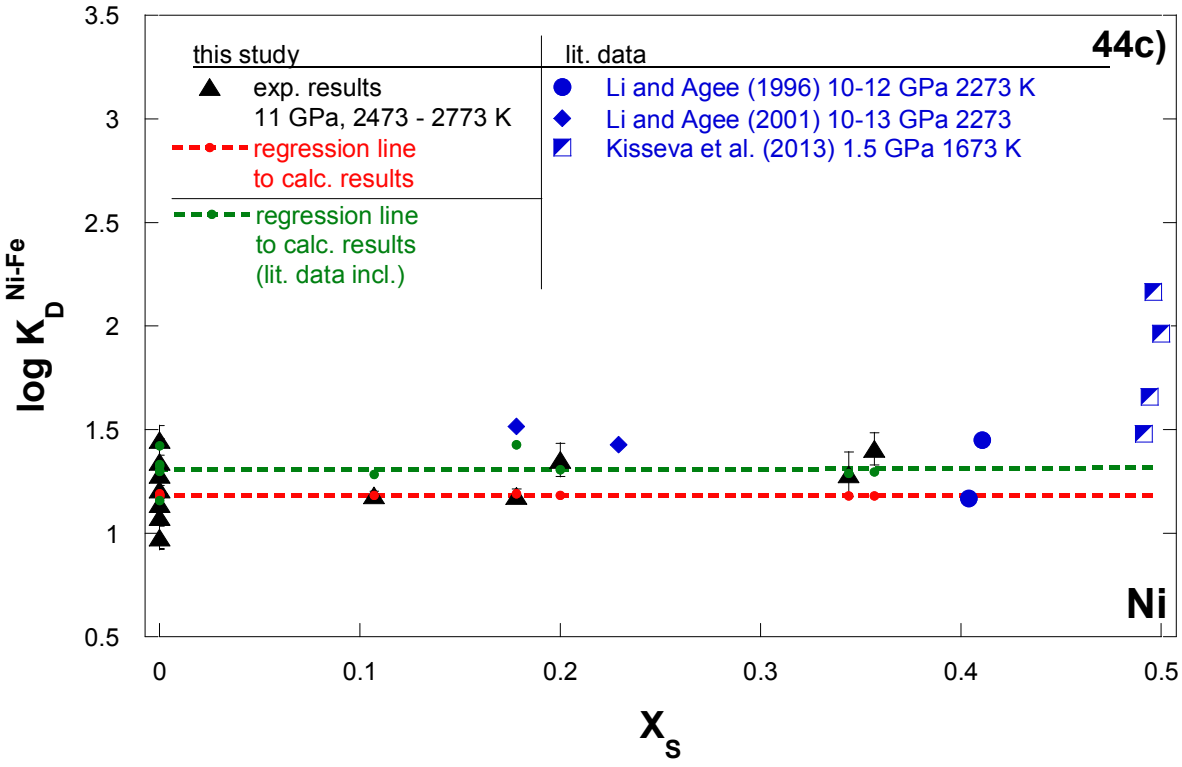

Figure 44a: *Experimentally determined logarithmic exchange coefficients minus the activity terms for Fe and Ni (equation [51]) are plotted against inverse temperature. The solid green and black lines represent the calculated temperature dependence of Ni partitioning with and without literature data being incorporated into the fit respectively.* ***b:*** *Comparison between the results of this study and the recalculated results from literature data sets for Ni. Experimentally obtained logarithmic exchange coefficient values are plotted against inverse temperature.* ***c:*** *The dependence of the metal – silicate partitioning of Ni on the S-content of the metal (mole fractions). The red and green dotted lines represent a linear regression to the recalculated results for a given* ε_S^{Ni} *value of 0.01 or -0.05 with the latter one being the result of the parameterization when literature data according to Table 18 was taken into account to better constrain the pressure and temperature dependence of Ni. Partly unfilled symbols in c) denote experiments that were conducted in graphite capsules. Literature: a) Siebert et al. (2011), b) Kegler et al. (2008), c) Siebert et el. (2013), d) Righter et al. (2010), e) Wade and Wood (2005), f) Gessmann et al. (1998).*

6.3.1.2 Cobalt

The liquid metal – liquid silicate partitioning behaviour of Co is weakly effected by changes in pressure and temperature. In fact only when incorporating literature data into the fit the parameterization of Co partitioning shows that increasing pressure slightly lowers the

siderophility of Co, but the calculated temperature trends at 11 GPa and 21 GPa are not distinguishable from one another (Figure 45a). This observation is similar to the results of Li and Agee (1996) (Figure 43a). However the parameterization of the results of this study and the combined parameterization that includes literature data with peridotitic silicate composition (compare Table 18) are, within the error, in agreement with one another. Moreover, similar to Ni, no evidence for a low pressure regime was found as it has been proposed by Kegler et al. (2008).

The data are furthermore in good agreement with other literature data sets, only the results of Righter et al. (2010) exhibit higher exchange coefficient values (Figure 45b).

As shown in Figure 45c the partitioning behaviour of Co is only effected very slightly by the presence of S in the metal phase. The results of this study are in agreement with the results of Li and Agee (1996 and 2001) and Kiseeva et al. (2013) even though the experiments of the latter study were conducted in C-capsules. Again red and green dotted lines represent regression lines to calculated results according to the fit of experiments solely from this study and the fit that included literature data according to Table 18 respectively.

Equations [54] and [55] show the parameterization of the partitioning behaviour of Co for this study and including literature respectively.

$$\log K_D^{Co-Fe}\,(this\ study) = 0.11 + \frac{1501}{T} - \frac{\ln(\gamma_M)}{\ln(10)} + \frac{\ln(\gamma_{Fe})}{\ln(10)} \quad (\pm 0.07)$$

with $\varepsilon_S^{Ni} = 0.58$ [54]

$$\log K_D^{Co-Fe}\,(this\ study + lit.) = 0.02 + \frac{2011}{T} - \frac{13 * P}{T} - \frac{\ln(\gamma_M)}{\ln(10)} + \frac{\ln(\gamma_{Fe})}{\ln(10)} \quad (\pm 0.1)$$

with $\varepsilon_S^{Ni} = 2.07$ [55]

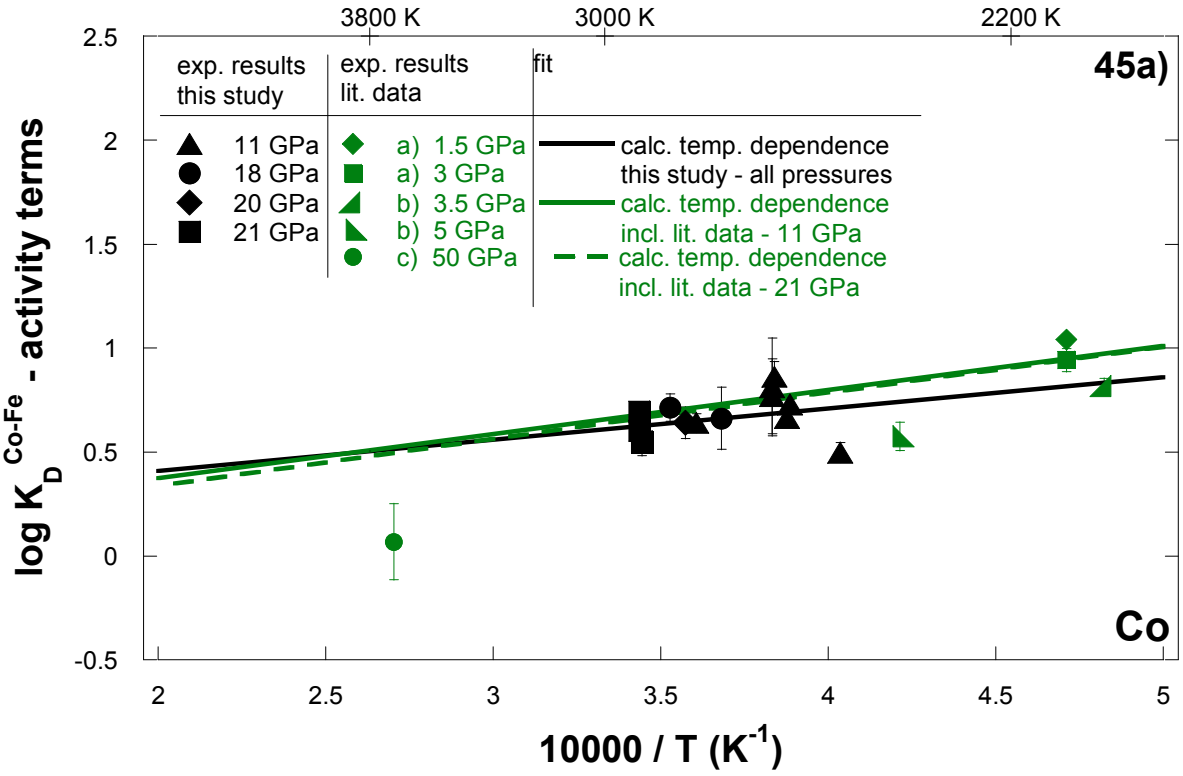
3800 K
3000 K
2200 K
45a)
exp. results this study
exp. results lit. data
fit
11 GPa
18 GPa
20 GPa
21 GPa
a) 1.5 GPa
a) 3 GPa
b) 3.5 GPa
b) 5 GPa
c) 50 GPa
calc. temp. dependence this study - all pressures
calc. temp. dependence incl. lit. data - 11 GPa
calc. temp. dependence incl. lit. data - 21 GPa
log K_D Co-Fe - activity terms
Co
10000 / T (K-1)

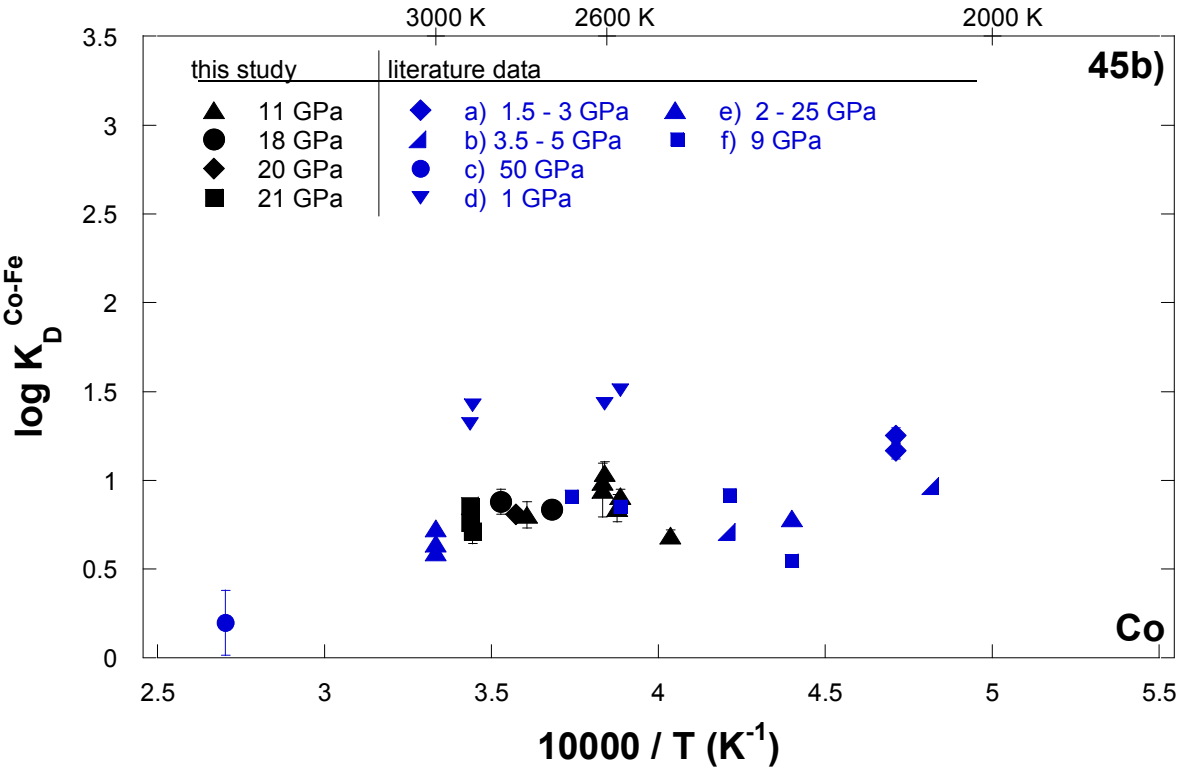
3000 K
2600 K
2000 K
45b)
this study
literature data
11 GPa
18 GPa
20 GPa
21 GPa
a) 1.5 - 3 GPa
b) 3.5 - 5 GPa
c) 50 GPa
d) 1 GPa
e) 2 - 25 GPa
f) 9 GPa
log K_D Co-Fe
Co
10000 / T (K-1)

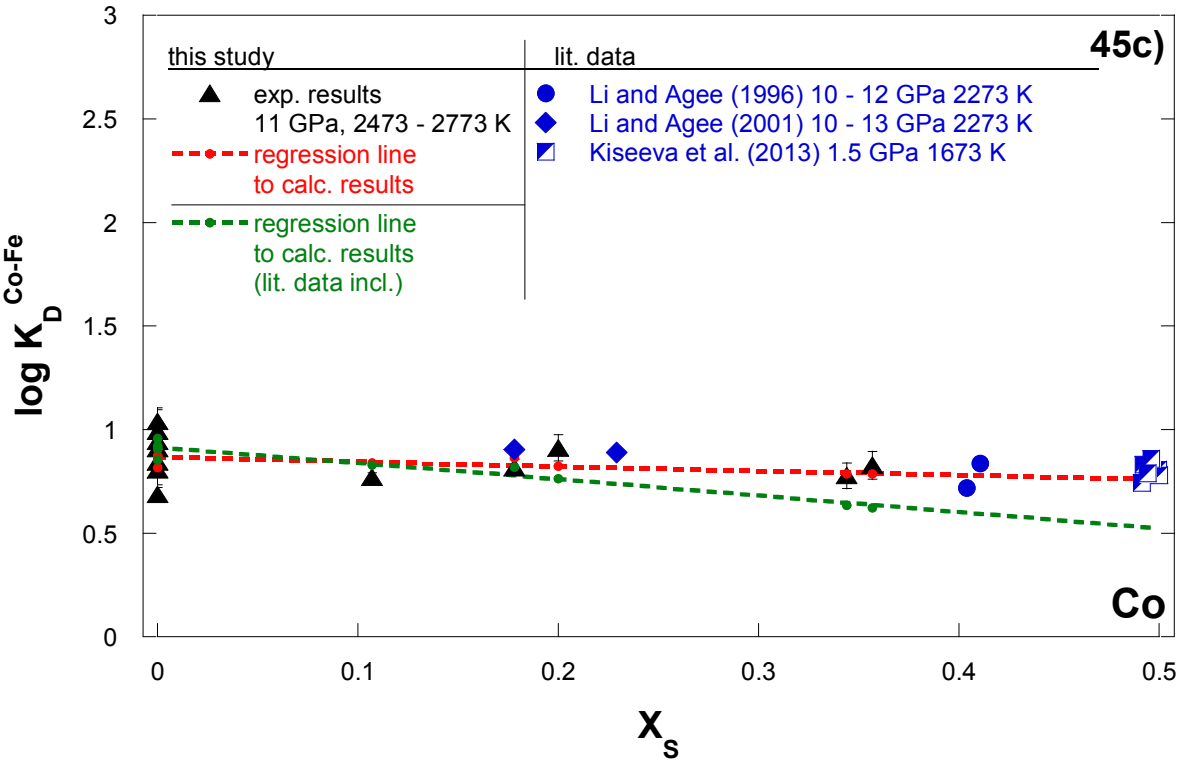

Figure 45a: *Experimentally determined logarithmic exchange coefficients minus the activity terms for Fe and Co (equation [51]) are plotted against inverse temperature. The solid green and black lines represent the calculated temperature dependence of Co partitioning with and without literature data being incorporated into the fit respectively. When literature data is included increasing pressure was found to slightly reduce the siderophility of Co. However the calculated temperature trends at 11 GPa and 21 GPa are hardly distinguishable from one another.* ***b:*** *Comparison between the results of this study and the recalculated results from literature data sets for Co. Experimentally obtained logarithmic exchange coefficient values are plotted against inverse temperature.* ***c:*** *The dependence of the metal – silicate partitioning of Co on the S-content of the metal (mole fractions). The red and green dotted lines represent a linear regression to the recalculated results for a given* ε_S^{Co} *value of 0.58 or 2.07 with the latter one being the result of the parameterization when literature data according to Table 18 was taken into account to better constrain the pressure and temperature dependence of Co. Partly unfilled symbols in c) denote experiments that were conducted in graphite capsules. Literature: a) Siebert et al. (2011), b) Kegler et al. (2008), c) Siebert et el. (2013), d) Righter et al. (2010), e) Wade and Wood (2005), f) Gessmann et al. (1998).*

6.3.2 Tetravalent element molybdenum

The partitioning behaviour of Mo was found to be insensitive to variations in pressure. The parameterization of the metal – silicate partitioning behaviour of Mo shows that increasing

temperature results in decreasing exchange coefficient values. This is also the case when literature data with peridotitic composition according to Table 18 is included into the parameterization. The results of the temperature dependence are shown in Figure 46a.

The experimental results are in good agreement with the observations by Righter et al. (2010), Siebert et al. (2011) and Wade et al. (2012). Because the first two studies are performed at comparatively low pressures and temperatures, this confirms the fact that a pressure dependence could not be parameterized (Figure 46b). However it should be noted that Siebert et al. (2011) found that the siderophility of Mo is decreased by increasing pressure. Therefore further experiments will be necessary to better parameterize the partitioning behaviour of Mo into which additionally the dependence on silicate melt composition should be taken into account.

The presence of S in the metal phase reduces the siderophility of Mo as shown in Figure 46c. Red and green dotted lines denote the results of the parameterization of the S-dependence of the Mo partitioning in the cases of fitting the experimental results without or with further literature data respectively. The results of this study are in excellent agreement with the data given by Wade et al. (2005). Equation [56] and [57] give the final parameterization of the partitioning behaviour of Mo of this study and of this study plus literature respectively.

$$\log K_D^{Mo-Fe}\ (this\ study) = 0.24 + \frac{1228}{T} - \frac{\ln(\gamma_M)}{\ln(10)} + \frac{\ln(\gamma_{Fe})}{\ln(10)} \quad (\pm 0.15)$$

$$\text{with } \varepsilon_S^{Mo} = 2.88 \qquad [56]$$

$$\log K_D^{Mo-Fe}\ (this\ study + lit.) = -1.04 + \frac{4813}{T} - \frac{\ln(\gamma_M)}{\ln(10)} + \frac{\ln(\gamma_{Fe})}{\ln(10)} \quad (\pm 0.26)$$

$$\text{with } \varepsilon_S^{Ni} = 4.65 \qquad [57]$$

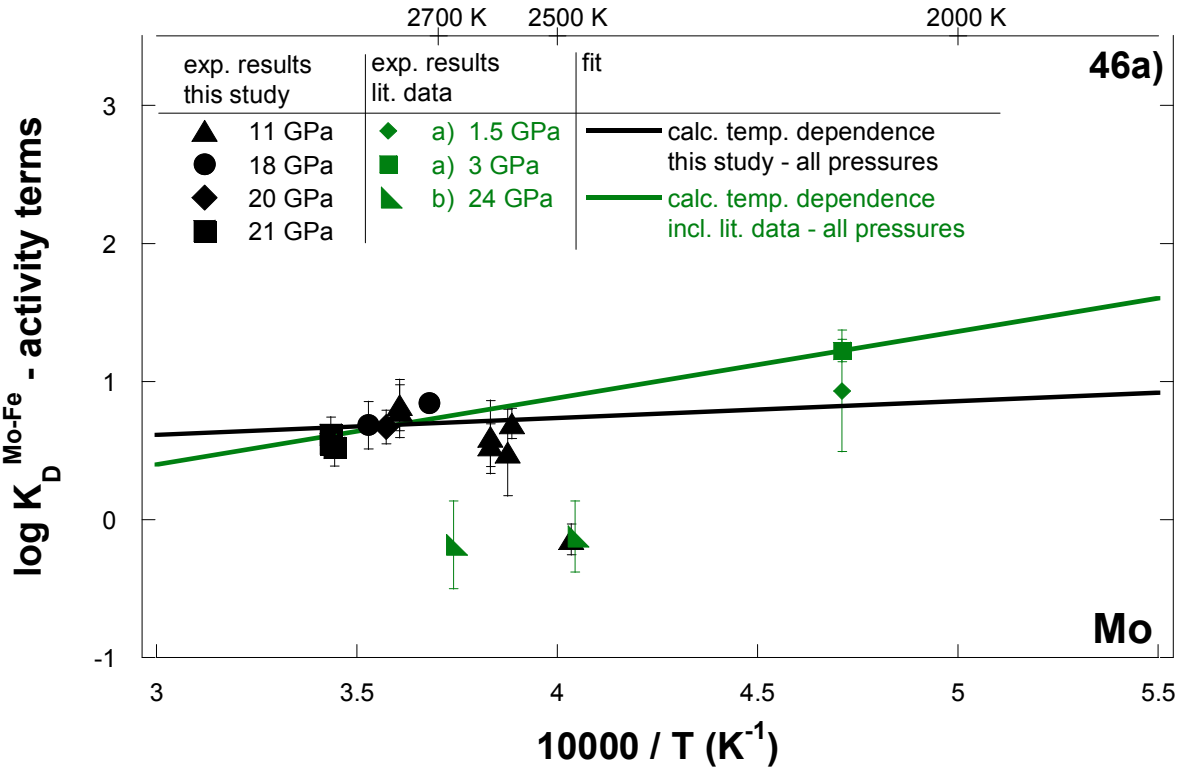
2700 K
2500 K
2000 K
exp. results this study
exp. results lit. data
fit
46a)
11 GPa
18 GPa
20 GPa
21 GPa
a) 1.5 GPa
a) 3 GPa
b) 24 GPa
calc. temp. dependence this study - all pressures
calc. temp. dependence incl. lit. data - all pressures
log K_D Mo-Fe - activity terms
Mo
10000 / T (K^-1)

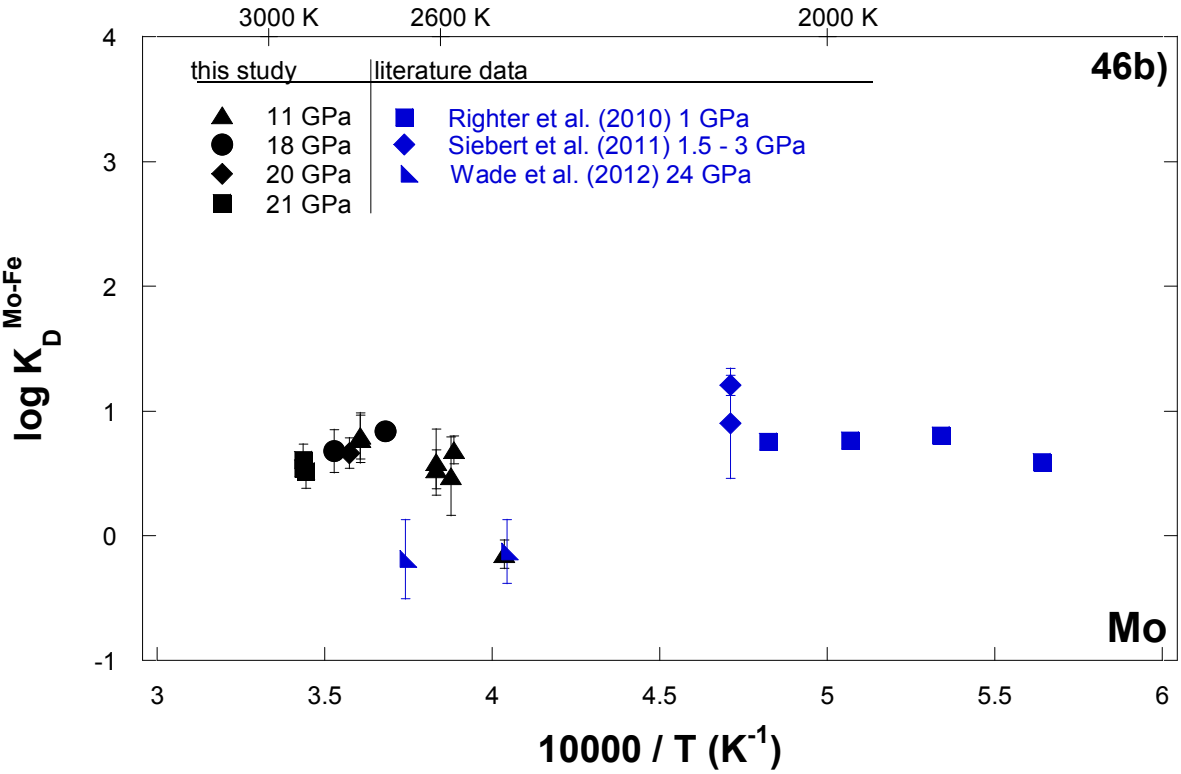
3000 K
2600 K
2000 K
this study
literature data
46b)
11 GPa
18 GPa
20 GPa
21 GPa
Righter et al. (2010) 1 GPa
Siebert et al. (2011) 1.5 - 3 GPa
Wade et al. (2012) 24 GPa
log K_D Mo-Fe
Mo
10000 / T (K^-1)

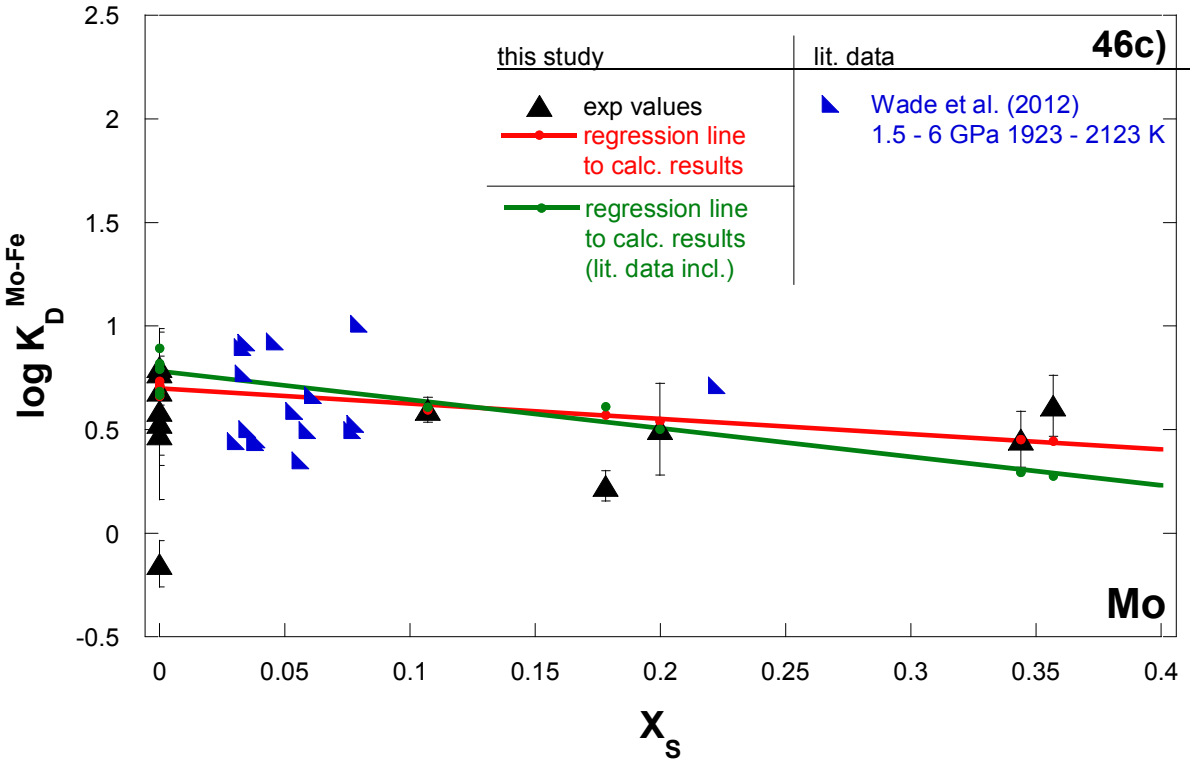

Figure 46a: *Experimentally determined logarithmic exchange coefficients minus the activity terms for Fe and Mo (equation [51]) are plotted against inverse temperature. The solid green and black lines represent the calculated temperature dependence of Mo partitioning with and without literature data being incorporated into the fit respectively. Literature: a) Siebert et al. (2011), b) Wade and Wood (2012).* ***b:*** *Comparison between the results of this study and the recalculated results from literature data sets for Mo. Experimentally obtained logarithmic exchange coefficient values are plotted against inverse temperature.* ***c:*** *The dependence of the metal – silicate partitioning of Mo on the S-content of the metal (mole fractions). The red and green dotted lines represent a linear regression to the recalculated results for a given* ε_S^{Mo} *value of 2.88 or 4.65 with the latter one being the result of the parameterization when literature data according to Table 18 was taken into account to better constrain the pressure and temperature dependence of Mo.*

6.3.3 Hexavalent element tungsten

The liquid metal – liquid silicate partitioning behaviour of W is strongly dependent on temperature with increasing temperatures resulting in higher K_D^{W-Fe} values. This is the case regardless of parameterizing the partitioning behaviour of W on the basis of the experiments of this study alone or incorporating literature data with peridotitic composition into the fit

(compare Table 18). The individual regressions are indistinguishable as can be seen in Figure 47a. No pressure dependence has been observed.

The data are in good agreement with the results published by Righter et al. (2010) and Ballhaus et al. (2013) and one experiment from the study of Cottrell et al. (2009 and 2010) that was conducted in a MgO capsule (Figure 47b).

Within the suite of studied refractory elements W exhibits the strongest dependence on the S content of the metal phase. Within the range of experimentally investigated S concentrations the logarithmic exchange coefficients of W decrease by one logarithmic unit. The data are not in good agreement with the data set of Wade et al. (2012). This might be due to differences in the silicate composition. The parameterization of the S-dependent partitioning behaviour of W is the same whether literature data are included into the fit or not (Figure 47c).

The parameterization of the partitioning behaviour of W with and without additional experiments from the literature is given by equations [58] and [59].

$$\log K_D^{W-Fe} = -0.02 - \frac{3247}{T} - \frac{\ln(\gamma_M)}{\ln(10)} + \frac{\ln(\gamma_{Fe})}{\ln(10)} \quad (\pm 0.15)$$

with ε_S^W = 10.46 [58]

$$\log K_D^{W-Fe} = -0.01 - \frac{3266}{T} - \frac{\ln(\gamma_M)}{\ln(10)} + \frac{\ln(\gamma_{Fe})}{\ln(10)} \quad (\pm 0.2)$$

with ε_S^W = 10.44 [59]

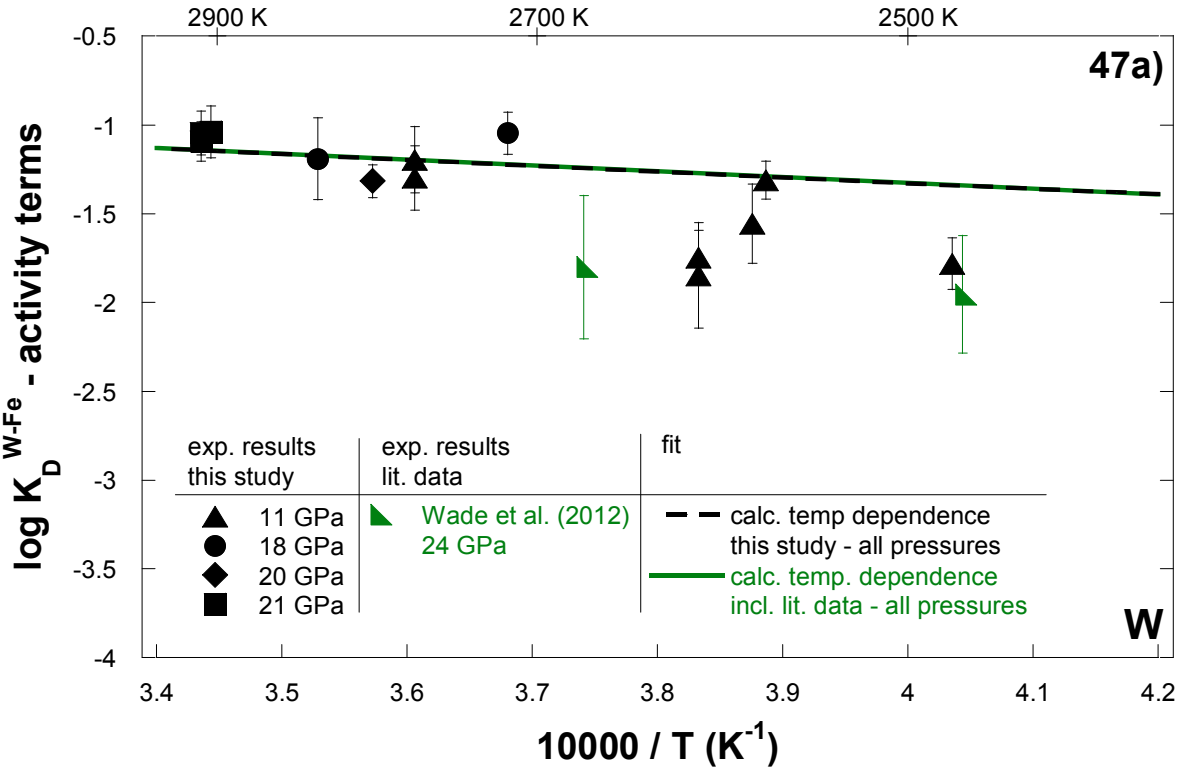
2900 K
2700 K
2500 K
47a)
log K_D^{W-Fe} - activity terms
-0.5
-1
-1.5
-2
-2.5
-3
-3.5
-4
exp. results this study
11 GPa
18 GPa
20 GPa
21 GPa
exp. results lit. data
Wade et al. (2012) 24 GPa
fit
calc. temp dependence this study - all pressures
calc. temp. dependence incl. lit. data - all pressures
W
3.4
3.5
3.6
3.7
3.8
3.9
4
4.1
4.2
10000 / T (K^{-1})

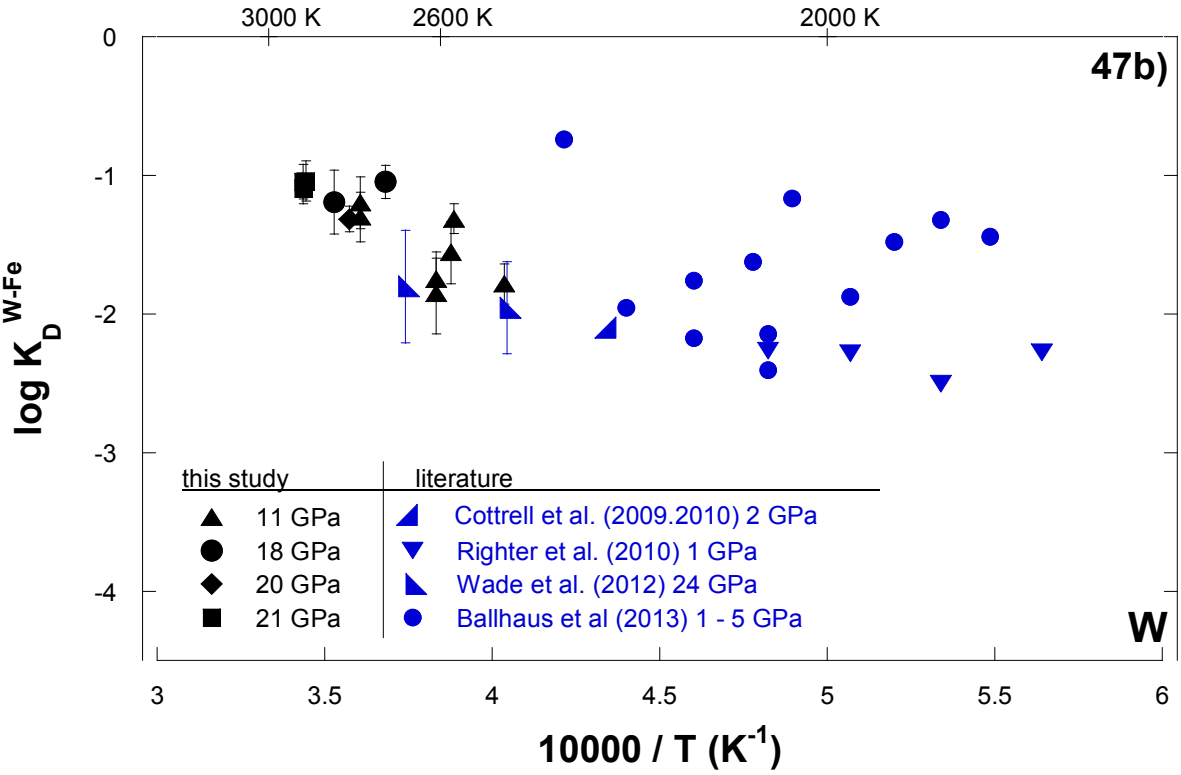
3000 K
2600 K
2000 K
47b)
log K_D^{W-Fe}
0
-1
-2
-3
-4
this study
11 GPa
18 GPa
20 GPa
21 GPa
literature
Cottrell et al. (2009.2010) 2 GPa
Righter et al. (2010) 1 GPa
Wade et al. (2012) 24 GPa
Ballhaus et al (2013) 1 - 5 GPa
W
3
3.5
4
4.5
5
5.5
6
10000 / T (K^{-1})

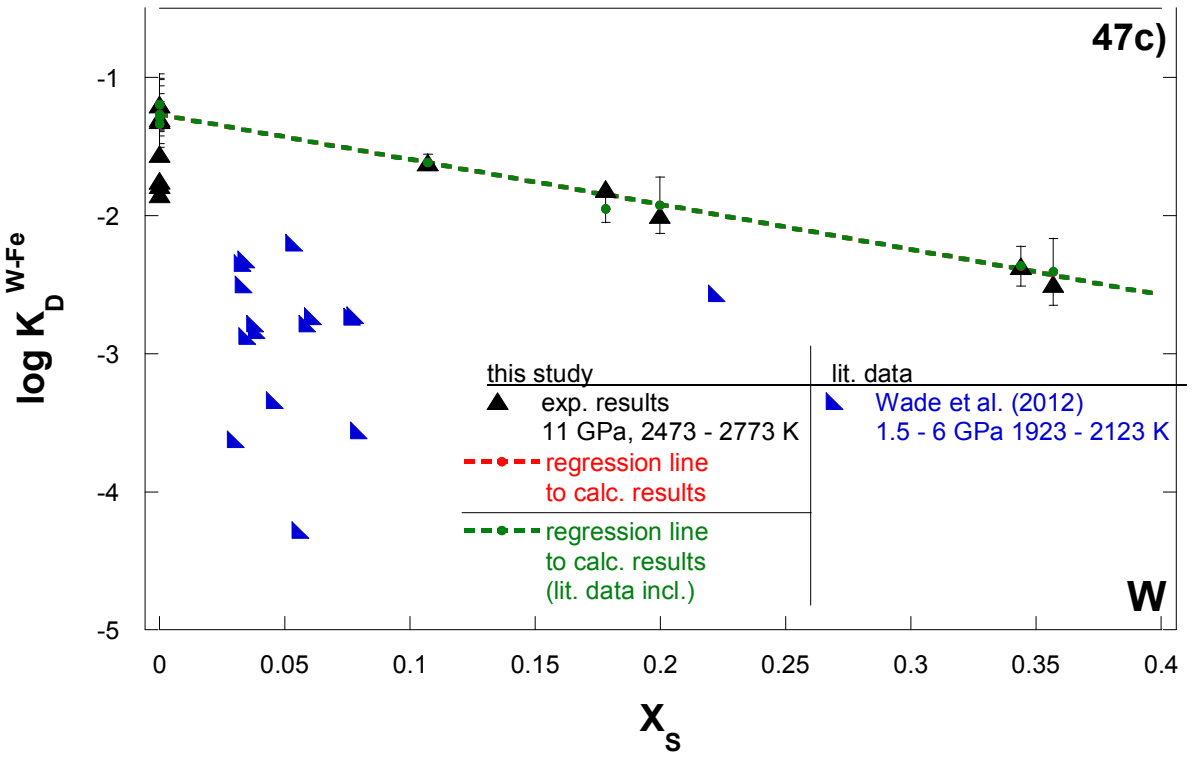

Figure 47a: *Experimentally determined logarithmic exchange coefficients minus the activity terms for Fe and W (equation [51]) are plotted against inverse temperature. The solid green and black lines represent the calculated temperature dependence of W partitioning with and without literature data being incorporated into the fit respectively.* ***b:*** *Comparison between the results of this study and the recalculated results from literature data sets for W. Experimentally obtained logarithmic exchange coefficient values are plotted against inverse temperature.* ***c:*** *The dependence of the metal – silicate partitioning of W on the S-content of the metal (mole fractions). The red and green dotted lines represent a linear regression to the recalculated results for a given* ε_S^W *value of 10.46 or 10.44 with the latter one being the result of the parameterization when literature data according to Table 18 was taken into account to better constrain the pressure and temperature dependence of W.*

6.4 Summary and implications

The liquid metal – liquid silicate partitioning has been studied and parameterized for the elements Ni, Co, Mo and W. The pressure and temperature ranges were 11 – 21 GPa and 2478 – 2773 K respectively.

In general it was found that the partitioning of the studied elements has, at most, a very weak dependence on pressure. With increasing temperatures the logarithmic exchange coefficient values of Ni, Co and Mo decrease, whereas W becomes more siderophile.

Increasing S contents on the metal phase significantly influence the partitioning behaviour of Mo and W by lowering their K_D^{M-Fe} values.

The results have additionally been parameterized including experiments from the literature that were comparable in terms of capsule material (MgO), silicate composition (peridotitic) and that did not exhibit significant amounts of Si or S in the metal phase. In the cases of Co, Mo and W the parameterization of their partitioning behaviours led to very similar results. In the case of Ni however, the parameterization of the influence of temperature changed significantly: when fitting the data of this study alone hardly any temperature dependence has been detected, whereas the addition of literature data clearly shows that increasing temperature lowers the siderophility of Ni. Unlike previous studies (e.g. Li and Agee, 1996; Kegler et al., 2008; Siebert et al., 2012) the partitioning behaviour of Ni was found to be independent of pressure, but strongly affected by temperature. Moreover an observation of two separate pressure regimes below and above 5 GPa, as proposed by Kegler et al. (2008), has not been identified for Ni and Co. Righter (2011) also proposed that the partitioning of Ni and Co does not differ between the two pressure regimes. The latter author argues that the observations of Kegler et al. (2008) are caused by variable silicate melt composition, which cannot be confirmed by the results of this study, because all experiments that were incorporated into the fit involved a peridotitic silicate composition.

All logarithmic exchange coefficient values have furthermore been compared to other literature data that were obtained at slightly different conditions. It was found that the results of this study are in excellent agreement with the results published by various authors. Minor differences might be the result of varying silicate composition.

Table 20 summarizes the fitted parameters a, b, c and ε_S^M that were derived in this study for each element. For each of the four studied elements a second set of parameterizations that includes literature data (Table 18) are given. By employing equations [48], [49] and [50], exchange coefficients can be derived as a function of pressure, temperature and metal composition. Interaction parameters ε_S^M are listed for a given temperature of 1873 K and thus need to be corrected to the temperature of interest using equation [39], Chapter 5. Additionally the uncertainty on each fit is given that has been calculated employing equation [41], Chapter 5.

Table 20: *Summary of fitted parameters that correspond to equation [48], [49] and [50]. Uncertainties were obtained by employing equation [41], Chapter 5. Additionally the parameterization of the combined results of this study and those mentioned in Table 18 are given.*

Element	a	b	c	ε_S^M	$\pm \log K_D^{M-Fe}$
Ni (this study)	1.05	21	-	0.01	0.10
Ni (this study + lit.)	-1.06	5824	-	-0.05	0.11
Co (this study)	0.11	1501	-	0.58	0.07
Co (this study + lit.)	0.02	2011	-13	2.07	0.10
Mo (this study)	0.24	1228	-	2.88	0.15
Mo (this study + lit.)	-1.04	4813	-	4.65	0.26
W (this study)	-0.02	-3247	-	10.46	0.15
W (this study + lit.)	-0.02	-3266	-	10.44	0.20

The derived interaction parameters between S and the elements of interest are compared to those derived from the mass related e-values in the Steelmaking Data Sourcebook in Table 21. The results for Ni and Co are in very good agreement with the values derived from the Steelmaking Data Sourcebook. In the cases of Mo and W it is consistently found that increasing S-contents of the metal phase lower the siderophility of both elements. However in this study a stronger dependence on the S-content of the metal phase for Mo and W has been observed than predicted by the values given in the Steelmaking Data Sourcebook.

Table 21: *Comparison between interaction parameters for non-volatile elements derived in this work and those given in the Steelmaking Data Sourcebook.*

Interaction Parameter	This study	This study + literature	Steelmaking Data Sourcebook
ε_S^{Ni}	0.01	-0.05	-0.05
ε_S^{Co}	0.58	2.07	0.58
ε_S^{Mo}	2.88	4.65	0.35
ε_S^{W}	10.46	10.44	6.05

The combined parameterization of the partitioning data of this study and literature data as given in Table 20 (this study + lit.) was finally incorporated into a simplified core formation model similar to that discussed in Chapter 5:

As before, the mantle and core abundances of the elements of interest have been adopted from McDounough (2003). The values are given in Table 22 together with the partition coefficient ratios of Ni/Co and Mo/W.

However because Ni, Co, W and Mo are classified as non-volatile it has been tried to model the absolute values of the partition coefficients of these elements in the Earth.

Table 22: *Abundance of Ni, Co, Mo and W in the Earth´s mantle and core adopted from McDonough (2003). Additionally the partition coefficient ratio of Ni/Co and Mo/W is given.*

Element	Mantle abundance (McDonough, 2003)	Core abundance (McDonough, 2003)	Partition coefficient ratio
Ni	1960 ppm	5.2 wt%	Ni/Co
Co	105 ppm	0.25 wt%	1.11
Mo	0.05 ppm	5 ppm	Mo/W
W	0.029 ppm	0.47 ppm	6.17

In a first approach only the influence of pressure and temperature has been modeled. The metal phase contained 85.5 wt% Fe plus the individual amounts of the elements of interest as given in Table 22. The temperature was fixed at the peridotitic liquidus as given by Liebske et al. (2012). As has been proposed by various authors (e.g. Li and Agee, 1996; Kegler et al., 2008) the partition coefficients of Ni and Co were found to converge with increasing pressure, since increasing pressure involves an increase in the peridotitic liquidus temperature. The absolute abundances of Ni and Co can only be matched at enormously high pressures of 126 and 116 GPa respectively (Figure 48).

The evolution of the partition coefficient ratio of Ni and Co with increasing pressure is shown in Figure 49. This in another way shows that high pressures can prevent the fractionation of Ni and Co, as these two elements were found to be depleted to the same amount in the Earth´s mantle relative to CI chondrites (Palme and O´Neill, 2003 and 2014, compare Chapter 1, Figure 4).

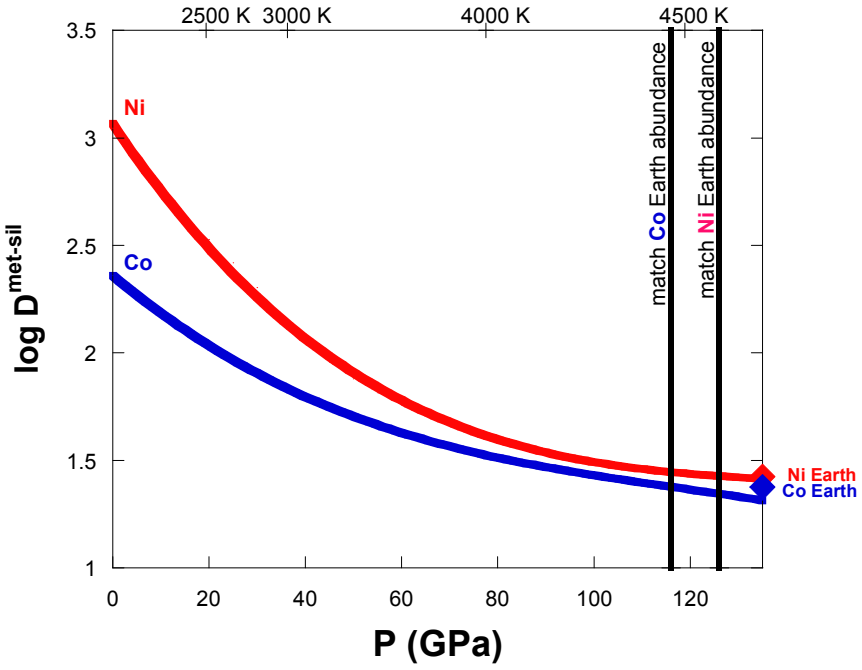

Figure 48: *Logarithmic partition coefficients are plotted against increasing pressure for the elements Ni and Co. The absolute abundances of both elements in the Earth are matched at 116 and 126 GPa for Co and Ni respectively.*

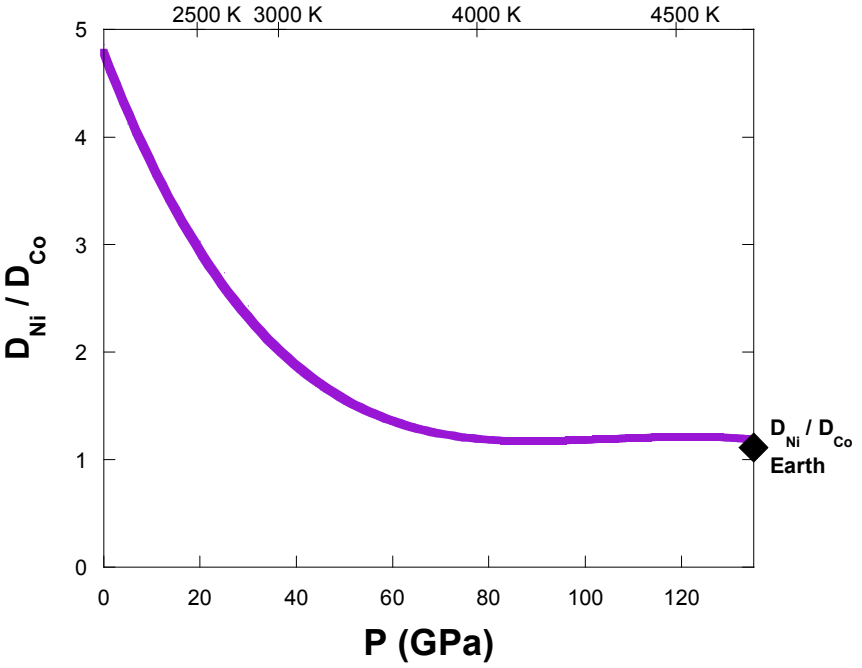

Figure 49: *The partition coefficient ratio of Ni and Co is plotted against increasing pressure. At high pressures the partition coefficient ratio approaches the Earth´s Ni/Co partition coefficient ratio.*

However extrapolated partition coefficients at very high pressures have high uncertainites because of which it cannot be excluded that the absolute abundances of Ni and Co and with it their partition coefficient ratio is matched at lower pressures. As can be seen in Figures 48

and 49 the trend of Ni and Co partitioning converges with the values for the Earth probably around 60 GPa.

In the case of W and Mo no pressure/temperature scenario led to the absolute abundance of both elements in the Earth´s mantle. Pressures above 65 GPa furthermore result in W being more siderophile than Mo, the opposite of which is observed for the Earth (Figure 50). The relative abundances of Mo and W however can be matched at 29 GPa as illustrated in Figure 51, in which the partition coefficient ratio of these elements is plotted against increasing pressure.

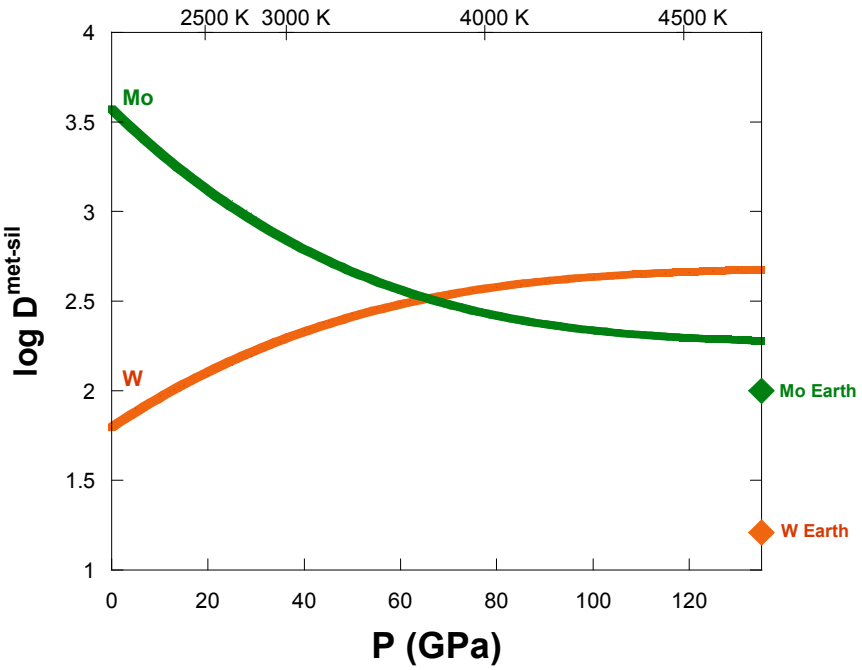

Figure 50: *Logarithmic partition coefficients are plotted against increasing pressure for the elements Mo and W. The absolute abundance of both elements in the Earth cannot be matched.*

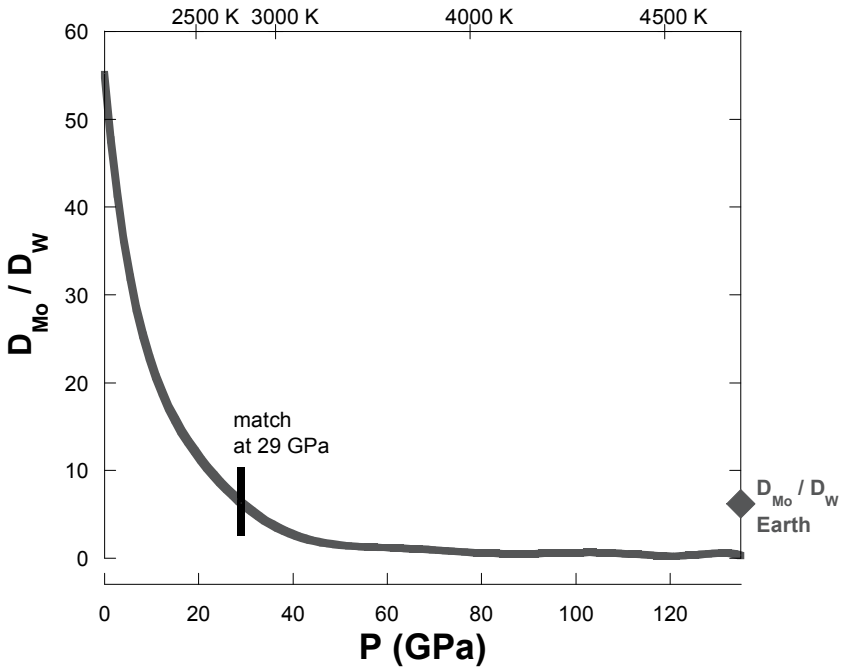

Figure 51: *The partition coefficient ratio of Mo and W is plotted against increasing pressure. At 29 GPa the partition coefficient ratio is consistent with the observation for the Earth.*

In a second step the influence of S on the partitioning behaviour was modeled either for Ni and Co or for Mo and W. Again very high pressures between 95 and 104 GPa together with small amounts of S (up to 0.4 wt%) can explain the Ni and Co abundances in the Earth. (Figure 52).

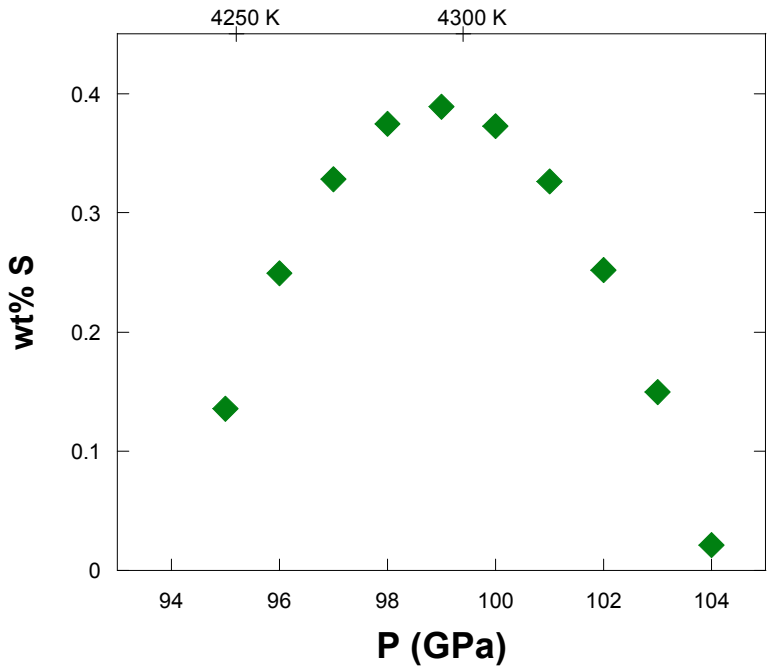

Figure 52: *The concentration of S in the metal phase necessary to match the abundance of the elements Ni and Co in the Earth is plotted against increasing pressure.*

It has been proposed by Wade et al. (2012) that the abundances of W and Mo in the Earth´s mantle can be explained if S is added to the growing Earth during the final 10 to 20 % of accretion. In this study it has been found that W is more strongly affected by the presence of S in the metal phase than Mo. Thus above 65 GPa high amounts of S in the metal phase can reverse the result of W being more siderophile than Mo. However no combination of pressure and S- metal contents with temperature being fixed at the peridotitic liquidus (Liebske et al. (2012) could exactly reproduce the absolute or relative abundances of Mo and W in the Earth.

However, in Figure 53 logarithmic partition coefficients of Mo and W are plotted against increasing S-content of the metal phase at a pressure of 65 GPa. At this point both elements exhibit the same partition coefficients if the metal phase is S-free. Therefore it can be visualized how increasing S-contents effect the partitioning behaviour of both elements to different extents.

One can see that the partition coefficients of Mo and W converge with the corresponding Earth abundances at high S-contents. Similarly the partition coefficient ratio of Mo and W approaches the partition coefficient ratio of these elements in the Earth with increasing S-content as illustrated in Figure 54. Considering that the derived partition coefficients have

high uncertainties these results show that the addition of a S-rich metal phase to the Earth could explain the depletions of Mo and W in the Earth´s mantle as similarly proposed by Wade et al. (2012).

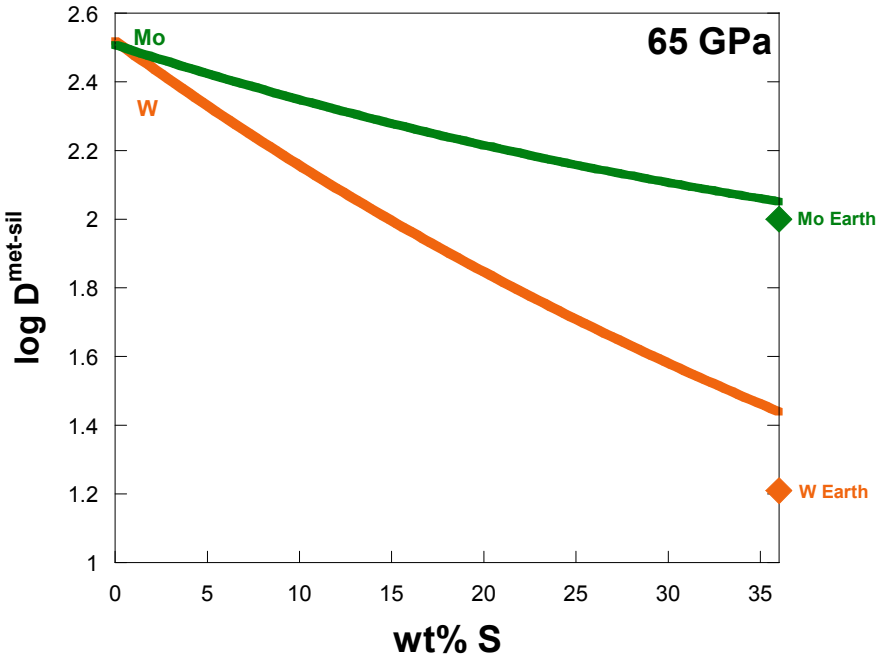

Figure 53: *Logarithmic partition coefficients of Mo and W are plotted against increasing S-contents of the metal phase at a pressure of 65 GPa with temperature being fixed at the peridotitic liquidus (Liebske et al., 2012).*

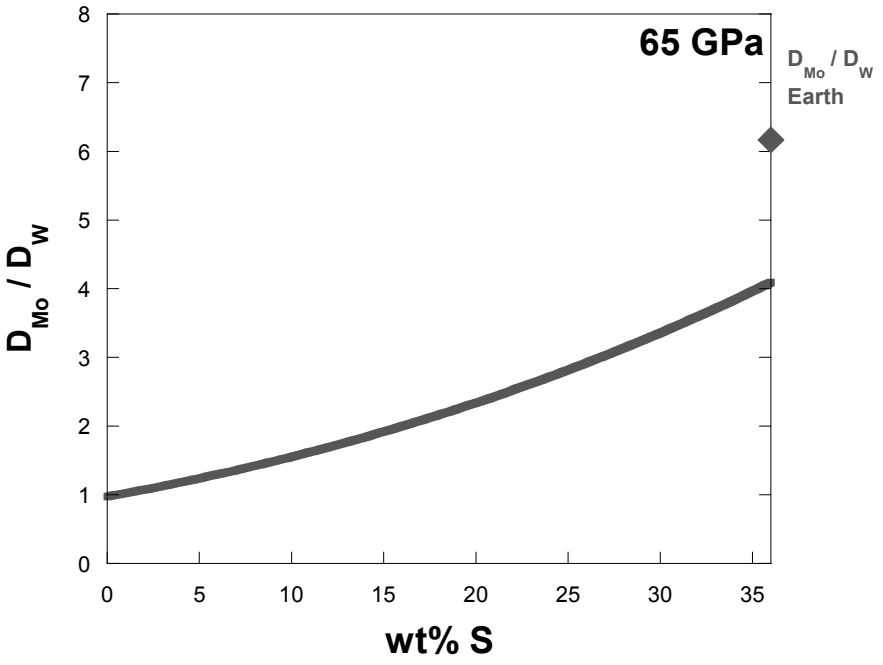

Figure 54: *The partition coefficient ratio of Mo and W are plotted against increasing S-contents of the metal phase at a pressure of 65 GPa with temperature being fixed at the peridotitic liquidus (Liebske et al., 2012).*

In summary it has been shown that high pressures can reproduce the partition coefficient ratio of the non-volatile element pairs Ni-Co and Mo-W, but a unique solution has not been found. The absolute abundances of Ni and Co are matched at extremely high pressures of 126 and 116 GPa respectively. The absolute abundances of Mo and W cannot be reproduced, regardless of modeling the pressure and temperature dependence alone or the additional influence of S on the partitioning behaviour of both elements, but it has been shown that the addition of S can cause the partitioning trends of both elements to converge with the respective core – mantle partition coefficients. Continuous core formation models will have to be employed to provide further constraints on the conditions that prevailed during core formation in the Earth. Additionally the influence of other light elements dissolved in the metal phase (e.g. O) or the influence of variable silicate composition have to be considered.

7. Summary and outlook

The liquid metal – liquid silicate partitioning behaviour of the non-volatile elements Ni, Co, Mo and W and the volatile elements Cu, Sn, Sb, Ge, Pb, Ag, Au, P and As has been studied at pressures between 11 and 23 GPa and temperatures between 2342 K to 2911 K. The 50 % condensation temperatures of these elements cover a range from 704 K (Sn) to 1789 K (W) and the depletions of these elements in the Earth´s mantle vary by around two orders of magnitude. This work has been primarily focused on volatile elements, because the literature and with it core formation models lack data of this group of elements. The experiments of this study contained a Fe-rich metal phase and a peridotitic silicate phase. However, the Earth´s core is known to exhibit a density deficit of around 9.3 wt% (McDonough, 2003), which is most likely caused by the presence of light elements such as S, Si and O (e.g. Birch, 1952; Jephcoat and Olson, 1987; Anderson and Issak, 2002). In order to investigate the influence of light elements dissolved in the metal phase on the partitioning of siderophile elements the starting metal powder was varied by the addition of different concentrations of S or Si.

A total of 104 successful experiments have been performed employing the multi-anvil apparatus. In the resulting samples the initially layered metal powder formed a spherical metal phase that is surrounded by quenched silicate matrix. Due to the use of MgO capsules ferropericlase has formed at the rim of the capsules and occasionally around the metal sphere. The composition of the ferropericlase phases has been used to calculate oxygen fugacity relative to the iron-wüstite buffer as described by Mann et al. (2009).

All metal and ferropericlase phases have been analysed with the electron probe micro-analyser, whereas the abundances of both major and trace elements in the silicate phase have been detected by employing the laser ablation inductively coupled plasma mass spectrometer. The results have been used to calculate partition and exchange coefficient values and finally the liquid metal – liquid silicate partitioning behaviour has been parameterized employing the ε-approach as formulated by Ma et al. (2001).

In a first step the influence of Si on the partitioning behaviour of volatile elements has been quantified in terms of interaction parameters ε_{Si}^{M}. It was found that the addition of Si to the metal phase of the partitioning experiments resulted in decreased siderophility for all elements studied. Since the addition of Si is accompanied by a decrease in oxygen fugacity this implies that for each element studied the interaction of Si with these counteracts the effect of low fO_2 which normally results in increased siderophile behaviour. This shows that reducing

conditions in the early stages of core formation do not necessarily result in complete or even strong depletion of siderophile elements when Si is present as a light element in the metal phase.

By parameterizing the effect of Si on the partitioning of volatile elements it was furthermore possible to derive the valence states of the elements of interest in the silicate phase. These are crucial to know if partitioning is expressed in form of exchange coefficient values and especially if partitioning data are used to extrapolate to higher pressure and temperature. Table 23 summarizes the derived valence states for the volatile elements studied in this work. In the case of P an unlikely valence of +6 was observed. More experiments are necessary to better parameterize the influence of Si on its partitioning behaviour. During the further procedure of this study P was treated as a 5+ cation as suggested by Siebert et al. (2011).

Table 23: *Valence state of volatile elements in the silicate phase derived in this study.*

Element	Cu	Ag	Au	Pb	Sn	Ge	Sb	As	(P)
Valence State	1+	1+	2+	2+	3+	3+	4+	5+	(6+)

Secondly the partitioning of all volatile elements has been investigated and quantified with regards to changes in pressure, temperature and Si- and S-metal contents. The interaction parameters ε_{Si}^{M} were refined by the addition of several more experiments. Additionally interaction parameters that describe the influence between S and the elements of interest have been investigated.

Lastly the effects of pressure, temperature and S-contents of the metal have been studied for the non-volatile elements Ni, Co, Mo and W. Again the interaction of S dissolved in the metal phase with the elements of interest was described in form of interaction parameter values. Table 24 provides the results of the parameterization of the metal – silicate partitioning behaviour of all elements. Interaction parameters refer to a temperature of 1873 K. The constants *a, b* and *c* are related to the entropy, enthalpy and volume change of a chemical reaction that involves the native element of interest plus FeO in exchange with pure Fe and an oxide of the element of interest. These constants can be used to calculate logarithmic exchange coefficient values employing equation [60]:

$$\log K_D^{M-Fe} = a + \frac{b}{T} + \frac{c\,P}{T} - \frac{\ln(\gamma_M)}{\ln(10)} + \frac{\frac{n}{2}\ln(\gamma_{Fe})}{\ln(10)}$$

[60]

In the cases of Ni, Co, Mo and W a further parameterization is provided in which literature data has been taken into account. To ensure comparability the selected literature data was carefully chosen on the basis of the same (peridotitic) silicate and metal composition. Furthermore only samples that have been conducted in MgO capsules have been incorporated into the fit in order to exclude the possibility of contamination of the metal phase by, for example, the dissolution of C from graphite capsules. Finally an uncertainty in the calculated logarithmic exchange coefficient values is given as calculated by equation [41].

Table 24: *Summary of the parameterization of the liquid metal - liquid silicate partitioning behaviour of volatile and non-volatile elements as derived in Chapters 5 and 6 respectively.*

Element	a	b	c	ε_{Si}^{M} (1873 K)	ε_{S}^{M} (1873 K)	Uncertainty on log K_D^{M-Fe}
Volatile						
Ag	2.73	-	-84	6.75	-4.07	0.17
Cu	0.17	3571	-	0.73	-2.58	0.07
Au	0.19	6521	-	23.06	0.49	0.23
Pb	0.22	5149	-	10.59	-0.60	0.10
Sn	0.18	753	63	17.79	6.34	0.09
Ge	1.24	-	-	16.76	13.04	0.24
Sb	1.35	-	-	28.51	12.95	0.45
As	0.21	-	178	43.47	2.64	0.52
P	-0.06	-5036	-	26.82	15.77	0.47
Non-volatile						
Ni (this study)	1.05	21	-	-	0.01	0.10
Ni (this study + lit.)	-1.06	5824	-	-	-0.05	0.11
Co (this study)	0.11	1501	-	-	0.58	0.07
Co (this study + lit.)	0.02	2011	-13	-	2.07	0.10
Mo (this study)	0.24	1228	-	-	2.88	0.15
Mo (this study + lit.)	-1.04	4813	-	-	4.65	0.26
W (this study)	-0.02	-3247	-	-	10.46	0.15
W (this study + lit.)	-0.02	-3266	-	-	10.44	0.20

Finally the parameterization of the liquid metal – liquid silicate partitioning behaviour has been used to derive constraints on the conditions that prevailed during core formation. The partitioning of non-volatile and volatile elements has been modeled with the aim of explaining the absolute or relative abundances in the Earth´s mantle. In the case of volatile

elements the partitioning of pairs of elements with similar 50% condensation temperatures as given by Lodders (2003) has been modeled in order to be able to neglect assumptions about the extent of volatility that these elements might have experienced. Therefore the ratio of the silicate mantle abundances has been employed as constraining parameter in the models. For both groups of elements, volatiles and non-volatiles, their abundances in the Earth´s core and mantle have been adopted from McDonough (2003). Oxygen fugacity was fixed by the present day FeO content of the Earth´s mantle as given by the latter study and the temperature was connected to the particular pressure as its corresponding liquidus temperature (Liebske et al., 2012).

It was found that increasing pressure facilitates the achievement of the correct relative abundances of Mo/W (29 GPa), Cu/Au (12 GPa), Cu/As (5 GPa) and Sn/Pb (21 GPa). It has to be considered that the derived partition coefficients have high uncertainties, because of which the individual partition coefficient ratios can possibly be explained by a range of pressures.

In the case of Ni and Co it was possible to explain their absolute abundances in the Earth by very high pressures of 126 and 116 GPa respectively. However a unique solution that simultaneously explains the abundances of all elements in the Earth has not been found. In the cases of Ag/Sb and Cu/As (> 5 GPa) increasing pressures even resulted in the opposite and fractionated the particular elements from one another.

Incorporating the influence of S on the partitioning behaviour of the elements of interest extended the pressure range that can explain the relative abundances of Ni/Co, Cu/Au, Cu/As, and Ag/Sb. In particular it has been found that the ratio of the element pairs Cu/Au and Cu/As can be explained at 7 GPa and 4.5 wt% S. The correct ratios of Cu/Au and Ag/Sb can simultaneously be matched at 2 GPa and 9 wt% S and in the case of Cu/As and Ag/Sb pressures of 9 GPa together with 12 wt% S in the metal phase are necessary to explain both ratios at the same time. These results clearly exceed the assumed abundance of around 2 wt% S in the Earth´s core (Dreibus and Palme, 1996), but it is not in conflict with the theory of a late S-rich accretionary component as proposed by O´Neill (1991). At pressures above 65 GPa the addition of S to the metal phase can furthermore prevent W becoming more siderophile than Mo as would be the result of pressure and temperature alone. However the addition of S to the metal phase did not provide an explanation to the relative abundances of Sn/Pb.

As Si is most likely one of the elements that contributes the most to the Earth´s core density deficit (Rubie et al., 2011; Fischer et al., 2012 and 2013) the combined effect of S- and Si-metal contents has been modeled at various pressure and temperature conditions. For each pair of volatile elements (Cu/Au, Cu/As, Ag/Sb and Sn/Pb) a combination of S and Si prevents their fractionation from one another at various pressures. In particular it was found that S and Si contents of each less than 1 wt % at pressures between 6 and 9 GPa can explain the relative abundances of Cu, Au and As, three elements with similar 50% condensation temperatures (Lodders, 2003). However still a single set of pressure, temperature, S- and Si-contents that could either be understood as a single stage core formation scenario or the averaged effect in a continuous core formation episode could not be determined.

In summary a single stage core formation event can be excluded by the results of this study. It seems that increasing pressure and with it increasing temperature facilitates the achievement of the relative mantle abundances of various element pairs. Best results have been obtained when the effects of Si- and S- metal contents have been taken into account simultaneously.

In order to better place constraints on the conditions that prevailed during core formation of the Earth the results of this study will have to be incorporated into continuous and heterogeneous core formation models that allow changes in oxygen fugacity, pressure, temperature and material with time. Furthermore it will be necessary to study the effect of other light elements, such as O, and different silicate compositions on the partitioning of siderophile elements.

With regards to this study the valence state of P needs to be clarified by several more experiments. Furthermore the partitioning behaviour of As, Ge and Sb should be studied in more detail in order to settle whether or not these elements are affected by changes in pressure and temperature.

8. References

Abe Y (1997) Thermal and chemical evolution of the terrestrial magma ocean. *Physics of the Earth and Planetary Interiors* **100**: 27–39.

Albaréde F (2009) Volatile accretion history of the terrestrial planets and dynamic implications. *Nature* **461**: 1227 – 1233.

Alfe A, Gillan MJ and Price GD (2002) Composition and temperature of the Earth's core constrained by combining ab initio calculations and seismic data. *Earth and Planetary Science Letters* **195**: 91 – 98.

Allégre CJ, Poirier J-P, Humler E and Hofmann AW (1995) The chemical composition of the Earth. *Earth and Planetary Science Letters* **134**: 515 – 526.

Amelin Y, Krot AN, Hutcheon ID and Ulyanov AA (2002) Lead isotopic ages of chondrules and calcium-aluminum–rich inclusions. *Science* **297**: 1678 – 1683.

Anderson OL and Isaak DG (2002) Another look at the core density deficit of Earth's outer core. *Physics of the Earth and Planetary Interiors* **131**: 19 – 27.

Asahara Y, Frost DJ and Rubie DC (2007) Partitioning of FeO between magnesiowüstite and liquid iron at high pressures and temperatures: Implications for the composition of the Earth's outer core. *Earth and Planetary Science Letters* **257**: 435 – 449.

Badro J, Fiquet G, Guyot F, Gregoryanz E, Occelli F, Antonangeli D, d'Astuto M (2007) Effect of light elements on the sound velocities in solid iron: Implications for the composition of Earth's core. *Earth and Planetary Science Letters* **254**: 233 – 238.

Baker J, Bizzarro M, Wittig N, Connelly J and Haack H (2005) Early planetesimal melting from an age of 4.5662 Gyr for differentiated meteorites. *Nature* **436**: 1127 – 1131.

Ballhaus C, Laurenz V, Münker CM, Fonseca ROC, Rohrbach FA, Lagos M, Schmidt MW, Jochum K-P, Stoll B, Weis U and Helmy HM (2013) The U/Pb ratio of the Earth's mantle - A signature of late volatile addition. *Earth and Planetary Science Letters* **362**: 237 – 245.

Benz W and Cameron AGW (1990) Terrestrial effects of the giant impact. In: Newsom HE and Jones JH (eds.) *Origin of the Earth*: 61 – 67, Oxford University Press.

Birch F (1952) Elasticity and constitution of the Earth's interior. *Journal of Geophysical Research* **69**: 227–286.

Borisov A and Palme H (1996) Experimental determination of the solubility of Au in silicate melts. *Mineralogy and Petrology* **56**: 297 – 312.

Botcharnikov RE, Linnen RL, Wilke M, Holtz F, Jugo PJ and Berndt J (2011) High gold concentrations in sulphide-bearing magma under oxidizing conditions. *Nature* **4**: 112 – 115.

Bottke WF, Walker RJ, Day AMD, Nesvorny D and Elkins-Tanton L (2010) Stochastic late accretion to Earth, the Moon, and Mars. *Science* **330**: 1527 – 1530.

Bouhifd MA, Andrault D, Bolfan-Casanova N, Hammouda T and Devidal JL (2013) Metal–silicate partitioning of Pb and U: Effects of metal composition and oxygen fugacity. *Geochimica et Cosmochimica Acta* **114**: 13 – 28.

Boujibar A, Andrault D, Ali Bouhifd M, Bolfan-Casanova N, Devidal J-L and Trcera N (2014) Metal silicate partitioning of sulphur, new experimental and thermodynamic constraints on planetary accretion. *Earth and Planetary Science Letters* **391**: 42 – 54.

Brandon AD and Walker RJ (2005) The debate over core–mantle interaction. *Earth and Planetary Science Letters* **232**: 211–225.

Brenan JM and McDonough WF (2009) Core formation and metal–silicate fractionation of osmium and iridium from gold. *Nature Geoscience* **2**: 798 – 891.

Brown GC and Mussett AE (1981) *The inaccessible Earth*: 235p., George Allen & Unwin.

Buffett BA and Seagle CT (2010) Stratifiation of the top of the core due to chemical interactions with the mantle. *Journal of Geophysical Research* **115**, B04407.

Buono AS, Dasgupta R, Lee C-TA and Walker D (2013) Siderophile element partitioning between cohenite and liquid in the Fe–Ni–S–C system and implications for geochemistry of planetary cores and mantles. *Geochimica et Cosmochimica Acta* **120**: 239 – 250.

Cameron AGW (2000) High-resolution simulations of the giant impact. In: Canup RM and Righter K (eds.) *Origin of the Earth and Moon*: 133 – 144, The University of Arizona Press.

Canup RM (2012) Forming a Moon with an Earth-like composition via a giant impact. *Science* **338**: 1052 – 1055.

Canup RM and Asphaug E (2001) Origin of the Moon in a giant impact near the end of the Earth's formation. *Nature* **412**: 708 – 712.

Capobianco CJ, DeAro JA, Drake MJ and Hillgren VJ (1994) Siderophile trace elements in silicate melts: Significance and status of unusual oxidation states. *25th Lunar and Planetary Science Conference*: 221 – 222.

Capobianco CJ, Drake MJ and De´Aro J (1999) Siderophile geochemistry of Ga, Ge, and Sn: Cationic oxidation states in silicate melts and the effect of composition in iron–nickel alloys. *Geochimica et Cosmochimica Acta* **63**: 2667 – 2677.

Chabot NL and Drake MJ (1999) Potassium solubility in metal: the effects of composition at 15 kbar and 1900ºC on partitioning between iron alloys and silicate melts. *Earth and Planetary Science Letters* **172**: 323 – 335.

Chabot NL, Draper DS and Agee CB (2005) Conditions of core formation in the Earth: Constraints from Nickel and Cobalt partitioning. *Geochimica et Cosmochimica Acta* **69**: 2141 – 2151.

Chambers JE (2004) Planetary accretion in the inner Solar System. *Earth and Planetary Science Letters* **223**: 241 – 252.

Chou CL (1978) Fractionation of siderophile elements in the Earth´s upper mantle. *Proceedings Lunar and Planetary Science Conference* **9**: 219 – 230.

Corgne A, Keshav S, Wood BJ, McDonough WF and Yingwei Fei Y (2008) Metal–silicate partitioning and constraints on core composition and oxygen fugacity during Earth accretion. *Geochimica et Cosmochimica Acta* **72**: 574 – 589.

Cottrell E, Walter MJ and Walker D (2009) Metal–silicate partitioning of tungsten at high pressure and temperature: Implications for equilibrium core formation in Earth. *Earth and Planetary Science Letters* **281**: 275 – 287.

Cottrell E, Walter MJ and Walker D (2010) Erratum to "Metal–silicate partitioning of tungsten at high pressure and temperature: Implications for equilibrium core formation in Earth". *Earth and Planetary Science Letters* **289**: 631 – 634.

Ćuk M and Stewart ST (2012) Making the Moon from a fast-spinning Earth: A giant impact followed by resonant despinning. *Science* **338**: 1047 – 1052.

Dahl TW and Stevenson DJ (2010) Turbulent mixing of metal and silicate during planet accretion – And interpretation of the Hf–W chronometer. *Earth and Planetary Science Letters* **295**: 177 – 186.

Danielson LR, Sharp TG and Hervig RL (2005) Implications for core formation of the Earth from high pressure – temperature Au partitioning experiments. *36th Lunar and Planetary Science Conference*: Abstract #1955.

Deguen R, Landeau M and Olson P (2014) Turbulent metal-silicate mixing, fragmentation, and equilibration in magma oceans. *Earth and Planetary Science Letters* **391**: 274 – 287.

Drake MJ and Righter K (2002) Determining the composition of the Earth. *Nature* **416**: 39 – 44.

Dreibus G and Palme H (1996) Cosmochemical constraints on the sulfur content in the Earth's core. *Geochimica et Cosmochimica Acta* **60**: 1125 – 1130.

Faure G (1998) *Principles and applications of geochemistry* (second edition): 600p., Prentice Hall.

Faure G and Mensing TM (2007) *Introduction to planetary science, The geological perspective*: 526p., Springer.

Fegley BJr (2000) Kinetics of gas-Grain Reactions in the Solar Nebula. *Space Science Reviews* **92**: 177 – 200.

Fischer RA, Campbell AJ, Caracas R, Reaman DM, Dera P and Prakapenka VB (2012) Equation of state and phase diagram of Fe–16 Si alloy as a candidate component of Earth's core. *Earth and Planetary Science Letters* **357 – 358**: 268 – 276.

Fischer RA, Campbell AJ, Reaman DM, Miller NA, Heinz DL, Dera P and Prakapenka VB (2013) Phase relations in the Fe–FeSi system at high pressures and temperatures. *Earth and Planetary Science Letters* **373**: 54 – 64.

Frost DJ (2003) Fe^{2+} -Mg partitioning between garnet, magnesiowüstite, and $(Mg,Fe)_2SiO_4$ phases of the transition zone. *American Mineralogist* **88**: 387 – 397.

Frost DJ, Asahara Y, Rubie DC, Miyajima N, Dubrovinsky LS, Holzapfel C, Ohtani E, Miyahara M and Sakai T (2010) Partitioning of oxygen between the Earth's mantle and core. *Journal of Geophysical Research: Solid Earth* **115**: 1 – 14.

Frost DJ, Liebske C, Langenhorst F, McCammon CA, Trønnes RG and Rubie DC (2004) Experimental evidence for the existence of iron-rich metal in the Earth´s lower mantle. *Nature* **428**: 409 – 412.

Frost DJ, Mann U, Asahara Y, Rubie DC (2008) The redox state of the mantle during and just after core formation. *Philosophical Transactions of the Royal Society of London* **A 366**: 4315 – 4337.

Frost DJ, Poe BT, Trønnes RG, Liebske C, Duba A and Rubie DC (2004) A new large-volume multianvil system. *Physics of the Earth and Planetary Interiors* **143–144**: 507 – 514.

Gaetani GA and Grove TL (1997) Partitioning of moderately siderophile elements among olivine, silicate melt, and sulfide melt: Constraints on core formation in the Earth and Mars. *Geochimica et Cosmochimica Acta* **61**: 1829 – 1846.

Geiss J and Rossi AP (2013) On the chronology of lunar origin and evolution, Implications for Earth, Mars and the Solar System as a whole. *The Astronomy and Astrophysics Review* **21**: 1 – 54.

Gessmann CK and Rubie DC (1998) The effect of temperature on the partitioning of nickel, cobalt, manganese, chromium, and vanadium at 9 GPa and constraints on formation of the Earth's core. *Geochimica et Cosmochimica Acta* **62**: 867 – 882.

Gessmann CK and Rubie DC (2000) The origin of the depletions of V, Cr and Mn in the mantles of the Earth and Moon. *Earth and Planetary Science Letters* **184**: 95 – 107.

Gessmann CK, Rubie DC and McCammon CA (1999) Oxygen fugacity dependence of Ni, Co, Mn, Cr, V, and Si partitioning between liquid metal and magnesiowüstite at 9 – 18 GPa and 2200°C. *Geochimica et Cosmochimica Acta* **63**: 1853 – 1863.

Gessmann CK, Wood BJ, Rubie DC and Kilburn MR (2001) Solubility of silicon in liquid metal at high pressure: implications for the composition of the Earth's core. *Earth and Planetary Science Letters* **184**: 367 – 376.

Goldschmidt VM (1937) The principles of distribution of chemical elements in minerals and rocks. *Journal of the Chemical Society*: 655 – 673.

Halliday AN (2004) Mixing, volatile loss and compositional change during impact-driven accretion of the Earth. *Nature* **427**: 505 – 506.

Halliday AN and Chambers JE (2007) The origin of the Solar System. In: McFadden LA, Weissman PR, Johnson TV (eds.) *Encyclopedia of the Solar System (second edition)*: 29 – 52, Elsevier, Academic Press.

Helffrich G and Kaneshima S (2004) Seismological constraints on core composition from Fe-O-S liquid immiscibility. *Science* **306**: 2239 – 2242.

Hillgren VJ, Gessmann CK and Li J (2000) An experimental perspective on the light element in Earth´s core. In: Canup RM and Righter K (eds.) *Origin of the Earth and Moon*: 245–264, The University of Arizona Press.

Holzheid A, Kegler Ph, Frost D, Rubie DC and Palme H (2007) Partitioning behaviour of copper and germanium: Implications for terrestrial core formation scenarios. *38th Lunar and Planetary Science Conference*: Abstract #2090.

Holzheid A, Sylvester P, O´Neill HStC, Rubie DC and Palme H (2000) Evidence for a late chondritic veneer in the Earth's mantle from high-pressure partitioning of palladium and platinum. *Nature* **406**: 396 – 399.

Humayun M and Cassen P (2000) Processes determining the volatile abundances of the meteorites and terrestrial planets. In: Canup RM and Righter K (eds.) *Origin of the Earth and Moon*: 3 – 23, The University of Arizona Press.

Ito W, Takahashi E and Matsui Y (1984) The mineralogy and chemistry of the lower mantle: an implication of the ultrahigh-pressure phase relations in the system MgO-FeO-SiO_2. *Earth and Planetary Science Letters* **67**: 238 – 248.

Jacobsen SB (2005) The Hf-W isotopic system and the origin of the Earth and the Moon. *Annual Review of Earth and Planetary Sciences* **33**: 531 – 570.

Jagoutz E, Palme H, Baddenhausen H, Blum K, Cendales M, Dreibus G, Spettel B, Lorenz V and Wänke H (1979) The abundances of major, minor and trace elements in the Earth´s mantle as derived from primitive ultramafic nodules. *Proceedings Lunar and Planetary Science Conference* **10**: 2031 – 2050.

Jana D and Walker D (1997) The influence of sulfur on partitioning of siderophile elements. *Geochimica et Cosmoehimica Acta* **61**: 5255 – 5277.

Javoy M (1997) The major volatile elements of the Earth: Their origin, behavior, and fate. *Geophysical Research Letters* **24**: 177 – 180.

Jephcoat A and Olson P (1987) Is the inner core of the Earth pure Iron? *Nature* **325**: 332 – 335.

Jones JH and Drake MJ (1986) Geochemical constraints on core formation in the Earth. *Nature* **322**: 221–228.

Karato S and Murthy VR (1997) Core formation and chemical equilibrium in the Earth - Physical considerations. *Physics of the Earth and Planetary Interiors* **100**: 61-79.

Kawai N and Endo S (1970) The generation of ultrahigh hydrostatic pressures by a split sphere apparatus. *The Review of Scientific Instruments* **41**: 1178 – 1181.

Kawai N, Togaya M and Onodera A (1973) New device for pressure-vessels. *Proceedings of the Japan Academy* **8**: 623–626.

Kegler Ph and Holzheid A (2011) Determination of the formal Ge-oxide species in silicate melts at oxygen fugacities applicable to terrestrial core formation scenarios. *European Journal of Mineralogy* **23**: 369 – 378.

Kegler Ph, Holzheid A, Frost DJ, Rubie DC, Dohmen R and Palme H (2008) New Ni and Co metal-silicate partitioning data and their relevance for an early terrestrial magma ocean. *Earth and Planetary Science Letters* **268**: 28 – 40.

Kegler Ph, Holzheid A, McCammon A, Rubie DC, Palme H (2009) Pressure and temperature dependent partitioning of copper: Implications for terrestrial core formation. *40th Lunar and Planetary Science Conference*: Abstract #1685.

Keil K, Stöffler D, Love SG and Scott ERD (1997) Constraints on the role of impact heating and melting in asteroids. *Meteoritics & Planetary Science* **32**: 349 – 363.

Keppler H and Frost DJ (2005) Introduction to minerals under extreme conditions. In: Miletich R (ed.) *European Mineralogical Union Lecture Notes in Mineralogy* **7** *Mineral Behaviour at Extreme Conditions*: 1 – 30.

Kilburn MR and Wood BJ (1997) Metal – silicate partitioning and the incompatibility of S and Si during core formation. *Earth and Planetary Science Letters* **152**: 139 – 148.

Kimura K, Lewis RS and Anders E (1974) Distribution of gold and rhenium between nickel iron and silicate melts: Implications for the abundance of siderophile elements on the Earth and Moon. *Geochimica et Cosmochimica Acta* **38**: 683 – 701.

Kiseeva ES and Wood BJ (2013) A simple model for chalcophile element partitioning between sulphide and silicate liquids with geochemical applications. *Earth and Planetary Science Letters* **383**: 68 – 81.

Kleine T, Palme H, Mezger K and Halliday AN (2005) Hf-W Chronometry of Lunar Metals and the Age and Early Differentiation of the Moon. *Science* **310**: 1671 – 1674.

Kleine T, Touboul M, Bourdon B, Nimmo F, Mezger K, Palme H, Jacobsen SB, Qing-Zhu Yin Q-Z and Halliday AN (2009) Hf–W chronology of the accretion and early evolution of asteroids and terrestrial planets. *Geochimica et Cosmochimica Acta* **73:** 5150 – 5188.

Lagos M, Ballhaus C Wohlgemuth–Ueberwasser C, Münker C, Berndt J and Kuzmin DV (2008) The Earth's missing lead may not be in the core. *Nature* **456**: 89 – 92.

Li J and Agee CB (1996) Geochemistry of mantle–core differentiation at high pressure. *Nature* **381**: 686 – 689.

Li J and Agee CB (2001) The effect of pressure, temperature, oxygen fugacity and composition on partitioning of nickel and cobalt between liquid Fe-Ni-S alloy and liquid silicate: Implications for the Earth's core formation. *Geochimica et Cosmochimica Acta* **65**: 1821 – 1832.

Li J and Fei Y (2003) Experimental constraints on core composition. In: Holland HD and Turekian KK (eds.) *Treatise on Geochemistry* **2**: *The Mantle and Core*: 521–546, Elsevier-Pergamon.

Liebske C and Frost DJ (2012) Melting phase relations in the MgO-$MgSiO_3$ system between 16 and 26 GPa: Implications for melting in Earth´s deep interior. *Earth and Planetary Science Letters* **345 – 348**: 159 – 170.

Lodders K (2003) Solar System aboundances and condensation temperatures of the elements. *The Astrophysical Journal* **591**: 1220 – 1247.

Longerich H, Jackson SE and Gunther D (1996) Laser ablation inductively coupled plasma mass spectrometric transient signal data acquisition and analyte concentration calculation analytical atomic spectrometry. *Journal of Analytical Atomic Spectrometry* **11**: 899 – 904.

Ma Z (2001) Thermodynamic Description for Concentrated Metallic Solutions Using Interaction Parameters. *Metallurgical and Materials Transactions* **B 32**: 87-103.

Mann U, Frost DJ and Rubie DC (2009) Evidence for high-pressure core-mantle differentiation from the metal–silicate partitioning of lithophile and weakly-siderophile elements. *Geochimica et Cosmochimica Acta* **73**: 7360 – 7386.

Mann U, Frost DJ, Rubie DC, Becker H and Audétat A (2012) Partitioning of Ru, Rh, Pd, Re, Ir and Pt between liquid metal and silicate at high pressures and high temperatures - Implications for the origin of highly siderophile element concentrations in the Earth's mantle. *Geochimica et Cosmochimica Acta* **84**: 593 – 613.

McDonough WF (2003) Compositional model for the Earth´s core. In: Holland HD and Turekian KK (eds.) *Treatise on Geochemistry* **2**: *The Mantle and Core*: 547 - 568, Elsevier-Pergamon.

McDonough WF and Sun S-s (1995) The composition of the Earth. Chemical Geology **120**: 223 – 253.

Melosh HJ (1990) Giant impacts and the thermal state of the early Earth. In: Newsom HE and Jones JH (eds.) *Origin of the Earth*: 69 – 83, Oxford University Press.

Murthy VR (1991) Early differentiation of the Earth and the problem of mantle siderophile elements: a new approach. *Science* **253**: 303 – 306.

Nebel O, Mezger K and van Westrenen W (2011) Rubidium isotopes in primitive chondrites: Constraints on Earth's volatile element depletion and lead isotope evolution. *Earth and Planetary Science Letters* **305**: 309 – 316.

Newsom HE (1990) Accretion and core formation in the Earth: evidence from siderophile elements. In: Newsom HE and Jones JH (eds.) *Origin of the Earth*: 273 – 288, Oxford University Press.

Nimmo F, O´Brian DP and Kleine T (2010) Tungsten isotopic evolution during late-stage accretion: Constraints on Earth–Moon equilibration. *Earth and Planetary Science Letters* **292**: 363 – 370.

Nishihara YU, Matsukage KN and Karato S (2006) Effects of metal protection coils on thermocouple EMF in multi-anvil high-pressure experiments. *American Mineralogist* **91**: 111 – 114.

O´Neill HStC (1991) The origin of the Moon and the early history of the Earth - A chemical model. Part 1: The Moon. *Geochemica et Cosmochimica Acta* **55**: 1135 – 1157.

O´Neill HStC (1991) The origin of the Moon and the early history of the Earth - A chemical model. Part 2: The Earth. *Geochemica et Cosmochimica Acta* **55**: 1159 – 1172.

O´Neill HStC and Eggins SM (2002) The effect of melt composition on trace element partitioning: An experimental investigation of the activity coefficients of FeO, NiO, CoO, MoO_2 and MoO_3 in silicate melts. *Chemical Geology* **186**: 151 – 181.

O´Neill HStC, Canil D and Rubie DC (1998) Oxide-metal equilibria to 2500°C and 25 GPa: Implications for core formation and the light component in the Earth´s core. *Journal of geophysical research: Solid Earth* **103**: 12239 – 12260.

Ohtani E and Ringwood AE (1984) Composition of the core, I. Solubility of oxygen in molten iron at high temperatures. *Earth and Planetary Science Letters* **71**: 85 – 93.

Ohtani E, Ringwood AE and Hibberson W (1984) Composition of the core, II. Effect of high pressure on solubility of FeO in molten iron. *Earth and Planetary Science Letters* **71**: 94 – 103.

Ohtani E, Yurimoto H and Seto S (1997) Element partitioning between metallic liquid, silicate liquid, and lower mantle minerals: implications for core formation of the Earth. *Physics of the Earth and Planetary Interiors* **100**: 97 – 114.

Palme H and O'Neill HSC (2003) Cosmochemical estimates of mantle composition. In: Holland HD and Turekian KK (eds.) *Treatise on Geochemistry* **2**: *The Mantle and Core*: 1 – 38, Elsevier-Pergamon.

Palme H and O'Neill HSC (2014) Cosmochemical estimates of mantle composition. In: Holland HD and Turekian KK (eds.) *Treatise on Geochemistry (second edition)* **3**: *The Mantle and Core*: 1 – 39, Elsevier.

Palme H, Larimer JW and Lipschutz ME (1988) Moderately volatile elements. In: Kerridge JF and Matthews MS (eds.) *Meteorites and the early Solar System*: 436 – 461, The University of Arizona Press.

Peach CL and Mathez EA (1993) Sulfide melt-silicate melt distribution coefficients for nickel and iron and implications for the distribution of other chalcophile elements. *Geochimica et Cosmochimica Acta* **57**: 3013 – 3021.

Poirier J-P (1994) Light elements in the Earth's outer core: A critical review. *Physics of the Earth and Planetary Interiors* **85**: 319 – 337.

Pritchard ME and Stevenson DJ (2000) Thermal aspects of a lunar origin by giant impact. In: Canup RM and Righter K (eds.) *Origin of the Earth and Moon*: 179 – 196, The University of Arizona Press.

Raymond SN, Quinn T and Lunine JI (2004) Making other Earths: dynamical simulations of terrestrial planet formation and water delivery. *Icarus* **168**: 1 – 17.

Raymond SN, Schlichting HE, Hersant F and Selsis F (2013) Dynamical and collisional constraints on a stochastic late veneer on the terrestrial planets. *Icarus* **226**: 671 – 681.

Ricolleau A, Fei Y, Corgne A, Siebert J and Badro J (2011) Oxygen and silicon contents of Earth's core from high pressure metal–silicate partitioning experiments. *Earth and Planetary Science Letters* **310**: 409 – 421.

Righter K (2011) Prediction of metal–silicate partition coefficients for siderophile elements: An update and assessment of PT conditions for metal–silicate equilibrium during accretion of the Earth. *Earth and Planetary Science Letters* **304**: 158 – 167.

Righter K and Drake MJ (2003) Partition coefficients at high pressure and temperature. In: Holland HD and Turekian KK (eds.) *Treatise on Geochemistry* **2**: *The Mantle and the Core*: 425 – 449, Elsevier-Pergamon.

Righter K, Drake MJ and Yaxley G (1997) Prediction of siderophile element metal-silicate partition coefficients to 20 GPa and 2800°C: The effects of pressure, temperature, oxygen fugacity, and silicate and metallic melt compositions. *Physics of the Earth and Planetary Interiors* **100**: 115–134.

Righter K, Humayun M and Campbell AJ (2009) Experimental studies of metal–silicate partitioning of Sb: Implications for the terrestrial and lunar mantles. *Geochimica et Cosmochimica Acta* **73**: 1487 – 1504.

Righter K, King C, Danielson L, Pando KM and Lee CT (2011) Experimental determination of the metal/silicate partition coefficient of Germanium: Implications for core and mantle differentiation. *Earth and Planetary Science Letters* **304**: 379 – 388.

Righter K, Pando KM, Danielson L and Lee C-T (2010) Partitioning of Mo, P and other siderophile elements (Cu, Ga, Sn, Ni, Co, Cr, Mn, V, and W) between metal and silicate melt as a function of temperature and silicate melt composition. *Earth and Planetary Science Letters* **291**: 1 – 9.

Righter K. (2005) Highly siderophile elements: constraints on Earth accretion and early differentiation. In: van der Hilst RD, Bass JD, Matas J and Trampert J (eds.) *Earth's deep mantle: Structure, composition and evolution*, *Geophysical Monograph Series* **160**: 201 - 218 American Geophysical Union.

Ringwood AE (1966) Chemical evolution of the terrestrial planets. *Geochimica et Cosmochimica Acta* **30**: 41 – 104.

Ringwood AE (1977) Composition of the core and implications for origin of the Earth. *Geochemical Journal* **11**: 111 – 135.

Rubie DC, Frost DJ, Mann U, Asahara Y, Nimmo F, Tsuno K , Kegler Ph, Holzheid A and Palme H (2011) Heterogeneous accretion, composition and core–mantle differentiation of the Earth. *Earth and Planetary Science Letters* **301**: 31 – 42.

Rubie DC, Gessmann CK and Frost DJ (2004) Partitioning of oxygen during core formation on the Earth and Mars. *Nature* **429**: 58 – 61.

Rubie DC, Melosh HJ, Reid JE, Liebske C and Righter K (2003) Mechanisms of metal-silicate equilibration in the terrestrial magma ocean. *Earth and Planetary Science Letters* **205**: 239 – 255.

Rubie DC (1999) Characterising the sample environment in multianvil high-pressure experiments. *Phase Transitions* **68**: 431 – 451.

Rubie DC, Frost DJ, Nimmo F, O´Brian DP, Mann U and Palme H (2010) Accretion of volatile elements to the Earth and Moon. *41st Lunar and Planetary Science Conference*: Abstract #1134.

Rubie DC, Nimmo F, and Melosh HJ (2007) Formation of Earth´s core. In: Stevenson D and Schubert G (eds.) *Treatise on Geophysics* **9**: *Evolution of the Earth*: 51 – 90, Elsevier.

Rubie DC, Nimmo F, and Melosh HJ (2015) Formation of Earth´s core. In: Stevenson D and Schubert G (eds.) *Treatise on Geophysics (second edition)* **9**: *Evolution of the Earth*, Elsevier. (in press)

Rubin AM (1995) Propagation of magma-filled cracks. *Annual Review of Earth and Planetary Sciences* **23**: 287 – 336.

Rudge JF, Kleine T and Bourdon B (2010) Broad bounds on Earth's accretion and core formation constrained by geochemical models. *Nature Geoscience* **3**: 439 – 443.

Rushmer T, Minarik WG and Taylor GJ (2000) Physical processes of core formation. In: Canup RM and Righter K (eds.) *Origin of the Earth and Moon*: 227 - 244, The University of Arizona Press.

Sakai T, Kanto T and Ohtani E (2006) Interaction between iron and post-perovskite at core-mantle boundary and core signature in plume source region. *Geophysical Research Letters* **33**: L15317.

Samuel H (2012) A re-evaluation of metal diapir breakup and equilibration in terrestrial magma oceans. *Earth and Planetary Science Letters* **313-314**: 105 – 114.

Schlichting HE, Warren PH and Yin Q-Z (2012) The last stages of terrestrial planet formation: Dynamical friction and the late veneer. *The Astrophysical Journal* **752:8**: 1 – 8.

Schönbächler M, Carlson RW, Horan MF, Mock TD and Hauri EH (2010) Heterogeneous accretion and the moderately volatile element budget of Earth. *Science* **328**: 884 – 887.

Seo JH, Guillong M, Aerts M, Zajacz Z and Heinrich CA (2011) Microanalysis of S, Cl, and Br in fluid inclusions by LA–ICP-MS. *Chemical Geology* **284**: 35 – 44.

Shannon MC and Agee CB (1996) High pressure constraints on percolative core formation. *Geophysical Research Letters* **23**: 2717 – 2720.

Shannon MC and Agee CB (1998) Percolation of core melts at lower mantle conditions. *Science* **280**: 1059 – 1061.

Siebert J, Badro J, Antonangeli D and Ryerson FJ (2012) Metal–silicate partitioning of Ni and Co in a deep magma ocean. *Earth and Planetary Science Letters* **321-322**: 189 –197.

Siebert J, Badro J, Antonangeli D and Ryerson FJ (2013) Terrestrial accretion under oxidizing conditions. *Science* **339**: 1194 – 1197.

Siebert J, Corgne A and Ryerson FJ (2011) Systematics of metal–silicate partitioning for many siderophile elements applied to Earth's core formation. *Geochimica et Cosmochimica Acta* **75**: 1451 – 1489.

Snow JE and Schmidt G (1998) Constraints on Earth accretion deduced from noble metals in the oceanic mantle. *Nature* **391**: 166 – 169.

Solomatov VS (2000) Fluid dynamics of a terrestrial magma ocean. In: Canup RM and Righter K (eds.) *Origin of the Earth and Moon*: 323 – 338, The University of Arizona Press.

Spohn T, Schubert G (1991) Thermal equilibration of the Earth following a giant impact. *Geophysical Journal International* **107**: 163 – 170.

Stevenson DJ (1981) Models of the Earth´s core. *Science* **214**: 611 – 619.

Stevenson DJ (1990) Fluid dynamics of core formation. In: Newsom HE and Jones JH (eds.) *Origin of the Earth*: 231 – 250, Oxford University Press.

Takafuji N, Hirose K, Mitome M and Bando Y (2005) Solubilities of O and Si in liquid iron in equilibrium with $(Mg,Fe)SiO_3$ perovskite and the light elements in the core. *Geophysical Research Letters* **32**: 1 – 4.

Taylor ST (2001) *Solar System evolution, A new perspective (second edition)*: 460p., Cambridge University Press.

Taylor ST and McLennan SM (2009) *Planetary crusts, Their composition, origin and evolution*: 378p., Cambridge University Press.

The Japan Society for the Promotion of Science and The Nineteenth Committee on Steelmaking (1988) Part 2: Recommended values of activity and activity coefficients, and interaction parameters of elements in iron alloys. In: Steelmaking Data Sourcebook: 273 – 297, Gordon and Breach.

Thibault Y and Walter MJ (1995) The influence of pressure and temperature on the metal-silicate partition coefficients of nickel and cobalt in a model Cl chondrite and implications for metal segregation in a deep magma ocean. *Geochimica et Cosmochimica Acta* **59**: 991 – 1002.

Thomas PC, Parker JW, McFadden LA, Russell CT, Stern SA, Sykes MV and Young EF (2005) Differentiation of the asteroid Ceres as revealed by its shape. *Nature* **437**: 224 – 226.

Thommes EW, Duncan MJ and Levison HF (2003) Oligarchic growth of giant planets. *Icarus* **161**: 431 – 455.

Tonks WB and Melosh HJ (1993) Magma ocean formation due to giant impacts. *Journal of Geophysical Research* **98**: 5319–5333.

Tsuno K, Frost DJ and Rubie DC (2013) Simultaneous partitioning of silicon and oxygen into the Earth's core during early Earth differentiation. *Geophysical Research Letters* **40**: 66 – 71.

Tuff J, Wood BJ and Wade J (2011) The effect of Si on metal–silicate partitioning of siderophile elements and implications for the conditions of core formation. *Geochimica et Cosmochimica Acta* **75**: 673 – 690.

Von Bargen N and Waff HS (1986) Permeabilities, interfacial areas and curvatures of partially molten systems: Results of numerical computations of equilibrium microstructures. *Journal of Geophysical Research* **91**: 9261 – 9276.

Wade J and Wood BJ (2005) Core formation and the oxidation state of the Earth. *Earth and Planetary Science Letters* **236**: 78 – 95.

Wade J, Wood BJ and Tuff J (2012) Metal–silicate partitioning of Mo and W at high pressures and temperatures: Evidence for late accretion of sulphur to the Earth. *Geochimica et Cosmochimica Acta* **85**: 58 – 74.

Walker D (2000) Core participation in mantle geochemistry: Geochemical Society Ingerson Lecture. *Geochimica et Cosmochimica Acta* **64**: 2897-2911.

Walker D, Carpenter MA and Hitch CM (1990) Some simplifications to multianvil devices for high pressure experiments. *American Mineralogist* **75**: 1020 – 1028.

Walker D, Norby L, Jones JH (1993) Superheating effects on metal-silicate partitioning of siderophile elements. *Science* **262**: 1858 – 1861.

Walter MJ, Newsom HE, Ertel W, and Holzheid A (2000) Siderophile elements in the Earth and Moon: Metal/silicate partitioning and implications for core formation. In: Canup RM and Righter K (eds.) *Origin of the Earth and Moon*: 365 – 290, The University of Arizona Press.

Waltera MJ and Trønnes R (2004) Early Earth differentiation. *Earth and Planetary Science Letters* **225**: 253 – 269.

Wänke H (1981) Constitution of the terrestrial planets. *Philosophical Transactions of the Royal Society of London* **A 303**: 287–302.

Wasson JT (1985) *Meteorites: Their records of early Solar-System history*, 267p., W.H. Freeman & Co Ltd.

Weidenschilling SJ (2000) Formation of planetesimals and accretion of the terrestrial planets. *Space Science Reviews* **92**: 295 – 310.

Weissman PR (2007) The Solar System and its place in the galaxy. In: McFadden LA, Weissman PR, Johnson TV (eds) *Encyclopedia of the Solar System (second edition)*: 1 – 28, Elsevier, Academic Press.

Wetherill GW (1989) The formation of the Solar System: Consensus, alternatives, and missing factors. In: Weaver HA and Danly L (eds.) *The formation and evolution of planetary systems*: 1 – 30, Cambridge University Press.

Wheeler KT, Walker D and McDonough W (2011) Pd and Ag metal-silicate partitioning applied to Earth differentiation and core-mantle exchange. *Meteoritics & Planetary Science* **46**: 199 – 217.

Wood BJ and Halliday AN (2010) The lead isotopic age of the Earth can be explained by core formation alone. *Nature* **465**: 767 – 771.

Wood BJ, Nielsen SG, Rehkämper M and Halliday AN (2008) The effects of core formation on the Pb- and Tl- isotopic composition of the silicate Earth. *Earth and Planetary Science Letters* **269**: 326 – 336.

Wood BJ, Wade J and Kilburn MR (2009) Core formation and the oxidation state of the Earth: Additional constraints from Nb, V and Cr partitioning. *Geochimica et Cosmochimica Acta* **72**: 1415 – 1426.

Wood BJ, Walter MJ and Wade J (2006) Accretion of the Earth and segregation of its core. *Nature* **441**: 825 – 833.

Yoshino T, Walter MJ and Katsury T (2003) Core formation in planetesimals triggered by permeable flow. *Nature* **422**: 154 – 157.

Zhang Y and Yin Q-Z (2012) Carbon and other light element contents in the Earth's core based on first-principles molecular dynamics. *Proceedings of the National Academy of Sciences of the United States of America* **109**: 19579 – 19583.

Ziegler K, Young ED, Schauble EA and Wasson JT (2010) Metal–silicate silicon isotope fractionation in enstatite meteorites and constraints on Earth's core formation. *Earth and Planetary Science Letters* **295**: 487 – 496.

Appendix

Table A1: *Average composition of all metal phases as detected by EPMA. The concentrations are given in wt% and the values in brackets give the error on the last digit (1 σ standard deviation). "N" stands for the number of analyses that have been averaged and column "Ø" lists the employed beam diameters. Shaded rows mark experiments the metal composition of which was calculated by Image Analyses. Given are the composition of the exsolutions (exs.) and the metal matrix and their relative fractions (by area).*

Exp.	Mg	Al	Si	Ca	Fe	O	S	Co	Ni	Mo	W	Cu	Ge	Sn	Sb	Pb	P	As	Au	Ag	N	Ø
11GPa																						
H3355a	0.001 (3)	0.005 (8)	0.06 (3)	-	93 (1)	0.38 (4)	0.02 (2)	-	-	-	-	2.2 (1)	1.0 (1)	0.76 (8)	0.62 (9)	1 (1)	-	-	-	-	34	10+20
H3355b	0.2 (6)	0.1 (2)	0.3 (6)	0.03 (8)	93 (4)	1 (2)	0.01 (1)	-	-	-	-	0.1 (4)	0.8 (2)	0.7 (1)	0.6 (2)	1 (1)	-	-	-	-	41	10+20
H3361a																						
Exs. 31.2%	-	0.004 (7)	0.003 (6)	-	85.9 (9)	0.35 (5)	5.5 (8)	-	-	-	-	2.4 (2)	1.5 (2)	1.22 (9)	1.2 (1)	0.5 (7)	-	-	-	-	30	10
Matrix 68.8%	0.003 (6)	0.003 (5)	0.005 (9)	-	65 (4)	3 (2)	19 (2)	-	-	-	-	8 (3)	0.6 (2)	1.8 (7)	2.2 (8)	2 (1)	-	-	-	-	31	10
H3361b	0.1 (5)	0.0 (2)	0.1 (4)	0.01 (7)	90 (5)	1 (1)	0.09 (9)	-	-	-	-	2 (2)	1.5 (5)	0.5 (7)	2.1 (9)	1.0 (9)	-	-	-	-	61	10
H3364a	0.001 (4)	0.005 (7)	0.002 (5)	-	82 (2)	0.4 (2)	10.7 (8)	-	-	-	-	1.3 (3)	1.2 (2)	1.5 (4)	1.6 (3)	1.3 (8)	-	-	-	-	34	10
H3364b																						
Exs. 1.5%	0.009 (8)	0.005 (6)	0.05 (4)	-	5.2 (8)	1.0 (7)	0.07 (9)	-	-	-	-	60 (10)	0.2 (2)	19 (3)	7.2 (9)	12 (21)	-	-	-	-	10	1
Matrix 98.5%	0.001 (2)	0.003 (6)	0.006 (8)	-	83 (2)	0.35 (6)	10 (2)	-	-	-	-	3.2 (8)	1.1 (3)	1.1 (2)	1.0 (2)	1.0 (8)	-	-	-	-	10	10
H3367b	0.00 (1)	0.003 (6)	0.01 (2)	-	81 (2)	0.4 (2)	10 (1)	-	-	-	-	2.5 (5)	1.0 (2)	1.5 (2)	1.0 (4)	1.1 (9)	-	-	-	-	49	10+20
H3371a	0.007 (9)	0.002 (5)	-	0.002 (3)	80 (1)	0.3 (4)	11 (1)	2.5 (1)	2.4 (1)	1.86 (8)	1.6 (2)	-	-	-	-	-	-	-	-	-	31	10
H3371b	0.01 (1)	0.002 (5)	-	0.006 (6)	83 (3)	0.20 (4)	0.25 (9)	2.5 (3)	2.3 (4)	3 (1)	3.8 (8)	-	-	-	-	-	-	-	-	-		
H3372a	0.02 (2)	0.004 (7)	-	0.012 (8)	83.2 (6)	0.45 (4)	6.3 (1)	2.15 (8)	2.02 (7)	3.05 (6)	2.1 (2)	-	-	-	-	-	-	-	-	-	30	10
H3372b	0.02 (2)	0.005 (7)	0.15 (1)	0.003 (4)	95.1 (5)	0.44 (4)	0.04 (2)	1.76 (7)	1.22 (7)	0.7 (2)	1.1 (3)	-	-	-	-	-	-	-	-	-	30	10
H3400a																						
Exs. 1.04%	0.10 (7)	0.12 (2)	0.04 (5)	0.07 (3)	4 (1)	0.9 (6)	0.004 (9)	-	-	-	-	-	-	-	-	-	0.007 (9)	0.2 (2)	36 (7)	64 (7)	12	1
Matrix 98.96%	0.001 (4)	0.006 (7)	0.004 (7)	0.015 (9)	92 (2)	0.15 (4)	0.02 (1)	-	-	-	-	-	-	-	-	-	0.3 (2)	1.3 (3)	1.4 (5)	0.06 (3)	29	10
H3400b																						
Exs. 1.6%	0.05 (4)	0.11 (2)	0.0 (1)	0.02 (1)	5 (3)	0.5 (2)	0.3 (4)	-	-	-	-	-	-	-	-	-	0.002 (5)	0.3 (2)	38 (13)	61 (12)	21	1
Matrix 98.4%	-	0.004 (5)	0.006 (9)	0.013 (7)	86.1 (6)	0.14 (3)	8.5 (4)	-	-	-	-	-	-	-	-	-	0.2 (2)	1.1 (3)	0.5 (3)	0.03 (2)	30	10
H3404a																						
Exs. 0.8%	0.06 (3)	0.05 (1)	0.01 (2)	0.02 (1)	3.9 (6)	0.9 (5)	0.00 (1)	-	-	-	-	-	-	-	-	-	-	0.2 (2)	51 (2)	49 (2)	10	1
Matrix 99.2%	-	0.003 (5)	0.005 (8)	0.003 (4)	92.2 (0.4)	0.27 (5)	0.02 (2)	-	-	-	-	-	-	-	-	-	0.74 (8)	1.7 (2)	1.7 (5)	0.03 (2)	20	20
H3404b																						
Exs. 1.6%	0.2 (3)	0.2 (1)	0.05 (8)	0.1 (1)	4 (2)	1 (1)	0.3 (3)	-	-	-	-	-	-	-	-	-	0.0 (1)	0.1 (2)	15 (5)	79 (6)	21	1
Matrix 98.4%	0.003 (6)	0.005 (7)	0.004 (6)	0.012 (8)	87.8 (6)	0.16 (3)	8.9 (4)	-	-	-	-	-	-	-	-	-	0.9 (3)	0.4 (3)	0.5 (4)	0.06 (3)	30	10
H3439a	-	0.007 (8)	0.02 (2)	0.002 (4)	93 (1)	0.27 (4)	-	-	-	-	-	-	-	-	-	-	0.4 (1)	1.0 (2)	1.8 (5)	0.2 (3)	50	20
H3439b	0.01 (1)	0.006 (8)	0.02 (1)	0.11 (1)	93 (2)	2.0 (4)	0.02 (1)	-	-	-	-	-	-	-	-	-	0.4 (1)	0.9 (3)	1.7 (5)	0.4 (5)	51	20
H3444a	0.01 (1)	0.005 (7)	0.30 (4)	0.003 (4)	98,5 (7)	0.36 (4)	-	-	-	-	-	-	-	-	-	-	-	-	-	0.6 (4)	30	20
H3444b	0.01 (1)	0.005 (9)	0.23 (7)	0.002 (3)	98.8 (4)	0.33 (7)	-	-	-	-	-	-	-	-	-	-	-	-	-	0.6 (2)	29	20
H3449a	0.005 (9)	0.002 (5)	0.11 (8)	0.013 (7)	99.6 (6)	0.6 (2)	-	-	-	-	-	-	-	-	-	0.9 (8)	-	-	-	-	30	20
H3449b	0.01 (1)	0.005 (8)	0.15 (6)	0.016 (7)	99.9 (6)	0.6 (1)	-	-	-	-	-	-	-	-	-	0.8 (6)	-	-	-	-	30	20
H3450a	0.002 (6)	0.004 (8)	0.05 (3)	-	94.5 (8)	0.30 (4)	-	-	-	-	-	1.32 (7)	0.8 (1)	0.9 (1)	0.08 (2)	-	-	-	-	-	30	20
H3455a	0.01 (1)	0.003 (5)	0.03 (5)	0.003 (4)	98.3 (8)	0.5 (4)	-	-	-	-	-	-	-	-	-	0.6 (6)	-	-	-	-	30	20
H3455b	0.006 (9)	0.005 (6)	0.007 (9)	0.004 (4)	92 (1)	0.22 (5)	-	-	-	-	-	-	-	-	-	0.7 (7)	-	-	-	-	30	20
H3497a	0.01 (1)	0.002 (6)	0.4 (4)	0.002 (4)	99.0 (9)	0.3 (2)	-	-	-	-	-	-	-	-	-	0.5 (3)	-	-	-	-	31	20
H3497b	0.006 (9)	0.003 (7)	0.28 (7)	0.003 (5)	98.7 (5)	0.26 (6)	-	-	-	-	-	-	-	-	-	-	-	-	-	0.2 (1)	31	20
H3586a	0.01 (2)	0.004 (7)	0.001 (5)	0.002 (3)	91.3 (5)	0.29 (5)	-	2.40 (8)	1.56 (6)	1.09 (8)	1.6 (2)	-	-	-	-	-	-	-	-	-	30	20
H3586b	0.005 (6)	0.003 (6)	0.05 (8)	0.003 (4)	93.4 (6)	0.4 (1)	-	2.03 (7)	1.26 (5)	0.8 (1)	1.2 (2)	-	-	-	-	-	-	-	-	-	30	20
H3704a	0.006 (8)	0.003 (5)	11.6 (2)	0.001 (2)	88.2 (8)	0.29 (5)	-	-	-	-	-	-	-	-	-	0.5 (5)	-	-	-	-	30	20
H3704b	0.01 (1)	0.004 (6)	6.38 (7)	0.002 (2)	94.5 (3)	0.05 (2)	-	-	-	-	-	-	-	-	-	0.17 (9)	-	-	-	-	31	20
H3707a	0.003 (7)	0.003 (6)	0.1 (2)	0.001 (2)	96.1 (8)	0.1 (2)	-	-	-	-	-	1.33 (7)	0.7 (1)	0.7 (1)	0.9 (1)	-	-	-	-	-	30	20
H3707b	0.01 (2)	0.02 (3)	11.6 (2)	0.002 (4)	83.0 (7)	0.2 (1)	-	-	-	-	-	1.5 (2)	0.8 (2)	0.9 (1)	1.6 (2)	-	-	-	-	-	26	20
H3718a	0.1 (5)	0.1 (2)	0.2 (7)	0.1 (4)	93 (3)	0 (1)	-	-	-	-	-	1.34 (7)	0.7 (1)	0.9 (2)	1.2 (2)	-	-	-	-	-	30	20
H3718b	0.001 (2)	0.006 (8)	3.94 (4)	0.001 (1)	91.5 (4)	0.19 (7)	-	-	-	-	-	1.05 (6)	0.7 (1)	0.99 (3)	0.80 (3)	-	-	-	-	-	30	20

Table A1 continued

Exp.	Mg	Al	Si	Ca	Fe	O	S	Co	Ni	Mo	W	Cu	Ge	Sn	Sb	Pb	P	As	Au	Ag	N	Ø
Z798a	0.005 (2)	0.005 (8)	0.34 (7)	0.002 (3)	99.4 (5)	0.31 (7)	-	-	-	-	-	-	-	-	-	-	-	-	-	0.6 (2)	30	20
Z798b	0.006 (9)	0.005 (7)	0.07 (4)	0.002 (3)	99.6 (5)	0.36 (8)	-	-	-	-	-	-	-	-	-	-	-	-	-	0.6 (2)	30	20
Z822a	0.1 (3)	-	0.4 (8)	0.1 (3)	93 (2)	1 (1)	-	-	-	-	-	1.37 (8)	1.0 (1)	1.0 (0.1)	0.06 (1)	-	-	-	-	-	30	20
Z822b	-	0.02 (4)	0.4 (8)	0.04 (9)	94 (1)	0.4 (6)	-	2.0 (1)	1.31 (6)	0.9 (1)	1.6 (2)	-	-	-	-	-	-	-	-	-	30	20
Z915a	0.007 (9)	0.005 (7)	6.13 (7)	0.002 (3)	94.2 (5)	0.05 (5)	-	-	-	-	-	-	-	-	-	-	-	-	-	0.3 (2)	30	20
Z915b	0.01 (1)	0.01 (2)	15.1 (1)	0.002 (3)	85.3 (5)	0.09 (5)	-	-	-	-	-	-	-	-	-	-	-	-	-	0.3 (3)	30	20
Z916a	-	0.01 (6)	0.3 (4)	0.02 (8)	98 (2)	0.2 (4)	-	-	-	-	-	-	-	-	-	-	-	-	-	0.5 (4)	40	20
Z916b	0.004 (7)	0.001 (3)	0.2 (2)	0.004 (4)	95.1 (6)	0.1 (1)	-	1.96 (8)	1.32 (6)	0.8 (1)	1.5 (2)	-	-	-	-	-	-	-	-	-	31	20
Z919a	0.01 (2)	0.01 (1)	0.4 (2)	0.01 (2)	100.2 (5)	0.1 (1)	-	-	-	-	-	-	-	-	-	0.4 (2)	-	-	-	-	31	20
Z919b	0.01 (1)	0.007 (9)	0.08 (9)	0.003 (6)	100.8 (6)	0.2 (2)	-	-	-	-	-	-	-	-	-	0.4 (3)	-	-	-	-	30	20
Z920b	0.02 (7)	0.01 (3)	0.2 (2)	0.01 (5)	99.5 (8)	0.2 (2)	-	-	-	-	-	-	-	-	-	0.3 (2)	-	-	-	-	30	20
Z922a	0.004 (4)	0.005 (8)	0.2 (1)	0.001 (2)	100.2 (6)	0.1 (1)	-	-	-	-	-	-	-	-	-	-	-	-	-	0.5 (3)	30	20
Z922b	0.1 (3)	-	0.2 (6)	0.1 (3)	100 (3)	0.3 (1)	-	-	-	-	-	-	-	-	-	-	-	-	-	0.5 (2)	30	20
Z926a	-	0.01 (5)	0.1 (2)	-	96 (1)	0.2 (3)	-	-	-	-	-	1.48 (8)	0.6 (2)	1.0 (3)	0.7 (2)	-	-	-	-	-	29	20
Z926b	0.03 (2)	0.003 (6)	0.06 (3)	0.001 (3)	95.3 (7)	0.23 (9)	-	-	-	-	-	2.25 (8)	0.6 (1)	1.1 (3)	0.8 (2)	-	-	-	-	-	29	20
Z941b	0.0001 (4)	0.004 (9)	0.2 (5)	0.001 (3)	94 (1)	0.3 (4)	-	-	-	-	-	1.40 (8)	0.9 (1)	0.9 (1)	1.4 (1)	-	-	-	-	-	29	20
Z1000a	-	0.003 (5)	0.02 (5)	0.003 (3)	91.3 (6)	0.2 (2)	-	-	-	-	-	-	-	-	-	-	1.27 (9)	0.9 (2)	1.5 (4)	-	40	20
Z1000b	0.01 (4)	0.01 (2)	0.03 (7)	0.02 (7)	91.8 (8)	0.1 (2)	-	-	-	-	-	-	-	-	-	-	1.3 (1)	0.9 (2)	1.6 (3)	-	40	20
Z1001a	0.1 (2)	0.03 (6)	0.2 (3)	0.3 (4)	56 (1)	1.3 (8)	38.9 (9)	-	-	-	-	-	-	-	-	0.5 (1)	-	-	-	-	31	20
Z1002a	0.000 (2)	0.005 (8)	7.8 (1)	0.011 (6)	79.6 (9)	0.4 (1)	-	-	-	-	-	-	-	-	-	-	0.28 (3)	0.2 (2)	2.2 (4)	-	30	20
Z1002b	-	0.002 (6)	2.2 (1)	0.006 (5)	92.9 (7)	0.23 (9)	-	-	-	-	-	-	-	-	-	-	0.8 (1)	0.8 (2)	1.2 (3)	-	39	20
Z1008a	0.3 (5)	0.1 (1)	0.2 (4)	0.1 (3)	53 (1)	2 (1)	38 (1)	-	-	-	-	3.5 (2)	0.08 (9)	0.7 (3)	0.7 (4)	-	-	-	-	-	60	20
Z1008b	-	0.004 (9)	0.2 (4)	0.006 (5)	94.5 (9)	0.3 (3)	0.05 (2)	-	-	-	-	-	-	-	-	-	0.66 (8)	1.0 (2)	1.1 (4)	-	50	20
Z1009b	0.004 (7)	0.004 (6)	0.002 (6)	0.005 (5)	78 (2)	0.3 (1)	12 (2)	2.4 (1)	2.2 (1)	1.7 (2)	1.2 (3)	-	-	-	-	-	-	-	-	-	51	20
Z1011a	0.0001 (4)	0.006 (7)	0.1 (2)	0.003 (4)	96 (1)	0.4 (5)	0.05 (2)	-	-	-	-	-	-	-	-	-	0.8 (1)	0.6 (2)	0.8 (3)	-	50	20
Z1011b	0.01 (1)	0.01 (1)	0.5 (9)	0.007 (5)	91 (1)	0.5 (7)	0.03 (1)	2.49 (8)	1.74 (6)	1.10 (8)	1.9 (2)	-	-	-	-	-	-	-	-	-	50	20
Z1013a	0.01 (1)	0.004 (6)	0.006 (9)	0.017 (7)	59.3 (3)	1.9 (1)	35.3 (2)	-	-	-	-	-	-	-	-	-	-	-	-	0.59 (6)	50	20
Z1016a	0.1 (2)	0.01 (3)	0.05 (9)	0.01 (1)	55.7 (8)	1.5 (4)	40.5 (6)	-	-	-	-	-	-	-	-	-	-	-	-	0.6 (1)	29	20
Z1016b	0.0 (1)	0.02 (4)	0.0 (1)	0.03 (3)	55 (1)	1.0 (6)	41.6 (1)	-	-	-	-	-	-	-	-	0.6 (3)	-	-	-	-	30	20
Z1019a	0.03 (4)	0.01 (2)	0.03 (5)	0.05 (4)	63.4 (4)	2.1 (3)	33.5 (4)	-	-	-	-	-	-	-	-	0.2 (1)	-	-	-	-	20	20
Z1019b	-	0.01 (2)	11.8 (2)	0.003 (4)	84.5 (5)	0.12 (8)	-	-	-	-	-	-	-	-	-	-	0.24 (5)	0.6. 2	0.6 (4)	-	40	20
Z1043a	0.001 (3)	0.004 (6)	0.01 (1)	0.006 (6)	71 (2)	0.5 (7)	24 (2)	-	-	-	-	-	-	-	-	-	0.007 (8)	1.4 (3)	1.2 (3)	-	53	20
Z1043b	0.0002 (9)	-	0.01 (1)	0.004 (5)	71 (2)	1.0 (9)	22 (2)	-	-	-	-	-	-	-	-	-	0.015 (8)	1.2 (2)	1.0 (4)	-	50	20
Z1051a	0.01 (1)	0.005 (8)	-	0.004 (5)	68 (2)	0.5 (5)	23 (2)	1.1 (1)	2.5 (0.6)	1.7 (1)	0.7 (2)	-	-	-	-	-	-	-	-	-	30	20
Z1051b	0.01 (1)	0.01 (5)	0.004 (8)	0.007 (5)	67 (2)	0.8 (6)	24 (2)	1.1 (1)	2.4 (3)	1.9 (1)	0.5 (2)	-	-	-	-	-	-	-	-	-	60	20
Z1062a	0.002 (4)	0.003 (5)	0.001 (2)	0.006 (5)	62 (3)	0.8 (1)	24 (2)	-	-	-	-	1.8 (3)	0.9 (2)	1.0 (3)	1.3 (3)	-	-	-	-	-	50	20
Z1062b	0.02 (3)	0.005 (7)	0.04 (5)	0.01 (1)	66 (2)	2 (1)	25 (2)	-	-	-	-	1.9 (2)	0.8 (2)	0.9 (2)	1.3 (2)	-	-	-	-	-	51	20
18 GPa																						
Z852a	0.006 (8)	0.005 (6)	0.06 (7)	0.005 (6)	99 (1)	0.4 (5)	-	-	-	-	-	-	-	-	-	-	-	-	-	0.07 (6)	31	20
Z854a	0.01 (1)	0.007 (8)	0.8 (1)	0.016 (7)	96.3 (9)	1.1 (2)	-	-	-	-	-	-	-	-	-	0.3 (1)	-	-	-	-	31	20
Z854b	0.01 (1)	0.003 (5)	0.7 (3)	0.030 (9)	97.9 (9)	1.0 (3)	-	-	-	-	-	-	-	-	-	-	0.09 (2)	0.1 (1)	0.1 (2)	0.6 (2)	31	20
Z858a	0.006 (7)	0.003 (6)	0.6 (2)	0.004 (5)	99.2 (7)	0.4 (1)	-	-	-	-	-	-	-	-	-	-	-	-	-	0.6 (3)	30	20
Z858b	0.006 (8)	0.001 (2)	0.7 (2)	0.005 (5)	99.7 (7)	0.5 (2)	-	-	-	-	-	-	-	-	-	0.5 (3)	-	-	-	-	30	20
Z859a	0.006 (8)	0.004 (6)	0.7 (5)	0.009 (7)	95 (1)	0.6 (5)	-	2.00 (7)	1.33 (5)	0.88 (9)	1.6 (3)	-	-	-	-	-	-	-	-	-	29	20
Z859b	-	0.005 (8)	0.4 (5)	0.006 (5)	94 (1)	0.5 (4)	-	-	-	-	-	1.33 (7)	0.9 (1)	1.0 (1)	1.4 (1)	-	-	-	-	-	40	20
Z865a	0.01 (1)	0.004 (6)	0.5 (3)	0.01 (1)	94.4 (9)	0.4 (2)	-	2.06 (8)	1.39 (5)	0.9 (1)	1.6 (2)	-	-	-	-	-	-	-	-	-	31	20
Z865b	0.002 (5)	0.003 (5)	0.4 (3)	0.002 (3)	94.9 (7)	0.4 (2)	-	-	-	-	-	1.44 (7)	0.9 (1)	0.9 (2)	0.05 (2)	-	-	-	-	-	31	20
Z869b	-	0.02 (3)	0 (1)	0.013 (8)	90 (4)	2 (1)	-	-	-	-	-	-	-	-	-	-	1.2 (3)	1.4 (3)	1.7 (6)	1 (1)	30	20
Z878a	-	0.005 (6)	04 (7)	0.003 (3)	94 (2)	0.2 (5)	-	-	-	-	-	-	-	-	-	-	1.2 (2)	1.3 (2)	1.5 (5)	1 (1)	30	20
Z878b	-	0.006 (8)	0.3 (9)	0.003 (4)	94 (2)	0.2 (7)	-	-	-	-	-	-	-	-	-	-	1.1 (2)	1.2 (3)	1.5 (5)	0.5 (8)	30	20
Z881a	0.01 (1)	0.003 (5)	0.70 (5)	0.02 (1)	98.8 (5)	0.5 (2)	-	-	-	-	-	-	-	-	-	0.3 (2)	-	-	-	-	30	20
Z881b	-	0.006 (7)	0.4 (6)	0.08 (2)	92 (3)	1.0 (5)	-	-	-	-	-	-	-	-	-	-	1.3 (2)	1.3 (2)	1.6 (6)	1 (2)	77	10+20
Z957b	-	0.002 (5)	0.02 (1)	0.001 (2)	93.0 (8)	0.08 (3)	-	-	-	-	-	-	-	-	-	-	1.2 (3)	1.2 (2)	1.7 (3)	-	20	51
20 GPa																						
Z929a	0.01 (1)	0.006 (9)	0.33 (8)	0.003 (3)	93.4 (7)	0.2 (1)	-	1.99 (7)	1.33 (5)	0.8 (1)	1.5 (2)	-	-	-	-	-	-	-	-	-	30	20
Z929b	0.002 (6)	0.003 (5)	0.2 (§)	0.002 (3)	94.4 (8)	0.2 (2)	-	-	-	-	-	1.39 (6)	0.8 (1)	0.9 (2)	1.3 (2)	-	-	-	-	-	30	20

Table A1 continued

Exp.	Mg	Al	Si	Ca	Fe	O	S	Co	Ni	Mo	W	Cu	Ge	Sn	Sb	Pb	P	As	Au	Ag	N	Ø
21 GPa																						
Z949b	0.001 (3)	0.004 (7)	1 (2)	-	95 (2)	1 (1)	-	-	-	-	-	1.39 (9)	0.9 (1)	1.0 (2)	1.4 (2)	-	-	-	-	-	30	20
Z950a	0.003 (6)	0.004 (7)	1 (1)	0.002 (3)	93 (2)	0.3 (8)	-	1.98 (9)	1.31 (7)	0.8 (1)	1.5 (2)	-	-	-	-	-	-	-	-	-	31	20
Z950b	0.001 (3)	0.003 (6)	0.6 (1)	0.001 (2)	95.0 (5)	0.1 (1)	-	-	-	-	-	1.40 (7)	0.9 (2)	0.8 (1)	1.2 (1)	-	-	-	-	-	30	20
Z969a	0.0001 (6)	0.004 (5)	0.3 (6)	0.009 (5)	93 (1)	0.4 (5)	-	-	-	-	-	-	-	-	-	-	1.0 (2)	1.0 (2)	1.8 (4)	-	41	20
Z969b	-	0.003 (5)	0.2 (2)	0.009 (7)	92.0 (7)	0.3 (1)	-	-	-	-	-	-	-	-	-	-	1.2 (2)	1.0 (2)	1.6 (5)	-	40	20
Z970a	0.01 (1)	0.005 (7)	0.7 (1)	0.005 (4)	94.1 (5)	0.2 (1	-	2.04 (7)	1.35 (5)	0.84 (8)	1.5 (2)	-	-	-	-	-	-	-	-	-	40	20
Z970b	0.01 (1)	0.003 (6)	0.7 (3)	0.003 (4)	93.8 (9)	0.2 (2)	-	2.07 (9)	1.37 (0.06)	0.8 (2)	1.5 (2)	-	-	-	-	-	-	-	-	-	40	20
Z977a	0.01 (1)	0.003 (6)	1.3 (2)	0.001 (2)	98.9 (6)	0.1 (1)	-	-	-	-	-	-	-	-	-	0.4 (2)	-	-	-	-	35	20
Z977b	0.007 (8)	0.003 (5)	1.0 (3)	0.002 (4)	96.5 (7)	0.1 (2)	-	-	-	-	-	-	-	-	-	-	-	-	-	0.5 (2)	45	20
Z980a	0.01 (1)	0.005 (9)	0.7 (4)	0.002 (3)	98 (1)	0.2 (3)	-	-	-	-	-	-	-	-	-	-	-	-	-	0.6 (3)	35	20
Z980b	0.006 (9)	0.004 (6)	1.1 (7)	0.001 (2)	97 (1)	0.3 (5)	-	-	-	-	-	-	-	-	-	0.4 (2)	-	-	-	-	75	20
23 GPa																						
H3518	0.01 (1)	0.003 (6)	1.0 (3)	0.01 (1)	98 (1)	0.4 (2)	-	-	-	-	0.1 (1)	-	-	-	-	0.5 (2)	-	-	-	-	32	20
H3536	0.01 (1)	0.005 (8)	0.6 (3)	0.009 (9)	97.9 (7)	0.4 (2)	-	-	-	-	0.8 (2)	-	-	-	-	0.6 (2)	-	-	-	-	32	20
H3581	0.001 (1)	0.003 (6)	0.4 (2)	0.018 (9)	97.8 (6)	0.8 (2)	-	-	-	-	-	-	-	-	-	0.4 (1)	-	-	-	-	31	10+20
H3606	0.02 (6)	0.005 (7)	1.5 (3)	0.02 (6)	98 (1)	0.5 (2)	-	-	-	-	-	-	-	-	-	-	-	-	-	0.06 (3)	31	20
H3629	0.004 (7)	0.003 (5)	1 (1)	0.003 (6)	99 (3)	1 (1)	-	-	-	-	-	-	-	-	-	0.4 (1)	-	-	-	-	30	20

Table A2: *Average composition of all ferropericlase phases as detected by EPMA. The concentrations are given in wt % and the values in brackets give the error on the last digit (1 σ standard deviation). "No" stands for the number of analyses that have been averaged. The beam diameter was set to 1μm in each case.*

Exp.	Mg	Al	Si	Ca	Fe	O	S	Co	Ni	Mo	W	Cu	Ge	Sn	Sb	Pb	P	As	Au	Ag	N
11GPa																					
H3355a	55.8 (9)	0.74 (6)	0.04 (1)	0.028 (6)	6.4 (6)	39.7 (7)	0.003 (3)	-	-	-	-	0.03 (3)	0.05 (6)	0.004 (7)	0.01 (1)	0.2 (4)	-	-	-	-	20
H3355b	54.4 (8)	0.98 (8)	0.05 (1)	0.036 (8)	7.5 (4)	39.7 (8)	0.002 (3)	-	-	-	-	0.02 (2)	0.04 (5)	0.01 (1)	0.01 (1)	0.3 (4)	-	-	-	-	18
H3361a	56 (2)	0.6 (1)	0.02 (1)	0.038 (7)	6 (2)	40 (1)	0.002 (3)	-	-	-	-	0.06 (3)	0.05 (5)	0.004 (6)	0.01 (1)	0.2 (2)	-	-	-	-	15
H3361b	55 (1)	0.6 (1)	0.02 (1)	0.03 (1)	5 (1)	38,9 (8)	0.002 (2)	-	-	-	-	0.04 (3)	0.03 (5)	0.006 (9)	0.002 (4)	0.4 (5)	-	-	-	-	31
H3364a	56 (2)	0.7 (2)	0.03 (1)	0.027 (8)	7 (2)	40 (1)	0.003 (4)	-	-	-	-	0.03 (3)	0.05 (6)	0.01 (1)	0.01 (2)	0.2 (3)	-	-	-	-	15
H3364b	55 (2)	0.06 (2)	0.03 (2)	0.026 (5)	7 (3)	40 (1)	0.002 (3)	-	-	-	-	0.07 (6)	0.05 (8)	0.005 (6)	0.01 (2)	0.5 (4)	-	-	-	-	16
H3367b	54 (2)	0.4 (2)	0.02 (2)	0.018 (8)	8 (2)	40 (1)	0.002 (2)	-	-	-	-	0.05 (4)	0.05 (7)	0.004 (8)	0.01 (2)	0.2 (4)	-	-	-	-	16
H3371a	56.2 (9)	0.65 (7)	0.02 (1)	0.037 (6)	6 (1)	39.3 (6)	0.003 (2)	0.03 (3)	0.02 (1)	0.005 (9)	0.06 (8)	-	-	-	-	-	-	-	-	-	16
H3371b	57 (1)	0.58 (9)	0.02 (1)	0.039 (8)	5 (1)	39.7 (6)	0.004 (4)	0.03 (3)	0.02 (3)	0.004 (8)	0.04 (4)	-	-	-	-	-	-	-	-	-	15
H3372a	55 (1)	0.8 (1)	0.03 (1)	0.028 (5)	7 (1)	39.5 (6)	0.004 (4)	0.04 (3)	0.03 (2)	0.008 (8)	0.02 (4)	-	-	-	-	-	-	-	-	-	16
H3372b	55.2 (4)	1.00 (7)	0.04 (1)	0.032 (8)	6.8 (4)	39.4 (4)	0.002 (3)	0.04 (3)	0.03 (3)	0.004 (5)	0.1 (1)	-	-	-	-	-	-	-	-	-	15
H3400a	53.4 (6)	1.37 (9)	0.07 (2)	0.035 (8)	9.2 (5)	39.2 (2)	0.009 (9)	-	-	-	-	-	-	-	-	-	0.01 (1)	0.10 (9)	0.1 (2)	0.01 (1)	22
H3400b	54.1 (7)	1.22 (5)	0.06 (2)	0.04 (1)	8.5 (4)	39.4 (4)	0.01 (1)	-	-	-	-	-	-	-	-	-	0.006 (7)	0.07 (9)	0.1 (2)	0.01 (1)	31
H3404a	57 (1)	0.7 (1)	0.03 (1)	0.031 (8)	6 (1)	40.1 (4)	0.006 (9)	-	-	-	-	-	-	-	-	-	0.004 (5)	0.07 (8)	0.1 (2)	0.01 (1)	31
H3404b	58 (1)	0.6 (1)	0.03 (1)	0.021 (5)	5 (1)	40.3 (5)	0.004 (7)	-	-	-	-	-	-	-	-	-	0.005 (7)	0.1 (1)	0.1 (2)	0.01 (1)	30
H3439a	53.9 (6)	0.9 (1)	0.04 (2)	0.026 (7)	7.3 (7)	38.0 (5)	-	-	-	-	-	-	-	-	-	-	0.002 (2)	0.1 (1)	0.1 (2)	0.002 (3)	30
H3439b	51 (2)	1.1 (2)	0.06 (1)	0.033 (8)	10 (1)	38 (1)	0.004 (5)	-	-	-	-	-	-	-	-	-	0.006 (5)	0.1 (1)	0.1 (2)	0.003 (4)	30
H3444a	53.7 (8)	0.84 (7)	0.04 (1)	0.024 (6)	7.9 (8)	39.5 (9)	-	-	-	-	-	-	-	-	-	-	-	-	-	0.01 (1)	31
H3444b	55 (2)	1.0 (3)	0.04 (2)	0.028 (8)	6 (2)	40 (1)	-	-	-	-	-	-	-	-	-	-	-	-	-	0.007 (9)	31
H3449a	52 (2)	1.3 (3)	0.07 (2)	0.039 (6)	9 (2)	39.7 (5)	-	-	-	-	-	-	-	-	-	0.3 (4)	-	-	-	-	31
H3449b	51.6 (6)	1.47 (8)	0.08 (1)	0.039 (8)	8.4 (5)	39.8 (5)	-	-	-	-	-	-	-	-	-	0.4 (5)	-	-	-	-	29
H3450a	55 (2)	1.0 (5)	0.04 (3)	0.03 (1)	5 (2)	38.5 (6)	-	-	-	-	-	0.02 (2)	0.03 (5)	0.005 (7)	0.001 (2)	-	-	-	-	-	32
H3455a	51 (2)	1.4 (3)	0.07 (2)	0.04 (1)	10 (2)	38.3 (7)	-	-	-	-	-	-	-	-	-	0.2 (4)	-	-	-	-	31
H3455b	53 (2)	1.2 (3)	0.07 (2)	0.030 (9)	8 (2)	39.1 (6)	-	-	-	-	-	-	-	-	-	0.4 (5)	-	-	-	-	29
H3497a	56 (1)	0.6 (1)	0.027 (9)	0.030 (6)	6 (2)	38.7 (4)	-	-	-	-	-	-	-	-	-	0.01 (2)	-	-	-	-	30
H3497b	55.8 (9)	0.66 (9)	0.03 (1)	0.023 (6)	6 (1)	38.7 (3)	-	-	-	-	-	-	-	-	-	-	-	-	-	0.002 (3)	30
H3586a	55 (2)	0.6 (1)	0.02 (1)	0.026 (6)	6 (2)	38.0 (8)	-	0.03 (3)	0.02 (2)	0.005 (6)	0.04 (6)	-	-	-	-	-	-	-	-	-	30
H3586b	55 (1)	0.9 (1)	0.04 (2)	0.05 (1)	5.3 (9)	38.3 (8)	-	0.02 (2)	0.01 (1)	0.004 (6)	0.06 (7)	-	-	-	-	-	-	-	-	-	30
H3704a	59.4 (8)	0.7 (2)	0.03 (2)	0.025 (6)	0.4 (1)	39 (1)	-	-	-	-	-	-	-	-	-	0.007 (9)	-	-	-	-	30
H3704b	58.7 (7)	0.8 (2)	0.03 (1)	0.026 (8)	0.9 (3)	39 (1)	-	-	-	-	-	-	-	-	-	0.01(1)	-	-	-	-	31
H3707a	55 (2)	0.7 (2)	0.026 (8)	0.026 (6)	7 (2)	38 (2)	-	-	-	-	-	0.02 (3)	0.05 (6)	0.005 (7)	0.003 (5)	-	-	-	-	-	33
H3707b	60 (1)	0.6 (1)	0.03 (2)	0.022 (4)	0.3 (1)	40 (2)	-	-	-	-	-	0.01 (2)	0.03 (4)	0.004 (7)	0.004 (5)	-	-	-	-	-	33
H3718a	55 (2)	0.8 (2)	0.04 (2)	0.030 (5)	7 (2)	38 (2)	-	-	-	-	-	0.02 (2)	0.04 (5)	0.003 (7)	0.004 (7)	-	-	-	-	-	33
H3718b	59 (1)	0.8 (1)	0.03 (1)	0.023 (6)	1.1 (3)	39 (2)	-	-	-	-	-	0.01 (2)	0.04 (4)	0.008 (1)	0.003 (5)	-	-	-	-	-	35
Z798a	55 (1)	0.9 (1)	0.04 (2)	0.024 (9)	7 (1)	39 (9)	-	-	-	-	-	-	-	-	-	-	-	-	-	0.007 (9)	29
Z798b	53.1 (8)	1.3 (1)	0.06 (2)	0.039 (7)	7.5 (6)	39.1 (9)	-	-	-	-	-	-	-	-	-	-	-	-	-	0.006 (9)	34
Z822a	54 (1)	0.7 (1)	0.03 (2)	0.017 (6)	7 (1)	38.5 (1)	-	-	-	-	-	0.02 (2)	0.02 (4)	0.006 (8)	0.002 (3)	-	-	-	-	-	30
Z822b	54.1 (9)	0.8 (1)	0.03 (1)	0.03 (1)	6.5 (9)	38.2 (7)	-	0.02 (2)	0.01 (2)	0.005 (6)	0.06 (9)	-	-	-	-	-	-	-	-	-	30
Z915a	59.9 (9)	0.5 (3)	0.03 (2)	0.026 (8)	0.5 (4)	39 (1)	-	-	-	-	-	-	-	-	-	-	-	-	-	0.004 (7)	31
Z915b	59.5 (8)	0.8 (1)	0.03 (2)	0.022 (5)	0.3 (1)	39 (1)	-	-	-	-	-	-	-	-	-	-	-	-	-	0.002 (5)	30
Z916a	56 (2)	0.7 (2)	0.03 (2)	0.032 (5)	5 (2)	39 (1)	-	-	-	-	-	-	-	-	-	-	-	-	-	0.003 (5)	33
Z916b	55 (1)	0.8 (2)	0.03 (1)	0.028 (6)	6 (1)	38.2 (8)	-	0.03 (2)	0.01 (2)	0.005 (8)	0.04 (7)	-	-	-	-	-	-	-	-	-	30
Z919a	56 (1)	0.8 (2)	0.03 (2)	0.030 (5)	5 (1)	38.9 (9)	-	-	-	-	-	-	-	-	-	0.01 (1)	-	-	-	-	31
Z919b	55 (2)	0.7 (1)	0.03 (1)	0.028 (6)	8 (2)	38.6 (8)	-	-	-	-	-	-	-	-	-	0.01 (1)	-	-	-	-	30
Z920b	56 (2)	0.8 (2)	0.03 (2)	0.027 (7)	6 (2)	38 (1)	-	-	-	-	-	-	-	-	-	0.005 (7)	-	-	-	-	25
Z922a	57 (2)	0.6 (2)	0.03 (2)	0.027 (7)	5 (1)	38 (1)	-	-	-	-	-	-	-	-	-	-	-	-	-	0.004 (5)	30
Z922b	53.6 (9)	0.8 (1)	0.03 (2)	0.030 (6)	8.5 (8)	38 (1)	-	-	-	-	-	-	-	-	-	-	-	-	-	0.003 (4)	33
Z926a	57 (2)	0.6 (2)	0.03 (2)	0.030 (6)	5 (2)	39 (1)	-	-	-	-	-	0.02 (2)	0.04 (5)	0.002 (4)	0.002 (4)	-	-	-	-	-	30
Z926b	56 (1)	0.7 (1)	0.03 (1)	0.024 (5)	6 (2)	39 (2)	-	-	-	-	-	0.03 (3)	0.03 (5)	0.004 (6)	0.004 (7)	-	-	-	-	-	30
Z941b	57 (2)	0.7 (3)	0.03 (2)	0.030 (9)	5 (2)	39.1 (7)	-	-	-	-	-	0.02 (2)	0.02 (4)	0.004 (6)	0.006 (8)	-	-	-	-	-	31
Z1000a	57 (1)	0.6 (1)	0.02 (1)	0.025 (5)	4 (2)	39.3 (5)	-	-	-	-	-	-	-	-	-	-	0.002 (3)	0.07 (9)	0.1 (1)	-	19
Z1000b	57 (2)	0.5 (2)	0.02 (2)	0.033 (9)	4 (1)	39.3 (7)	-	-	-	-	-	-	-	-	-	-	0.004 (4)	0.04 (5)	0.1 (1)	-	23
Z1001a	56.9 (9)	0.7 (2)	0.03 (2)	0.018 (5)	3.5 (7)	40 (1)	0.005 (5)	-	-	-	-	-	-	-	-	0.01 (2)	-	-	-	-	30
Z1002a	58.9 (5)	0.68 (6)	0.02 (1)	0.021 (6)	0.39 (5)	40.0 (7)	-	-	-	-	-	-	-	-	-	-	0.002 (3)	0.04 (7)	0.1 (1)	-	19
Z1002b	58.1 (5)	0.9 (2)	0.04 (2)	0.027 (9)	1.4 (3)	40 (1)	-	-	-	-	-	-	-	-	-	-	0.001 (2)	0.07 (9)	0.1 (1)	-	24

Table A2 continued

Exp.	Mg	Al	Si	Ca	Fe	O	S	Co	Ni	Mo	W	Cu	Ge	Sn	Sb	Pb	P	As	Au	Ag	N
Z1008a	58 (1)	0.4 (3)	0.02 (2)	0.015 (5)	2 (2)	39.0 (4)	0.004 (4)	-	-	-	-	0.02 (2)	0.04 (6)	0.01 (1)	0.0001 (5)	-	-	-	-	-	30
Z1008b	57 (2)	0.5 (4)	0.02 (2)	0.026 (6)	3 (2)	38.9 (6)	0.003 (4)	-	-	-	-	-	-	-	-	-	0.006 (5)	0.07 (9)	0.1 (1)	-	28
Z1009b	57 (3)	0.6 (3)	0.03 (2)	0.023 (7)	4 (3)	38.8 (7)	0.004 (4)	0.02 (2)	0.01 (2)	0.001 (3)	0.04 (5)	-	-	-	-	-	-	-	-	-	20
Z1011a	54 (2)	0.7 (2)	0.03 (1)	0.029 (6)	7 (2)	38.5 (6)	0.003 (5)	-	-	-	-	-	-	-	-	-	0.002 (3)	0.06 (9)	0.1 (1)	-	30
Z1011b	57 (2)	0.6 (3)	0.03 (1)	0.033 (7)	3 (2)	38.9 (6)	0.003 (4)	0.02 (2)	0.01 (2)	0.01 (1)	0.04 (5)	-	-	-	-	-	-	-	-	-	34
Z1013a	53.3 (9)	1.1 (2)	0.05 (2)	0.020 (7)	7.4 (9)	38.3 (3)	0.004 (5)	-	-	-	-	-	-	-	-	-	-	-	-	0.005 (6)	30
Z1016a	54.7 (1)	1.0 (2)	0.04 (2)	0.021 (4)	5.8 (8)	38.7 (4)	0.004 (5)	-	-	-	-	-	-	-	-	-	-	-	-	0.005 (7)	30
Z1016b	57.3 (9)	0.7 (2)	0.03 (1)	0.021 (6)	3.1 (9)	39.2 (3)	0.004 (5)	-	-	-	-	-	-	-	-	0.01 (1)	-	-	-	-	28
Z1019a	54.0 (8)	0.8 (1)	0.04 (2)	0.018 (6)	8 (1)	38.8 (5)	0.003 (4)	-	-	-	-	-	-	-	-	0.01 (2)	-	-	-	-	31
Z1019b	59.0 (6)	0.9 (3)	0.04 (2)	0.026 (7)	0.3 (1)	40 (1)	-	-	-	-	-	-	-	-	-	-	0.002 (3)	0.05 (7)	0.1 (1)	-	38
Z1043a	56 (2)	0.7 (3)	0.03 (2)	0.023 (5)	5 (2)	39.8 (9)	0.002 (4)	-	-	-	-	-	-	-	-	-	0.002 (3)	0.06 (9)	0.1 (2)	-	30
Z1043b	56 (2)	0.7 (2)	0.03 (2)	0.02 (2)	5 (2)	38.7 (9)	0.004 (4)	-	-	-	-	-	-	-	-	-	0.002 (4)	0.07 (8)	0.1 (2)	-	45
Z1051a	56 (2)	0.9 (5)	0.06 (8)	0.03 (5)	4 (2)	39 (9)	0.003 (3)	0.02 (2)	0.02 (2)	0.004 (7)	0.03 (5)	-	-	-	-	-	-	-	-	-	29
Z1051b	55 (2)	0.8 (3)	0.03 (2)	0.021 (7)	5 (2)	39.0 (4)	0.004 (4)	0.03 (2)	0.02 (2)	0.01 (1)	0.04 (6)	-	-	-	-	-	-	-	-	-	32
Z1062a	58 (2)	0.4 (2)	0.02 (2)	0.017 (6)	2 (2)	39.1 (4)	0.004 (4)	-	-	-	-	0.02 (2)	0.04 (5)	0.01 (1)	0.001 (2)	-	-	-	-	-	33
Z1062b	55 (1)	0.7 (2)	0.03 (2)	0.022 (6)	6 (1)	38.8 (5)	0.003 (5)	-	-	-	-	0.02 (2)	0.02 (4)	0.01 (1)	-	-	-	-	-	-	29
18 GPa																					
Z852a	57 (2)	0.5 (2)	0.04 (2)	0.03 (2)	4 (2)	38.8 (5)	-	-	-	-	-	-	-	-	-	-	-	-	-	-	31
Z854a	55 (1)	0.7 (1)	0.04 (1)	0.035 (6)	6 (1)	37.7 (4)	-	-	-	-	-	-	-	-	-	0.1 (1)	-	-	-	-	30
Z854b	55.1 (9)	0.80 (8)	0.05 (2)	0.033 (5)	6 (1)	38.6 (4)	-	-	-	-	-	-	-	-	-	-	0.007 (7)	0.04 (8)	0.1 (1)	0.004 (9)	27
Z858a	56 (2)	0.6 (2)	0.04 (2)	0.033 (6)	5 (3)	37.8 (6)	-	-	-	-	-	-	-	-	-	-	-	-	-	0.009 (9)	30
Z858b	56 (1)	0.7 (1)	0.04 (2)	0.033 (5)	5 (2)	37.6 (6)	-	-	-	-	-	-	-	-	-	0.01 (1)	-	-	-	-	35
Z859a	55 (2)	0.8 (2)	0.04 (2)	0.032 (9)	7 (2)	37.8 (5)	-	0.03 (2)	0.02 (2)	0.01 (1)	0.04 (7)	-	-	-	-	-	-	-	-	-	25
Z859b	54 (1)	0.74 (8)	0.02 (4)	0.025 (7)	7 (1)	38.3 (4)	-	-	-	-	-	0.03 (2)	0.04 (6)	0.006 (7)	0.003 (6)	-	-	-	-	-	25
Z865a	57 (2)	0.6 (3)	0.04 (2)	0.04 (2)	5 (3)	38.2 (6)	-	0.02 (2)	0.01 (2)	0.004 (7)	0.04 (5)	-	-	-	-	-	-	-	-	-	30
Z865b	57 (3)	0.6 (3)	0.04 (2)	0.05 (2)	5 (4)	38.3 (8)	-	-	-	-	-	0.3 (3)	0.05 (6)	0.004 (7)	0.008 (9)	-	-	-	-	-	30
Z869b	56 (1)	0.6 (1)	0.04 (2)	0.030 (8)	4 (2)	38.8 (5)	-	-	-	-	-	-	-	-	-	-	0.004 (5)	0.06 (9)	0.1 (2)	0.01 (1)	31
Z878a	56 (1)	0.67 (8)	0.04 (2)	0.028 (5)	5.3 (9)	38.8 (9)	-	-	-	-	-	-	-	-	-	-	0.004 (5)	0.04 (7)	0.2 (2)	0.00 (1)	25
Z878b	56 (2)	0.6 (2)	0.03 (1)	0.029 (6)	5 (2)	39.0 (8)	-	-	-	-	-	-	-	-	-	-	0.004 (5)	0.05 (8)	0.1 (2)	0.005 (8)	25
Z881a	56 (2)	0.7 (3)	0.04 (2)	0.027 (9)	5 (2)	38.8 (5)	-	-	-	-	-	-	-	-	-	0.01 (2)	-	-	-	-	30
Z881b	56.2 (5)	0.78 (5)	0.05 (1)	0.026 (5)	4.9 (5)	37.9 (5)	-	-	-	-	-	-	-	-	-	-	0.004 (3)	0.05 (7)	0.1 (2)	0.005 (6)	23
Z957b	58 (2)	0.5 (2)	0.03 (2)	0.031 (6)	3 (2)	39.3 (7)	-	-	-	-	-	-	-	-	-	-	0.001 (2)	0.06 (7)	0.1 (2)		31
20 GPa																					
Z929a	57 (3)	0.6 (3)	0.04 (2)	0.026 (5)	4 (3)	39 (1)	-	0.01 (1)	0.01 (1)	0.005 (7)	0.04 (5)	-	-	-	-	-	-	-	-	-	30
Z929b	57 (2)	0.6 (3)	0.04 (2)	0.03 (2)	5 (3)	39 (1)	-	-	-	-	-	0.03 (4)	0.02 (4)	0.004 (5)	0.003 (7)	-	-	-	-	-	30
21 GPa																					
Z949b	55 (1)	0.70 (7)	0.05 (1)	0.038 (6)	8 (1)	38.6 (7)	-	-	-	-	-	0.04 (3)	0.04 (6)	0.003 (4)	0.004 (5)	-	-	-	-	-	30
Z950a	54 (3)	0.7 (2)	0.06 (2)	0.05 (2)	8 (3)	38 (2)	-	0.04 (3)	0.02 (3)	0.003 (5)	0.02 (5)	-	-	-	-	-	-	-	-	-	28
Z950b	56 (2)	0.6 (2)	0.05 (2)	0.034 (8)	5 (2)	38 (2)	-	-	-	-	-	0.04 (3)	0.03 (5)	0.01 (1)	0.004 (6)	-	-	-	-	-	28
Z969a	56 (1)	0.7 (1)	0.05 (2)	0.036 (7)	5 (2)	38 (2)	-	-	-	-	-	-	-	-	-	-	0.004 (4)	0.1 (1)	0.1 (2)	-	29
Z969b	55 (3)	0.6 (3)	0.05 (2)	0.04 (1)	5 (2)	39 (2)	-	-	-	-	-	-	-	-	-	-	0.004 (4)	0.09 (9)	0.1 (1)	-	37
Z970a	58 (3)	0.4 (3)	0.04 (2)	0.05 (1)	3 (3)	39 (1)	-	0.02 (2)	0.01 (2)	0.005 (7)	0.04 (7)	-	-	-	-	-	-	-	-	-	34
Z970b	55 (1)	0.7 (2)	0.05 (2)	0.04 (1)	6 (2)	38 (1)	-	0.03 (2)	0.01 (2)	0.01 (1)	0.04 (7)	-	-	-	-	-	-	-	-	-	35
Z977a	44 (17)	0.6 (3)	0.1 (1)	0.03 (1)	4 (3)	31 (13)	-	-	-	-	-	-	-	-	-	0.01 (1)	-	-	-	-	26
Z977b	56 (1)	0.71 (5)	0.06 (2)	0.04 (1)	6 (1)	38 (1)	-	-	-	-	-	-	-	-	-	-	-	-	-	0.01 (1)	30
Z980a	55 (2)	0.7 (1)	0.03 (2)	0.04 (1)	7 (2)	39 (1)	-	-	-	-	-	-	-	-	-	-	-	-	-	0.01 (1)	29
Z980b	51 (5)	0.7 (1)	0.04 (4)	0.04 (1)	5 (2)	38 (2)	-	-	-	-	-	-	-	-	-	0.01 (1)	-	-	-	-	59
23 GPa																					
H3518	57 (1)	0.52 (2)	0.05 (2)	0.03 (1)	4 (1)	39.1 (4)	-	-	-	-	0.06 (9)	-	-	-	-	0.02 (3)	-	-	-	-	30
H3536	56 (3)	0.06 (1)	0.06 (2)	0.04 (1)	5 (4)	39 (1)	-	-	-	-	0.1 (1)	-	-	-	-	0.02 (2)	-	-	-	-	26
H3581	55 (2)	0.57 (8)	0.05 (2)	0.034 (7)	7 (2)	38 (6)	-	-	-	-	-	-	-	-	-	0.007 (8)	-	-	-	-	30
H3606	55.9 (9)	0.68 (7)	0.05 (1)	0.036 (7)	6 (1)	36.9 (3)	-	-	-	-	-	-	-	-	-	-	-	-	-	0.001 (1)	30
H3629	56 (2)	0.6 (1)	0.05 (2)	0.032 (7)	6 (2)	38.3 (5)	-	-	-	-	-	-	-	-	-	0.01 (1)	-	-	-	-	33

Table A3: *Average composition of all silicate phases as detected by LA-ICP-MS. The concentrations of the main elements (oxides) are given in wt %, whereas the abundances of the elements of interest are given in ppm (native element). Depending on the standard used, the concentration of S is either given in wt % (Afghanite) or in ppm (Botcharnikov) (blue and pink shaded cells respectively). The values in brackets give the error on the last digit (1 σ standard deviation). "N" stands for the number of analyses that have been averaged and column "Ø" lists the employed beam diameters.*

	MgO	Al_2O_3	SiO_2	CaO	FeO	S	Co	Ni	Mo	W	Cu	Ge	Sn	Sb	Pb	P	As	Au	Ag	N	Ø
11GPa																					
H3355a	43.6 (2)	3.38 (7)	42.7 (3)	4.28 (7)	5.99 (3)	-	-	-	-	-	605 (20)	5.9 (3)	34.2 (5)	1.00 (5)	372 (4)	-	-	-	-	5	80
H3355b	42.2 (5)	4.3 (2)	41.9 (1)	5.2 (3)	6.4 (4)	-	-	-	-	-	37 (5)	9 (5)	47 (14)	4 (5)	431 (54)	-	-	-	-	4	80
H3361a	46 (1)	2.8 (1)	40 (1)	4.0 (1)	7.1 (1)	0.228 (8)	-	-	-	-	2142 (15)	115 (15)	367 (32)	18 (12)	633 (11)	-	-	-	-	3	80
H3361b	45.1 (4)	2.8 (1)	42.4 (9)	4.29 (9)	5 (1)	-	-	-	-	-	731 (274)	27 (40)	67 (65)	7 (13)	386 (99)	-	-	-	-	4	80
H3364a	42.0 (7)	4.0 (2)	41.2 (3)	5.2 (3)	7.6 (2)	0.11 (1)	-	-	-	-	373 (42)	75 (18)	320 (38)	10 (6)	547 (118)	-	-	-	-	5	80
H3364b	44 (1)	3.33 (9)	41. (1)	3.92 (6)	8.1 (3)	0.11 (1)	-	-	-	-	1633 (327)	93 (8)	369 (15)	26 (15)	719 (30)	-	-	-	-	4	80
H3367b	36.5 (8)	5.9 (3)	39.5 (3)	6.0 (4)	12.1 (4)	0.086 (2)	-	-	-	-	926 (16)	119 (5)	542 (6)	18 (2)	1408 (132)	-	-	-	-	5	80
H3371a	45.3 (4)	2.9 (1)	41.2 (2)	4.5 (3)	6.2 (3)	0.17 (1)	230 (15)	95 (3)	37 (5)	189 (20)	-	-	-	-	-	-	-	-	-	4	40+50
H3371b	45 (1)	2.82 (8)	42.7 (8)	4.5 (2)	4.9 (3)	-	184 (20)	79 (13)	9 (2)	50 (15)	-	-	-	-	-	-	-	-	-	4	70
H3372a	43.1 (4)	3.5 (2)	42.7 (3)	3.9 (2)	6.8 (1)	0.13 (2)	232 (6)	85 (3)	29 (4)	181 (11)	-	-	-	-	-	-	-	-	-	5	80
H3372b	42.2 (9)	4.4 (3)	42.8 (3)	4.9 (4)	5.6 (3)	-	166 (7)	59 (6)	19 (1)	51 (9)	-	-	-	-	-	-	-	-	-	5	80
H3400a	38.9 (9)	5.7 (4)	41.7 (2)	6.4 (4)	7.2 (3)	-	-	-	-	-	-	-	-	-	-	265 (68)	1.4 (3)	1.5 (3)	487 (25)	5	80
H3400b	40.4 (7)	5.3 (2)	40.4 (5)	7.1 (2)	6.9 (1)	0.12 (1)	-	-	-	-	-	-	-	-	-	2464 (100)	4 (1)	2.1 (4)	525 (24)	3	80
H3404a	44.9 (3)	3.1 (1)	42.2 (3)	4.1 (2)	5.63 (7)	-	-	-	-	-	-	-	-	-	-	142 (13)	1.0 (2)	6.7 (4)	502 (13)	5	80
H3404b	45.8 (3)	3.0 (2)	42.3 (3)	3.8 (2)	5.2 (2)	0.19 (1)	-	-	-	-	-	-	-	-	-	708 (24)	3 (1)	5 (2)	521 (17)	4	80
H3439a	40.8 (4)	3.8 (2)	44.7 (1)	4.1 (2)	6.6 (1)	-	-	-	-	-	-	-	-	-	-	26 (2)	-	0.42 (9)	357 (10)	5	80
H3439b	37. 3 (9)	5.5 (4)	43.5 (3)	6.1 (4)	7.6 (2)	-	-	-	-	-	-	-	-	-	-	105 (8)	8 (7)	0.8 (3)	404 (22)	4	80
H3444a	41.7 (4)	3.59 (6)	44.3 (7)	4.2 (2)	6.3 (2)	-	-	-	-	-	-	-	-	-	-	-	-	-	282 (16)	5	80
H3444b	39 (1)	5.2 (2)	43.82 (8)	6.1 (3)	5.6 (4)	-	-	-	-	-	-	-	-	-	-	-	-	-	254 (11)	4	80
H3449a	37 (1)	5.9 (3)	43.3 (2)	6.4 (3)	7.3 (3)	-	-	-	-	-	-	-	-	-	327 (13)	-	-	-	-	4	80
H3449b	36 (1)	6.4 (7)	43.3 (5)	7.7 (5)	6.6 (4)	-	-	-	-	-	-	-	-	-	326 (17)	-	-	-	-	5	80
H3450a	37.3 (8)	6.6 (2)	43.3 (2)	6.5 (2)	6.2 (3)	-	-	-	-	-	358 (14)	4 (2)	27.8 (8)	1.2 (6)	-	-	-	-	-	5	80

Table A3 continued

	MgO	Al_2O_3	SiO_2	CaO	FeO	S	Co	Ni	Mo	W	Cu	Ge	Sn	Sb	Pb	P	As	Au	Ag	N	Ø
H3455a	41 (9)	5.8 (5)	37 (7)	8 (2)	8 (1)	-	-	-	-	-	-	-	-	-	714 (266)	-	-	-	-	4	40+50+80
H3455b	38 (3)	6.2 (3)	42 (2)	6.4 (4)	6.9 (6)	-	-	-	-	-	-	-	-	-	1206 (168)	-	-	-	-	5	80
H3497a	44.5 (4)	3.07 (6)	42.9 (2)	3.8 (1)	5.8 (1)	-	-	-	-	-	-	-	-	-	165 (7)	-	-	-	-	5	80
H3497b	43.8 (7)	3.0 (2)	43.4 (4)	4.3 (2)	5.5 (3)	-	-	-	-	-	-	-	-	-	-	-	-	-	221 (9)	6	80
H3586a	47 (2)	2.1 (4)	42 (1)	3.7 (9)	5 (1)	-	116 (32)	35 (12)	4 (2)	64 (17)	-	-	-	-	-	-	-	-	-	6	20
H3586b	43 (1)	3.6 (3)	42.0 (5)	6.5 (4)	5.0 (2)	-	85 (3)	24 (4)	4 (1)	37 (11)	-	-	-	-	-	-	-	-	-	4	30
H3704a	47.3 (7)	3.31 (9)	45.4 (7)	3.5 (1)	0.45 (2)	-	-	-	-	-	-	-	-	-	87 (4)	-	-	-	-	5	80
H3704b	45.9 (5)	3.6 (2)	45.4 (1)	4.1 (3)	0.96 (6)	-	-	-	-	-	-	-	-	-	33 (2)	-	-	-	-	5	80
H3707a	42.9 (5)	3.1 (1)	42.7 (5)	4.0 (2)	7.3 (4)	-	-	-	-	-	405 (46)	6.0 (7)	34 (4)	1.3 (2)	-	-	-	-	-	6	80
H3707b	48.0 (3)	2.9 (1)	45.2 (2)	3.5 (3)	0.35 (6)	-	-	-	-	-	103 (4)	1.7 (3)	13.1 (8)	1.2 (3)	-	-	-	-	-	5	80
H3718a	42.4 (3)	3.3 (1)	42.86 (9)	3.9 (2)	7.6 (1)	-	-	-	-	-	427 (25)	3.6 (3)	42 (2)	0.66 (8)	-	-	-	-	-	5	80
H3718b	45.8 (5)	3.3 (1)	45.6 (2)	4.0 (2)	1.25 (7)	-	-	-	-	-	142 (15)	1.1 (2)	11 (3)	0.17 (6)	-	-	-	-	-	7 (Ge 5, Sb 6)	80
Z798a	42 (1)	4.0 (2)	44.3 (4)	4.3 (3)	5.8 (4)	-	-	-	-	-	-	-	-	-	-	-	-	-	249 (16)	4	80
Z798b	37.9 (3)	5.7 (2)	43.4 (3)	6.6 (2)	6.4 (1)	-	-	-	-	-	-	-	-	-	-	-	-	-	281 (7)	4	80
Z822a	44.1 (8)	3.1 (2)	42.5 (2)	3.9 (3)	6.4 (3)	-	-	-	-	-	398 (24)	8 (2)	47 (2)	1.7 (5)	-	-	-	-	-	5	80
Z822b	44.2 (9)	3.1 (2)	42.9 (3)	4.1 (4)	5.7 (3)	-	118 (2)	38 (2)	3.4 (6)	27 (3)	-	-	-	-	-	-	-	-	-	5	80
Z915a	46.9 (4)	3.51 (8)	44.7 (4)	3.7 (1)	1.13 (4)	-	-	-	-	-	-	-	-	-	-	-	-	-	97 (4)	5	80
Z915b	47.6 (9)	3.2 (3)	45.1 (5)	3.8 (3)	0.24 (2)	-	-	-	-	-	-	-	-	-	-	-	-	-	56 (5)	5	80
Z916a	43.5 (4)	3.7 (1)	42.6 (3)	6.3 (2)	3.94 (6)	-	-	-	-	-	-	-	-	-	-	-	-	-	246 (15)	5	80
Z916b	42.9 (5)	3.7 (1)	42.6 (2)	4.3 (2)	6.5 (4)	-	150 (23)	59 (21)	7 (5)	64 (29)	-	-	-	-	-	-	-	-	-	4	80
Z919a	42.8 (5)	3.4 (1)	43.8 (2)	4.1 (2)	5.9 (3)	-	-	-	-	-	-	-	-	-	167 (27)	-	-	-	-	7	80
Z919b	41.1 (7)	3.1 (1)	43.4 (1)	4.4 (3)	7.9 (3)	-	-	-	-	-	-	-	-	-	218 (13)	-	-	-	-	7	80
Z920b	42.8 (6)	3.4 (2)	43.3 (3)	4.2 (3)	6.4 (4)	-	-	-	-	-	-	-	-	-	143 (7)	-	-	-	-	6	80
Z922a	43.6 (6)	3.5 (2)	42.2 (3)	4.1 (2)	6.6 (4)	-	-	-	-	-	-	-	-	-	-	-	-	-	216 (20)	5	80
Z922b	43 (1)	3.3 (2)	42.0 (2)	4.0 (3)	8.0 (7)	-	-	-	-	-	-	-	-	-	-	-	-	-	219 (25)	5	80
Z926a	43.4 (8)	3.01 (9)	42.2 (9)	4.2 (2)	7.2 (2)	-	-	-	-	-	459 (20)	3.6 (5)	47 (3)	0.5 (1)	-	-	-	-	-	5	80
Z926b	43.1 (7)	3.0 (2)	42.91 (9)	4.1 (3)	6.8 (2)	-	-	-	-	-	590 (39)	3 (1)	33 (8)	0.7 (2)	-	-	-	-	-	5	80

Table A3 continued

	MgO	Al_2O_3	SiO_2	CaO	FeO	S	Co	Ni	Mo	W	Cu	Ge	Sn	Sb	Pb	P	As	Au	Ag	N	Ø
Z941b	44 (1)	3.6 (2)	42.6 (7)	4.1 (3)	5.2 (1)	-	-	-	-	-	378 (31)	9 (2)	38 (2)	2.6 (4)	-	-	-	-	-	5	80
Z1000a	48 (2)	2.6 (4)	41 (2)	4 (1)	5 (2)	-	-	-	-	-	-	-	-	-	-	575 (173)	-	5 (6)	-	2	30
Z1000b	45.0 (4)	3.1 (1)	42.5 (4)	5.1 (1)	4.35 (5)	-	-	-	-	-	-	-	-	-	-	303 (23)	0.4 (2)	2.7 (7)	-	5 (As 4)	80
Z1001a	46.9 (3)	3.1 (1)	41.8 (1)	3.3 (2)	4.8 (1)	5873 (308)	-	-	-	-	-	-	-	-	187 (10)	-	-	-	-	5	80
Z1002a	49.1 (6)	3.3 (3)	43 (1)	4.2 (4)	0.39 (7)	-	-	-	-	-	-	-	-	-	-	191 (225)	1 (1)	3 (1)	-	5	50
Z1002b	46.6 (9)	3.7 (3)	43.5 (3)	4.7 (4)	1.39 (8)	-	-	-	-	-	-	-	-	-	-	17 (9)	0.086 (4)	1.1 (4)	-	4 (As 2)	80
Z1008a	49 (1)	3.1 (2)	39 (1)	3.5 (3)	5.3 (2)	17041 (7259)	-	-	-	-	406 (28)	1748 (84)	1069 (101)	840 (100)	-	-	-	-	-	6	80
Z1008b	44.7 (9)	3. (4)	41.7 (2)	4.4 (5)	5.5 (4)	-	-	-	-	-	-	-	-	-	-	53 (18)	0.15 (3)	0.89 (8)	-	5	80
Z1009b	45 (1)	3.6 (5)	40.8 (5)	-	-	997 (165)	188 (18)	62 (10)	21 (10)	282 (89)	-	-	-	-	-	-	-	-	-	6	80
Z1011a	44 (1)	3.4 (3)	39.9 (4)	4.1 (6)	8.7 (5)	-	-	-	-	-	-	-	-	-	-	66 (23)	0.17 (3)	1.1 (2)	-	6 (As 3)	80
Z1011b	45.8 (9)	3.3 (3)	41.7 (3)	4.1 (4)	5.1 (4)	-	98 (11)	27 (4)	3 (1)	18 (6)	-	-	-	-	-	-	-	-	-	6	80
Z1013a	42.8 (8)	4.3 (2)	41.0 (3)	4.3 (3)	7.6 (2)	3326 (200)	-	-	-	-	-	-	-	-	-	-	-	-	61 (4)	6	80
Z1016a	45.4 (6)	3.9 (3)	42.0 (2)	4.1 (3)	4.6 (1)	5687 (325)	-	-	-	-	-	-	-	-	241 (8)	-	-	-	-	5	80
Z1016b	45.2 (8)	3.7 (3)	41.6 (4)	3.6 (3)	6.0 (1)	4265 (131)	-	-	-	-	-	-	-	-	-	-	-	-	45 (3)	6	80
Z1019a	44 (1)	3.5 (2)	41.4 (6)	2.9 (2)	8.2 (3)	3641 (403)	-	-	-	-	-	-	-	-	168 (8)	-	-	-	-	5	80
Z1019b	45.0 (5)	5.0 (2)	44.1 (1)	5.6 (2)	0.23 (1)	-	-	-	-	-	-	-	-	-	-	6.6 (9)	0.37 (8)	1.1 (3)	-	5	80
Z1043a	45.9 (6)	3.4 (3)	41.6 (2)	3.4 (2)	5.8 (1)	2237 (65)	-	-	-	-	-	-	-	-	-	769 (42)	7.5 (7)	5.8 (9)	-	5	80
Z1043b	45.7 (7)	3.12 (8)	41.3 (8)	3.6 (1)	6.2 (1)	1684 (11)	-	-	-	-	-	-	-	-	-	1138 (18)	2.2 (5)	1.7 (3)	-	5	80
Z1051a	44.9 (3)	3.7 (1)	42.6 (1)	3.8 (2)	5.0 (1)	2500 (162)	103 (4)	72 (7)	20 (6)	316 (24)	-	-	-	-	-	-	-	-	-	5	80
Z1051b	45 (1)	3.8 (4)	42.0 (1)	4.2 (5)	5.5 (4)	1877 (189)	101 (8)	60 (6)	19 (6)	391 (44)	-	-	-	-	-	-	-	-	-	6	80
Z1062a	46. 3 (7)	3.0 (1)	39.6 (7)	3.5 (1)	7.6 (3)	3418 (174)	-	-	-	-	449 (21)	781 (45)	716 (44)	68 (2)	-	-	-	-	-	5	80
Z1062b	44.7 (5)	3.4 (1)	40.8 (2)	3.9 (1)	7.2 (1)	2607 (260)	-	-	-	-	372 (21)	685 (33)	613 (41)	42 (13)	-	-	-	-	-	3	80
18 GPa																					
Z852a	36 (2)	3.6 (2)	49 (1)	5.5 (2)	5.9 (2)	-	-	-	-	-	-	-	-	-	-	-	-	-	309 (25)	4	50+70
Z854a	39.1 (3)	3.64 (9)	46.8 (4)	4.02 (6)	6.4 (1)	-	-	-	-	-	-	-	-	-	177 (9)	-	-	-	-	4	50+70
Z854b	39.3 (7)	3.9 (2)	46.8 (3)	4.3 (2)	5.7 (1)	-	-	-	-	-	-	-	-	-	-	-	-	-	260 (14)	4	70

Table A3 continued

	MgO	Al_2O_3	SiO_2	CaO	FeO	S	Co	Ni	Mo	W	Cu	Ge	Sn	Sb	Pb	P	As	Au	Ag	N	Ø
Z858a	38.8 (7)	3.5 (1)	46.7 (1)	4.1 (1)	6.9 (3)	-	-	-	-	-	-	-	-	-	-	-	-	-	314 (10)	4	70
Z858b	37 (1)	3.6 (2)	49 (1)	3.9 (2)	6.2 (3)	-	-	-	-	-	-	-	-	-	172 (38)	-	-	-	-	4	40+50
Z859a	38.7 (6)	3.85 (6)	46.4 (6)	4.08 (5)	6.9 (1)	-	166 (5)	47 (3)	3.8 (3)	28 (6)	-	-	-	-	-	-	-	-	-	5	70
Z859b	39 (1)	3.6 (1)	47.3 (6)	4.0 (2)	6.6 (3)	-	-	-	-	-	442 (31)	8 (4)	30 (3)	3 (3)	-	-	-	-	-	5	70
Z865a	39.6 (6)	3.75 (7)	46.1 (5)	4.00 (9)	6.6 (1)	-	147 (22)	48 (12)	5 (2)	32 (16)	-	-	-	-	-	-	-	-	-	5	70
Z865b	39 (1)	3.6 (1)	45.1 (7)	3.9 (2)	8.1 (1)	-	-	-	-	-	647 (28)	7 (1)	49 (2)	2.0 (5)	-	-	-	-	-	4	70
Z869b	44 (3)	3.2 (2)	43 (2)	4.0 (6)	5.8 (3)	-	-	-	-	-	-	-	-	-	-	158 (37)	1.1 (6)	3.1 (6)	423 (22)	3	40
Z878a	40.8 (5)	3.23 (9)	46.3 (6)	4.0 (1)	5.7 (2)	-	-	-	-	-	-	-	-	-	-	57 (4)	1.2 (6)	4.1 (7)	451 (17)	5	50
Z878b	40 (1)	3.2 (2)	46 (1)	3.7 (4)	7.1 (2)	-	-	-	-	-	-	-	-	-	-	54 (3)	0.232 (5)	2.4 (3)	503 (47)	4 (As 2)	50
Z881a	41.0 (7)	4.0 (2)	45.1 (2)	4.3 (2)	5.6 (2)	-	-	-	-	-	-	-	-	-	150 (12)	-	-	-	-	4	80
Z881b	42.0 (3)	3.71 (7)	45.2 (2)	2.09 (6)	5.0 (1)	-	-	-	-	-	-	-	-	-	-	67 (5)	0.08 (2)	1.4 (8)	430 (15)	5 (As 3)	80
Z957b	43.7 (7)	3.8 (1)	42.5 (9)	4.4 (4)	5.5 (2)	-	-	-	-	-	-	-	-	-	-	110 (4)	0.19 (2)	1.7 (2)	-	3 (As 2)	80
20 GPa																					
Z929a	40 (5)	4.1 (1)	44.6 (4)	3.9 (1)	6.8 (1)	-	176 (7)	51 (3)	5 (1)	45 (5)	-	-	-	-	-	-	-	-	-	5	80
Z929b	40.6 (7)	4.2 (1)	44.9 (5)	4.6 (2)	5.8 (2)	-	-	-	-	-	375 (18)	2.4 (2)	21 (1)	0.7 (1)	-	-	-	-	-	5	80
21 GPa																					
Z949b	37.6 (6)	3.79 (7)	46.9 (5)	4.9 (2)	6.9 (2)	-	-	-	-	-	595 (39)	7 (3)	29 (6)	3 (2)	-	-	-	-	-	4	80
Z950a	37 (2)	4.07 (4)	46 (2)	4.6 (2)	8.3 (4)	-	264 (3)	93 (21)	11 (2)	44 (11)	-	-	-	-	-	-	-	-	-	5	80
Z950b	39 (5)	3.96 (8)	46.8 (5)	4.6 (2)	5.7 (2)	-	-	-	-	-	479 (33)	8 (1)	32 (7)	3 (2)	-	-	-	-	-	6	80
Z969a	40 (2)	3.8 (1)	45 (1)	4.4 (3)	6.4 (3)	-	-	-	-	-	-	-	-	-	-	146 (26)	0.25 (5)	2.8 (8)	-	6 (As 2, 70µm)	70 + 50
Z969b	39.4 (5)	4.2 (1)	46.2 (5)	4.76 (9)	5.4 (2)	-	-	-	-	-	-	-	-	-	-	161 (23)	0.22 (4)	1.3 (4)	-	6 (As 3)	80
Z970a	38 .0 (5)	4.24 (6)	46.0 (4)	3.8 (1)	7.0 (4)	-	204 (21)	67 (8)	7 (1)	30 (4)	-	-	-	-	-	-	-	-	-	5	80
Z970b	38.3 (6)	4.16 (4)	46.2 (4)	4.8 (2)	6.6 (2)	-	-	54 (4)	6 (1)	23 (5)	-	-	-	-	-	-	-	-	-	5	80
Z977a	39. 2 (6)	4.3 (1)	46.1 (6)	4.7 (1)	5.7 (1)	-	-	-	-	-	-	-	-	-	147 (20)	-	-	-	-	6	80
Z977b	38.9 (8)	4.12 (8)	46.4 (5)	5.0 (2)	5.5 (5)	-	-	-	-	-	-	-	-	-	-	-	-	-	283 (20)	5	80

Table A3 continued

	MgO	Al_2O_3	SiO_2	CaO	FeO	S	Co	Ni	Mo	W	Cu	Ge	Sn	Sb	Pb	P	As	Au	Ag	N	Ø
Z980a	37.8 (6)	4.07 (3)	46.8 (4)	4.97 (9)	6.3 (3)	-	-	-	-	-	-	-	-	-	-	-	-	-	305 (17)	5	80
Z980b	39.3 (7)	3.8 (1)	46.2 (3)	4.6 (1)	6.1 (2)	-	-	-	-	-	-	-	-	-	175 (4)	-	-	-	-	5	80
23 GPa																					
H3518	38 (1)	2.71 (8)	52 (1)	4.2 (2)	4 (1)	-	-	-	-	-	-	-	-	-	174 (23)	-	-	-	-	4	20+30
H3536	69 (9)	2.2 (3)	22 (8)	1 (2)	6 (4)	-	-	-	-	-	-	-	-	-	178 (84)	-	-	-	-	4	20
H3581	38.7 (5)	3.5 (2)	47.2 (5)	4.4 (2)	6.1 (6)	-	-	-	-	-	-	-	-	-	174 (4)	-	-	-	-	3	50
H3606	36 (1)	3.6 (1)	50 (1)	4.2 (2)	5.5 (5)	-	-	-	-	-	-	-	-	-	-	-	-	-	343 (63)	5	30+40+50
H3629	35.2 (8	4.1 (1)	50 (7)	4.28 (5)	6.4 (2)	-	-	-	-	-	-	-	-	-	151 (6)	-	-	-	-	3	40+50

Acknowledgement

I´d like to thank my supervisor Dr. David C. Rubie for giving me the great opportunity of working at the University of Bayreuth, for his support and advice during my time in Bayreuth and for numerous helpful thoughts and comments that significantly helped to improve this work. Moreover I would like to gratefully acknowledge to have been given the chance to participate in many scientific conferences all over the world – a wonderful experience.

I´d like to give my warm thanks to Prof. Dr. Daniel J. Frost for introducing me to the experimental work of this study, for all his help with the data treatment, derivations and calculations and especially for the possibility to get help, answers and support at any time.

Desweiteren möchte ich mich ganz herzlich bei Herrn Prof. Dr. Palme bedanken, der mich erst auf die Position als Doktorandin am Bayerischen Geoinstitut aufmerksam gemacht, mich stets unterstützt und sich ausserdem bereit erklärt hat als Zweitgutachter für diese Arbeit zu fungieren (sofern durch das Leitungsgremium ausgewählt).

Für Hilfe bei Kalibrationen und Fragen zu Mikrosondenmessungen möchte ich mich herzlichst bei Herrn Detlef Krauße und Frau Ulrike Trenz bedanken. Herrn Dr. Andreas Audétat gilt zudem mein großer Dank für die Unterstützung bei sämtlichen LA-ICP-MS Messungen und für das zur Verfügung Stellen des Excel-basierten Programms für die Datenauswertung.

Für viele hilfreiche Diskussionen möchte ich mich bei meiner Kollegin Dr. Vera Laurenz bedanken.

Mein herzlicher Dank gilt zudem dem gesamten technischen und administrativen Personal des Bayerischen Geoinstituts Bayreuth. Hierbei möchte ich mich besonders für die hervorragende Probenvorbereitung und -präparation durch Herrn Heinz Fischer, Herrn Hubert Schulze und Herrn Raphael Njul bedanken.

Ich möchte mich ausserdem bei meinen Freunden Frau Dr. Linda Lerchbaumer, Frau Asiye Shabestari Hassani Saddat, Herrn Dr. Dennies Harries, Frau Dr. Natalia Solopova, Herrn Christopher Beyer, Frau Dr. Geertje Ganskow, Herrn Dr. Jochen Bammert, Herrn Dr. Kolja Stremmel, Frau Sara Rölver, Herrn Stefan Bretz, Frau Julia Werle und meinen Schwiegereltern Herrn Dr. Helmut und Frau Inge Bretz für ihre Freundschaft und vielen aufmunternden Worte ganz herzlich bedanken, sowie bei Bruno und Pünktchen Bretz für ihre Zuneigung und Aufmunterungen.

Für ihre Liebe, Unterstützung und stetigen Zuspruch während meiner ganzen Arbeit gilt mein herzlichster Dank meiner Familie, meinen Eltern Herrn Dipl. Theol. Dietrich und Frau Elisabeth Vogel und meiner Schwester Frau Kirsten Vogel und ihrem Partner Herrn Andreas Raschke.

Aus tiefstem Herzen möchte ich mich schließlich bei meinem Ehemann und besten Freund Herrn Dr. Markus Bretz für seine Liebe und unglaubliche Unterstützung während meiner gesamten Zeit als Doktorandin bedanken. Mein allerherzlichster Dank gilt ihm für seine stets aufmunternden Worte, seine Hilfe und fortwährende Motivation und ganz besonders für seinen grenzenlosen Optimismus.

(Eidesstattliche) Versicherungen und Erklärungen

(§ 8 S. 2 Nr. 6 PromO)

Hiermit erkläre ich mich damit einverstanden, dass die elektronische Fassung meiner Dissertation unter Wahrung meiner Urheberrechte und des Datenschutzes einer gesonderten Überprüfung hinsichtlich der eigenständigen Anfertigung der Dissertation unterzogen werden kann.

(§ 8 S. 2 Nr. 8 PromO)

Hiermit erkläre ich eidesstattlich, dass ich die Dissertation selbstständig verfasst und keine anderen als die von mir angegebenen Quellen und Hilfsmittel benutzt habe.

(§ 8 S. 2 Nr. 9 PromO)

Ich habe die Dissertation nicht bereits zur Erlangung eines akademischen Grades anderweitig eingereicht und habe auch nicht bereits diese oder eine andere gleichartige Doktorprüfung endgültig nicht bestanden.

(§ 8 S. 2 Nr. 10 PromO)

Hiermit erkläre ich, dass ich keine Hilfe von gewerblichen Promotionsberatern bzw. –vermittlern in Anspruch genommen habe und auch künftig nicht nehmen werde.

Bayreuth, den 16.09.2014